

FIBER OPTIC SENSOR NETWORK FOR THE MONITORING OF CIVIL ENGINEERING STRUCTURES

PRESENTEE AU DEPARTEMENT DE GENIE CIVIL

ECOLE POLYTECHNIQUE FEDERALE DE LAUSANNE

POUR L'OBTENTION DU GRADE DE DOCTEUR ES SCIENCES TECHNIQUES

PAR
Daniele INAUDI

Diplômé en Physique
de l'École Polytechnique Fédérale de Zurich
de nationalité suisse

Jury:

Prof. L. Pflug, rapporteur
Prof. G. Guekos, corapporteur
Dr. A. D. Kersey, corapporteur
Dr. M. Pedretti, corapporteur
Prof. Ph. Robert, corapporteur
Prof. L. Vulliet, corapporteur

Lausanne, EPFL
Mai 1997

Outline

Acknowledgments	v
Summary	ix
Résumé	xi
Zusammenfassung	xiii
Préface du Prof. L. Pflug	xv
Table of contents	xvii
1. Introduction	1-1
2. Fiber optic smart sensing	2-1
3. Selection of the sensing technology	3-1
4. Optical fibers as intrinsic sensors	4-1
5. Low-coherence interferometry	5-1
6. SOFO design and fabrication	6-1
7. Multiplexing	7-1
8. Applications	8-1
9. Conclusions	9-1
General Bibliography	A-1
Curriculum vitae	A-7
Author's Bibliography	A-9

Acknowledgments

This work was carried out at the Laboratory of Stress Analysis (IMAC) of the Swiss Federal Institute of Technology in Lausanne (EPFL) under the direction of Prof. L. Pflug.

Many peoples and institutions have contributed to the realization of this dissertation. I would especially like to thank:

Prof. Léopold Pflug IMAC EPFL	For his encouragement, support and enthusiasm and for giving us the possibility of working in a stimulating environment.
Prof. Laurent Vulliet LMS EPFL	For believing in the potential of the SOFO system for geostructural monitoring and contributing to the development of both the reading unit and the sensors.
Dr. Alain D. Kersey Naval Research Lab.	For lighting in me the passion for fiber optic sensor during a course in Norway, for his useful discussion at many congresses and for giving me feedback on different chapters of this work.
Prof. Georg Guekos IQE ETHZ	For his support during my graduation work in his laboratory, and for taking part to the jury.
Prof. Philippe Robert MET EPFL	For the interesting discussion with him and the researchers of his group as well as for taking part to the jury.
The Council of the Swiss Federal Institutes of Technology	For financing my work through a ETHZ-EPFL exchange scholarship.
CTI Commission pour la Technologie et l'Innovation	For their continuous financial support to the SOFO project.
The EPFL direction.	For their encouragement on the application of new technologies to engineering and to the needs of the industry.

My special thanks goes to all persons having worked with me day by day, encouraged me, given invaluable feedback and contributed with their competence to the development of the SOFO project:

Samuel Vurpillot	For sharing his passion for civil engineering with me, teaching me most that I know in this field and contributing in a decisive matter to the success of this project. Sharing our office with him was a real pleasure. I wish Sam good luck for his own PhD.
Nicoletta Casanova	For contributing to the many applications of the SOFO system and for sharing the adventure of starting SMARTEC SA.
Pascal Kronenberg Annette Osa-Wyser Xavier Rodicio Branco Glisic Adil Elamari	For contributing to the many applications of the SOFO system and for giving invaluable input to its design and improvements.
Charles Gilliard Aleksander Micsiz	For helping in the design and realization of the SOFO reading unit and other electronic components.
Raymond Délez	For his many mechanical realizations and for solving many small and not so small practical problems.
Alain Herzog	For his beautiful pictures of our ugly sensors and for taking care of my plants during my many absences.
Antonio Scano Pascal Kronenberg Sandra Lloret Dénis Clément	Who contributed to the project by working on different aspects of the SOFO system during their graduation works.
Xavier Colonna de Lega Mathias Lehmann Mauro Facchini Alma di Tullio	For the many interesting discussion we had on our respective works and for contributing to the pleasant working atmosphere at IMAC.
Pramod K. Rastogi	For his support and for the many technical and philosophical discussions we had. I thank him for encouraging me to participate in his editorial projects.
Pierre Jacquot	For many useful discussion and for supporting this project.
Jean-Marc Ducret	For believing in the potential of the SOFO system and

Pierre Mivelaz letting us use their experiments to test and improve the system.

Colin Forno For his interesting comments on many chapters of this dissertation.

I would like to acknowledge the essential technical, financial and human contribution of our industrial partners. It was a real pleasure to work with them and I am very grateful for their consistent engagement even during difficult periods.

Mauro Pedretti
Rinaldo Passera
Passera+Pedretti SA The SOFO project and the creation of SMARTEC were possible thanks to the invaluable contribution of these two engineers who believe in new technology and support its development and application.

Paolo Colombo
and the whole team at
IMM For contributing to many of the applications and helping to the diffusion of the SOFO system outside the laboratory.

Ing. Silvio Marazzi
Hans Gerber
Maria Fornera
Joseph Kaelin
and the whole R&D team
at DIAMOND SA For industrializing the SOFO sensor and giving invaluable feedback to our team. DIAMOND contributed in a decisive way to the industrial development of the system and to the creation of SMARTEC.

Stefano Trevisani
SMARTEC SA For sharing with us the fascinating experience of starting a new company.

José Piffaretti
François Cochet
CABLOPTIC SA For giving us precious information about optical fibers and coating and for supplying most of the optical fibers used in this project.

A special thank also to all my family and friends and particularly to:

Mum and Dad For their moral and material support during my whole education and for always giving me the freedom to follow my inclinations and interests.

Paola Pellandini For being there in good and less good times.

Thanks to all these people and to the many others that have contributed with a little of their time, energy and enthusiasm to the realization of the SOFO project.

Summary

The security of civil engineering works demands a periodical monitoring of the structures. The current methods (such as triangulation, water levels, vibrating strings or mechanical extensometers) are often of tedious application and require the intervention of specialized operators. The resulting complexity and costs limit the frequency of these measurements. The obtained spatial resolution is in general low and only the presence of anomalies in the global behavior urges a deeper and more precise evaluation.

There is therefore a real need for a tool allowing an automatic and permanent monitoring from within the structure itself and with high precision and good spatial resolution.

In this framework, the concept of smart structures has proved its effectiveness in other domains such as the monitoring of composite materials or in aerospace applications. This type of structures are instrumented with an internal array of optical fiber sensors allowing the monitoring of different parameters critical for its security and useful for a cost efficient planning of the maintenance interventions. This includes the measurement of deformations, temperatures, pressures, penetration of chemicals, and so on.

Fiber optic sensors present important advantages compared to more traditional measurement methods, including their low cost, versatility to measure different parameters, insensitivity to electromagnetic fields (power lines, trains, thunderstorms) and to corrosion, their small size and the high density of information they can deliver even remotely.

The application of the smart structure concept to the specific needs of civil engineering opens new perspectives in the long-term monitoring of all works of some importance such as bridges, tunnels, dams, airport runways, domes, unstable soils and rocks, just to name a few.

The SOFO measurement system (French acronym for Surveillance d'Ouvrages par Fibre Optique or Structural Monitoring by Optical Fibers), is based on low-coherence interferometry and has been developed in the framework of this dissertation in cooperation with several industrial partners.

This systems includes a portable, waterproof and computer controlled reading unit as well as a number of sensors adapted to different structures and materials such as: concrete, metallic, timber and mixed structures, underground works, anchorage and pre-stressing cables and new construction materials.

Furthermore, different multiplexing techniques have been developed and tested in order to measure a large number of sensors without any operator's assistance.

This instrument was developed especially to measure small deformations over periods up to a few years and was tested successfully on a number of structures including bridges, tunnels, dams and laboratory models.

Résumé

La sécurité des ouvrages de génie civil nécessite un contrôle périodique des structures. Les méthodes actuellement utilisées (telles que triangulation, niveau d'eau, cordes vibrantes ou extensomètres mécaniques) sont souvent d'application lourde voire fastidieuse et demandent la présence d'un ou plusieurs opérateurs spécialisés. La complexité et les coûts élevés qui en découlent limitent la fréquence des mesures. La résolution spatiale obtenue est en général faible et seule la présence d'anomalies dans le comportement global incite à poursuivre l'analyse avec plus de détails et de précision. Il y a donc un besoin réel, manifesté à l'échelle internationale, d'un outil permettant une surveillance automatique et permanente à l'intérieur même de la structure avec une grande précision et une bonne résolution dans l'espace.

Dans cette optique, le concept de structure intelligente (en anglais smart structure) a déjà prouvé son efficacité dans plusieurs branches des sciences de l'ingénieur notamment dans le domaine de l'aéronautique et des matériaux composites. Ce type de structure est équipée d'un réseau interne de capteurs à fibres optiques permettant de surveiller différents paramètres critiques pour la sécurité et utiles pour une planification efficace des interventions de maintenance, notamment déformation, température, pression, pénétration d'agents chimiques, etc.

Ces senseurs à fibres optiques présentent d'importants avantages par rapport aux méthodes de mesure plus traditionnelles. Citons leur faible coût, la grande plage de paramètres mesurables, l'insensibilité aux champs électromagnétiques (lignes à haute tension, trains, orages) et à la corrosion, leur petite taille, leur souplesse d'utilisation et la grande densité d'information qu'ils peuvent fournir. L'application du concept de structure intelligente aux problèmes spécifiques du génie civil ouvre de nouvelles voies dans le domaine de la surveillance à long terme des ouvrages de quelque importance tels que ponts, tunnels, barrages, pistes d'aéroport, couvertures de grande portée, mécanique des roches et des sols, etc.

Le système de mesure SOFO (Surveillance d'Ouvrages par Fibre Optique), est basé sur le principe de l'interférométrie en basse cohérence et à été développé en collaboration avec plusieurs partenaires industriels. Ce système se compose d'une unité de lecture portable, étanche et entièrement contrôlée par ordinateur ainsi que d'une série de capteurs adaptés à l'installation dans différentes structures et matériaux tels que: les structures en béton, métal, bois et mixte, les ouvrages souterrains, les câbles d'ancrage et précontrainte ainsi que les nouveaux matériaux de construction.

Plusieurs techniques de multiplexage qui permettent la mesure automatique d'un grand nombre de senseurs ont aussi été développées et testées.

De par son principe même, cet instrument est adapté à la mesure de faibles déplacements sur des périodes pouvant atteindre plusieurs années. Il a été testé avec succès sur plusieurs structures civiles et notamment dans des ponts, des barrages, des tunnels et des modèles de laboratoire.

Zusammenfassung

Im Bauwesen fordert die Sicherheit eine periodische Überwachung der Strukturen. Die derzeit benutzten Methoden (wie z.B. die Triangulation, Wasserpegel, Schwingungskabel oder mechanische Extensometer) sind oft schwierig und langwierig in der Anwendung und erfordern die Anwesenheit eines oder mehrerer Fachleute. Die Komplexität und die daraus entstehenden hohen Kosten haben eine Einschränkung der periodisch durchzuführenden Kontrollen zur Folge. Die erhaltene räumliche Auflösung ist im allgemeinen schwach, und nur bei der Feststellung von Anomalien im allgemeinen Verhalten wird man eine detailliertere und genauere Analyse vornehmen. Es existiert also ein reeller Bedarf an einem Mittel, das eine automatische und permanente Überwachung im Inneren der Struktur mit höchster Präzision und mit einer befriedigenden räumlichen Auflösung ermöglicht.

In dieser Hinsicht hat sich das Konzept der intelligenten Struktur (*smart structure*) in vielen Bereichen des Ingenieurwesens, insbesondere in den Bereichen der Aeronautik und der Verbundbaustoffe als wirksam erwiesen. Eine solche Struktur ist mit einem internen Netz von Sensoren aus Glasfasern ausgestattet, das die Überwachung unterschiedlicher kritischer Parameter für die Sicherheit oder für eine wirksame Planung der Unterhaltsarbeiten ermöglicht, wie z.B. Deformation, Temperatur, Druck, Eindringen von chemischen Substanzen, usw.

Diese Sensoren aus Glasfasern weisen gegenüber herkömmlichen Messmethoden erhebliche Vorteile auf. Erwähnt seien hier die niedrigen Kosten, das große Spektrum von meßbaren Parametern, die Unempfindlichkeit auf elektromagnetische Felder (Hochspannungsleitungen, Züge, Gewitter) und auf Korrosion, die kleinen Abmessungen, die Flexibilität in der Anwendung und die grosse Menge an Informationen, die gewonnen werden kann. Die Anwendung des Konzepts der intelligenten Struktur im Bauwesen erschließt neue Wege auf dem Gebiet der langfristigen Überwachung von bedeutenden Bauwerken wie Brücken, Tunnels, Staumauern, Landepisten, größere Überdeckungen, Fels- und Bodenmechanik, usw. Das Messsystem SOFO (*Surveillance d'Ouvrages par Fibres Optiques*) beruht auf dem Prinzip der Interferometrie in niederer Kohärenz und wurde in Zusammenarbeit mit mehreren industriellen Partnern entwickelt. Das System besteht aus einer tragbaren und von einem Computer völlig kontrollierten Leseinheit und einer Serie von Sensoren, die für die Installation in verschiedenartigen Strukturen und Materialien geeignet sind; zum Beispiel Strukturen aus Beton, Metall und Holz, unterirdische Strukturen, Verankerungs- und Vorspannkabel, neuartige Baustoffe.

Verschiedene Multiplexing-Methoden wurden entwickelt und getestet. Sie bezwecken eine höhere Dichte von Messpunkten, die vom Apparat ohne manuelle Betätigung abgelesen werden können.

Dem Herstellungsprinzip gemäß ist das Gerät für eine Messung geringer Deformationen geeignet, die sich auch über mehrere Jahre erstrecken kann. Das SOFO System wurde auf verschiedenen Strukturen wie Brücken, Tunnels und Dämmen erfolgreich getestet.

Préface

L'infrastructure d'un pays dépend pour une large part des prestations de l'ingénieur civil, que l'on pense au réseau routier ou à celui des chemins de fer, aux barrages, aux tunnels ou aux installations portuaires, pour ne citer que ces exemples.

Dans le contexte actuel, en Suisse en particulier, les missions dévolues au praticien s'infléchissent de manière accrue vers les tâches d'entretien ou de maintenance du patrimoine existant : il s'agit de garantir la longévité des ouvrages en toute sécurité, au besoin en les rendant aptes à des exigences nouvelles.

Dans cette optique, la nécessité de méthodes d'auscultation efficaces, peu onéreuses et susceptibles de fournir des indications permanentes apparaît à chacun. Il résulte de cette exigence un flux de données considérable, dont la signification concrète doit être présentée sous une forme adéquate afin d'être réellement utile au praticien. C'est dire qu'il s'agit non seulement de mesurer des paramètres significatifs en grand nombre, mais encore de dépouiller ces mesures sans qu'il soit nécessaire de recourir à un opérateur humain et de manière à inscrire ces résultats dans les schémas familiers à l'ingénieur constructeur.

C'est ainsi que, par exemple, les allongements mesurés aux fibres extrêmes d'une poutre peuvent être directement transformés en courbures puis en flèche, et le tracé de la déformée effective rendu graphiquement et de manière quasiment instantanée.

Le travail remarquable de Monsieur Inaudi s'inscrit dans cette perspective de développement de nouvelles méthodes d'auscultation et de l'appareillage qu'elles impliquent. Le mérite du candidat est d'avoir transposé au domaine très exigeant des ouvrages en phase de construction les techniques d'apparition récentes exploitées dans le domaine des télécommunications. Non content d'adapter ces nouvelles technologies, Monsieur Inaudi a conçu puis mis en oeuvre des procédés inédits d'exploitation du potentiel considérable recelé par les fibres optiques, en particulier en multipliant les points de mesure situés sur une seule et même fibre.

Une fois démontré la validité du principe de fonctionnement, le candidat a poursuivi la réflexion qui lui a permis de conférer au système proposé la nécessaire maturité à son engagement dans les conditions réelles rencontrées sur le chantier.

L'achèvement d'une thèse constitue toujours un motif de satisfaction : une idée ou un concept inédit prend naissance puis se développe, ses assises sont structurées, ses limites explorées et au besoin étendues. S'agissant d'une technique de mesure inédite, sensibilité, précision, plage de mesure font l'objet d'analyses et de comparaisons minutieuses. De manière générale, quelques essais convenablement choisis au laboratoire attestent la plupart du temps le bien fondé de l'innovation proposée.

Ici, non seulement la technique et son instrumentation ont subi l'épreuve des conditions de chantier à répétées reprises, mais encore avant même de quitter le milieu académique, le candidat a fondé sa propre entreprise destinée à valoriser le système d'auscultation qu'il a proposé et réalisé dans le cadre de sa thèse.

Cet esprit de pionnier mérite à mes yeux d'être souligné. A l'heure où tant de médias véhiculent pessimisme ou morosité, il est réjouissant de voir un jeune ingénieur entreprendre, réussir et persévérer.

Professeur L. Pflug

Table of contents

1. INTRODUCTION	1-1
1.1 CIVIL STRUCTURES, THEIR SAFETY, THE ECONOMY AND THE SOCIETY	1-2
1.2 MONITORING DURING BIRTH, LIFE AND DEATH OF A STRUCTURE	1-3
1.2.1 NEW STRUCTURES, CONSTRUCTION AND TESTING	1-4
1.2.2 TESTING	1-4
1.2.3 IN-SERVICE MONITORING	1-4
1.2.4 AGING STRUCTURES: RESIDUAL LIFE ASSESSMENT	1-5
1.2.5 REFURBISHING	1-5
1.2.6 RECYCLING OR DISMANTLING	1-5
1.2.7 KNOWLEDGE IMPROVEMENTS	1-5
1.2.8 SMART STRUCTURES	1-6
1.3 EXISTING DEFORMATION MONITORING SYSTEMS	1-6
1.3.1 VISUAL INSPECTION	1-6
1.3.2 MECHANICAL GAGES	1-6
1.3.3 ELECTRICAL GAGES	1-7
1.3.4 ELECTROMECHANICAL METHODS	1-7
1.3.5 OPTICAL METHODS	1-7
1.3.6 FIBER OPTIC SENSORS	1-7
1.3.7 GPS	1-7
1.4 NEW MONITORING NEEDS	1-8
1.4.1 REPLACEMENT OR IMPROVEMENTS OF CONVENTIONAL INSTRUMENTATION	1-8
1.4.2 ENABLING INSTRUMENTATION	1-9
1.5 CONCLUSIONS	1-10
1.6 OUTLINE	1-10
1.7 BIBLIOGRAPHY	1-11
2. FIBER OPTIC SMART SENSING	2-1
2.1 INTRODUCTION	2-2
2.2 FIBER OPTIC SMART SENSING	2-3
2.3 SMART SENSING SUBSYSTEMS	2-3
2.4 SENSOR SELECTION	2-6
2.4.1 STRAIN, DEFORMATION AND DISPLACEMENT MEASUREMENTS	2-6
2.4.2 ABSOLUTE, RELATIVE AND INCREMENTAL MEASUREMENTS	2-8
2.4.3 SENSITIVITY, PRECISION AND DYNAMIC RANGE	2-9
2.4.4 DYNAMIC, SHORT-TERM AND LONG-TERM MEASUREMENTS	2-9
2.4.5 INDEPENDENT MEASUREMENT OF STRAIN AND TEMPERATURE	2-10
2.4.6 MULTIPLEXING TOPOLOGIES AND REDUNDANCY	2-10

2.4.7 INSTALLATION TECHNIQUES	2-14
2.4.8 REMOTE SENSING	2-16
2.5 FIBER OPTIC SENSOR TECHNOLOGIES	2-17
2.5.1 MICROBENDING SENSORS	2-17
2.5.2 FIBER BRAGG GRATING SENSORS	2-17
2.5.3 INTERFEROMETRIC SENSORS	2-18
2.5.4 LOW COHERENCE SENSORS	2-18
2.5.5 BRILLOUIN SENSORS	2-19
2.5.6 OVERVIEW	2-20
2.6 OUTLOOK	2-21
2.7 REFERENCES	2-23

3. SELECTION OF THE SENSING TECHNOLOGY **3-1**

3.1 INTRODUCTION	3-2
3.2 REQUIREMENTS	3-3
3.2.1 DEFORMATION SENSING	3-3
3.2.2 SENSOR LENGTH	3-3
3.2.3 RESOLUTION AND PRECISION	3-3
3.2.4 DYNAMIC RANGE	3-3
3.2.5 STABILITY	3-4
3.2.6 TEMPERATURE SENSITIVITY	3-4
3.3 CONCLUSIONS	3-5

4. OPTICAL FIBERS AS INTRINSIC SENSORS **4-1**

4.1 INTRODUCTION	4-2
4.2 OPTICAL FIBER CHARACTERISTICS	4-2
4.2.1 OPTICAL CHARACTERISTICS	4-2
4.2.2 PHYSICAL CHARACTERISTICS	4-4
4.3 OPTICAL FIBERS AS PART OF AN INTERFEROMETRIC SENSOR	4-5
4.3.1 FIBER LENGTH SENSITIVITY	4-6
4.3.2 AXIAL STRAIN SENSITIVITY	4-6
4.3.3 TEMPERATURE SENSITIVITY	4-7
4.3.4 COATINGS	4-8
4.3.5 EMBEDDED OPTICAL FIBER SENSORS	4-11
4.4 ERROR ESTIMATION	4-13
4.5 CONCLUSIONS	4-13
4.6 BIBLIOGRAPHY	4-14

5. LOW-COHERENCE INTERFEROMETRY **5-1**

5.1 INTRODUCTION	5-2
5.2 PERFECTLY COHERENT INTERFEROMETERS	5-2
5.3 PARTIALLY COHERENT INTERFEROMETERS	5-4
5.3.1 MONOCHROMATIC SOURCE	5-5
5.3.2 MULTIPLE MONOCHROMATIC SOURCES	5-6
5.3.3 RECTANGULAR SPECTRA	5-6

5.3.4 GAUSSIAN SPECTRA	5-7
5.3.5 LORENZIAN SPECTRA	5-8
5.3.6 WAVELENGTH SELECTIVE MIRRORS	5-9
5.3.7 CONCLUSIONS	5-9
5.4 PATH-MATCHING INTERFEROMETERS	5-10
5.4.1 SPECTRAL APPROACH	5-10
5.4.2 WAVE PACKETS APPROACH	5-13
5.5 BIREFRINGENCE AND POLARIZATION EFFECTS	5-16
5.6 SIGN AMBIGUITIES	5-18
5.7 CONCLUSIONS	5-19
5.8 BIBLIOGRAPHY	5-20
<u>6. SOFO DESIGN AND FABRICATION</u>	<u>6-1</u>
6.1 INTRODUCTION	6-2
6.2 REQUIREMENTS	6-2
6.3 OVERVIEW	6-5
6.4 EVOLUTION: THE HISTORY OF SOFO	6-8
6.4.1 PMD / FORMOS	6-9
6.4.2 SOFO	6-11
6.4.3 INDUSTRIAL VERSION OF SOFO	6-14
6.5 LIGHT SOURCE	6-15
6.5.1 REQUIREMENTS	6-15
6.6 SENSORS	6-19
6.6.1 REQUIREMENTS	6-19
6.6.2 FIBER AND COATING TYPES	6-20
6.6.3 REFERENCE FIBER	6-21
6.6.4 LOCAL VS. DISTRIBUTED COUPLING	6-23
6.6.5 DISTRIBUTED COUPLING SENSORS	6-23
6.6.6 LOCAL COUPLING SENSORS	6-25
6.6.7 MIRRORS	6-31
6.6.8 EXTERNAL OPTICAL COUPLER	6-31
6.6.9 OPTICAL CONNECTORS	6-33
6.6.10 OPTICAL CABLES	6-34
6.7 ANALYZER	6-35
6.7.1 OPTICAL SETUP	6-35
6.7.2 BEAM COLLIMATOR	6-37
6.7.3 REFLECTOR	6-38
6.7.4 TRANSLATION STAGE	6-44
6.7.5 COUPLER	6-45
6.7.6 REFERENCE ARM	6-45
6.8 DETECTION	6-46
6.9 SIGNAL PROCESSING	6-47
6.9.1 LOCK-IN AMPLIFIER	6-47
6.9.2 ANALOG ENVELOPE EXTRACTION	6-48
6.9.3 ALL DIGITAL PROCESSING	6-48
6.10 DATA PROCESSING AND INTERFACE	6-53
6.10.1 ACQUISITION SOFTWARE	6-53
6.10.2 DATA ANALYSIS SOFTWARE	6-56
6.10.3 OUTLOOK: SMART CIVIL STRUCTURES	6-57
6.11 ADDITIONAL ELEMENTS	6-58

6.11.1 INTERNAL PROCESSOR	6-58
6.11.2 COMMUNICATION LINKS	6-58
6.11.3 POWER SUPPLIES	6-59
6.11.4 CASE AND CONNECTORS	6-59
6.12 PERFORMANCES	6-61
6.12.1 READING UNIT PRECISION	6-61
6.12.2 SENSOR ACCURACY	6-62
6.12.3 STABILITY	6-62
6.12.4 REMOTE SENSING CAPABILITY	6-63
6.13 OUTLOOK	6-63
6.14 BIBLIOGRAPHY	6-63

7. MULTIPLEXING **7-1**

7.1 INTRODUCTION	7-2
7.2 LATERAL MULTIPLEXING	7-3
7.2.1 OPTICAL SWITCHING	7-3
7.2.2 ELECTRICAL SWITCHING	7-5
7.2.3 MULTI-CHANNEL DELAY COILS.	7-5
7.2.4 COHERENCE MULTIPLEXING	7-7
7.2.5 WAVELENGTH MULTIPLEXING	7-9
7.3 LONGITUDINAL MULTIPLEXING	7-10
7.3.1 COHERENCE MULTIPLEXING	7-11
7.3.2 PEAK RECOGNITION: PEAK FORM	7-12
7.3.3 REFLECTOR RECOGNITION: SPATIAL POSITION	7-19
7.4 MIXED MULTIPLEXING	7-35
7.5 PARTIAL REFLECTOR MANUFACTURING	7-36
7.5.1 REFLECTOR'S OPTIMIZATION	7-37
7.5.2 AIR-GAP CONNECTORS	7-40
7.5.3 ETALONS	7-41
7.5.4 BUBBLE REFLECTORS, BAD SPLICES	7-41
7.5.5 BROADBAND FIBER BRAGG GRATINGS	7-42
7.5.6 PHOTO-INDUCED FRESNEL REFLECTORS	7-42
7.5.7 MODAL REFLECTORS, INDEX PROFILES MISMATCH	7-42
7.6 CONCLUSIONS	7-42
7.7 BIBLIOGRAPHY	7-43

8. APPLICATIONS **8-1**

8.1 HOLOGRAPHIC TABLE	8-2
8.2 HIGH PERFORMANCE CONCRETE TENDON	8-4
8.3 TIMBER-CONCRETE SLAB	8-7
8.4 STEEL-CONCRETE SLAB	8-9
8.5 PARTIALLY RETAINED CONCRETE WALLS	8-11
8.6 TENDONS	8-13
8.7 VERTICAL DISPLACEMENT MEASUREMENTS: TIMBER BEAM	8-15
8.8 VERTICAL DISPLACEMENT MEASUREMENTS: CONCRETE BEAM	8-18
8.9 VENOGE BRIDGE	8-20

8.10 MOESA BRIDGE	8-23
8.11 VERSOIX BRIDGE	8-25
8.12 LULLY VIADUCT	8-27
8.13 LUTRIVE BRIDGE	8-29
8.14 EMOSSON DAM	8-31
8.15 OTHER APPLICATIONS	8-33
8.15.1 RAILS	8-33
8.15.2 PILES IN MORGES	8-33
8.15.3 VIGNES TUNNEL	8-33
8.15.4 HIGH TEMPERATURE SENSORS FOR A NUCLEAR POWER PLANT MOCK-UP	8-34
8.15.5 FATIGUE TESTS	8-34
8.16 CONCLUSIONS	8-34
9. CONCLUSIONS	9-1
<hr/>	
9.1 SUMMARY	9-2
9.2 MAIN ACCOMPLISHMENTS	9-2
9.2.1 SENSORS	9-2
9.2.2 READING UNIT	9-3
9.2.3 MEASUREMENT AND ANALYSIS SOFTWARE	9-3
9.2.4 MULTIPLEXING	9-4
9.2.5 APPLICATIONS	9-4
9.3 OUTLOOK	9-5
9.3.1 EXTENSIONS OF THE SOFO SYSTEM	9-5
9.3.2 POSSIBLE SPIN-OFFS	9-6
9.3.3 OTHER POSSIBLE APPLICATIONS OF THE SOFO SYSTEM	9-7
9.4 EPILOGUE	9-8

1. Introduction

“On doit se proposer de faire tous les ouvrages, surtout les ouvrages publics, en premier lieu bien solidement au second lieu avec économie. Le motif d’économie n’est que secondaire et subordonné au premier.” (“All structures, and especially the public ones, should be made solid and with economy. The economy concern are secondary and subordinate to the first one.”)

Perronet 1708-1794

This section analyzes the monitoring needs in civil engineering structures. After giving an overview of the different phases in a structure’s life that can benefit from a deformation measuring system, we will analyze the characteristics of the existing monitoring methods. Finally we will discuss the possibility of developing a new generation of sensors based on fiber optics and their applications as replacement of existing measurement methods or as enabling technology to open new possibilities in structural monitoring.

1.1 Civil structures, their safety, the economy and the society

Civil engineering accounts for 15% of Switzerland's gross internal product which represents 46'000 Millions Sfr of investments per year. This shows the importance of this branch for the economy and, on the other hand, the consequences that it can have on the society. It is for example calculated that about 40% of the 500'000 highway bridges in the USA are structurally deficient and would need to be repaired or rebuilt. This would represent an investment starting at 90 billions USD. More than 130'000 bridges have imposed load restrictions and approximately 5'000 are closed. In any year between 150 and 200 spans suffer partial or complete collapse [1]. Interestingly, a strong correlation was found between the maintenance of a bridge and its health state, while the age, climatic conditions and traffic load have only a minor influence. Other studies show that the situation in Europe is only slightly better and Switzerland is certainly not the happy exception that we would hope.

As citizens and daily users of civil structures such as bridges tunnels and buildings, we take their safety for granted. The size and the apparent solidity of the materials they are build from, naturally suggest a sense of security and eternity.

It should therefore be a priority of each public and private owner of a structure to build and maintain it cost-efficiently but without compromises to the safety of the users. This points to the application of total quality management concepts that have already been applied successfully in many industry domains. It is rejoicing to see a steady shift in this direction as shown for example by the creation of a chair for structure's maintenance in our department. More and more investments are nowadays shifted from the construction to the maintenance and life-span extension of existing structures.

In the framework of total quality management, a special concern is directed toward the definition of measurable quantities that can describe the state of a given process. In civil engineering this means that we will have to rely more and more on standardized tests and objective measurements, especially during the structure's construction, but also during its whole life span. In many fields, like underground works and dams, constant monitoring is an established concept and the professionals are often eager to test and apply new monitoring systems that can ease their work, provide new data or replace outdated and cumbersome equipment. In other fields, like bridge and building construction, it seems that the need for a long-term monitoring of structures is only a more recent concern and a real measurement culture has still to be established. It is still sometimes argued that a well designed and well-built structure does not need any monitoring at all. The recent history shows how misleading and costly these arguments can be. Bridges built only years ago and meant to last for a century, already need repair. The cause has been traced back to a poor quality of the construction materials, to the insufficient knowledge on concrete chemistry and sometimes to risky design. It is undeniable that a closer monitoring of these structures could have avoided, at least partially, the same problems to appear on similar structures built later and would have allowed a more prompt intervention to stop the progression of the damages.

A permanent monitoring starting with the construction of the structure adds a cost. This small added cost is however counterbalanced from the increased value of the structure that pays back in the long term. This is probably the main obstacle to a generalized application of the quality concepts to civil engineering: the costs of poor quality and the benefits of good quality turn into economical consequences only after years or tens of years. This tends to reduce the personal concern and can lead to the well known “Not my problem in twenty years” syndrome.

The work presented in this dissertation aims to give a small contribution towards a better understanding and a permanent monitoring of new and existing structures. Its main objective has been the design and realization of a deformation monitoring system based on optical fiber sensors and adapted to the specific needs of civil engineering. This system is named SOFO, the French acronym for “Surveillance d’Ouvrages par Fibres Optiques” or structural monitoring by optical fiber sensors.

1.2 Monitoring during birth, life and death of a structure

The monitoring of a new or existing structure can be approached either from the material or from the structural point of view. In the first case, monitoring will concentrate on the local properties of the materials used in the construction (e.g. concrete, steel, timber,...) and observe their behavior under load or aging. Short base-length strain sensors are the ideal transducers for this type of monitoring approach. If a very large number of these sensors are installed at different points in the structure, it is possible to extrapolate information about the behavior of the whole structure from these local measurements.

In the structural approach, the structure is observed from a geometrical point of view. By using long gage length deformation sensors with measurement bases of the order of one to a few meters, it is possible to gain information about the deformations of the structure as a whole and extrapolate on the global behavior of the construction materials. The structural monitoring approach will detect material degradation like cracking or flow only if they have a direct impact on form of the structure. This approach usually requires a reduced number of sensors when compared to the material monitoring approach.

The availability of reliable strain sensors like resistance strain gages or, more recently, fiber Bragg gratings have historically concentrated most research efforts in the direction of material monitoring rather than structural monitoring. This latter has usually been applied using external means like triangulation, dial gages and invar wires. Interferometric fiber optic sensors offer an interesting means of implementing structural monitoring with internal or embedded sensors.

In the next paragraphs we will give an overview of the different parameters that can be monitored during the whole life-span of a bridge using long gage sensors.

1.2.1 New structures, construction and testing

For new structures, the construction phase presents a unique opportunity to install sensors and gather data that will be useful for their whole life-span. For concrete structures it is even possible to embed the deformation sensors right inside the different structural parts. It is possible to follow the setting reaction of concrete in its

expansion and shortening phases and assess the conformity of the material to the prescribed standards. In the case of structures constructed in successive phases, the sensors can help to optimize the time between successive concrete pours, by evaluating the curing stage of the precedent sections. If the structure includes pre-stressed elements, the cable tensioning and the associated deformations can also be monitored and the forces can be adjusted to achieve the desired shape. For pre-fabricated elements, the sensors can be installed right at the factory and serve both as an additional quality test of each element separately and as a deformation sensor for the assembled structure.

Problems in bridge and building construction often come from the foundations. Long deformation sensor can also be used to monitor these critical parts. Many structures are particularly vulnerable to external agents like wind, small earthquakes and thermal loading before they are completed. A deformation sensor network can quantify any damage undergone by the structure before it reaches its final static configuration.

1.2.2 Testing

Many structures of some importance and bridges in particular are load-tested before being put in service. Typically the bridge is loaded with pre-defined patterns of sand-loaded trucks and the induced vertical displacements are compared with the ones calculated by the engineers. The measurements are normally performed with conventional techniques like triangulation and dial gages that are installed for this test only. Embedded and/or surface mounted deformation sensors can replace or supplement these measurements and help compare these extreme loading patterns to the ones that will be encountered by the structure once in service. The appearance of cracks or other degenerative phenomena during these tests can also be observed.

1.2.3 In-service monitoring

Once the structure is in-service, its monitoring becomes even more important, since the security of the user is involved. Ideally, all deformations produced by traffic, wind and thermal loading (sunshine, seasonal temperature variations,...) should be reversible. However, all construction materials tend to degrade with age. Concrete cracks and flows, steel is subject to fatigue and rust. A degradation of the building materials usually has an influence on the static behavior of the bridge and can be detected by the deformation sensors. These measurements can lead to early warnings and prediction of potential problems and help in the planning of the necessary maintenance interventions.

In a bridge, the sensor network can monitor the load patterns associated with traffic and record any abnormal (but unfortunately not unusual) overflow of the prescribed carrying capacity. In the case of excessive deformations resulting from partial structural deficiency or an excessive wind or traffic load, the monitoring system can automatically stop or slow the traffic on the bridge.

In seismic areas, one of the most challenging tasks in structural monitoring is the damage assessment after earthquakes, even of modest amplitude. Bridges can remain inaccessible for a long time before their safety is re-certified and they can be re-opened for use. An internal sensor network can obviously accelerate this process and discover damages undetectable by visual inspection.

1.2.4 Aging structures: residual life assessment

Deformation sensors can also be used to determine the residual carrying capacity of a bridge by observing its deformation under known mechanic or thermal solicitations. In this case it should be possible to install the sensors on the surface of the structure or inside ad-hoc grooves. Once in place, the monitoring system will follow the structure during the rest of its life.

1.2.5 Refurbishing

Many concrete bridges constructed 20 to 30 years ago already need refurbishment due to degenerative processes like carbonation, chemical aggressions (e.g. deicing salts), steel corrosion and use of poor construction materials. Typically, the damaged surface of concrete is removed and a new concrete or mortar shell is applied to the bridge. To ensure a durable repair it is necessary to guarantee an excellent cohesion between the old and the new concrete, otherwise the new layers will fall-off after a short time destroying all repairing efforts. Material testing is therefore fundamental and has to be performed both on concrete samples analyzed in the laboratory but also with in-situ measurements. In this case the shrinkage, cracking and plasticity of the new layer have to be measured by embedding sensors at different positions between the old concrete and the surface of the new one.

These sensors, once in place, can serve as a long-term monitoring system, without the need to mount sensors on the structure's surface. Embedded sensors are indeed better protected and less subject to external disturbances like direct sunshine, wind and rain.

1.2.6 Recycling or dismantling

Temporary and re-usable structures need efficient monitoring systems to assess possible damages before recycling.

When a structure has reached the end of its life-span and repairing becomes exceedingly costly or the structure does not respond the increased needs, dismantling becomes necessary. A deformation monitoring system helps to follow this phase that can be as delicate as the bridge construction.

1.2.7 Knowledge improvements

Besides the knowledge that can be gathered on a particular structure instrumented with a sensor network, more general information can be collected and used to refine the knowledge of the real behavior of structures and eventually improve design, construction and maintenance techniques. If similar structures are constructed in succession, the so-called design-by-testing approach can be used to continuously improve on the design and verify the consequences on the new structures. The measured deformations can be inserted into a feed-back loop to the finite elements programs used to calculate the structure.

Deformation sensors can also be used in the laboratory to experiment with new construction materials and techniques before application to real structures. Testing on reduced-scale models allows the evaluation of new or extreme solutions with reduced costs and risks.

1.2.8 Smart structures

Fiber optic sensors are often cited as the first building block of smart structures, i.e. structures able to respond to internal and external stimuli with appropriate actions using a series of actuators. The smart structure concept has usually been applied to relatively small structures, but could also find interesting application to civil structures. Possible examples include actively damped and adaptive structures. In the first case the structure (e.g. a bridge) would be capable of actively damping vibrations produced by traffic, wind or seismic loads, increasing the comfort of the user and slowing the fatigue damages. This application, however, requires huge forces and energies that are not easy to generate. Adaptive structures react much slower and only compensate to quasi-static loads or creep and flow effects. This could be achieved for example by changing the force in the post-tensioning cables according to the measured deformations.

1.3 Existing deformation monitoring systems

In the next paragraphs we analyze some of the most widely used deformation monitoring systems, their performances, advantages and limitations [2].

1.3.1 Visual inspection

The human eye and brain constitute a remarkable monitoring system. By visual inspection it is possible to recognize a great variety of problems and defects in many structures. Our eye is very sensitive to deviations from regular patterns and straight lines, which allows a fast recognition of structural problems that provoke a deformation. The effectiveness of this method is however related to the skill and experience of the observer and only macroscopic problems are identifiable. The observation is generally limited to the external surface of the structure¹, quantitative and objective measurements are difficult and the intervention of an operator tends to increase the monitoring costs. Visual inspection remains an invaluable tool to help evaluate a situation after a problem is detected by other measurement means.

1.3.2 Mechanical gages

Dial gages and other types of mechanical gages are still widely used in a variety of deformation monitoring tasks. They allow a very simple and precise measurement of small deformation with a sensitivity down to a few microns. These methods rely on a mechanical amplification of the small deformations. Typical examples include rockmeters (steel or invar bars fixed at the bottom of a bore-hole and measured at the top with a dial gage) and mechanical gages used to measure concrete shrinkage. The inverse pendulum used to monitor dam deflections is another example. The measurement basis can extend from a few millimeters up to 100 m and more. If special precaution is not taken, these systems tend to be quite temperature sensitive. This is not a problem for many underground applications where the temperature is fairly constant, but can constitute a major drawback in other situations. From the installation point of view, these methods usually require access to one or both ends of

¹ Except for endoscopic methods.

the region to be measured. They tend to be subject to corrosion problems and require an operator to carry out the measurements.

1.3.3 Electrical gages

Electrical gages are the natural extension of the mechanical ones. The two main categories include resistive foil strain gages which are attached directly to the surface of the structure (mostly on metals) and inductive sensors that replace dial gages for measuring larger deformations. Both methods are well established and can be brought to automatic and remote monitoring. The main drawbacks include their sensitivity to temperature and corrosion. Furthermore the electrical nature of the measurements makes them incompatible with environments where electromagnetic disturbances are present.

1.3.4 Electromechanical methods

A special case is constituted by vibrating string sensors, where a deformation over a distance of a few centimeters is transformed into a variation of the vibration frequency of a strained wire and detected by a pickup similar to the one found in an electric guitar. Its temperature sensitivity can be corrected by the integrated temperature sensor. Measurement bases are limited to a few decimeters.

1.3.5 Optical methods

Optical methods include triangulation and leveling. These methods are well suited to the measurement of relatively large deformations (of the order of the millimeter) even on very large structures. Some systems have been adapted to automatic and remote monitoring, but these methods usually require the presence of a specialized operator. The measurements are once again restricted to the structure's surface.

1.3.6 Fiber optic sensors

Optical fibers, initially developed for the telecommunication industry, are also interesting as deformation sensors. Practical applications of these methods are few but steadily promising. A more detailed description of the different methods available will be found in section 2 and the relative bibliography.

1.3.7 GPS

The satellite based GPS system is becoming increasingly interesting for structural monitoring. While it is generally possible to obtain cm grade precision from commercially available systems in differential configurations, recent experiments at ARL in Austin (Texas, USA) showed that mm-grade precision might be reached in the near future. With this kind of precision these system could become an interesting system for structural monitoring. It has however to be pointed out that the topology of Switzerland might prove an obstacle in the application of such techniques.

1.4 New monitoring needs

The new monitoring needs in civil engineering can be subdivided in two broad categories. On one hand, some outdated monitoring methods can be replaced by modern equipment that responds better to today's necessities. On the other hand,

new techniques can enable measurements in structures that traditionally lack of adequate monitoring systems.

1.4.1 Replacement or improvements of conventional instrumentation

Many monitoring systems presently in use do not fully respond to the expectations of their users. Some of the main complains raised by the specialists about conventional deformation sensors include:

1. Difficult to use, requiring specialized operators, slow and inefficient.
2. Difficult or impossible automatic and/or remote measurement.
3. Requiring calibration and re-calibration.
4. Sensitive to temperature, humidity and other environmental variations.
5. Sensitive to electromagnetic fields produced by thunderstorms, railway lines and power lines as well as vagabond currents.
6. Sensitive to corrosion.
7. Large size.
8. High operational costs, including base costs, per-measurement costs and maintenance costs.

Any new monitoring system has to solve at least a few of these problems in order to succeed as a replacement of existing equipment.

Some applications that could benefit from a new monitoring system responding to most of the above requirements include:

- **Geostructures.** Tunnels, underground works, foundations, piles, unstable rocks and soils all need deformation monitoring. This is generally carried out with electromechanical sensors like rockmeters (fixed and sliding) or by triangulation. In many cases, a system insensitive to humidity and corrosion and amenable to remote measurement would present a real interest.
- **Railway bridges and tunnels.** The presence of strong electromagnetic fields and vagabond currents discourages or makes extremely painful the in-situ monitoring of rail bridges and structures. A system using dielectric sensors is sometimes the only possible solution.
- **Dams.** Dams (especially shell dams) are heavily instrumented with many types of sensors and are regularly measured by triangulation. Some of the equipment could be replaced by more efficient ones allowing better accuracy as well as automatic and remote surveillance. Currents generated by thunderstorms are also a concern because of the large size of the dam and the absence of reinforcing bars in concrete. Conducting instruments like rockmeters tend to capture and conduct these currents that can damage the monitoring equipment.
- **Laboratory experiments.** Besides in-situ measurements, laboratory experiments on reduced-scale models constitute an interesting test-bed for any new equipment. These models tend to be heavily instrumented and an increased accuracy as well as a reduced sensor size are often welcome by the researchers.

1.4.2 Enabling instrumentation

Some structures and materials are not or insufficiently monitored because no adequate measurement system is available. This creates, on one hand, a fertile ground for new instruments but, on the other hand, makes it sometimes difficult to introduce new

techniques when no measurement culture exists. Bringing together and establishing communication between the specialists needing and offering a monitoring system is not always a trivial task!

Some fields that could benefit from a new deformation monitoring system (e.g. based on optical fiber sensors) include:

- **Concrete monitoring during the cure.** This requires a system insensitive to temperature variations and capable to measure small deformations inside the concrete itself (the surface is not accessible before the framework is removed). Concrete monitoring is useful to supplement laboratory tests and help establish the quality of the deployed materials and their compatibility with their function in the structure. This is especially true in the case of refurbishing and mixed structures, where layers of different materials (steel and concrete, old and new concrete,...) have to adhere and interact. In structures built in successive sections it is possible to optimize the process by characterizing the progression of the cure. Sensors can also be used for quality control in prefabrication.
- **Monitoring of concrete structures.** Being concrete an in-homogeneous material, local and surface measurements, as those performed with electrical strain gages, are not well adapted or require an excessive number of sensors. A more distributed measurement over bases of the order of the meter can give more general information about the material and structure's state. Internal sensors, embedded directly into concrete during construction allow a more representative measurement than those installed on the surface.
- **Geometrical monitoring of structures.** Many structures such as bridges, trusses, towers, walls and other can be monitored from a geometrical point of view, i.e. by measuring the distance variations between a network of fixed points on structure. This approach concentrates on the global mechanical properties of the structure rather than the local behavior of the constituent materials.
- **Monitoring with large temperature variations.** Structures like tanks, boilers, cryogenic reservoirs and space trusses can undergo large and sudden temperature variations. The measurement of the associated deformations is generally a difficult task because of the temperature sensitivity of most conventional sensors.
- **Measurements over curved shapes.** Most traditional sensors do not allow the measurement of curved surfaces like those of a pipe or a tank.
- **Measurement of other quantities** that can be converted into a deformation, like force, temperature, humidity, pH, rust,...
- **Laboratory experiments.** New types of measurements (like deformations during concrete setting or inside the structure) allow experiments that would be impossible without them. The knowledge of the real behavior of structures has always progressed in parallel with the development of sensors and testing other equipment.

1.5 Conclusions

The previous paragraphs show that a real need for new deformation monitoring systems exists in many fields of civil engineering, both in the industry as in the research community. The SOFO system that constitutes the result of this doctoral work and

will be presented in the next sections, responds to many of requirements expressed above for replacing and complementing the existing monitoring means.

Of course, the development of this system has been initially driven more by scientific curiosity than from a real end-user demand. Once that the first prototypes of SOFO started to work outside the laboratory, a large interest was nevertheless encountered and the research project expanded more and more in the direction of applications. The interested professionals have helped to define the real strengths and weaknesses of the system and the most promising application fields. In the course of this work we had the occasion to participate in a large palette of projects including new and refurbished bridges (road, highway and railway), tunnels, geostructures and dams. In some cases it was possible to compare the results obtained with our system with the ones delivered by more established measurement method. These comparisons have helped to refine our system and to convince the end-users about its performances.

The SOFO system is now commercialized by SMARTEC², a spin-off company born from the cooperation between the Swiss Federal Institute of Technology, the civil engineering company Passera + Pedretti², the institute of material mechanics IMM² and the fiber optic components manufacturer DIAMOND³. These precious industrial partners have paralleled the SOFO project and helped focusing on the practical aspects associated with in-situ applications and industrial production.

1.6 Outline

- **Section 2** introduces the concept of *Smart Sensing*, a fascinating and new domain aiming to the optimal combination of sensors and information processing tools to achieve a better knowledge and representation of the real behavior of structures.
- **Section 3** shows the requirements for monitoring deformations in civil engineering structures.
- **Section 4** explains how optical fibers can be used as sensors of strain, deformation and temperature and how the sensors interact with the host structure.
- **Section 5** deals with the principles of low-coherence interferometry, the optical technique on which the SOFO system relies.
- **Section 6** presents the design process and issues behind the development of the basic SOFO system. This system, adapted to the conditions of civil engineering, allows the measurement of single sensors with high accuracy, excellent long-term stability and insensitivity to electromagnetic fields, corrosion and temperature variations.
- **Section 7** shows a variety of multiplexing techniques that can be used to measure a large number of sensors with a single reading unit. The sensors can be arranged in chains and in star configurations.
- **Section 8** gives an overview of the applications that were realized using the SOFO system.
- Finally, **section 9** presents the general conclusions, summarizes the main achievements of this work and gives an outlook to the future of the SOFO project.

² Grancia, Switzerland

³ Losone, Switzerland

The bibliography can be found at the end of each chapter. A general bibliography, a list of the publications realized during this work, the acknowledgments and a biography of the author appear at the end of the dissertation.

1.7 Bibliography

- [1] K. Danker, B. G. Rabbat, “Why America’s Bridges are crumbling”, Scientific American, March 1993, 66-70
- [2] I. F. Markey, “Enseignements tirés d’observations des déformations de ponts en béton et d’analyses non linéaires”, Thèse EPFL n° 1194, 1993

2. Fiber Optic Smart Sensing

This section gives a general overview on Fiber Optic Smart Sensing. We will first introduce the most important concepts behind this emerging field of optical metrology and then compare different sensing techniques that are attracting increasing research interest. This will help to situate this work in a more general framework.

Parts of this section have appeared as a chapter in “Optical Measurement Techniques and Applications”, Artech House, edited by Pramod K. Rastogi.

2.1 Introduction

Smart sensing [1,2,3,4] is a recent and fast growing field of optical metrology. Although, as we will see, the concepts behind it are not necessarily bound to optical methods, smart sensing is usually implemented in conjunction with fiber optic sensors. Smart sensing is also closely linked to structural monitoring and is normally considered to be the first building block of a smart structure, the others being processing and actuation. This field is so young that the smart structure community itself has yet to come up with a generally accepted definition of what smart sensing really is. Since most definitions rely, at least partially, on biological parallels, we will try to define smart sensing through a comparison with the properties of the human body.

Imagine you close your eyes and then move one of your arms. Even if you do not see it directly, you know where your arm is and what shape it has at any particular moment. This is usually known as the self-awareness of our body. Now let another person put a weight in your hand. In some cases the shape of your arm does not change after adding this extra load, for example if the arm is extended along your body. Nevertheless you are aware of the increased load and if this load is increased further you eventually start to feel pain. If at this point the load is removed, the pain disappears. If the load was excessive and extended in time, the pain will however remain to indicate permanent damage to the arm. Thanks to the amazing self-repairing capability of our body, this pain will dissipate after some time meaning that the initial functionality of the arm has been restored. This example shows that our nervous system can perform different monitoring activities on our body, including shape and position analysis, load analysis, excessive load alarms and damage detection. All these features are produced by a combination of sensors (nerves), information carriers (the spinal cord) and processing units (the lower brain and the brain cortex). Moving up in this processing chain, the information from different sensors is combined, filtered, analyzed and delivered to the person's consciousness only when needed or transmitted to other subconscious processes. If the processing unit decides that an action is required, it will send appropriate orders to the muscles. The result of this actions will be further analyzed by the sensing chain realizing a closed loop feedback system.

Now imagine an artificial structure like a bridge, an airplane wing or a space station, having the same capabilities as our body. This 'sensitive structure' could know its shape and position in space, could analyze its stress state, deliver alarms if some structural parts are excessively loaded and record a history of past load patterns and intensities. These measurements could extend from the fabrication and assembly of the structure, through its whole life span and even to its dismantling, disposal or recycling. Smart sensing can be seen as the combination of technologies (sensors, information carriers, information processors, and interfaces) allowing the realization of such a 'sensitive structure'. Combining these sensing capabilities with an ad-hoc array of actuators, it would be possible to create a structure with self-repairing, shape control or vibration damping capabilities: a smart structure.

Structures with at least some of these capabilities already exist (think of a modern airplane, a dam, an actively damped skyscraper or a power plant), but new and promising applications are only appearing at the horizon. This chapter will try to give an overview on new applications of smart sensing and on the enabling technologies that will allow the transfer of the smart sensing concepts from the research laboratories to mainstream applications. Emphasis will be given to civil engineering structural monitoring. Civil structures are indeed attracting rising interest in the smart structures community and the smart sensing concept has been successfully demonstrated in

a number of in-field applications. Furthermore, since we see bridges, tunnels and dams in our everyday lives, it will be easy to explain the smart sensing concepts with examples accessible to all readers.

2.2 Fiber optic smart sensing

The sensors used to monitor the different parameters necessary to quantify the state of a given structure could be of any type. However, fiber optic sensors (FOS) are the natural choice for this kind of application [5,6,7,8,9]. The most important advantage of FOS resides in their passive nature. All electronics can be confined in the reading unit, while the sensors that are installed in the structure are electrically passive elements. The dielectric nature of optical fibers [10] ensures a high degree of immunity to external disturbances like electromagnetic fields and parasite currents. An equivalent electromechanical sensor would require a bulky shielding to achieve the same performances and this would increase its size and cost. FOS are very small and an array of many sensors can be multiplexed on the same fiber line thanks to the enormous bandwidth of optical fibers. Furthermore silica fibers are chemically inactive and can therefore be embedded (with an appropriate coating) in most materials including composites [11,12], concrete [13], mortars [14] and timber aggregates, without altering significantly their mechanical properties. Finally, FOS are mostly based on standard telecommunication and photonics components with continuously falling prices, thanks to the developments driven by the respective markets. All these characteristics lead to potentially cheap, small and reliable sensor arrays that can be imbedded in any structure of some importance. It is interesting to point out that the optical fibers used in a smart sensing architecture, are at the same time the sensors and the information carriers. This simplifies greatly the realization of a sensor array.

For all these reasons, FOS are the first choice of sensing technology for the realization of a smart sensing system. We will therefore limit the discussion in this chapter to FOS arrays. Other technologies like electrical and electromechanical sensors (of force, position, angle, acceleration, temperature,...) or special systems like GPS (Global Positioning System) can be used in conjunction with FOS to deliver additional information on a structure and its environment.

2.3 Smart sensing subsystems

Not unlike its biological counterparts, any smart sensing system can be subdivided into five main subsystems: the sensors, the information carriers, the reading unit, the processing unit and the external interface.

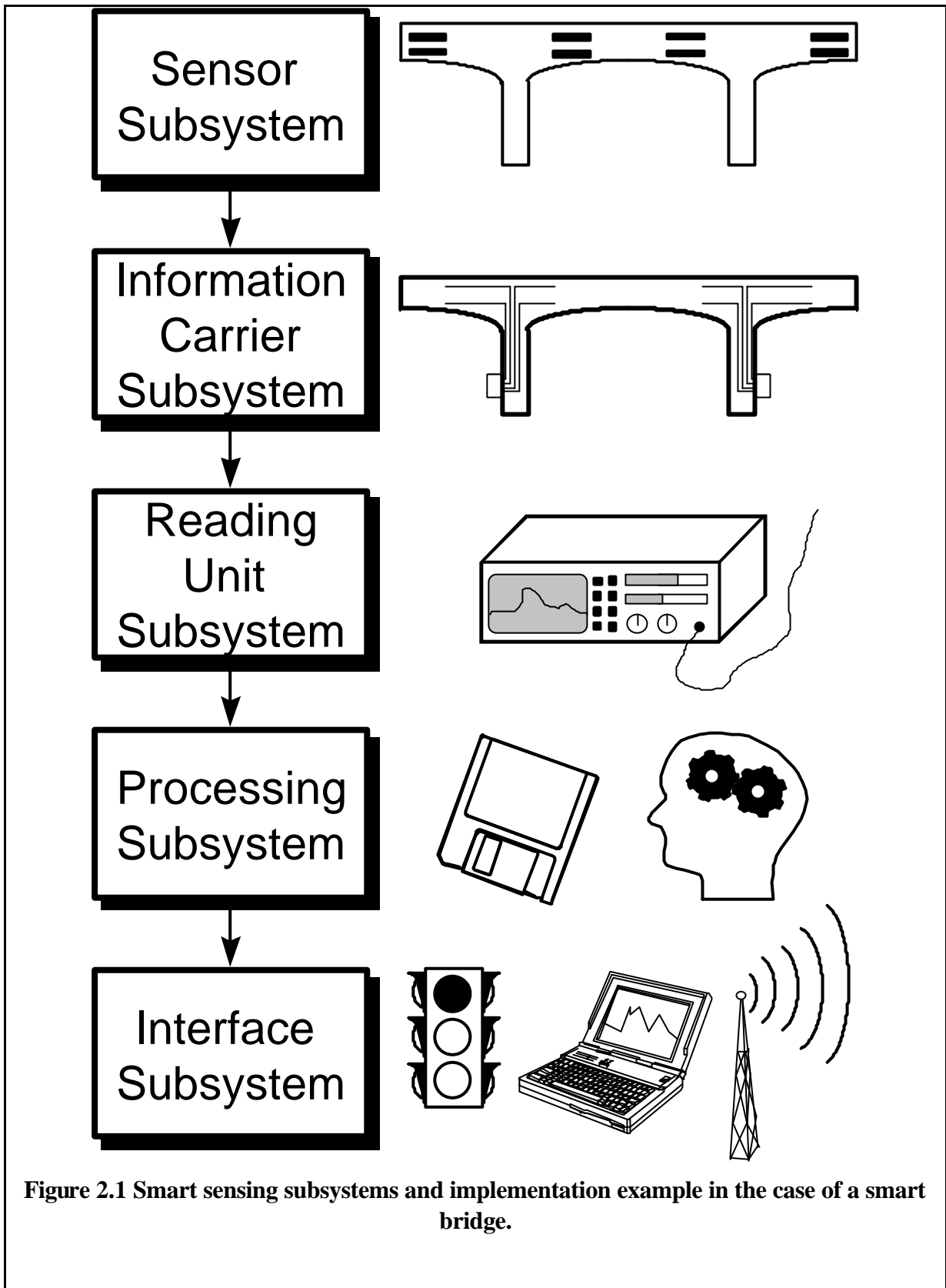
- The sensor subsystem includes the FOS itself and all additional parts that are required to install it into or onto the host structure. This includes the fiber coatings, additional protections, pipes, attachment points, glues and so on. The function of the sensor subsystem is to transform the quantity to be measured (strain, position, temperature, chemical composition,...) into a variation of the radiation carried by the optical fiber (transmitted or reflected intensity, wavelength, phase or polarization). The sensor should be insensitive to all environmental changes other than the one it is supposed to measure. The sensor subsystem is the one that most depends on the particular application and has to be fine-tuned to each new host material or structure type.
- The information carrier subsystem links the sensors to the reading unit. The optical link is usually a fiber that does not alter the information encoded by the sensor. These fibers have

to be protected from external agents that could affect their transmission properties or damage them mechanically. Other important aspects of this subsystem are the ingress-egress points, since the reading unit is usually separated from the structural elements containing the sensors. These points can often constitute a delicate link in the information chain since the signals from many sensors travel through a single location and a failure can lead to a large information loss. The design of ingress and egress points is often a major challenge especially in the case of composite materials or for civil structures that are built in sections (bridges, tunnels and so on). The multiplexing architecture of the sensor array is also implemented at this level. The signals produced by different sensors have to be combined into a reduced number of access points and fiber links. This reduces the complexity of the system and takes advantage of the large bandwidth of optical fibers.

- The reading unit subsystem demultiplexes the signals from the sensors and transforms them into values that are representative of the measured quantities at the sensor locations. These values are usually expressed in digital form and transmitted to the processing subsystem for further analysis. The reading unit is often an optoelectronic device of a complexity, size and cost far superior than that of the sensors. However, one reading unit can address a multitude of sensors and be located outside the monitored structure. This subsystem is in many cases less failure-sensitive than the sensors and the optical links since it is possible to replace a faulty unit with only a small information loss. This is obviously not the case when the smart sensing system has an active structural function.
- The processing subsystem combines the readings from all sensors installed in the structure, measuring either the same quantity at different points or monitoring different parameters. It then extracts the relevant information that characterizes the structure's state and behavior. This subsystem is a key element for the successful application of the smart sensing concept, since a single structure could be instrumented with hundreds of sensors addressed many times each second. It is therefore impossible to analyze this huge data flow manually or even semi-automatically. Important information about an anomaly or a failure could disappear in the flood of data. In some cases, the relevant structural parameters can be obtained only by combining the values from different sensors.
- The interface subsystem delivers the parameters extracted by the processing unit to other external systems. In the case of a smart structure this system is an array of actuators acting back on the structure to modify its shape or stress state. In this case the smart system would work in a closed feedback loop. In most other cases the interface would simply inform about the present state of the structure. If an anomaly is detected, all actions required to ensure safety and reliability would be performed manually. It is also possible for the interface unit to deliver alarms or, for example, turn a traffic light red to stop the traffic on a failing bridge. When a problem is detected, this subsystem can deliver more information according to the type and importance of the anomalies detected in the structure.

Figure 2.1 summarizes the different subsystems found in a smart sensing system and gives an example of how these elements would be implemented in the case of a smart bridge.

Only an adequate combination of all subsystems leads to a successfully working smart sensing system. In the next paragraphs we will analyze some of the aspects that have to be considered in the design process as well as the enabling technologies that can be combined into a smart sensing system.



2.4 Sensor selection

The first step in the design process of a smart sensing structure resides in the analysis of the parameters that need to be monitored, in the choice of the best suited sensor technology (or

technologies) and in evaluation of the number and position of measurement points required. These issues are best discussed with the structural engineers who design the structure. Even if every structure is a case by itself, some key decisions are common to most applications and are summarized in the next paragraphs. We will concentrate our discussion to strain and displacement sensors. These are often the most important parameters to be monitored in a structure and a great variety of sensors have been designed for this purpose requiring particular attention in their choice. Other types of sensors include temperature, pressure and chemical sensors.

2.4.1 Strain, deformation and displacement measurements

Strain, deformation and displacement measurements constitute the most interesting parameters to be monitored in the vast majority of structures. There is however often some confusion among these three types of measurements and this confusion can lead to the choice of an inadequate sensor technology.

Strain refers to the internal compressive, tensile and shear state of a material and gives a measurement of the loading of the structure at a given point. Unfortunately there is no such thing as a real strain sensor (except for photoelasticity that is suited only for the study of some specific transparent materials). All other so-called strain sensors [15] are actually deformation sensors with a very short measurement base. If it can be assumed that the strain state \mathbf{e} of the structure is almost constant along this short measurement path L , the measured deformation ΔL will be given by:

$$\Delta L = \mathbf{e} L . \quad (9.1)$$

By measuring ΔL , it is therefore possible to obtain an indirect measurement of \mathbf{e} .

The sensor is usually made of a material different from the one of the host structure. Therefore, it is important to ensure that the strain field is entirely transferred to the sensor and that the sensor does not alter this strain field in a significant way [16,17,18]. This is generally achieved using a sensor that has a rigidity (given by the product of the elastic modulus and the sensor section) far inferior to the one of the surrounding material. Furthermore, it does not make sense to measure strain over a length of the same order of magnitude or even shorter than the transverse dimension of the sensor. On this scale, the strain field will be significantly altered by the presence of the sensor.

In the case of inhomogeneous materials like concrete, timber or composites, the microscopic strain field will vary in an important way if observed on a scale comparable to the dimension of the material components. It would be much more regular if integrated over a length by at least an order of magnitude larger than the granularity of the material. It is therefore necessary to choose a sufficiently large sensor length, if the measurement is intended to obtain information about the behavior of the material as a whole. A sensor embedded in a concrete mix with a granulometry up to 20 mm should have a measurement base of at least 100 mm in order to obtain macroscopic information about the concrete behavior (see Figure 2.2). On the other hand it could be interesting in some special cases to study the microscopic strain field of dimensions smaller than the material inhomogeneities [19]. This type of measurement is however delicate because of the interaction between the sensor and the host material.

From now on we will define strain sensing as a deformation measurement over a base length larger than the characteristic size of the components of the host material but short enough to consider the macroscopic strain field constant. This type of measurement is best suited to monitor the local behavior of the materials rather than the global behavior of the structure. Strain sensors will therefore be placed at critical points of the structure where high strains are expected that could approach or surpass the material resistance.

Deformation refers to an internal shape variation of a structure. A deformation is usually accompanied by a change of the strain field. A deformation measurement will however concentrate on the geometrical changes of the structure and not on the variation of its loading state. The measurement base could extend for many meters or even hundreds of meters for particular applications (e.g. geosstructural monitoring or long suspended bridges). When the macroscopic strain field is not constant inside the structure, the deformation sensor will integrate the strain over its measurement base. Deformation measurements are useful in the case of structures that have to show dimensional stability. In this type of structures the load state is usually far lower than the material failure limit and local strain measurements are therefore uninteresting. Good examples of this type of structure are concrete bridges that can sink at mid-span because of flow effects. This causes the well-known roller coaster effect that reduces the comfort of the vehicles passing on the bridge but has normally no consequence on its structural safety and could even reduce the strain in the girders. Another example is given by a base

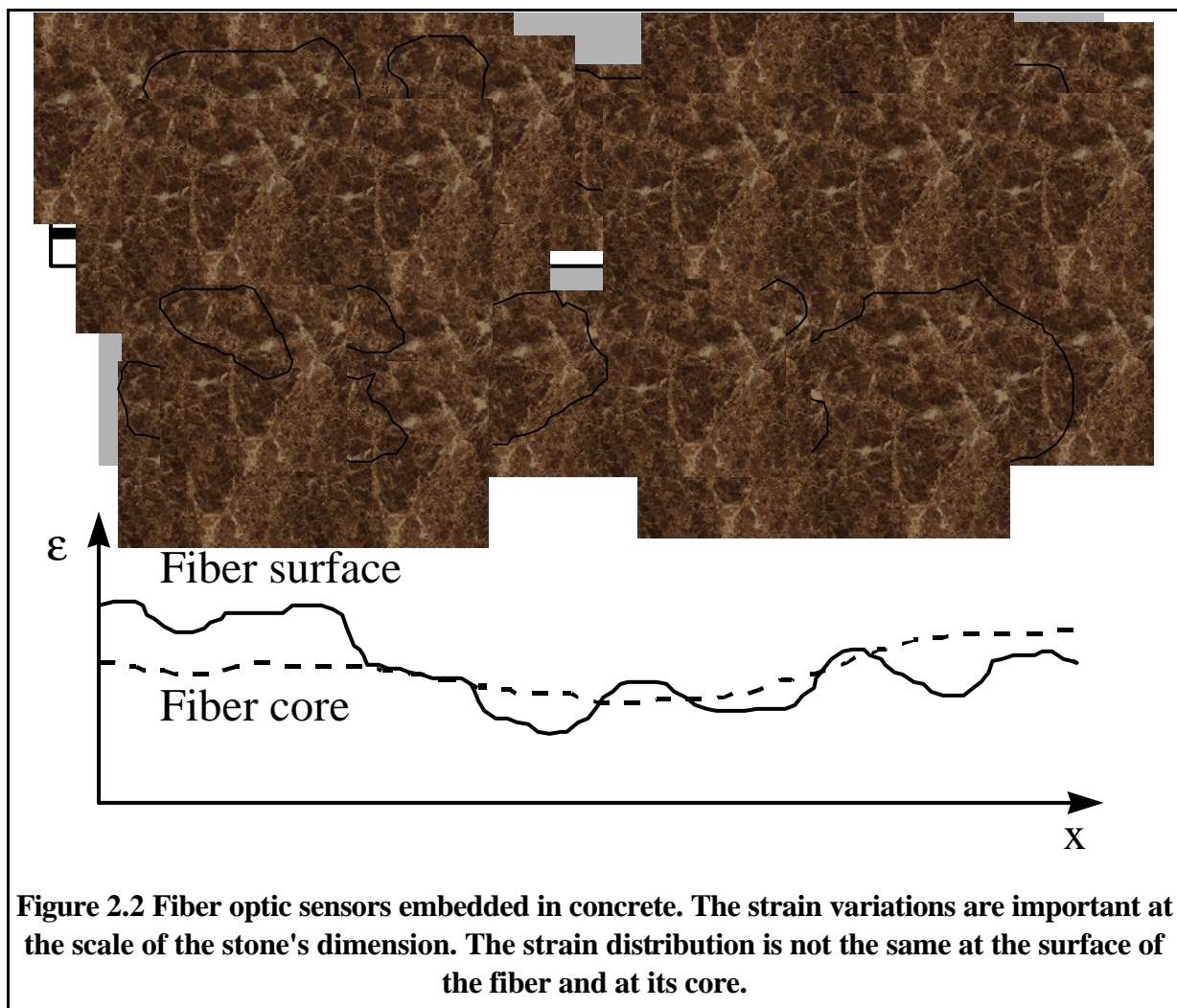


Figure 2.2 Fiber optic sensors embedded in concrete. The strain variations are important at the scale of the stone's dimension. The strain distribution is not the same at the surface of the fiber and at its core.

supporting precision equipment, where dimensional variations lead to misalignments of the supported components.

Finally, displacement refers to a movement between different parts of a structure. This can occur without a change of the strains in the structure. A displacement sensor monitors the distance variations between two given points. Examples of displacement measurements are the monitoring of rocks sliding one respect to another, of the relative position of a piston in its cylinder or the displacement of a bridge with respect to the ground. Most sensors used for deformation monitoring can also be used for displacement measurements.

Strain, deformation and displacement sensors (sometimes based on the same technology) can be used together in complex structures to achieve a complete understanding of the global and local behavior. The choice of the sensor technology (or technologies) usually leads to a first estimation of the number and of the emplacement of the sensors needed to monitor a given structure.

2.4.2 Absolute, relative and incremental measurements

An absolute strain measurement gives a value relative to the unstrained state of the materials and is therefore useful to establish the loading state of the structure. Most sensors will however give a value that is relative to the one measured at the time of the installation of the sensor on the host material. If the installation is performed on an already loaded structure (even only under its own weight), the reading will just give an indication on the variation of the structure's load (or of creep and flow effects) and it will become difficult to establish if the material is approaching its failure limit. To obtain an absolute strain measurement it is therefore important to install the sensor on (or in) an unstrained material or on a material in a predictable strain state.

A deformation or displacement measurement is by definition relative to a defined initial state. It is not interesting to measure the length of a structure with micrometer precision while it could be important to follow its deformations with this resolution. Fiber optic sensor technologies are however available in the rare cases where a precise and absolute length measurement is required.

In both cases of relative strain or displacement measurements, the sensor could give incremental or non-incremental readings. In the case of incremental reading each variation in the strain or in the deformation by a given value will produce a particular signal. These signals have to be counted in order to reconstruct the total strain variation or displacement undergone by the structure between successive times. This requires the reading unit to be continuously connected to the sensor in order not to lose any of these signals. Non-incremental sensors will give readings that can be directly compared with all precedent and successive values, without the need of a continuous monitoring. Measuring the distance you have traveled by counting the telegraph poles along the highway is an example of incremental measurement, while watching the mileage signposts is a non-incremental measurement. Interferometric fiber optic sensors are a typical example of incremental sensors, while Bragg grating sensors are non-incremental. Incremental sensors tend to be simpler and therefore cheaper than non-incremental ones. For long-term measurements, non-incremental sensors offer however a higher reliability since a short failure of a component does not lead to data losses. Furthermore, a single non-incremental reading unit can be used to monitor a large number of sensors and even structures.

2.4.3 Sensitivity, precision and dynamic range

Once the type of measurement required to monitor a given structure has been established, it is necessary to quantify the values that will be measured. The performances of a sensing system are measured in terms of sensitivity, precision and dynamic range. The sensitivity of a sensing system (sensor and reading unit) is defined as the minimal variation of the measured quantity that gives a just measurable variation in the sensor response. The sensitivity therefore limits the measurement of small values. The precision is defined as the root mean square (RMS) difference between the real and the measured values. It is usually expressed as a fraction of the measured value. The precision can be worse than the sensitivity in the case of sensors with non-linear response and limits the measurement quality of values much larger than the sensitivity. The dynamic range gives an indication of the maximal variations that can be recorded by a sensing system.

Consider a stick supposed to be one meter long, but really only 99 cm long, and subdivided into thousand one millimeter marks. If we use this stick to measure a length, the sensitivity will be of about one millimeter, the precision of 1% and the dynamic range of one meter.

2.4.4 Dynamic, short-term and long-term measurements

The performances analyzed in the previous paragraph are not independent of time. In some cases a measurement requires a certain time to be completed or the performance of the sensing system is reduced if the measurement time is decreased. Other sensors can not guarantee a constant precision if the measurements are too much spaced in time. It is therefore useful to distinguish three broad categories of time resolved measurements.

Dynamic measurements require many readings each second. They are usually related to vibration measurements at or out of resonance condition. In general, the smaller the structure the higher the measurement frequency will be. Typical frequencies for civil structure are between 0.1 and 30 Hz, while metallic and composite structures can require frequencies extending in the kilohertz range. Drift is in most cases not a concern and, since the strain variations are often appreciable, the sensitivity does not need to be pushed to its limits.

Short-term measurements can extend from a couple of seconds to one week. In this case, the drift of the reading unit can become appreciable, but other parameters like aging of the sensors and reproducibility of the connection can be neglected. This is the time domain where most sensors give their best performances. Typical short-term measurements include quasi-static loading tests.

Long-term measurements require highly stable sensor techniques to guarantee a sufficient precision for readings that can be spaced by month or years and last up to a century. In this case the aging of components such as fibers, sources and mechanical parts can not be neglected. A failure of one of the subsystems of the smart sensing setup can not be ruled out. Therefore redundancy, modular and evolutive design as well as self testing capabilities are important issues to be addressed for this time domain. Typical examples include the monitoring of aging civil structures and the monitoring of slow phenomena like landslides and creep in some composite materials.

2.4.5 Independent measurement of strain and temperature

As a general rule any sensor is also a temperature sensor. If temperature variations are expected during the measurements, it is important to consider their influence on the precision. Two

approaches are possible in order to reduce the temperature influence: either choose a sensor that has intrinsically a low temperature dependence or measure the temperature at the same time. The simultaneous measurement of strain and temperature usually consists in a sensor responding only to temperature variations and a second one sensitive to both strain and temperature in a linear way [13]. The data from the temperature sensor is then used to correct the strain or displacement values. The two sensors can be based on different technologies but are often (and more elegantly) based on the same type of sensor. In this case two identical sensors are installed side by side. The first, usually called the measurement sensor is installed in mechanical contact with the structure, the other, called the reference sensor, is mechanically uncoupled from but in thermal contact with the structure. Other setups have been proposed where the temperature and strain measurements are performed on both sensors but with different linear response coefficients. It is even possible to use only one fiber to measure both quantities. Examples include the simultaneous measurement of phase and dispersion in the same fiber [20,21], the phase of different modes in a multimode or multiple-cores fiber [22], or the phase at two different wavelengths [23]. In general the relation between the two measured quantities A and B , the strain \mathbf{e} and the temperature T will be written in the form:

$$\begin{pmatrix} A \\ B \end{pmatrix} = \begin{bmatrix} a & b \\ c & d \end{bmatrix} \begin{pmatrix} \mathbf{e} \\ T \end{pmatrix} \quad (9.2)$$

In order to solve the linear system for \mathbf{e} and T , the matrix should have a non zero determinant. Furthermore it is desirable that a small error in the measurement of A and B should not result in a large variation of \mathbf{e} and T (well-conditioned system).

In some cases the temperature of the structure is not constant but is nevertheless well determined (for example an element tested in a temperature controlled cabinet). In this case it is possible to correct the strain reading using the known temperature value.

It is important to note that, in general, a temperature insensitive sensor will not give a zero reading when the temperature changes. A temperature change will result in a shape variation of the structure and possibly in a change of its stress state that should be detected by the sensors. A temperature variation can lead to a deformation without any change in the structure stress state. A so-called stress sensor should therefore return a zero reading even if a displacement is observed over its short measurement base. This is usually not the case, since the sensor has a thermal expansion coefficient different from the one of the host structure. It will then be impossible to tell if the measured deformation is the result of a strain or of a temperature variation (or a combination of the two). To obtain a 'real' strain measurement in a structure subject to temperature variations it is therefore always necessary to measure temperature and strain simultaneously.

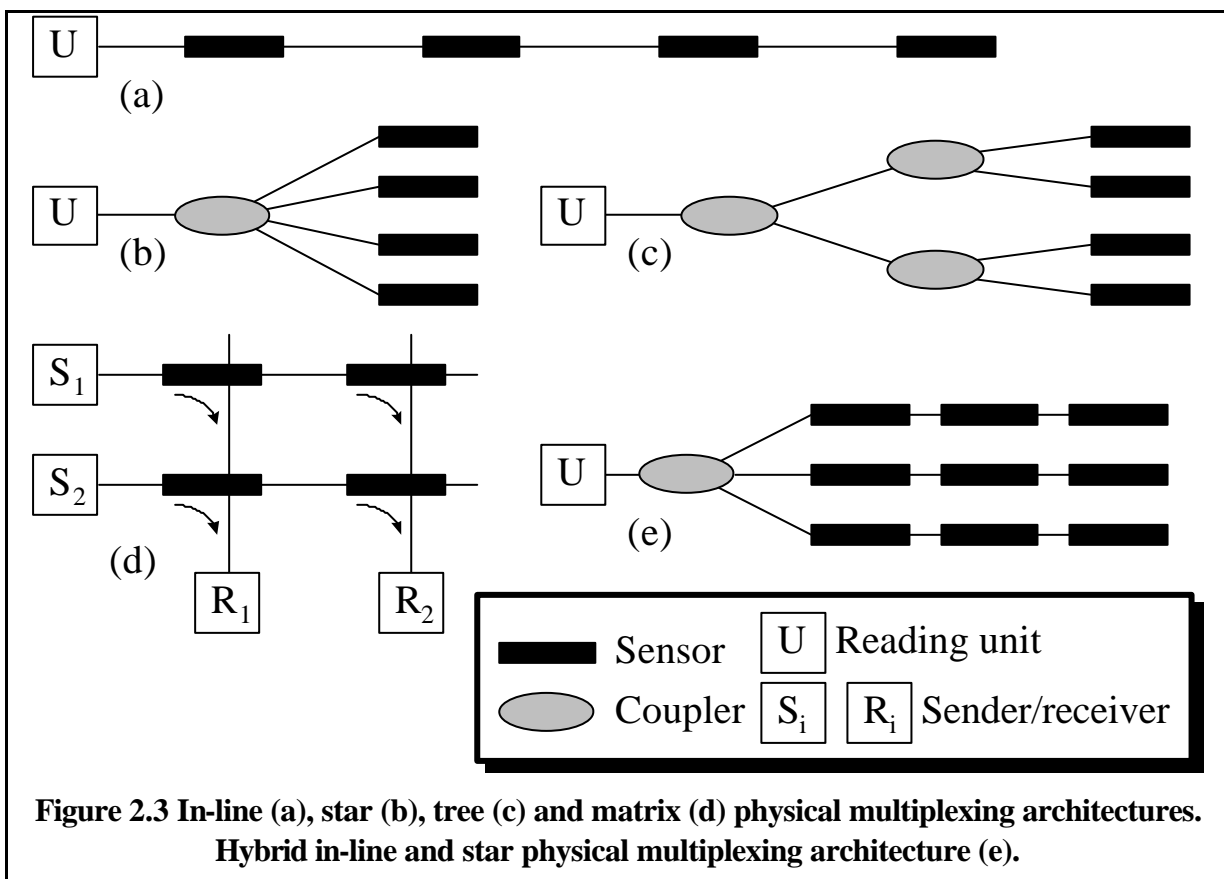
2.4.6 Multiplexing topologies and redundancy

When the type of measurement is decided (strain deformation and/or displacement) it is generally possible to obtain a first estimation of the number of sensors that will be needed to instrument the structure and of their emplacement. At this point it is necessary to design a multiplexing topology to read these sensors. The number of access points where the termination of the information carrier subsystem meets the reading units often has to be limited. Depending on the sensor technology it will be possible to read a number of sensors with one and the same reading unit. In some cases it is even possible to read many sensors simultaneously.

A multiplexing architecture [5,7,8,24,25] has to be analyzed at two different and interdependent levels. The physical architecture deals with the disposition of the sensor in the structure and with the arrangement of the connections between the sensors and the reading unit (or units). The signal architecture deals with the optical and electronic setup used to address the sensors independently. The signal architecture also determines the timing of the measurements.

At the physical level, all architectures can be broadly subdivided into four categories: in-line, star, tree and matrix topologies (see Figure 2.3). In the in-line topology, the sensors are installed along a single line. In some cases the connections between the nodes of this chain will be passive (e.g. in a strain sensor array), while in other cases (e.g. in a displacement sensor array) the connections themselves will act as sensors. Both these types of sensor chains are known as quasi-distributed sensors. In other cases the fiber line is sensitive along its whole length and the measurements can be obtained continuously with a given spatial resolution. This type of sensor is referred to as a distributed sensor. These configurations are particularly vulnerable, since the failure of a single connection can isolate a large section of the sensor chain from the reading unit. For some types of sensor it is however possible to address the sensor chain from both ends, which brings an important security factor in the case of failures. Even if the sensors are arranged sequentially along the same fiber line, it is always possible to install this line in a serpentine to cover an area or even a volume in the structure.

In the case of a star topology, the connections from each sensor converge at a single point where they are either combined into a single cable or switched sequentially. Most sensor technologies can be easily brought to a star topology. However, this type of setup usually requires a large number of connections and signal lines, which is not without consequences on the price and complexity of the system. The star architecture is on the other hand very resistant to failures that,



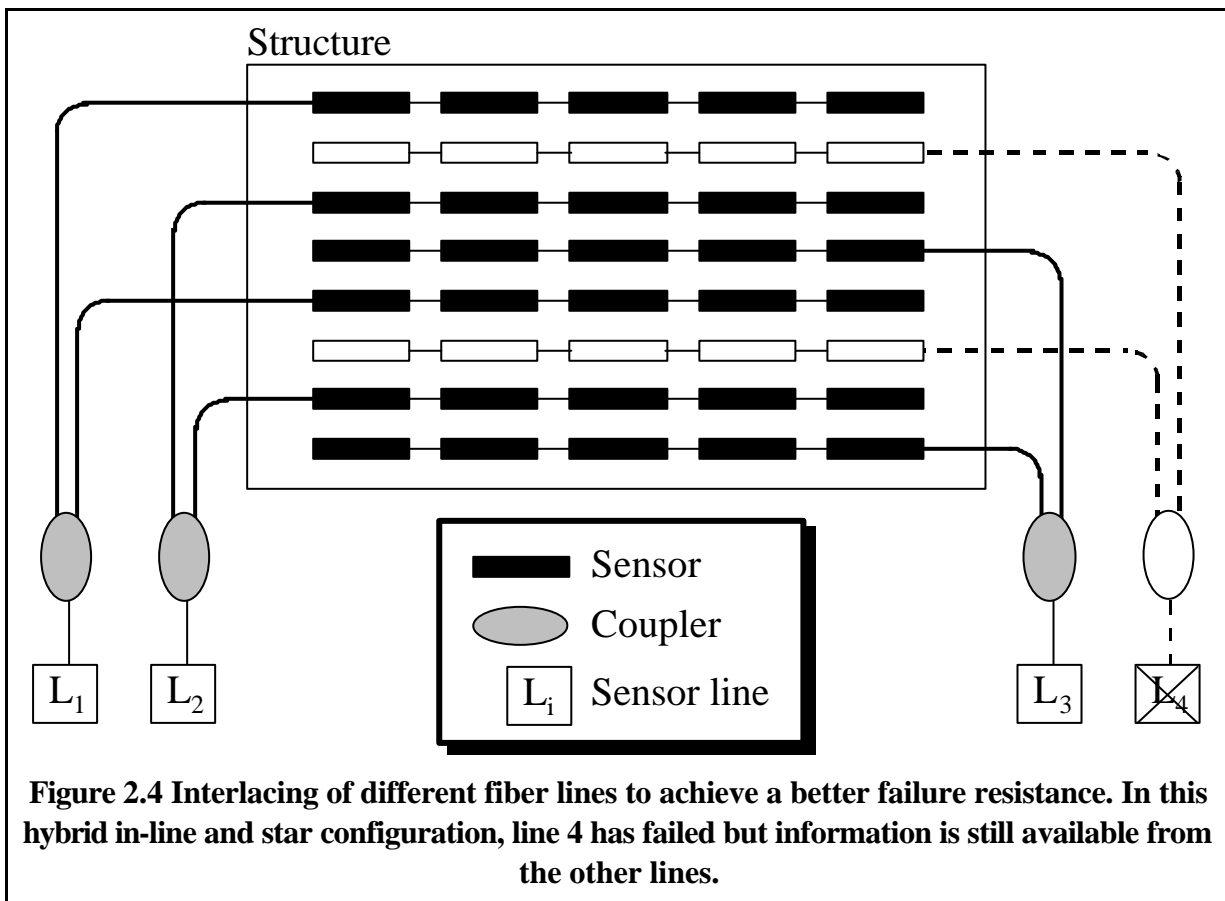
in most cases, isolate only one of the sensors.

In the tree configuration, the sensors are arranged in a branched structure that combines more and more signals from the different fibers as it approaches the reading unit. This topology is very flexible and can be easily adapted to different structures. Its resistance to failure falls between the in-line and the star configurations. A failure near the root will have more important consequences than one near the sensors.

Finally, a matrix configuration configures the sensors at the crossings of a two-dimensional array where the 'horizontal' lines correspond to the lead-in fibers while the 'vertical' lines are used as lead-outs. The matrix configuration can lead to a high density of sensors and, because of the high number of ingress and egress lines, a good fault tolerance can be achieved.

Hybrid solutions combine different basic topologies to address an even higher number of sensors. A typical hybrid solution includes both the in-line and the star configuration. In these cases the ends of the sensor chains are combined or switched at a single location (see Figure 2.3 (e)).

When designing the physical structure of a smart sensing system, it is important to consider the possibility of failure of some of the components. If the information of a given sensor is fundamental, the sensor should be doubled by another sensor that is not supposed to fail at the same time (e.g. it should not be on the same sensor chain). In most cases, the failure of a single sensor will not affect dramatically the performance of the monitoring system, since the relevant parameters about the structural behavior are obtained by a combination of the values from a number of sensors. However if a large number of sensors fail, the quality and precision of the results will drop significantly. If a certain amount of the installed sensors are expected to fail, the sensor density should be increased so that sufficient information results even after the worst case



failure. Failure of a single element leading to the loss of all sensors in a certain volume of the structure should also be avoided. This can be achieved by interlacing the fiber lines as shown in Figure 2.4. Finally, special care must be taken to protect the most sensitive parts of the sensor network, for example the concentration point in a star configuration or the ends of a sensor line. In some architectures it is even possible that the signals from all sensors transit in a single fiber at some points. If this dangerous concentration can not be avoided, this section should be carefully protected and made easily replaceable.

The signal architecture deals with the optical and electrical addressing of the individual sensors. The main types of signal multiplexing fall into the following categories: time division multiplexing (TDM), wavelength division multiplexing (WDM), frequency division multiplexing (FDM), coherence domain multiplexing (CDM) and polarization division multiplexing (PDM). The TDM technique is especially adapted to the in-line configurations where the signals need more time to reach the analyzer from the sensors at the end of the chain. Using additional delay lines, like a simple fiber spool of appropriate length, it is possible to adapt the TDM to all other physical architectures. In the case of intensity-based sensors the reading unit will be an optical time domain reflectometer (OTDR) [26]. The WDM technique relies on the sharing of the optical bandwidth between the different sensors, so that each one uses a distinct wavelength range. The key technologies are in this case the wavelength separation components like fiber Bragg gratings [27] for in-line WDM or wavelength splitting couplers for star and tree topologies. In a FDM multiplexing array, the signals from different sensors are modulated at different frequencies and can therefore be separated electronically after the detection. This technique can be applied to in-line architectures using a chirped light source and differently unbalanced interferometers [28] or to matrix setups with intensity modulated light sources and synchronous demodulation [29]. Coherence domain multiplexing is used in conjunction with interferometric sensors and can be adapted to most physical architectures. Each sensor introduces a different path unbalance between the two interfering paths [30]. The path unbalances are compensated by the reading unit, separately for each sensor. Finally, polarization division multiplexing offers a very limited multiplexing potential and should be considered only in special cases. Table 2.1 explores some of the most used combinations between the physical and the signal multiplexing architectures.

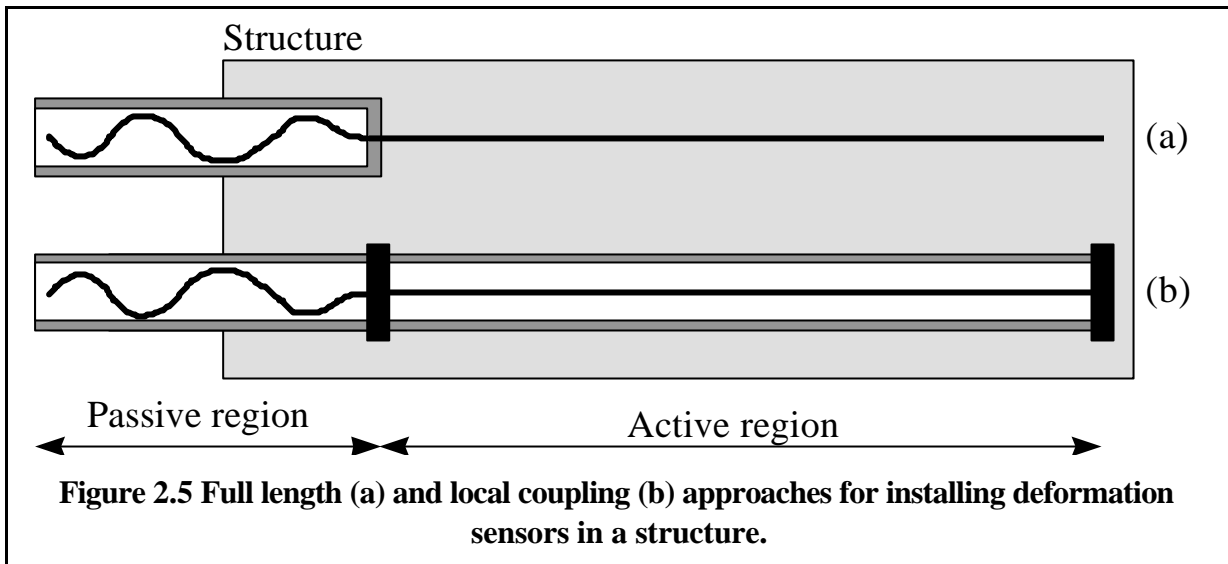
	In-line	Star	Tree	Matrix
Time Division Multiplexing (TDM)	Optical time domain reflectometer (OTDR)	OTDR with different delay lines for each arm	OTDR with different delay lines for each arm	OTDR with different delay lines for ingress and egress line
Wavelength Division Multiplexing (WDM)	Wavelength selective reflectors (for example fiber Bragg gratings)	Wavelength division couplers	Wavelength division couplers	Wavelength division couplers, multiple wavelength sources and detectors
Frequency Division Multiplexing (FDM)	Chirped wavelength modulation and unbalanced interferometers	Active modulator with different frequencies in each arm		Modulation of the sources at different frequencies and synchronous detection (lock-in amplifiers)
Coherence Domain Multiplexing (CDM)	Broadband partial reflector pairs on both interferometer arms	Different path unbalance in each arm	Different path unbalance in each arm	
Polarization Division Multiplexing (PDM)	Birefringence measurements	Polarization division couplers		Polarization division couplers

Table 2.1 Combination examples between physical and signal multiplexing architectures.

2.4.7 Installation techniques

Due to the variety of materials and environmental conditions that can be found in the different fields where the smart sensing concept can be applied, it is difficult to give general guidelines for the installation of the sensors and the optical links. However, some critical points are common to the different fields and should be considered attentively in the design process. The first concern is the installation of the sensors themselves into or onto the host material. On one hand it is necessary to guarantee a good mechanical contact between the fiber sensor and the structure, while on the other hand it is important to protect the fibers mechanically [31]. In the case of a strain sensor, it is difficult to add additional layer of protection to the fibers without altering the sensor response. In this case the sensor has to be adhered or embedded in the structure directly. For example it is possible to glue a Bragg grating sensor to the re-bars before concrete is poured or to imbed the sensor into a composite material. In other cases the strain sensor can be first embedded in a buffer material that is mechanically compatible with the surrounding material (for example a mortar prism for the installation in a concrete material) [32].

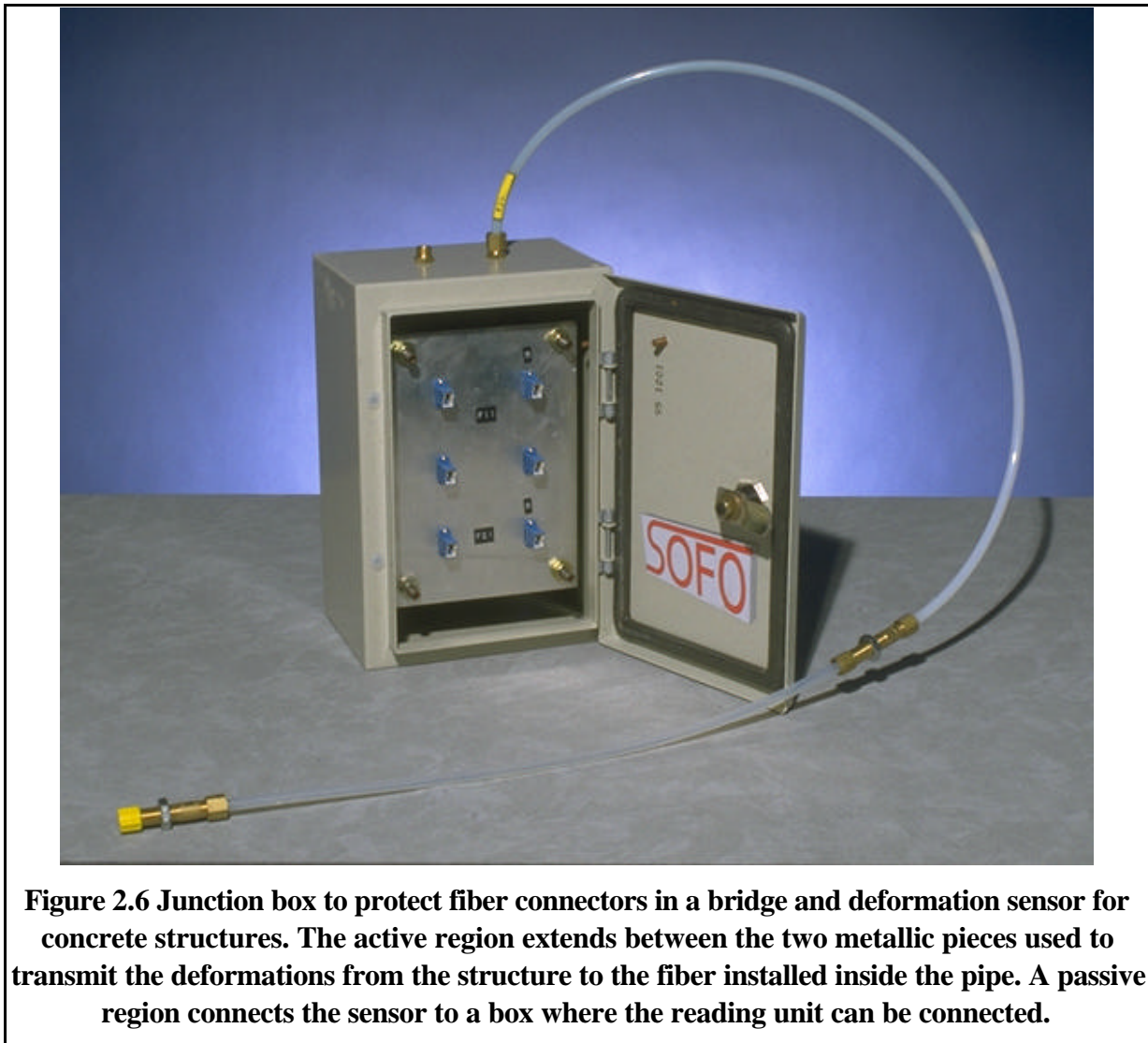
When a fiber is completely surrounded by the host or the buffer material, it is possible that a parasite sensitivity appears in the strain components transversal to the fiber axis. This is particularly true in the case of interferometric sensors (including Bragg grating sensors), where a transverse pressure will change the fiber's index of refraction. This change will be incorrectly interpreted as an axial strain variation. This may be overcome by a proposed method using two superposed Bragg gratings written in a birefringent fiber [33]



In the case of deformation sensors with a measurement base far longer than the fiber diameter, two installation approaches are possible: full length and local coupling [34]. In the first case the fiber is in mechanical contact with the host structure along its whole active length. In the second case the fiber is attached to the structure only at the ends of the active region and pre-stressed in-between (see Figure 2.5). In the case of full-length coupling the strain between the fiber and the surrounding material will be distributed over the whole sensor length. The fiber has to be directly attached to the material as in the case of a strain sensor making it difficult to protect it sufficiently. Full-length coupling should therefore be considered only when the fibers can be directly embedded in the host material without a significant failure risk. It is generally admitted that for sufficiently long sensors, it is possible to transmit small efforts through the primary acrylate coating or even through a tight nylon buffer coating without any slipping of the fiber. If the Poisson's ratio of the coating and the one of the host material are very different, a de-bonding of the sensor can not be ruled out.

On the other hand, local coupling offers the advantage of a higher degree of protection from external agents at the expense of an increased sensor size. In this case all the efforts will be transmitted from the structure to the fiber at the attachment points. Special care should be taken in the choice of the appropriate glue and coating in order to ensure a perfect mechanical contact and to avoid any creeping or slipping problems. Gluing on the acrylate primary coating should be avoided. Mechanically removing the coating always results in a significant reduction of the fiber resistance to traction. It is however possible to obtain a good mechanical contact through the much thinner polyimide coating.

The ingress and egress points of the fibers in the structure are other critical details to be considered. These points often represent an important failure source, especially in the case of host materials that require external finishing (e.g. removal of the casting forms from a concrete structure or cutting of a composite panel). In the case of concrete structures these problems can usually be solved by installing appropriate reservation boxes containing and protecting the fiber connectors or splices (see Figure 2.6).



In many cases, the installation of the sensors in the structure constitutes a serious problem that should not be underestimated. Many trials (and errors!) are often necessary before a reliable and efficient procedure can be established. It is desirable that the installation technique is included from the beginning in the design process and early trials should be carried out in real conditions, even before the whole sensing system is operational.

2.4.8 Remote sensing

When monitoring a structure through a smart sensing system, it is sometimes desirable or even necessary to observe its behavior from a remote location. If, for example, the sensors are placed in a tunnel vault to monitor the rock movements, the resulting data should appear in the control room at the entrance of the tunnel. We have seen in the previous paragraph that a certain degree of remote access can be achieved through the signal carrier subsystem. In this case the optical signals from the different sensors are brought to the reading unit through a series of optical cables. The reading unit resides near the operator terminal where the information is displayed and recorded. Depending on the multiplexing architecture that is chosen, this can however result in a large number of cables and for some type of sensors (e.g. intensity based sensors) in a degradation of the system's performance. If the sensors are more than a few hundred meters

from the operator, it is more interesting to transmit the data in a digital form. In this case the reading unit would be placed near the sensors and the long link would be established between the reading unit and the data treatment subsystem. This link can be electrical (Local Area Network, telephone line, serial link), optical (fiber network) or radio (cellular phone, radio link). By this means it is possible to monitor a structure from any location, even hundreds of kilometers away. For example, all bridges and tunnels along a highway section can be monitored from a single location. Once the data from the processing subsystem is available on a computer network it becomes possible for many persons to access the data at different levels for monitoring, maintenance, statistical or financial purposes.

2.5 Fiber optic sensor technologies

In this paragraph we will analyze the performances and the possible application of some of the most popular or promising fiber optic sensor technologies. Other types of fiber optic sensors have been demonstrated and could be of interest for specific applications. However, the technologies presented here cover the great majority of the research efforts going on worldwide.

2.5.1 Microbending sensors

Microbending sensors are based on the bend induced losses in optical fibers (generally multimode) and are therefore intensity based sensors. This type of sensor has been demonstrated for both strain and distributed deformation measurements, as well as for fire and humidity detection [35]. These sensors can be read either in transmission or in reflection (observing the attenuation of the Rayleigh scattering). In this second case the reading unit will be an optical time domain reflectometer (OTDR) of the same type used to monitor telecommunication fibers. If the measurements are done in reflection, the system can be easily brought to in-line multiplexing. Other architectures are possible by using appropriate passive delay lines. Sensitivities of the order of the micron have been demonstrated over short periods. Since the information is encoded in the intensity of the radiation, microbending sensors are subject to important performance degradation when applied to long-term measurements. Aging fibers, light sources, detectors and connections can decrease the amount of light independently from the deformations of the structure. Therefore, the long term drift has to be expected. These sensors can however find useful applications for the long-term monitoring of sudden events like a partial structural failure or the appearance of a crack. These events will produce a rapid change in the detected intensity that can be easily separated from the drift. The effect of temperature has to be compensated by using unstrained reference sensors. The reading units are usually rather inexpensive and simple, but specially manufactured fibers are required.

2.5.2 Fiber Bragg grating sensors

Fiber Bragg grating sensors are wavelength-shift based sensors that can be applied to both strain, displacement and, of course, temperature monitoring. These sensors are only sensitive to strain in the grating region that can be up to a few centimeters long. To obtain a displacement sensor, the fiber containing the Bragg grating has to be pre-stressed between two points at the extremities of the active region. Any deformation will change the distance between the two points and therefore the strain state of the grating. To obtain reliable measurements, the fiber has to be completely free and with a uniform tension. This usually requires the fiber to be installed in pipes with a sufficiently large diameter. Furthermore, the displacement precision will decrease with increasing sensor length. For these reasons, the Bragg grating sensors are better suited for strain

monitoring. The gratings are glued directly to the host material. In this case, sensitivities down to $1 \mu\epsilon$ can be achieved on the field. Methods have been even proposed to resolve the strain inside the grating itself. Since the fiber and the glue act as mechanical strain integrators, these measurements are well suited to detect a starting sensor debonding. The microscopic strain structure of the host material can be measured only if the grating is at least one centimeter long. The temperature apparent strain can be compensated with a reference grating or by using dual overlaid gratings at two well separated wavelengths.

The fiber Bragg gratings are written in the fiber core by a lateral UV exposure. The periodic structure is created either by interference or by using an appropriate mask. In both cases the fiber does not have to be coated at the time of exposure. Since stripping the fiber and reapplying a coating reduces the fiber resistance, techniques have been demonstrated to write the grating directly in the draw tower before the primary coating is applied [36]. These systems will probably bring the unit price of these sensors down to a few dollars a piece. Fiber Bragg grating sensors can be multiplexed in most physical architectures. Many types of reading architectures have been demonstrated in order to analyze the spectral content of the light returned by the gratings. The price and the size of the reading units vary according to their resolution, but portable reading units are now available for in-field applications [37].

Wavelength division multiplexing is obviously the first choice but time division multiplexing can further increase the number of addressable sensors.

2.5.3 Interferometric sensors

When high sensitivity is required, interferometric sensors are often the only choice. Although fiber Bragg grating sensors are also based on optical interference, the term ‘interferometric sensor’ is usually applied to two-path interferometers. The three main categories of interferometric sensors are the Mach-Zehnder, the Michelson and the Fabry-Perot types. In all cases the length change in one of the interferometer arms induces a change in the relative phase between the two interfering arms and therefore produces a sinusoidal intensity variation on the detector. Most interferometric sensors are incremental and require continuous monitoring. On the other side, sensitivities in the nanometer range can be achieved by appropriate demodulation of the interferometric signals. Depending on the length of the arms, both strain and deformation sensors can be realized. Useful interferometric strain sensor for structural monitoring are the external Fabry-Perot interferometer (EFPI) [38] and the in-line fiber étalon [39].

Many multiplexing architectures have been demonstrated including in-line, star, tree and matrix multiplexing. Being phase-based, these sensors are relatively immune to aging problems and long term monitoring is possible. However, because of the incremental nature of the signals, a failure of the reading unit usually leads to irrecoverable data losses. If the path unbalance between the arms becomes important, the wavelength stability of the laser source becomes a critical parameter. The reading unit can be very small and relatively inexpensive.

2.5.4 Low coherence sensors

Low-coherence systems use the same sensors as the interferometric ones but the reading unit is now based on a broadband source with a limited coherence length [40,13]. This solves the ambiguity between the fringes and transforms the sensors into a non-incremental system. In this type of setup the path unbalance introduced by the sensors is entirely compensated in the reading unit. This is done with a delay line that usually includes bulk optics and/or moving parts. The reading unit therefore tends to be rather expensive and bulky. However, because of the non-

incremental nature of the signals, one reading unit can be used to monitor lots of sensors or even different structures. Low-coherence interferometry has been demonstrated for deformation and strain measurements. It is particularly adapted to the measurement of deformations over long bases, where the interferometric principle offers high precision without the drawback of incremental encoding. Depending on the demodulation technique, sensitivities as high as those of coherent systems can be attained. The SOFO system is based on low coherence interferometry.

2.5.5 Brillouin sensors

The Brillouin effect consists in an interaction between the photons and the phonons in an optical fiber that results in a frequency shifted radiation traveling in the opposite direction of the monochromatic pump beam. The frequency shift depends on both the temperature and the strain of the fiber. By adding an appropriate modulation, it is possible to obtain a distributed sensor with a spatial resolution of some tens of meters [41,42]. This is insufficient for many structures but could be enough for larger ones like dams or for the temperature monitoring of garbage dumps. These sensors are used for the monitoring of power lines and can detect dangerous heating points.

2.5.6 Overview

In Table 2.2 we summarize the performances of the main sensor technologies presented in the previous paragraphs and analyzes their multiplexing capabilities at both the physical and the signal levels.

	Fiber Bragg Gratings	External Fabry-Perrot Interferometers (EFPI)	Microbending sensors	Interferometric sensors (incl. Low-coherence), e.g. SOFO
Sensor type	Strain sensor, amenable to deformation and displacement sensing	Strain sensor, amenable to deformation and displacement sensing	Deformation and displacement sensor	Deformation and displacement sensor
Measurement basis	Up to 2 cm, up to about 10 m for indirect deformation sensing	about 1cm	10 cm to about 1 km	Few cm to about 1 km
Resolution (field conditions)	down to 1 microstrain	down to 1 microstrain	about 1-20 μm for short periods	down to 10 nm, typical 1-10 μm
Linearity	Very good	Very good	Good	Very good
Long term stability	Very good	Very good for interferometric reading	Poor	Very good
Measurement type	Absolute	Incremental, absolute for low-coherence	Absolute	Incremental, absolute for low-coherence
Temperature sensitivity	High, can be compensated with reference gratings	Potentially low, depends on embedding technique	High, can be compensated with reference sensor	High, low, if both interferometer arms have the same temperature.
Multiplexing potential	Very high	Low	Good, especially in-line	High
Possible physical multiplexing architectures	In-line, star / tree (with additional couplers)	Star (with additional couplers), in-line	In-line, star / tree (with additional couplers and delay lines)	In-line, star / tree, matrix
Possible signal multiplexing architectures	WDM and TDM, without the need of any additional components	CDM, TDM	TDM	CDM, FDM, TDM, WDM
Price	High, but potentially low for on-the-drawing-tower writing	Medium	Medium, uses special cables	Low, uses standard telecom fibers

Table 2.2 Performance and multiplexing potential comparison between current fiber optic sensor technologies.

2.6 Outlook

Smart sensing is not an isolated and self-sufficient research and industrial field. Smart sensing is a new way to combine and enhance existing technologies to achieve innovative results in the field of structural monitoring.

In the first decade of smart sensing technology, most efforts were concentrated on the different subsystems. The reading unit and the multiplexing subsystems have seen important developments and many technologies are today mature for field and industrial applications. Some techniques have emerged like fiber Bragg grating sensors, low-coherence sensors and external Fabry-Perot interferometers, others are living a second youth like intensity based sensors. New technologies, like Brillouin scattering, are still in the development phase and many more will certainly emerge in the future. Portable reading units are getting smaller each year and have been successfully operated in demanding environment like those found in marine and civil engineering applications. In these last few years, the maturity of the reading unit subsystems has driven toward the development of reliable sensors and installation techniques. Fiber optic sensors have been embedded successfully in a number of materials and structures including composites, concrete, timber and metals. Some of these efforts are leading to industrial products and this will allow the instrumentation of structures with an increasing number of sensor at reasonable prices. This progress will be helped by the continuous development of fiber optic components like fibers, cables, connectors, couplers and optical switches driven by the much larger telecommunication market.

With structures equipped with hundreds or even thousands of sensors, measuring different parameters each second, the need of automatic data analysis tools will become increasingly urgent. Efforts have already been directed in this direction. Unfortunately, each type of structure and sensor needs specific processing algorithms. Vibration and modal analysis have attracted many research efforts and geometrical analysis like the curvature measurements can be easily applied to many types of structures like bridges, tunnels or spatial structures. Many other concepts like neural networks, fuzzy logic, artificial intelligence, genetic algorithms and data mining tools will certainly find an increasing interest for smart processing applications.

The ubiquity of digital networks and cellular communication tools increases the flexibility of the interface subsystems and makes remote sensing not only possible but even economically attractive. Of course every remote sensing system has to be based on reliable components since the need of manual interventions obviously reduces the interest of such systems.

Smart structures will both demand and produce sophisticated smart sensing and processing systems. Continuous developments in actuators based on piezoelectric materials and shape memory alloys complement ideally the progress made in sensor and processing technology. Most efforts are directed towards vibration damping, noise reduction and shape control, mainly for the aeronautics and space industry. Civil engineering is also producing interesting smart structures applications in particular for seismic control and many experiments have been conducted at least on reduced scale models. Other applications like vibration and modal control of large civil structures like suspended bridges could be potentially interesting but the forces required to achieve these results are still exceedingly high.

In a first phase we can expect that smart structures will be used to increase the comfort of the users and the life-span of the structures by reducing the amplitude of its oscillations under seismic, traffic or aerodynamic loads. These systems will not have a major structural role and their failure would not lead to important structural damages. The acceptance of smart structures

where the control system plays a structural role will require well-proved and reliable systems and will probably appear first in high-risk structures like fighter airplanes or space structures. More than the developments in each of the smart sensing subsystems, it is however the successful integration of different technologies that will lead to increasingly useful applications. This integration is possible only in highly multidisciplinary teams including structural, material and sensor engineers. The necessary competencies already exist in many industries and universities but have to be brought together and adapted to each other needs. The final judge of all smart sensing system will however be the market. Even well designed and perfectly functioning systems will have to prove their economic interest in order to succeed. Unfortunately the evaluation of the benefits of a smart sensing system is often difficult and the initial additional investments are paid back only in the long run. Furthermore it is not easy to quantify the benefits of the increased security of one structure or of a better knowledge of its aging characteristics. In many fields including civil engineering and aeronautics we are however witnessing an investment shift from the construction of new structures to the maintenance and the life-span extension of the existing ones. In these domains, smart sensing technologies have certainly an important role to play.

2.7 References

- [1] Smart Structures and Materials 1993: Smart sensing, processing, and instrumentation, Albuquerque, NM, Feb. 1-4, 1993, SPIE Vol. 1918
- [2] Smart Structures and Materials 1994: Smart sensing, processing, and instrumentation, Orlando, FL, Feb. 14-16, 1994, SPIE Vol. 2191
- [3] Smart Structures and Materials 1995: Smart sensing, processing, and instrumentation, San Diego, CA, Feb. 27- Mar. 1, 1995, SPIE Vol. 2444
- [4] Udd, E., Fiber optic smart structures, Wiley, New York, 1995
- [5] Udd, E., Fiber Optic Sensors, New York, NY, Wiley, 1991
- [6] Dakin, J., Culshaw, B., Optical fiber sensors, Norwood, MA, Artech House, 1988
- [7] Optical Fiber Sensor Conference Series OFS: 1 London 1983, 2 Stuttgart 1984, 3 San Diego 1985, 4 Tokyo 1986, 5 New Orleans 1988, 6 Paris 1989, 7 Sydney 1990, 8 Monterey 1991, 9 Florence 1993
- [8] Tenth International Conference on Optical Fiber Sensors, Glasgow, UK, Oct. 11-13, 1994, SPIE Vol. 2360
- [9] Bruinsama, A.J., Culshaw, B., Fiber Optic Sensors: Engineering and applications, The Hague, The Netherlands, Mar. 14-15, 1991, SPIE Vol. 1511
- [10] Murata, H., Handbook of optical fibers and cables, New York, NY, Dekker, 1988
- [11] Measures, R. M., et al. "Structurally Integrated Fiber Optic Damage Assessment System for Composite Materials," Applied Optics, Vol. 28, 1989, pp. 2626-2633
- [12] Chang, C.-C., Sirkis, J., "Optical Fiber Sensors Embedded in Composite Panels for Impact Detection," Smart Structures and Materials 1995: Smart sensing, processing, and instrumentation, San Diego, CA, Feb. 27- Mar. 1, 1995, SPIE Vol. 2444, pp. 502-513
- [13] Inaudi, D., Elamari, S., Pflug, L., Gisin, N., Breguet, J., Vurpillot, S., "Low-coherence deformation sensors for the monitoring of civil-engineering structures," Sensor and Actuators A, Vol. 44, 1994, pp. 125-130.
- [14] Habel, W. R., Höpcke, M., Basedau, F., Polster H., "The Influence of Concrete and Alkaline Solutions on Different Surfaces of Optical Fibers for Sensors," Second European Conference on Smart Structures and Materials, Glasgow, UK, Oct. 12-14, 1994, SPIE Vol. 2361, pp. 168-171
- [15] Butter, C. D., Hocker G. B., "Fiber Optics Strain Gauge," Applied Optics, Vol. 17, 1978, pp. 2867-2869
- [16] Sirkis, J. S., "Unified Approach to Phase-Strain-Temperature Models for Smart Structure Interferometric Optical Fiber Sensors: Part 1, Development," Optical Engineering, Vol. 32, 1993, pp. 752-761
- [17] Sirkis, J. S., "Unified Approach to Phase-Strain-Temperature Models for Smart Structure Interferometric Optical Fiber Sensors: Part 2, Applications," Optical Engineering, Vol. 32, 1993, pp. 762-773
- [18] Sirkis, J. S., Mathews, C. T., "Experimental Investigation of Phase-Strain-Temperature Models for Structurally Embedded Interferometric Fiber-optic Sensors," Experimental Mechanics, vol. 33, 1993, pp. 26-31

- [19] Huang, S. H., Ohn, M. M., LeBlanc, M., Lee, R. Measures, R. M., "Fiber Optic Intra-grating Distributed Strain Sensor," Distributed and Multiplexed Fiber Optic Sensors IV, San Diego, CA, Sept. 1994, SPIE Vol. 2294
- [20] Gusmensoli, V., Martinelli, M., "Non-incremental Interferometric Fiber-optic measurement method for simultaneous detection of temperature and strain," Optics Letters, Vol. 19, 1994, pp. 2164-2166
- [21] Flavin, D. A., McBride, R., Jones, J. D. C., Burnett, J. G., Greenaway, A. H., "Combined Temperature and Strain Measurement with a Dispersive Optical Fiber Fourier-transform Spectrometer," Optics Letters, Vol. 19, 1994, pp. 2167-2169
- [22] Vengsarkar, A. M., Michie, W. C., Jankovic, L., Culshaw, B., Claus, R. O., "Fiber-optic Dual-technique for Simultaneous Measurement of Strain and Temperature," Journal of Lightwave Technology, Vol. 12, 1994, pp. 170-177
- [23] Xu, M. G., Archambault, J.-L., Reekie, L., Dakin, J. P., "Discrimination Between Strain and Temperature Effects Using Dual-wavelength fiber grating sensors," Electronics Letters, vol. 30, 1994, pp. 1085-1087
- [24] Distributed and multiplexed fiber optic sensors IV, San Diego, CA, Jul. 27-28, 1994, SPIE Vol. 2294
- [25] Distributed and multiplexed fiber optic sensors V, Munich, FRG, Jun. 22-23, 1995, SPIE Vol. 2507
- [26] Barnoski, M. K., Jensen, S. M., "A Novel Technique for Investigating Attenuation Characteristics," Applied Optics, Vol. 15, 1976, pp. 2112
- [27] Kersey, A. D., Berkoff, T. A., Morey, W. W., "Multiplexed Fiber Bragg Grating Strain-sensor System with a Fiber Fabry-Perot Wavelength Filter," Optics Letters, Vol. 18, 1993, pp. 1370-1372
- [28] Giles, I. P., Uttam, D., Culshaw, B., Davies, D. E. N., "Coherent Optical Fiber Sensors with Modulated Laser Sources," Electronics Letters, Vol. 20, 1983, pp. 14
- [29] Dandridge, A., Tveten, A. B., Kersey, A. D., Yurek, A. M. "Multiplexing of Interferometric Sensors Using Phase Generated Carrier Techniques," IEEE Journal of Lightwave Technology, Vol. 5, 1987, PP. 947
- [30] Inaudi, D., "Coherence Multiplexing of In-line Displacement and Temperature Sensors," Optical Engineering, Vol. 34, 1995, pp. 1912-1915
- [31] Inaudi, D., Elamari, A., Vurpillot, S. "Low-coherence Interferometry for the monitoring of Civil Engineering Structures," Second European Conference on Smart Structures and Materials, Glasgow, UK, Oct. 12-14, 1994, SPIE Vol. 2361, pp. 216-219
- [32] Habel, W. R., Hofmann, D., "Strain Measurements in Reinforced Concrete Walls During the Hydration Reaction by Means of Embedded Fiber Interferometers," Second European Conference on Smart Structures and Materials, Glasgow, UK, Oct. 12-14, 1994, SPIE Vol. 2361, pp. 180-183
- [33] Udd, E., Three axis and temperature fiber optic grating sensor, Smart Structures and Materials 1996, San Diego, CA, Feb. 27- 29, 1996, SPIE Vol. 2718
- [34] Inaudi, D., Vurpillot, S., Casanova, N., Osa-Wyser, A. "Development and Field Test of Deformation Sensors for Concrete Embedding," Smart Structures and Materials 1996: Industrial and Commercial Applications of Smart Structures Technologies, San Diego, CA, Feb. 27- 29, 1996, SPIE Vol. 2721-16

- [35] Michie, W. C., Culshaw, B., McKenzie, I., Konstantakis, M., Graham, N. B., Moran, C., Santos, F., Bergqvist, E., Carlstrom, B., "Distributed Sensor for Water and pH Measurements Using Fiber Optics and Swellable Polymeric Systems," *Optics Letters*, Vol. 20, 1995, pp. 103-105
- [36] Askins, C. G., Putman, M. A., Williams, G. M., Friebele, E. J., "Contiguous Fiber Bragg Grating Arrays Produced On-line During Fiber Draw," *Smart Structures and Materials 1994: Smart sensing, processing, and instrumentation*, Orlando, FL, 1994, SPIE Vol. 2191, pp. 80-85
- [37] Davis, M. A., Bellemore, D. G., Berkoff, T. A., Kersey, A. D. "Design and Performance of a Fiber Bragg Grating Distributed Strain Sensor System," *Smart Structures and Materials 1995: Smart Systems for Bridges, Structures, and Highways*, San Diego, CA, Feb. 28 - Mar. 3, 1995, SPIE Vol. 2446, p. 227-235
- [38] Mason, B., Valis, T., Hogg, D., "Commercialization of Fiber-optic Strain Gauge Systems," *Fiber optic and laser sensors X*, Boston, MA, Sept. 8-11, 1992, SPIE Vol. 1795, p. 215-222.
- [39] Sirkis, J. S., Brennan, D. D., Putman, M. A., Berkoff, T. A., Kersey, A. D., Friebele, E. J., "In-line Fiber Etalon for Strain Measurements," *Optics Letters*, Vol. 18, 1993, pp. 1973-1975
- [40] Koch, A., Ulrich, R., "Fiber-optic Displacement Sensor with 0.02 micron Resolution by White-light Interferometry," *Sensors and Actuators A*, Vol. 25-27, 1991, pp. 201-207
- [41] Shimitzu, K., Horiguchi, T., Koyamada, Y., "Measurement of Distributed Strain and Temperature in a Branched Optical Fiber Network by Use of Brillouin Optical Time-Domain Reflectometry," *Optics Letters*, Vol. 20, 1995, pp. 507-509
- [42] Niklès, M., Thévenaz, L., Robert, P. A., "Simple Distributed Temperature Sensor Based on Brillouin Gain Spectrum Analysis," *Tenth Optical Fiber Sensors Conference*, Glasgow, UK, Oct. 11-13, 1994, SPIE Vol. 2360, pp. 138-141

3. Selection of the sensing technology

This section shows the requirements for monitoring deformations in civil engineering structures. Low-coherence interferometry will be shown in section 5 and 6 to respond to all these requirements.

3.1 Introduction

The selection of a measurement technique to be developed in the framework of a research project like SOFO must pursue two main objectives. On one hand a new system has to respond to a real need of the end-users (as described in section 1). On the other hand it should constitute an innovative approach in the domain of metrology and present some originality compared to the work of other research laboratories active in the same field.

From the point of view of the end-users, we have seen that a real need exists for short and long gage-length sensors based on fiber optics. These techniques offer the advantage of a small size, insensitivity to electromagnetic fields, currents, corrosion and in some cases temperature variations. Furthermore, optical fibers can be used at the same time as sensors and information carriers, reducing the complexity of the system and potentially allowing the multiplexing of a great number of sensors on a reduced number of transmission lines.

In the domain of short-gage fiber optic sensors, the optical replacements of resistive strain-gages, great research efforts have been conducted worldwide and have produced interesting solutions including intrinsic, extrinsic and in-line Fabry-Perot interferometers and fiber Bragg grating sensors (see also section 2). These sensors have or are evolving to commercial applications.

Fiber optic deformation sensors, the optical equivalent of rockmeters and inductive sensors, have attracted considerable research interest at the beginning of fiber optic sensor history, especially in the interferometric configuration. Michelson and Mach-Zehnder interferometers with coherent sources (typically gas and semiconductor lasers) were used in the first demonstrations of fiber sensing. Two drawbacks have stopped these techniques from reaching main-stream applications: the incremental nature of the interferometric signal (requiring a continuous connection between the sensor and the demodulator) and the extreme sensitivity of the methods making it difficult to isolate the quantities to be measured from external disturbances, especially phase fluctuation in the lead fibers. Other techniques for deformation sensing rely on micro-bending to encode the deformation in a change of the transmitted or reflected intensity. Some of these techniques have turned into industrial applications. Microbending sensors offer the advantage of a relatively good sensitivity and precision, combined with the simplicity of the reading units that should have made them extremely affordable. Furthermore they offer a certain potential for distributed sensing, but at the price of a reduced resolution. Unfortunately the intensity nature of the deformation encoding makes these methods prone to drifts resulting from fluctuation in the source power, degradation of the transmission properties of fibers and connectors as well as changes in the characteristics of the receiver's electronics. These sensors are therefore indicated for short-term and dynamic measurements but are less effective for long-term monitoring.

An interesting and relatively unoccupied niche in the research panorama exists therefore for mid- and long-term deformation monitoring systems . Low-coherence

interferometry fits into this niche and offers the sensitivity advantage of the coherent methods but without the problems associated with incremental measurements and especially the need of continuous measurements. Furthermore, the coherence encoding of the deformation information frees the method from any intensity-related drift.

3.2 Requirements

The requirements that a deformation sensor for short (but not dynamic) and long-term monitoring should meet are examined in the next few paragraphs. Low-coherence interferometry in singlemode optical fiber sensors responds to all these requirements.

3.2.1 Deformation sensing

A deformation sensor has to measure the distance variation between two given points fixed to the structure. When possible, the sensor should be embeddable inside the construction materials in order to provide a more representative measurement of the structure's behavior when compared to surface mounted sensors¹. The extremities of the sensor's active region (i.e. the region over which the deformation is measured) should be easily defined and identified.

3.2.2 Sensor length

Because of the great variety of structures encountered in civil engineering it is impossible to find a standard sensor length that fits all applications. An all-purpose sensor should allow measurements over length from a few centimeters to a hundred meters and more. The active region can sometimes be up to a few kilometers away from the reading unit.

3.2.3 Resolution and precision

The resolution requirements also greatly vary with the application. If the sensors are considered as replacement of conventional techniques like dial gages, it is important to guarantee at least the same resolution. A resolution of a few microns can therefore be considered sufficient for most applications. For applications where large deformations are expected this resolution largely exceeds the real needs. A precision of 1% of the measured deformation is usually considered as sufficient.

3.2.4 Dynamic range

For applications in conventional civil structures, in-service deformations larger than 0.1-1% of the gage length are rare. For geotechnical structures, deformations of a few percents are on the contrary found in some applications. However, this means that for a 10 m long sensor, deformation of a few centimeters are expected. In this case a precision of a few microns is certainly overkill and other simpler methods (e.g. a rule) are certainly more appropriated than fiber optic sensors.

¹ The surface represents a special and not always representative case of the structural behavior.

3.2.5 Stability

Since long-term applications are aimed, the resolution and precision cited above should remain valid even for measurements spaced by years.

3.2.6 Temperature sensitivity

All deformation sensors are also to some extent temperature sensors. It is therefore interesting to study the influence of temperature on the deformation measurements. This helps to define what kind of temperature compensation is best suited for a given application.

Any sensor will transform a deformation into a change of a certain quantity X . This can be a mark count (in a dial gage) a resistance, an inductance, a phase, an intensity,...

In general the variations of X as a function of the variations of the strain \mathbf{e} and temperature T will be given by:

$$\Delta X = \Delta \mathbf{e} \frac{dX}{d\mathbf{e}} + \Delta T \frac{dX}{dT} \quad (1)$$

The first term represents the sensor response to strain variations. The second term represents the sensitivity to temperature variations.

Furthermore:

$$\Delta \mathbf{e} = \Delta \mathbf{e}_M + \Delta T \frac{d\mathbf{e}}{dT} \quad (2)$$

The first term accounts for the mechanically induced strain variation in the sensor. The second term represents the strain variations due to a temperature change. Therefore we can write:

$$\Delta X = \Delta \mathbf{e}_M \frac{dX}{d\mathbf{e}} + \Delta T \frac{dX}{dT} + \Delta T \frac{dX}{d\mathbf{e}} \mathbf{a} \quad (3)$$

where \mathbf{a} represents the thermal expansion coefficient (either of the sensor or of the structure).

If the sensor is mounted on a structure S it will inherit its strain, temperature and thermal expansion coefficient and (3) will become:

$$\Delta X_S = \Delta \mathbf{e}_M \frac{dX}{d\mathbf{e}} + \Delta T \frac{dX}{dT} + \Delta T \frac{dX}{d\mathbf{e}} \mathbf{a}_S \quad (4)$$

In this equation, the temperature induced strain variations in the structure are represented by the third term in the sum. The strain variations produced by external forces and constrains as well as relaxation and other similar phenomena are accounted for in the first term. The second term represents the parasitic sensor's response to temperature. If the temperature variation ΔT is measured separately, it is possible to correct the results numerically to eliminate the second term (provided that the sensor's response to temperature variations is linear and known). This is for example the approach used in the vibrating-string sensors. If the thermal expansion coefficient \mathbf{a}_S of the structure is also known it is possible to eliminate the influence of the third term, too.

Another common approach consists in placing a second reference sensor R near the first one and isolate it from the strain variations. Its response will be given by:

$$\Delta X_R = \Delta T \frac{dX}{dT} + \Delta T \frac{dX}{de} \mathbf{a}_R \quad (5)$$

where \mathbf{a}_R is now the thermal expansion coefficient of the free sensor. By subtracting the two readings we obtain:

$$\Delta X_{M-R} = \Delta X_M - \Delta X_R = \Delta \mathbf{e}_M \frac{dX}{de} + \Delta T \frac{dX}{de} (\mathbf{a}_S - \mathbf{a}_R) \quad (6)$$

The direct sensor sensitivity to temperature has now been eliminated. An indirect sensor sensitivity to temperature however remains in the form of the term containing \mathbf{a}_R . Two interesting cases are now possible. In the first case the reference sensor is mounted on a free piece of the same material that the structure is made of. In this case we obtain $\mathbf{a}_S = \mathbf{a}_R$ and (6) becomes simply:

$$\Delta X_{M-R} = \Delta \mathbf{e}_M \frac{dX}{de} \quad (7)$$

This is the approach used for resistive strain gages mounted on metals (e.g. steel). It is effective only if the thermal expansion coefficient of the host structures is known, constant and can be reproduced on the small sample to which the reference sensor is mounted to. This is not the case, for example in concrete structures where \mathbf{a}_S is far from constant, especially during concrete setting. A good temperature compensation of \mathbf{a}_S by \mathbf{a}_R is therefore impossible.

Another approach is to choose a sensor with $\mathbf{a}_R \ll \mathbf{a}_S$. In this case (6) becomes:

$$\Delta X_{M-R} = \Delta \mathbf{e}_M \frac{dX}{de} + \Delta T \frac{dX}{de} \mathbf{a}_S \cong \Delta \mathbf{e}_M \frac{dX}{de} \quad (8)$$

This represents the real total deformation undergone by the structure. This is the only solution that does not make any assumption on the material properties of the host structure. The SOFO system is based on this approach, as explained in section 4. The thermal expansion coefficient of silica fibers is about twenty times lower than the one of steel and concrete.

3.3 Conclusions

In section 4 (optical fibers as intrinsic sensors), section 5 (low-coherence interferometry) and section 6 (SOFO design and fabrication) we will show that low-coherence interferometry in singlemode optical fibers is able to respond to all requirements listed above and can be used to implement a reliable deformation measuring system.

4. Optical fibers as intrinsic sensors

The use of singlemode optical fiber as sensors is discussed in this section. The physical and optical characteristics of the commonly used optical fibers will be introduced briefly. We will then describe the behavior of these fibers when used as a part of an interferometric system. The variations of the optical path length as a function of the applied strain and temperature will be investigated for the free, coated and embedded fibers. Recommendations on the type of fibers and coatings to be used in a sensor system, will be given at the end of the section.

4.1 Introduction

Optical fibers are widely used as information carriers in the telecommunication industry. Their small size, large bandwidth and low attenuation make them ideal to transmit signals over long distances¹. Driven by the large telecommunication market the manufacturing industry has made important progress in the mass-production of optical fibers with excellent optical and mechanical characteristics, while progressively lowering their cost².

Since the beginning of this relatively young technology, these same fibers have been used as sensors [1] for different parameters such as strain, temperature, pressure, acceleration or current, only to name a few. These fiber sensors are usually divided into two main categories: *intrinsic* and *extrinsic*.

In the case of intrinsic sensors, the fiber itself reacts to a change of the quantity to be measured by modifying the radiation it carries. This can result in a variation of the intensity, the phase, the polarization state or the spectral content of the light transmitted through the fiber. The sensitivity of an intrinsic sensor to different parameters is determined by the setup conditions and in particular by the fiber coatings and the fiber attachments. This type of sensors is usually sensitive along the whole length of the fiber and can therefore be used for distributed or integrated measurements.

In the extrinsic sensors, the optical fibers are only used to carry the information from the transducer, which is usually installed at one end of the fiber, to the remote reading unit. The transducer can alter the incoming light or produce a radiation responding to the variations of the external quantity to be measured. In this case, the sensor is usually sensitive only at the position of the transducer (or transducers) and is best suited for local or point measurements.

In this work we have chosen to focus on the measurement of displacements by low-coherence interferometry. We will therefore deal with sensor of intrinsic type and analyze in detail the response of a singlemode optical fiber to an applied external strain or a variation of the local temperature.

4.2 Optical fiber characteristics

Many different types of fibers are produced for the telecommunication market and a few specifically for sensing applications. In the next paragraphs we discuss the different optical and mechanical characteristics of optical fibers and choose the types that are best suited to be used as part of a low-coherence interferometric setup.

4.2.1 Optical characteristics

All optical fibers present a core surrounded by a cladding with a lower index of refraction. The light is therefore guided by the core and propagates along the fiber axis [2]. Most common optical fibers are made of fused silica³ and the required variations of index are obtained with appropriate doping. A preform with the desired index profile, measuring typically two meters in length and 200 mm in diameter, is fabricated by chemical vapor deposition and then drawn

¹ Depending on the bit-rate, links up to 100 km are possible without repeaters.

² Standard singlemode fibers cost less than 0.10 Sfr per meter.

³ Plastic fibers are used in telecommunication but rarely for sensors applications. Vitreous materials other than silica are used to at wavelength other than 850, 1300 and 1550 nm to deliver laser radiation over short distances.

in a drawing tower to a wire of 125 μm diameter and sometimes more than 100 km in length [1, chapter 2]. Silica fibers are exceptionally transparent around two optical window at 1300 nm and 1550 nm. The attenuation at these two wavelength can be as low as 0.3 dB/km and 0.2 dB/km, respectively. The refractive index is of about 1.46.

Optical fibers [3] are usually divided between *singlemode* and *multimode* types.

Multimode fibers have larger cores (commonly 50 μm in diameter) and can transmit multiple transversal eigenmodes having, in general, different propagation speeds. This produces a *modal dispersion* and makes this type of fibers unsuited for interferometric applications since each eigenmode can be considered as a coupled interferometer between the source and the detector.

Only singlemode fibers will therefore be used in all experiments presented in this work. This type of fibers has an index profile (see Figure 4.1) that allows only the fundamental transversal mode to propagate, while all higher-order modes will be dissipated. Typical core sizes are

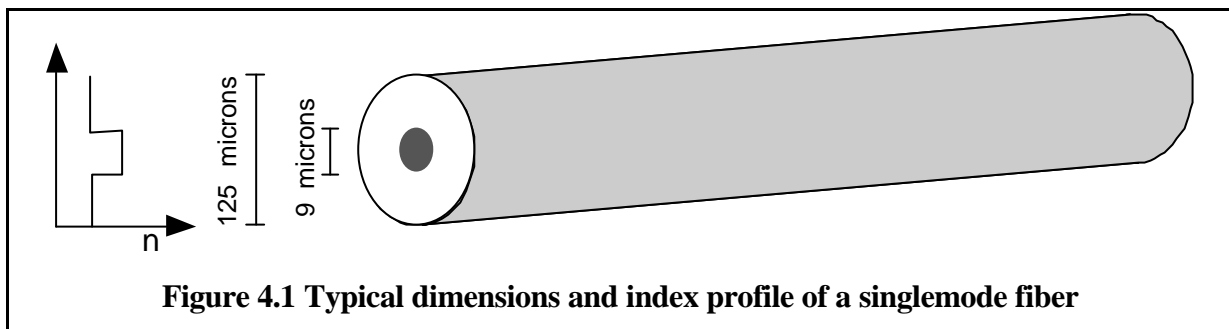


Figure 4.1 Typical dimensions and index profile of a singlemode fiber

between 3 μm and 9 μm with an index increase between 0.2% and 0.8%. Singlemode fibers are not affected by modal dispersion and allow therefore interferometric measurements. These fibers are however affected by *chromatic dispersion*, *wave-guide dispersion* and *polarization mode dispersion*.

Chromatic dispersion is the result of a wavelength dependent index of refraction and is a material characteristic. For silica fibers the value of chromatic dispersion is about zero at 1300 nm and around 20 ps/(km nm) at 1550 nm.

Wave-guide dispersion is produced by a wavelength dependence of the effective index of refraction, i.e. of the propagation constant. It is produced by the index profile of the fiber⁴ and can therefore be modified using ad-hoc dopants structures. By combining the effects of chromatic and wave-guide dispersions, it is possible to obtain fibers with a desired total dispersion at a given wavelength. *Dispersion-shifted* fibers show a dispersion minimum at a wavelength other than 1300 nm, e.g. at 1550 nm. *Dispersion flattened* fibers offer a reduced dispersion over a wide wavelength range. *Compensating fibers* can be added at the end of a dispersive fiber link and compensate its dispersion.

Recently, another type of dispersion, *polarization mode dispersion*, has attracted rising attention. It is produced by the combined effects of the fiber birefringence and the polarization mode coupling. The value of this type of dispersion can vary greatly during one day and can not be compensated efficiently.

⁴ A change in the wavelength produces a change in the form of mode that propagates in the fiber. Since the index profile remains the same the mode will see a different effective index.

Finally, some fibers are fabricated with index profiles that have not a cylindrical symmetry. These fibers are therefore intrinsically birefringent and can propagate a linear polarization unaltered.

Since in this work we will deal mostly with fibers of reduced length and sources at 1300 nm, most dispersive phenomena can be neglected and special index profiles do not offer a significant improvement in the performances to justify their use. Unless otherwise specified, all the sensors described in this work are based on the use of standard silica singlemode fibers.

4.2.2 Physical characteristics

Since the optical fibers will be used as strain, displacement and temperature sensors, it is useful to summarize here the main physical characteristics of silica and silica fibers [3].

Silica (SiO_2) is a vitreous material with a density of $2.2 \cdot 10^3 \text{ kg/m}^3$, a Young's modulus of 72 kN/mm^2 and can withstand an elongation up to 2-8%. Optical fibers have usually a diameter of $125 \mu\text{m}$, giving a Hooke constant of 884 kN (a force of 884 g will therefore produce an elongation of 1%). An elongation of 1% is by at least one order of magnitude higher than the maximal possible elongation of concrete. Silica fibers are therefore ideal as displacement sensors for concrete structures. Some metals can show larger elongation, but these occur only rarely in real structures.

Silica has a very low thermal expansion coefficient of $5 \cdot 10^{-7} \text{ } 1/^\circ\text{C}$ that will help avoiding parasitic sensitivities to temperature variations (see paragraph 4.3.3).

The main optical and mechanical characteristics of silica fibers, steel and concrete are summarized in Table 4.1.

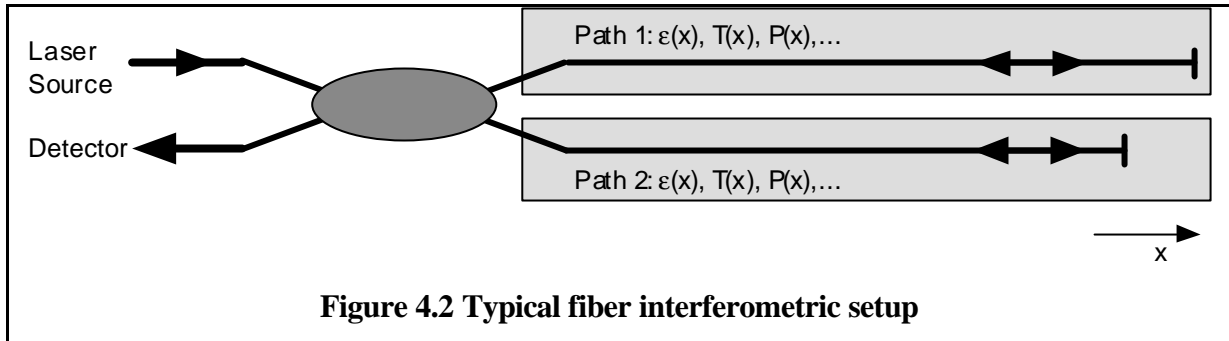
Propriety	Silica	Steel	Concrete (approx.)
Chemical composition	SiO_2	$\text{Fe}_{0.99} \text{C}_{0.01}$	-
Density [10^3 kg / m^3]	2.2	7.9	2.7
Tensile strength [kN/mm^2]	5	0.46	0.003
Young's modulus [kN/mm^2]	72	210	30
Poisson's ratio	0.17	0.3	0.17 - 0.2
Maximal elongation [%]	2-8	5-25	0.3
Thermal expansion coefficient [$10^{-6} / ^\circ\text{C}$]	0.5	12	10
Fusion point [$^\circ\text{C}$]	1665	1535	-
Index of refraction	1.46	-	-
Typical attenuation [dB/km]	0.3	-	-
Typical dispersion @ 1550 nm [ps/(km nm)]	20	-	-

Table 4.1. Physical and optical properties of silica, steel and concrete.

4.3 Optical fibers as part of an interferometric sensor

Since we have chosen an interferometric setup as measuring technique, we will now restrain our study on the response of optical fibers to the case of singlemode intrinsic sensors.

Figure 4.2 shows a typical Michelson interferometer setup. The coherent emission of a laser source is split by means of a directional coupler and sent into two distinct fiber lines. The external quantity to be measured, e.g. the strain or the temperature, will act differently on each



of the fibers and introduce therefore a path unbalance between the two interferometer arms. This will produce a variation of the relative phase and therefore of the intensity measured by the detector.

For this reason it is interesting to study the relationship between the applied perturbation and the resulting path unbalance. This unbalance is calculated as the difference between the optical path in the two arms. To avoid any confusion⁵, we will from now on express all path unbalances as delays, i.e. as the difference in the time of flight between photons traveling in the two arms. The delay $\mathbf{d}t$ is therefore given by:

$$\mathbf{d}t = \frac{2}{c} \int_{Path 2} n_2(x) dx - \frac{2}{c} \int_{Path 1} n_1(x) dx \quad (1)$$

Where:

$n_i(x)$ is the local refractive index along the path i and

c is the vacuum speed of light

The factor two comes from the double pass typical of the Michelson interferometer.

If we assume that the refraction index is constant along both arms, (1) becomes:

$$\mathbf{d}t = 2 \frac{n_2 L_2 - n_1 L_1}{c} \quad (2)$$

Where:

L_i is the physical length along path i

To measure a change of the externally applied quantity, it is interesting to compare the value of $\mathbf{d}t$ at different times and define:

$$\Delta t \equiv \mathbf{d}t'' - \mathbf{d}t' \quad (3)$$

Where the upper index refers to different times.

Moving to infinitesimal variations and considering that the perturbation is applied only to one of the arms we obtain:

$$dt = \frac{2}{c} d(n L) = \frac{2}{c} (n dL + L dn) \quad (4)$$

⁵ A length could be interpreted as a displacement, a cut in the fiber, the equivalent path unbalance in vacuum,...

Were n and L are the refractive index and the physical length of the perturbed fiber. Since the light propagates in a wave-guide, the index n should be replaced by the effective refractive index n_{eff} which lies between the index of the core and the one of the cladding. This finally gives:

$$dt = \frac{2}{c} (n_{eff} dL + L dn_{eff}) \quad (5)$$

Since for standard singlemode fibers the core index is less than 1% higher than the cladding index we can assume:

$$n_{eff} = n_{cladding} \equiv n \quad (6)$$

Lets now consider the behavior of this differential under variations of the fiber length, of the applied strain and of the temperature. The different proportionality constants that will be introduced in the next paragraphs, are summarized in Table 4.3 at the end of this section.

4.3.1 Fiber length sensitivity

If we cut the fiber and therefore introduce a dL , (5) becomes:

$$\frac{dt}{dL} = \frac{2}{c} \left(n \frac{dL}{dL} + L \frac{dn}{dL} \right) \quad (7)$$

Since n is independent from L we obtain:

$$\frac{dt}{dL} = \frac{2}{c} n \quad (8)$$

Or, for a finite ΔL :

$$\Delta t = \frac{2n}{c} \Delta L \quad (9)$$

We can define k_{cut} as:

$$\Delta L \equiv k_{cut} \Delta t \quad (10)$$

with $n = 1.46$ and $c = 300 \frac{m}{ps}$ we obtain:

$$k_{cut} = \frac{c}{2n} = 103 \frac{m}{ps} \quad (11)$$

This material constant gives the length of fiber that has to be cut (without being strained) in order to obtain a unitary change in the delay.

4.3.2 Axial strain sensitivity

If we pull the fiber by dL and therefore introduce a strain ϵ , (5) becomes:

$$\frac{dt}{dL} = \frac{2}{c} \left(n \frac{dL}{dL} + L \frac{dn}{dL} \right) \quad (12)$$

In this case the second term in the equation can no longer be neglected since the index of the stressed fiber will be different. The change in the core diameter will produce a change of n_{eff} .

This effect can however be shown to be negligible [4].

The second term of the sum can be expressed as a function of the strain-optic tensor p_{ij} and the Poisson ratio \mathbf{m} of silica:

$$\frac{dt}{dL} = \frac{2n}{c} \left(1 - \frac{n^2}{2} [(1 - \mathbf{m})p_{12} - \mathbf{m}p_{11}] \right) \quad (13)$$

For typical silica: $m=0.17$, and $p_{11}=0.121$ and $p_{12} \cong 0.270$, giving:

$$\frac{dt}{dL} = \frac{2n}{c}(1-0.21) = 0.79 \frac{2n}{c} \quad (14)$$

The decreasing index will therefore partially cancel the effect of an increased length.

We define k_{stress} as:

$$\Delta L \equiv k_{stress} \Delta t \quad (15)$$

and obtain:

$$k_{stress} = \frac{1}{0.79} k_{cut} = 130 \frac{mm}{ps} \quad (16)$$

This material constant gives the elongation (strain times length) that has to be given to a fiber to obtain a unitary variation of the delay.

In Figure 4.3 we plot an experimental curve showing the measured delay as a function of the deformation applied to the fiber by a micro-metric displacement table. The fiber was glued at two points 1495 mm apart, one fixed and the other on the displacement table. The flat part of the curve corresponds to a loose fiber. As soon as the fiber exhibits stress, the curve becomes linear giving a $k_{stress} = 128 \frac{mm}{ps}$. This value differs slightly from the theoretical one found in (16). This figure was confirmed by a number of calibration experiments and has been adopted as standard.

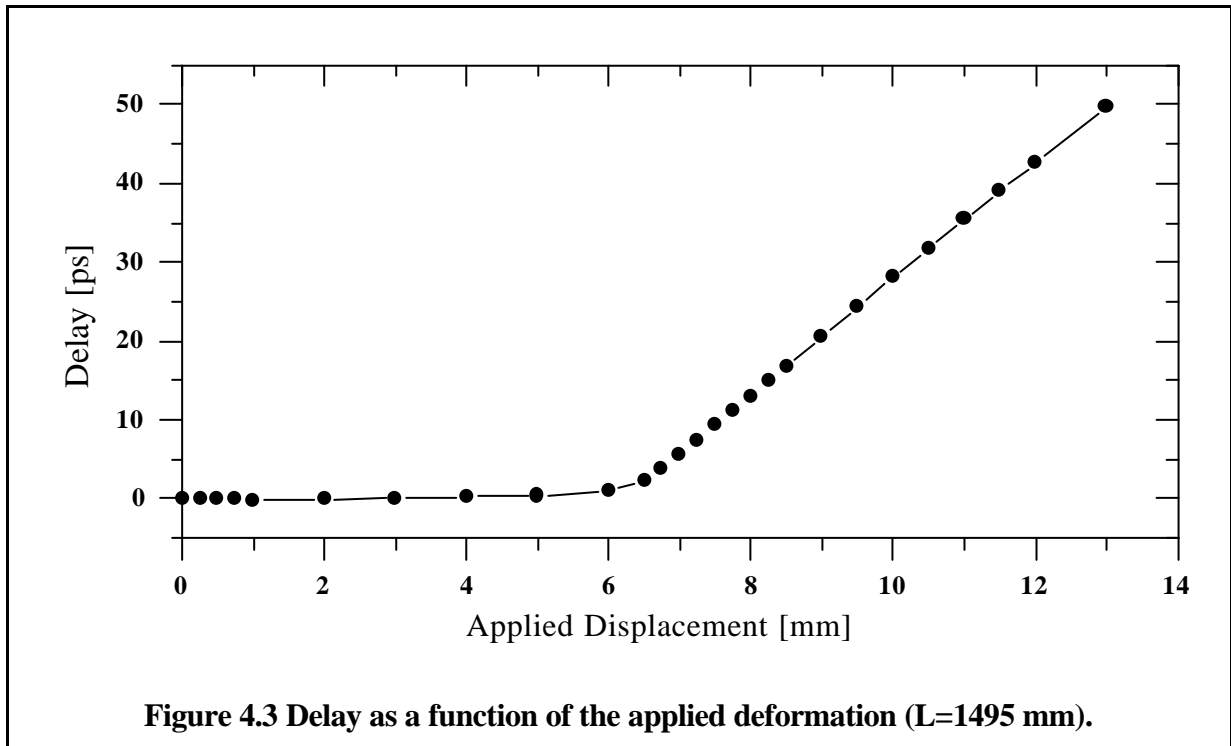
4.3.3 Temperature sensitivity

If we change the temperature of the fiber by dT , (5) becomes [5]:

$$\frac{dt}{L dT} = \frac{2}{c} \left(\frac{n}{L} \frac{dL}{dT} + \frac{dn}{dT} \right) \quad (17)$$

We have once again assumed that n_{eff} equals n .

The first term in the sum represents the length variation of the fiber due to the non zero thermal



expansion coefficient, while the second represents the contribution given by the temperature dependence of the index of refraction.

As seen in chapter 4.2.2:

$$\frac{n}{L} \frac{dL}{dT} = 0.73 \cdot 10^{-6} / ^\circ C \quad (18)$$

and [3]:

$$\frac{dn}{dT} = 10^{-5} / ^\circ C \quad (19)$$

The index change is therefore (and somehow surprisingly) the dominating effect.

This gives us from (17) and for finite temperature variations:

$$L \Delta T = k_{TF} \Delta t \quad (20)$$

with

$$k_{TF} = 14.0 \frac{^\circ C m}{ps} \quad (21)$$

This material constant gives the necessary temperature variation that has to be imposed to a free fiber to obtain a unitary change in the delay.

We also define a constant taking into account only the contribution of the temperature dependent refractive index:

$$k_{Tn} = \frac{c}{2} \frac{1}{dn/dT} = 15 \frac{^\circ C m}{ps} \quad (22)$$

4.3.4 Coatings

Most fibers are manufactured with coatings to protect them from aging agents like humidity. Since these coatings have, in general, a much higher thermal expansion coefficient than the one of silica, we should consider their influence on the thermal expansion coefficient of the system. Lets consider an optical fiber and a coating with elasticity modules E_f and E_c , thermal expansion coefficients \mathbf{a}_f and \mathbf{a}_c as well as cross-sections A_f and A_c .

If we assume that under temperature changes the fiber sections remains plain⁶ and therefore impose the same deformation for both material or an opposed force between the two, we obtain:

$$\frac{dL}{L dT} = \frac{\mathbf{a}_f E_f A_f + \mathbf{a}_c E_c A_c}{E_f A_f + E_c A_c} \equiv \mathbf{a}_{fc} \quad (23)$$

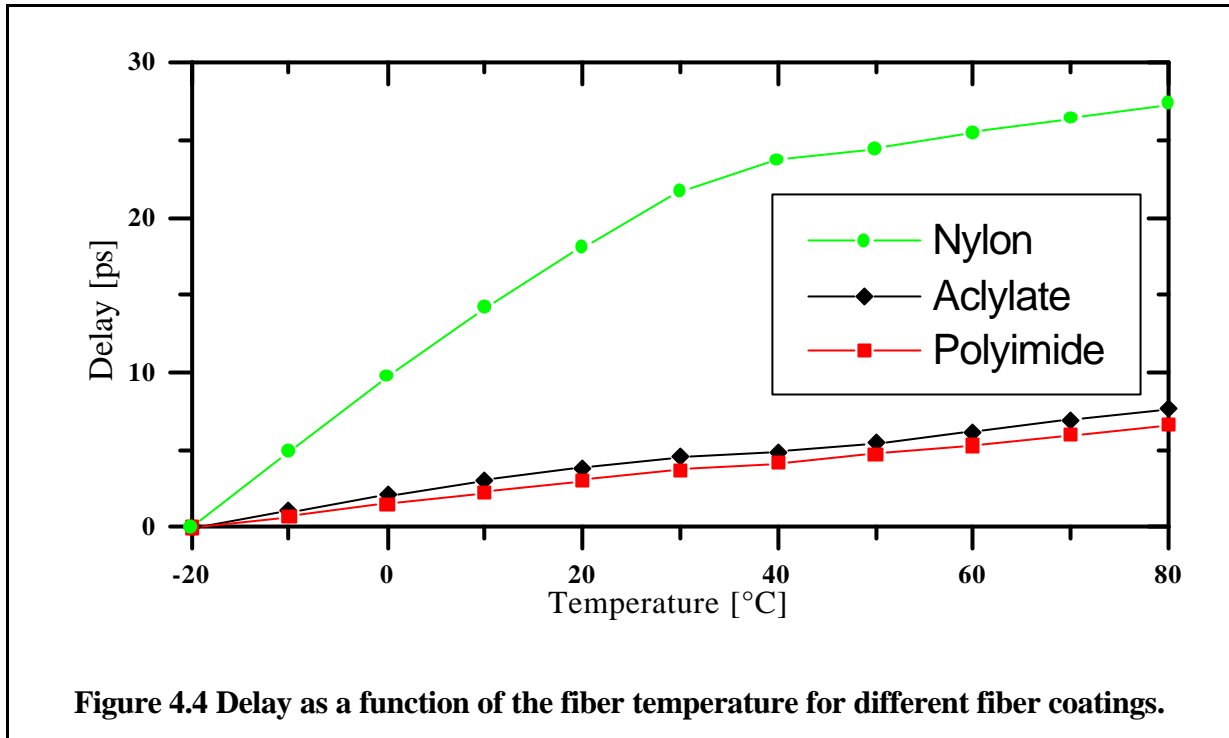
The fiber will therefore undergo a deformation of $L \mathbf{a}_{fc} \Delta T$ instead of the free deformation $L \mathbf{a}_f \Delta T$. This gives:

$$\Delta t = \frac{\Delta T}{k_{TF}} + \frac{\Delta L}{k_{stress}} = \frac{\Delta T}{k_{TF}} + \frac{L (\mathbf{a}_{fc} - \mathbf{a}_f) \Delta T}{k_{stress}} \quad (24)$$

and finally:

$$L \Delta T = \frac{1}{\frac{1}{k_{TF}} + \frac{\mathbf{a}_{fc} - \mathbf{a}_f}{k_{stress}}} \Delta t = k_{TC} \Delta t \quad (25)$$

⁶ i.e. the fiber does not slide inside its coating



We can therefore define a new constant k_{TC} :

$$k_{TC} = \frac{1}{\frac{1}{k_{TF}} + \frac{\mathbf{a}_{fc} - \mathbf{a}_f}{k_{stress}}} \quad (26)$$

It is also useful to define a constant k_{Tm} taking into account only the mechanical effect of the coating on the fiber and excluding the effect of the temperature dependence of the refractive index.

$$k_{Tm} = \frac{1}{\frac{1}{k_{TC}} - \frac{1}{k_{Tn}}} \quad (27)$$

In the (not so unusual) case of fibers with multiple layers of coating, all the coatings can be reduced to a single coating. To reduce n coatings with an elasticity modules E_n , thermal expansion coefficients \mathbf{a}_n as well as a cross-sections A_n , one can define an equivalent thermal expansion coefficient:

$$\mathbf{a}_c = \frac{\sum_n \mathbf{a}_n E_n A_n}{\sum_n E_n A_n} \quad (28)$$

and an equivalent Hooke constant:

$$E_c A_c = \sum_n E_n A_n \quad (29)$$

These equivalent values can than be used in equation (23) and (26).

Since it is not always possible to know the material constants of all coating layers, the constant k_{TC} is best measured experimentally.

In Figure 4.4 we plot an experimental curve showing the measured delay as a function of the fiber temperature and for different fiber coatings. The fibers were placed in a temperature controlled cabinet. It is evident that the nylon coated fiber undergoes a transition near 30°C. It seems that at this temperature the fiber starts to slip inside the nylon coating and assumes therefore a thermal expansion coefficient close to the one of an acrylate coated fiber. It must be recalled that the nylon coating is deposited on top of an acrylate coating. This same behavior has been found in embedded acrylate coated fibers. We can therefore conclude that this transition is due to a softening of the first (inner) acrylate coating.

Fiber coating	External fiber diameter [μm]	k_{TC} [$^{\circ}\text{C}.\text{m}/\text{ps}$]	k_{Tm} [$^{\circ}\text{C}.\text{m}/\text{ps}$]	Price [SFr/m]
none (theoretical data)	125	14	210	-
acrylate (2 layers)	250	10.9	39.6	0.1
polyimide	145	13.3	120	3
nylon tight buffered fiber gray	900	2.29	2.7	0.5

Table 4.2. Temperature variation required to introduce a variation of 1 ps in the time of flight for different fiber coatings. The indicative price per meter is also listed.

In Table 4.2 we compare the thermal expansion coefficient of differently coated fibers. It is clear from these results that the acrylate and polyimide coatings do not alter in a significant way the thermal expansion coefficient of the fibers. This is due to the reduced thickness and stiffness of these coatings. Nylon tight buffered fibers show, on the other hand, a dramatic increase of the temperature sensitivity due to the large thermal expansion coefficient of nylon and the significant thickness of the coating.

Since differently coated fibers show different thermal expansion coefficients, it is possible to use pairs of such fibers to measure integrated temperature variations [6]. If both fibers are installed side by side and have the same temperature, the differential thermal expansion coefficient of the coatings will produce a variation of the measured delay proportional to the integrated temperature variation:

$$\Delta t = \frac{1}{k_{1TC} - k_{2TC}} \int_{Path} \Delta T dL \quad (30)$$

Where

k_{iTC} is the effective thermal expansion coefficient of fiber i

If the temperature variation is constant along the path we find:

$$\Delta T L = (k_{1TC} - k_{2TC}) \Delta t \quad (31)$$

A fiber pair with, respectively, primary coating and nylon coating shows a sensitivity of about $3.45^{\circ}\text{C}.\text{m}/\text{ps}$. The response is however linear only between -25°C and $+30^{\circ}\text{C}$. At higher temperatures, the fiber seems to slip inside its coating.

This type of sensor will measure only temperature variations and not the absolute temperature. If the delay is first measured for a given temperature, e.g. in a temperature controlled cabinet, an absolute measurement becomes possible. These sensors should be used only in the linear temperature range of both coatings.

4.3.5 Embedded optical fiber sensors

For most sensing applications, one of the fibers will be in mechanical contact to the host structure in order to measure its displacement. We have seen in chapter 4.3.2 how the fiber sensor would react to length variations of the host structure. In this case we assume that the fiber is stressed only axially and no external force is applied transversally. In this latter case it would be impossible to separate the three stress components with only one measurement. For most sensor setups proposed in this work, no transversal stress will be applied to the fibers and the results of chapter 4.3.2 can be used without modifications.

It is now important to study the influence of the structure temperature on the measured delay. If the measurement fiber is in mechanical contact with the host structure, it will inherit its thermal expansion coefficient. If we consider the structure as a coating with infinite stiffness, equation (25) becomes:

$$L \Delta T = \frac{1}{\frac{1}{k_{TF}} + \frac{\mathbf{a}_s - \mathbf{a}_f}{k_{stress}}} \Delta t = k_{TS} \Delta t \quad (32)$$

Besides the desired sensitivity to the temperature induced length variation of the structure, we obtain a parasitic sensitivity due to the temperature dependence of the index and the strain of the fiber.

It is possible to reduce this sensitivity further by installing (e.g. in a pipe) a reference fiber which is not subject to the strain variations induced by the host structure but has its same temperature and measure the variations of the path unbalance between the two. In this case the effects of the temperature dependence of the refractive index will cancel between the two fibers. The free fiber will however maintain its (low) thermal expansion coefficient⁷

$$\frac{n}{L} \frac{dL}{dT} = 0.73 \cdot 10^{-6} / ^\circ C .$$

We consider now the case of a free structure undergoing at the same time a deformation ΔL and a temperature variation ΔT . We assume that the reference fiber is installed near the measurement fiber and has the same temperature. The linear thermal expansion coefficient of the host structure is given by \mathbf{a}_s .

The measurement fiber (i.e. the one attached to the structure) will introduce the delay:

$$\Delta t_m = \frac{\Delta L}{k_{stress}} + \frac{L \Delta T}{k_{TS}} \quad (33)$$

while the reference fiber (i.e. the one installed in the pipe) will introduce the delay:

$$\Delta t_n = \frac{L \Delta T}{k_{TC}} \quad (34)$$

If we measure the difference between the two we obtain:

$$\Delta t = \frac{\Delta L}{k_{stress}} + L \Delta T \left(\frac{1}{k_{TF}} + \frac{\mathbf{a}_s - \mathbf{a}_f}{k_{stress}} - \frac{1}{k_{TF}} - \frac{\mathbf{a}_{fc} - \mathbf{a}_f}{k_{stress}} \right) \quad (35)$$

or

$$\Delta t = \frac{\Delta L}{k_{stress}} + \frac{\mathbf{a}_s L \Delta T}{k_{stress}} - \frac{\mathbf{a}_{fc} L \Delta T}{k_{stress}} \quad (36)$$

⁷ We assume here that a fiber with a thin or loose coating is used.

The first two terms correspond to real length variations of the structure, while the latest is a parasitic sensitivity in the temperature introduced by the reference fiber and its coating. It is interesting to notice that the effect of the temperature dependence of the refractive index has been eliminated.

Since the coefficient \mathbf{a}_{fc} depends on the fiber coating it can be chosen to achieve different effects. If we choose a fiber with a very low \mathbf{a}_{fc} (e.g. a fiber with the primary coating, only) we obtain a sensor with very low temperature dependence. This would allow the measurement of the temperature-induced deformations in the structure. For typical concrete we find:

$$\mathbf{a}_s = 10 \frac{\mathbf{m}}{^\circ\text{C}\cdot\text{m}} \quad (37)$$

while for the bare reference fiber we find:

$$\mathbf{a}_{fc} = \mathbf{a}_f = 0.5 \frac{\mathbf{m}}{^\circ\text{C}\cdot\text{m}} \quad (38)$$

which is twenty times smaller.

In general, if we use a reference fiber with a given \mathbf{a}_{fc} and interpret incorrectly a temperature induced parasitic delay as a deformation we will find an apparent displacement of:

$$\Delta L_T = \mathbf{a}_{fc} L \Delta T \quad (39)$$

For a fiber with only the primary coating, this parasitic temperature dependence is half of the one of an invar bar.

Another interesting case is the one where the fiber coating is chosen in order to obtain: $\mathbf{a}_s = \mathbf{a}_{fc}$. In this case we are able to compensate the temperature induced displacements in the structure by an identical displacement in the reference fiber. Since the \mathbf{a}_{fc} required to compensate the thermal induced displacements of a concrete structure lies between the ones of primary coated fibers and 900 μm nylon coated fibers, it should be possible to manufacture a special fiber with the appropriate nylon coating thickness. This derivation is valid only for free structures where one can actually calculate the deformation by multiplying \mathbf{a}_s with the temperature variation ΔT . For structures that are bound to external constraints or have particular shapes and are submitted to gravity⁸ this approximation could give unreliable results. Furthermore, the thermal expansion coefficient of many construction materials (e.g. concrete) can be variable and therefore unpredictable.

To achieve even higher precision, it is necessary to separate the effects of temperature and strain by measuring the integrated temperature variations. This can be done by adding a second reference fiber with a different coating as seen in paragraph 4.3.4.

4.4 Error estimation

As seen in the previous section, to obtain a measurement of a relative quantity ΔQ , one measures a delay Δt and then multiplies it by a coefficient k .

$$\Delta Q = k \Delta t \quad (40)$$

In general k and Δt are known with an error $\mathbf{d}k$ and $\mathbf{d}\Delta t$, respectively. The error $\mathbf{d}\Delta Q$ on the measurement will therefore be given by:

$$\mathbf{d}\Delta Q = \mathbf{d}k \Delta t + k \mathbf{d}\Delta t \quad (41)$$

⁸ Like most structures on earth and neighboring planets. The approximation is however satisfactory in the interesting case of free falling or orbiting structures...

The first term is given by an error in the estimation of the proportionality factor k and is proportional to the measured ΔQ or Δt . This term is therefore dominant for large variations of Q . The second term is given by the error in the measurement of the delay Δt and is independent from ΔQ and Δt and therefore dominant for small variations of Q .

It is interesting to notice that both terms are independent from the length L of the measurement base. The relative precision will therefore increase linearly for increasing measurement bases.

4.5 Conclusions

We have demonstrated that optical fibers are excellent displacement sensors. They show linear response to strain and can accept displacements up to 2-8%. These fibers are however subject to thermal apparent strain, this is mostly the result of the temperature dependent refractive index. It is suggested to use a reference fiber that has the same temperature that the measurement fiber. In this case we obtain only a small temperature dependence given by the thermal expansion coefficient of the reference fiber. In the case of free fibers (e.g. the reference fiber) special care must be taken in the choice of the fiber coatings. These can have a dramatic influence on the thermal sensitivity of the fibers and can therefore be used as integrated temperature sensors. By choosing an appropriate coating for the reference fiber, it is possible to achieve interesting temperature effects like a compensation of the thermal deformations of the structure itself.

In Table 4.3 we resume the different coefficient introduced in this chapter.

Coefficient	Symbol	Unit	Typical value
Time of flight variations without strain (cutting fibers).	k_{cut}	$\frac{m}{ps}$	103
Time of flight variations under strain (displacement sensor).	k_{stress}	$\frac{m}{ps}$	128
Time of flight variations under temperature changes (free and uncoated fiber).	k_{TF}	$\frac{^{\circ}C m}{ps}$	14
Time of flight variations under temperature induced variations of the refractive index.	k_{Tn}	$\frac{^{\circ}C m}{ps}$	15
Time of flight variations under temperature changes (free and coated fiber).	k_{TC}	$\frac{^{\circ}C m}{ps}$	depends on the coating
Time of flight variations under temperature changes (free and coated fiber) excluding index variations.	k_{Tm}	$\frac{^{\circ}C m}{ps}$	depends on the coating
Time of flight variations under temperature changes (fiber embedded or attached to a structure).	k_{TS}	$\frac{^{\circ}C m}{ps}$	depends on the structure

Table 4.3. Proportionality coefficient for different types of perturbation.

4.6 Bibliography

- [1] E. Udd "Fiber Optic Sensors", Wiley, 1990
- [2] E. Hecht "Optics", Addison-Wesley, 1974-1987
- [3] H. Murata "Handbook of optical fibers and cables", Dekker, 1988
- [4] C. D. Butter and G. B. Hocker "Fiber optics strain gage", Applied Optics, Vol. 17, No. 18, Sept. 1978
- [5] G. B. Hocker "Fiber-optic sensing of pressure and temperature", Applied Optics, Vol. 18, No. 9, May 1979
- [6] D. Inaudi "Coherence multiplexing of in-line displacement and temperature sensors", Optical Engineering, Vol. 34, Nr.7, July 1995

5. Low-coherence interferometry

"If, however, the source is not homogeneous, the clearness or visibility of the fringes will diminish as the difference in the path of the two interfering pencils increases, and in general will vary in manner depending on the nature of the source".

Albert A. Michelson
Studies on Optics, 1927

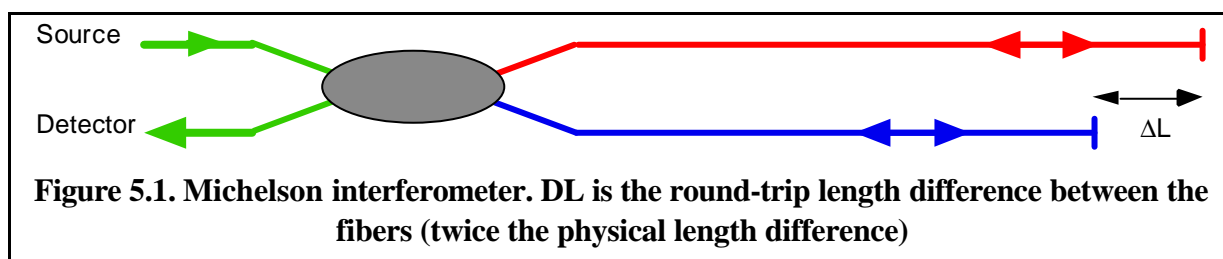
The principle of low coherence interferometry is discussed in this section. We will first introduce the concept of optical interference for an ideally coherent source and then extend it to partially coherent sources. Path-matching or coherence-recovery interferometers are described in detail with emphasis on their use for demodulating interferometric sensors. The effects of polarization and optical fibers birefringence are also analyzed. We will finally discuss the limiting factors for using such an interferometric arrangement in a remote sensing setup.

5.1 Introduction

Interferometric sensors are based on the principle of optical interference. This phenomenon is one of the results of the wave-nature of electromagnetic radiation. The propagation of light¹ can be expressed by a complex vector field describing the intensity and phase of the electric (or magnetic) field in each point of the space. This field has to be a solution of the Maxwell equations or, in the case where no charges or magnetic dipoles are present, by the wave equations. Since all the detectors we can use to observe this radiation (e.g. our eyes, a photodiode or a pyrometer) are sensitive only to the intensity of this radiation (not its amplitude) and have a detection bandwidth by many orders of magnitude lower than the oscillation frequency of light², we cannot measure the phase of the incoming radiation directly. Since the electromagnetic field is unique, it is however possible to superpose two light-waves having a constant phase relationship and obtain locally a constructive or destructive combination, i.e. a sum or subtraction of the amplitudes that results in an increased or decreased detected intensity. This effect is called *interference* and can be used to obtain an indirect measurement of the phase and therefore allows the realization of highly sensitive measurements. These sensors are however of incremental type and a continuous monitoring of the sequence of constructive and destructive interference is necessary. The constant phase relationship between two waves is referred as *coherence* [1 cp. 5 , 2]. We will show that the coherence properties are directly related to the spectral characteristics of the source used to produce the light-waves. A source with a reduced coherence can be used in order to obtain absolute (non incremental) measurement with interferometric precision.

5.2 Perfectly coherent interferometers

In order to introduce the concept of optical fiber interferometers, we will first consider a Michelson setup (see Figure 5.1) with an ideally coherent light source.



All the fibers are supposed to be of monomode type. It should be noted that these fibers usually propagate two independent orthogonal polarization. The effect of polarization will be analyzed in chapter 5.5, and we will, for the time being, restrict to a scalar EM field.

The electric component of the EM emitted by the source can be described by:

$$E(x, t) = \text{Re} \left(E_0 e^{i(\omega t - kx + \Phi_0)} \right) \quad (1)$$

¹ We use the word "light" to describe any form of EM radiation and not only visible light.

² This is not the case for radio waves that have much lower oscillation frequencies.

Where $\boldsymbol{w} = 2\boldsymbol{p}n$ is the optical angular velocity, $k = 2\boldsymbol{p}n/\boldsymbol{l}$ the propagation constant and Φ_0 the initial phase. E_0 represents the amplitude of the electric field. We will from now on drop the Re operator and consider a complex electric field. We will furthermore assume $E_0 = 1$.

It is evident from Figure 5.1 that the light can propagate from the source to the detector following two independent path of total length L_1 and L_2 . Part of these path is common (the lead-in and lead-out fibers) while other is separate (the two interferometer arms). The amplitude at the detector will therefore be given by:

$$E(x_D, t) = E_1 e^{i(\boldsymbol{w} - kL_1 + \Phi_0)} + E_2 e^{i(\boldsymbol{w} - kL_2 + \Phi_0)} \quad (2)$$

Where E_i indicates the amplitude returned by each path.

The detector will measure the intensity of this field and integrate it over a period much longer than $2\boldsymbol{p}/\boldsymbol{w}$ and therefore obtain:

$$I_D = \langle E(x_D, t) E^*(x_D, t) \rangle = E_1^2 + E_2^2 + 2E_1E_2 e^{ik\Delta L} \quad (3)$$

where $\langle \rangle$ indicates an integral over the integration time of the detector.

If we define:

$$I_1 = E_1^2 \text{ and } I_2 = E_2^2 \quad (4)$$

representing the intensities returned by each arm, (3) becomes:

$$I_D = I_1 + I_2 + 2\sqrt{I_1I_2} \cos(k\Delta L) \quad (5)$$

Or:

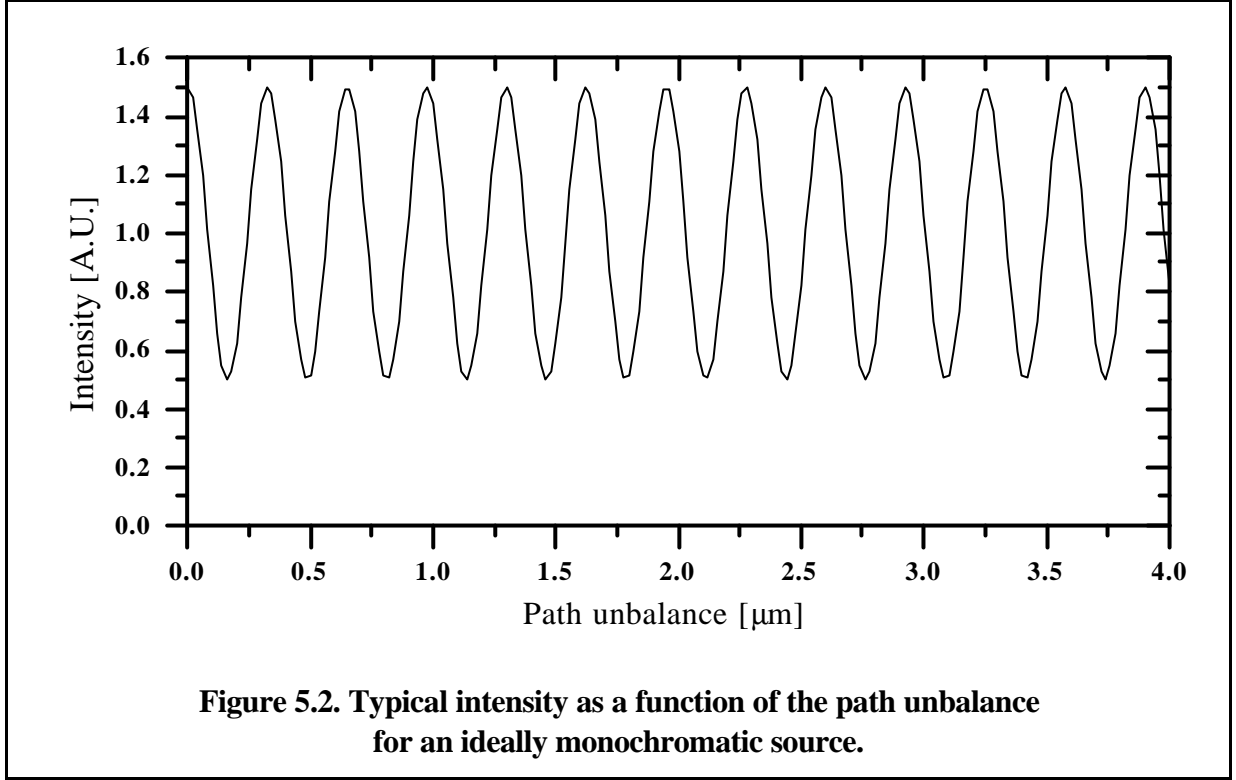
$$I_D = I_0(1 + V \cos(k\Delta L)) \quad (6)$$

with:

$$I_0 = I_1 + I_2 \quad (7)$$

and the visibility of the interference fringes given by:

$$V = \frac{I_{\max} - I_{\min}}{I_{\max} + I_{\min}} = \frac{2\sqrt{I_1I_2}}{(I_1 + I_2)} \quad (8)$$



In Figure 5.2. we plot the measured intensity as a function of the path unbalance between the two interferometer arms. The sinusoidal intensity modulation has the same visibility independently from the magnitude of the path unbalance. Knowing the phase in a single point of the interferogram, it is possible to predict it for every other path unbalance. The coherence of the source is therefore infinite.

5.3 Partially coherent interferometers

We will now consider the case of an interferometer using a source with a finite coherence length (i.e. with a non-zero spectral bandwidth) and a normalized power emission. The spectrally resolved intensity of the source will be given by:

$$I_S = I_S(k) \text{ with } \int_k I_S(k) = 1 \quad (9)$$

For each wavelength we obtain an amplitude which is given by (3). Since the detector is wavelength-blind the amplitude must be integrated and we obtain:

$$I_D(\Delta L) = \int_k I_{Det}(k) I_S(k) \left(E_1(k)^2 + E_2(k)^2 + 2E_1(k)E_2(k) e^{ik\Delta L} \right) dk \quad (10)$$

Where we have considered an explicit wavelength dependence of the reflectivity of the two interferometer arms. If the detector has a wavelength independent efficiency we can assume $I_{Det}(k) = 1$. If we define:

$$I_0 = \int_k I_S(k) \left(E_1(k)^2 + E_2(k)^2 \right) dk \quad (11)$$

as the incoherent power spectra returned by the two arms, we obtain:

$$I_D(\Delta L) = I_0 + \int_k 2E_1(k)E_2(k) I_S(k) e^{ik\Delta L} dk \quad (12)$$

Equation (12) shows that the path unbalance dependence of the detected intensity is given (except for an additive constant) by the Fourier transform of the intensity spectrum of the source multiplied by the reflectivity of the two interferometer arms.

In some case it is interesting to consider a source with an emission centered around a given wavevector k_0 . In this case (12) becomes:

$$I_D(\Delta L) = I_0 + e^{i k_0 \Delta L} \int_{\Delta k} 2E_1(k_0 + \Delta k)E_2(k_0 + \Delta k) I_s(k_0 + \Delta k) e^{i\Delta k \Delta L} d(\Delta k) \quad (13)$$

or

$$I_D(\Delta L) = I_0(1+V(\Delta L) e^{i k_0 \Delta L}) \quad (14)$$

with:

$$V(\Delta L) = \frac{\int_{\Delta k} 2E_1(k_0 + \Delta k)E_2(k_0 + \Delta k) I_s(k_0 + \Delta k) e^{i\Delta k \Delta L} d(\Delta k)}{I_0} \quad (15)$$

where V is the visibility of the fringes.

Equation (15) is almost identical to (6) except for the fact that the visibility term depends now on the path unbalance ΔL .

Furthermore, if we define the Fourier transform³ of the power spectra:

$$\tilde{I}_s(\Delta L) = \int_{\Delta k} I_s(k_0 + \Delta k) e^{i\Delta k \Delta L} d(\Delta k) \quad (16)$$

we find assuming a constant reflectivity of the mirrors inside the emission spectra:

$$V(\Delta L) = \frac{2 E_1(k_0)E_2(k_0) \tilde{I}_s(\Delta L)}{I_0} \quad (17)$$

Let's now consider a few interesting cases:

5.3.1 Monochromatic source

In first approximation a monomode laser can be considered as a monochromatic source. This case has already been considered in chapter 5.2. If we want to consider this case in the Fourier transform formalism we have to use a Dirac function at k_0 as the spectral power distribution:

$$I_s(k) = \mathbf{d}(k - k_0) \quad (18)$$

Which gives:

$$V(\Delta L) = \frac{2 E_1(k_0) E_1(k_0)}{E_1^2(k_0) + E_1^2(k_0)} \quad (19)$$

Since the Fourier transform of a Dirac function centered in zero gives a constant. This result is identical to the one given in (8).

³ "constants free" and after translation to k_0 .

5.3.2 Multiple monochromatic sources

The emission of a longitudinally multimode laser can be considered as a superposition of monochromatic sources with n wavevectors k_i . The spectral power distribution becomes:

$$I_s(k) = \sum_{i=0}^{n-1} r_i \mathbf{d}(k - k_i) \quad (20)$$

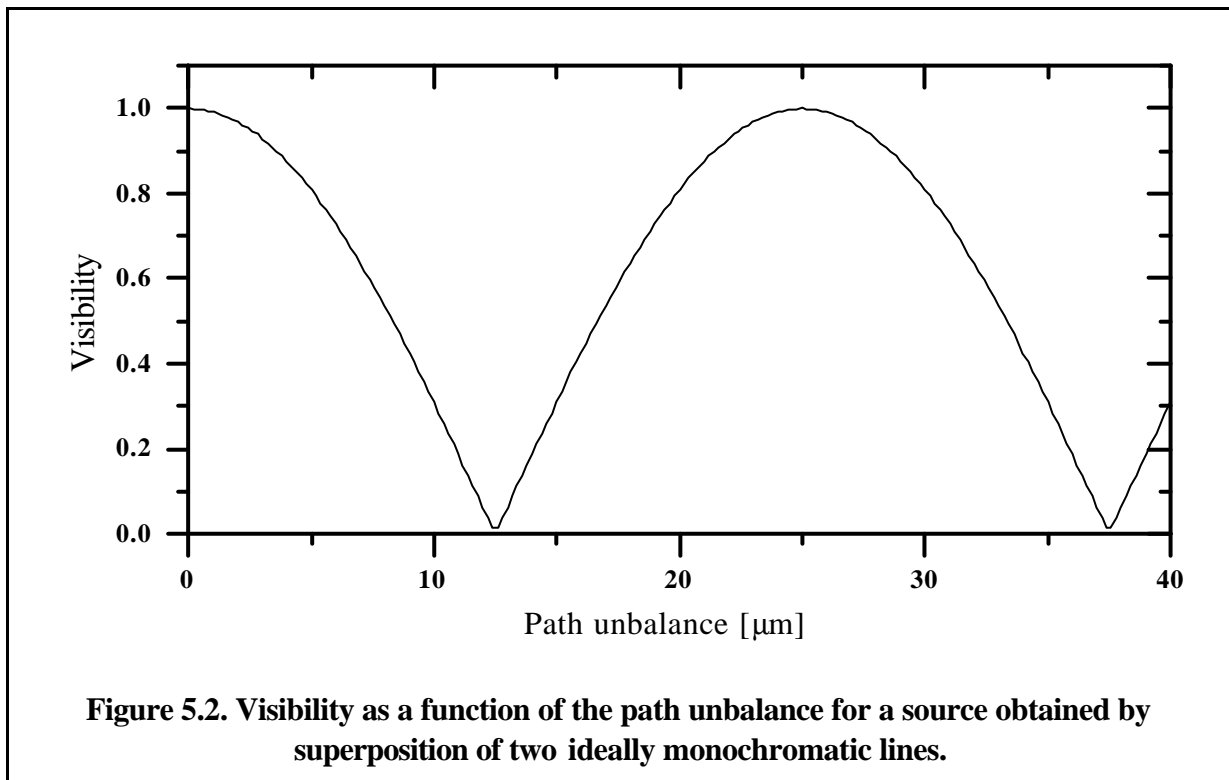
where r_n is the relative intensity of the emission lines and:

$$\sum_{i=0}^{n-1} r_i = 1 \quad (21)$$

In this case the visibility becomes:

$$V(\Delta L) = \sum_{i=1}^{n-1} 2 r_i e^{i(k - k_0)\Delta L} \quad (22)$$

The visibility varies therefore periodically in a typical beating figure. The period of this beating will increase with decreasing spacing between the modes. If the different emission lines have comparable intensities the visibility can drop to very low figures.



5.3.3 Rectangular spectra

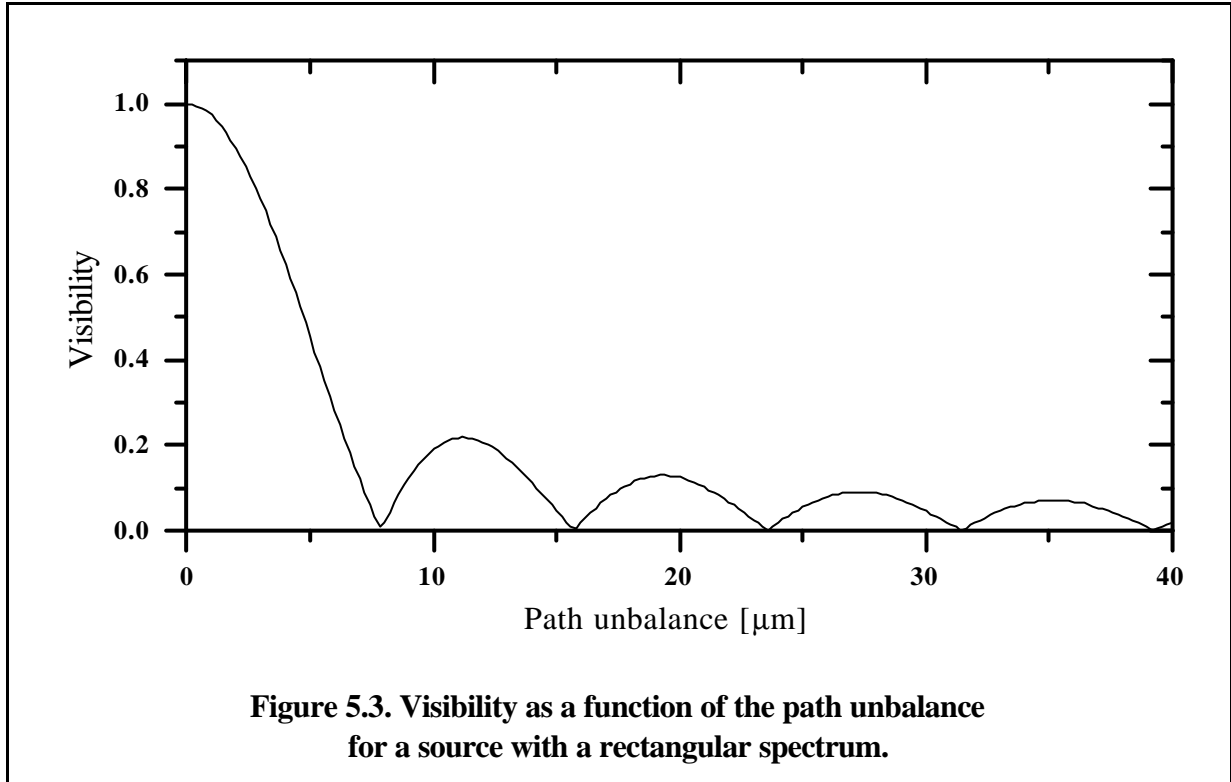
If the source emits over a rectangular wavelength domain:

$$I_s(k) = \text{rect}_{\frac{\mathbf{d}k}{2}}(k - k_0) = \begin{cases} \frac{1}{\mathbf{d}k} & \text{for } |k - k_0| < \frac{\mathbf{d}k}{2} \\ 0 & \text{otherwise} \end{cases} \quad (23)$$

The visibility becomes:

$$V(\Delta L) = \frac{\sin\left(\frac{\Delta L \mathbf{d}k}{2}\right)}{\frac{\Delta L \mathbf{d}k}{2}} \quad (24)$$

The visibility will therefore decrease with increasing path unbalance.



5.3.4 Gaussian spectra

Gaussian spectra are typical for the emission of thermal sources (e.g. an halogen lamp), low pressure discharge lamps as well as of the amplified spontaneous emission occurring in a superluminescent diode. In this case the power spectrum is given by:

$$I_s(k) = \frac{1}{\sqrt{2\mathbf{p}}} e^{-\left(\frac{k-k_0}{2\mathbf{d}k}\right)^2} \mathbf{d}k \quad (25)$$

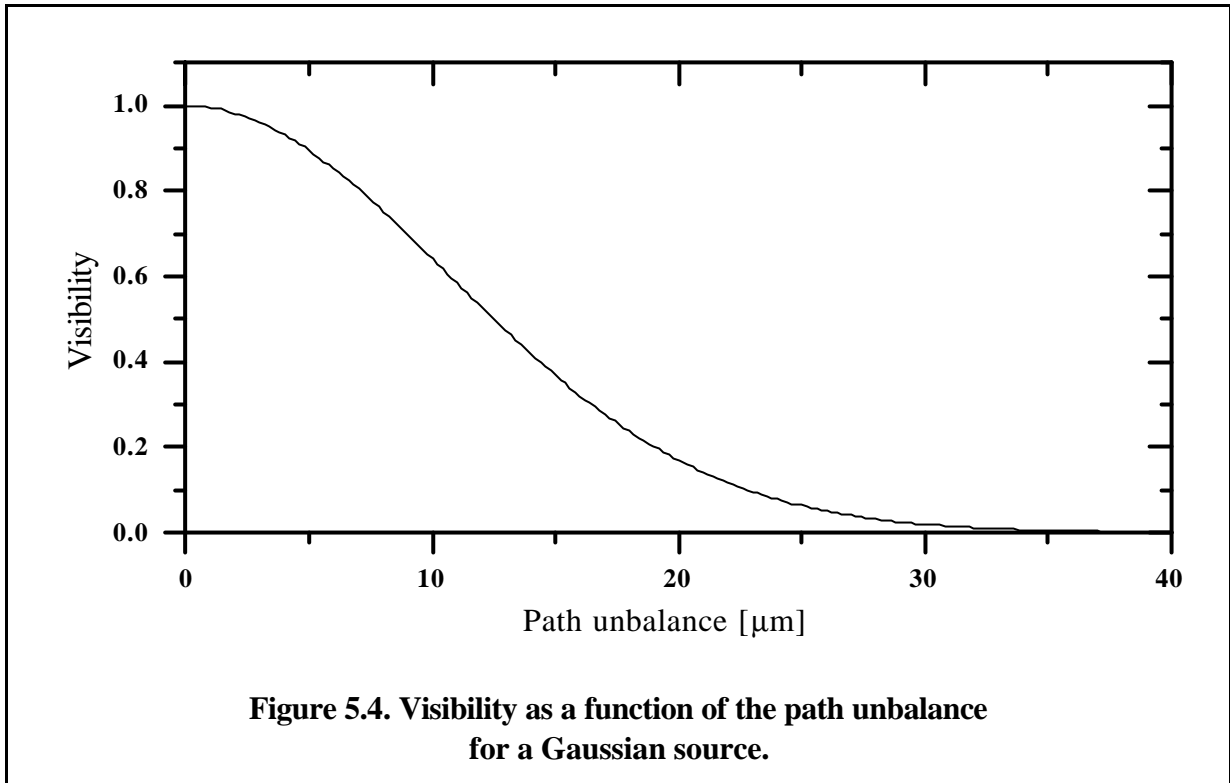
where $\mathbf{d}k$ represents the spectral width of the source.

The visibility will be given by:

$$V(\Delta L) = 2 \frac{e^{-\left(\frac{\Delta L \mathbf{d}k}{2}\right)^2}}{\mathbf{d}k} \quad (26)$$

The visibility function is also Gaussian, its width being proportional to the inverse of the spectral width. The visibility will fade for path unbalances greater than the coherence length:

$$L_c = \frac{2\mathbf{p}}{\mathbf{d}k} \quad (27)$$



5.3.5 Lorentzian spectra

Lorentzian spectral distributions are common for high-pressure discharge lamps and laser diodes below a threshold:

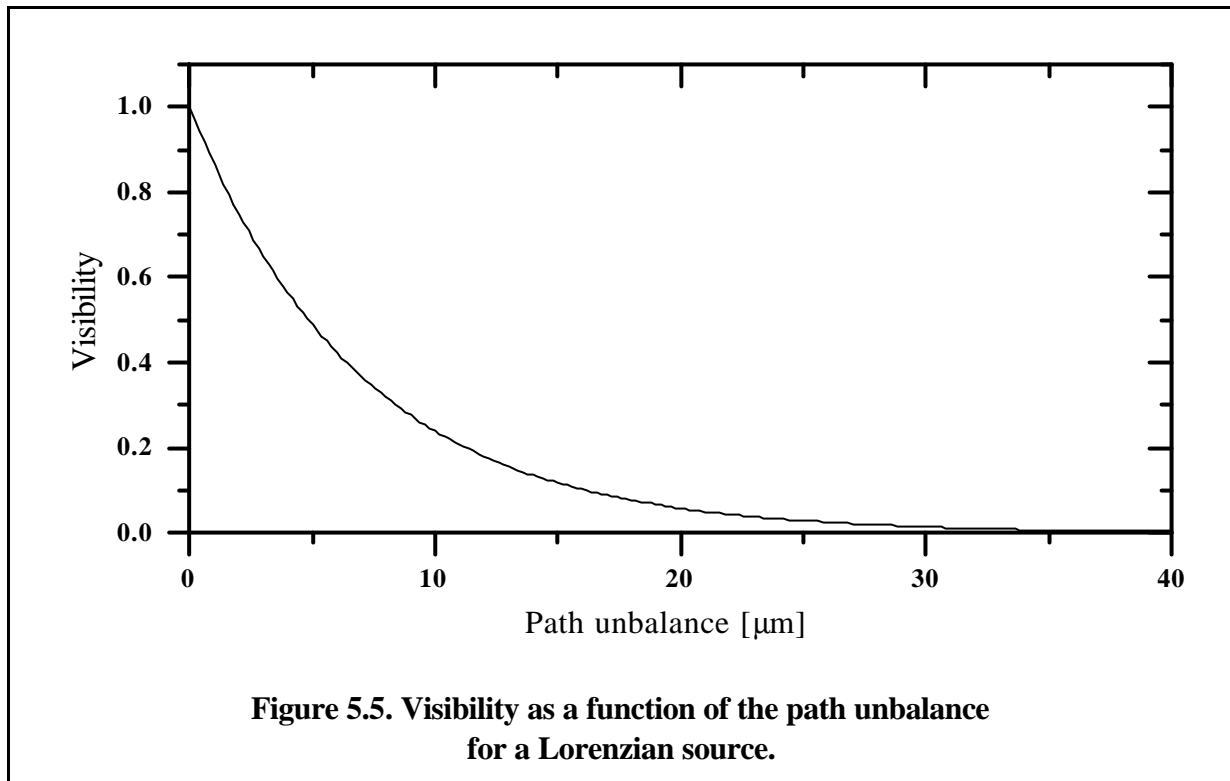
$$I_s(k) = \frac{2 \mathbf{d}k}{\mathbf{p}(\mathbf{d}k^2 + 4(k - k_0)^2)} \quad (28)$$

In this case the visibility is given by:

$$V(\Delta L) = e^{-\mathbf{p} \mathbf{d}k \Delta L} \quad (29)$$

and the visibility of the fringes fades for path unbalances greater than:

$$L_c = \frac{2\mathbf{p}}{\mathbf{d}k} \quad (30)$$



5.3.6 Wavelength selective mirrors

If the two arms of the interferometer are spectrally selective, equation (15) show that the visibility can also be affected. For each wavelength that is not emitted and transmitted by both arms, the integrand will vanish. For most cases the component with the most restrictive optical bandwidth will be the source, but in some cases (e.g. fiber Bragg gratings) the spectral reflectivity of the interferometer arms will dominate and therefore influence the visibility of the fringes and increase the coherence length of the source.

5.3.7 Conclusions

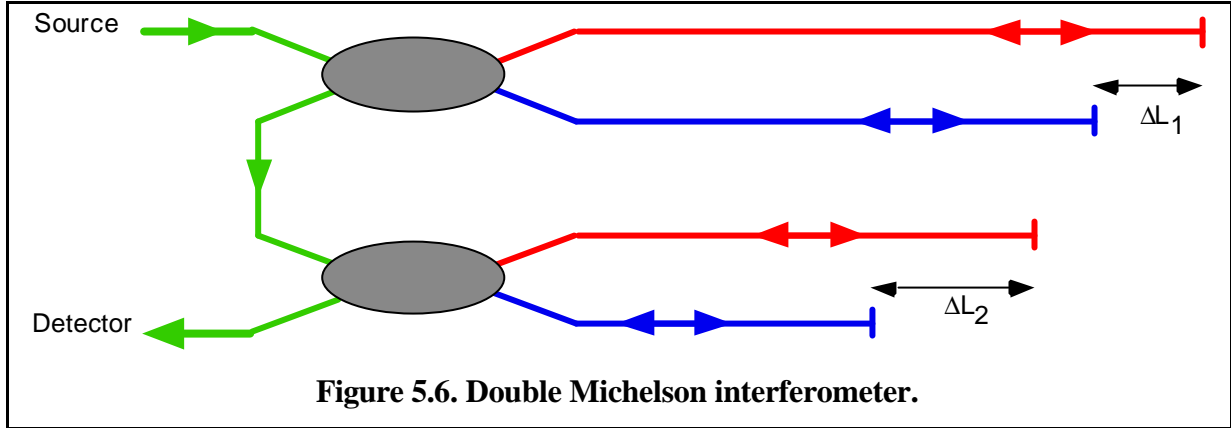
The choice of the spectral profile of the source used in an interferometric setup depends on the type of demodulation that will be used. In the case of high-coherence interferometer, where the variations of ΔL are measured incrementally by fringe counting and/or phase tracking, it is interesting to use a source giving a visibility function as flat as possible over large ΔL ranges. In this case a laser will be the most appropriate source. A good wavelength stability and a narrow spectral emission are very important in this case. Distributed feedback or multiple section laser diodes with temperature stabilization offer sufficient performances for this type of measurements, even for large path unbalances.

In this work we have decided to concentrate on low coherence interferometry. In this case we use the fading of the visibility resulting from a finite optical bandwidth, in order to get an absolute measurement of the path unbalance. From the previous examples it is clear that for most sources the maximum visibility is obtained for a vanishing path unbalance. In order to find this maximum precisely, it is interesting to use a source with a rapidly decreasing visibility

function. Broadband sources with Gaussian or Lorentzian profiles have this characteristic and are therefore well suited for this type of measurement.

5.4 Path-matching interferometers

We will now consider an interesting setup that allow the demodulation of the interferogram obtained by a Michelson interferometer as the one described in the previous chapters. Since the spectrum returned by the interferometer contains information about the path unbalance ΔL , it should be possible to measure it by an appropriate spectral analysis.



This can be done in an elegant way by adding a second *analyzing* Michelson interferometer after the first *measurement* interferometer as shown in Figure 5.6 [3,4]. The second interferometer will be used to perform a Fourier spectroscopy analysis of the spectra returned by the first interferometer.

The functional principle of this double interferometer can also be explained in terms of wavepackets. Both the spectral and the wave-packet analysis offer distinct advantages to explain some of the phenomena we will encounter later and are therefore introduced in the following chapters.

5.4.1 Spectral approach

The first (measurement) interferometer acts as a spectral filter and modifies the spectra content of the radiation coming from the source. The power spectra at its output will be given by:

$$I_1(k, \Delta L_1) = I_S(k) \left(E_{11}(k)^2 + E_{12}(k)^2 + 2E_{11}(k)E_{12}(k) e^{ik\Delta L_1} \right) \quad (31)$$

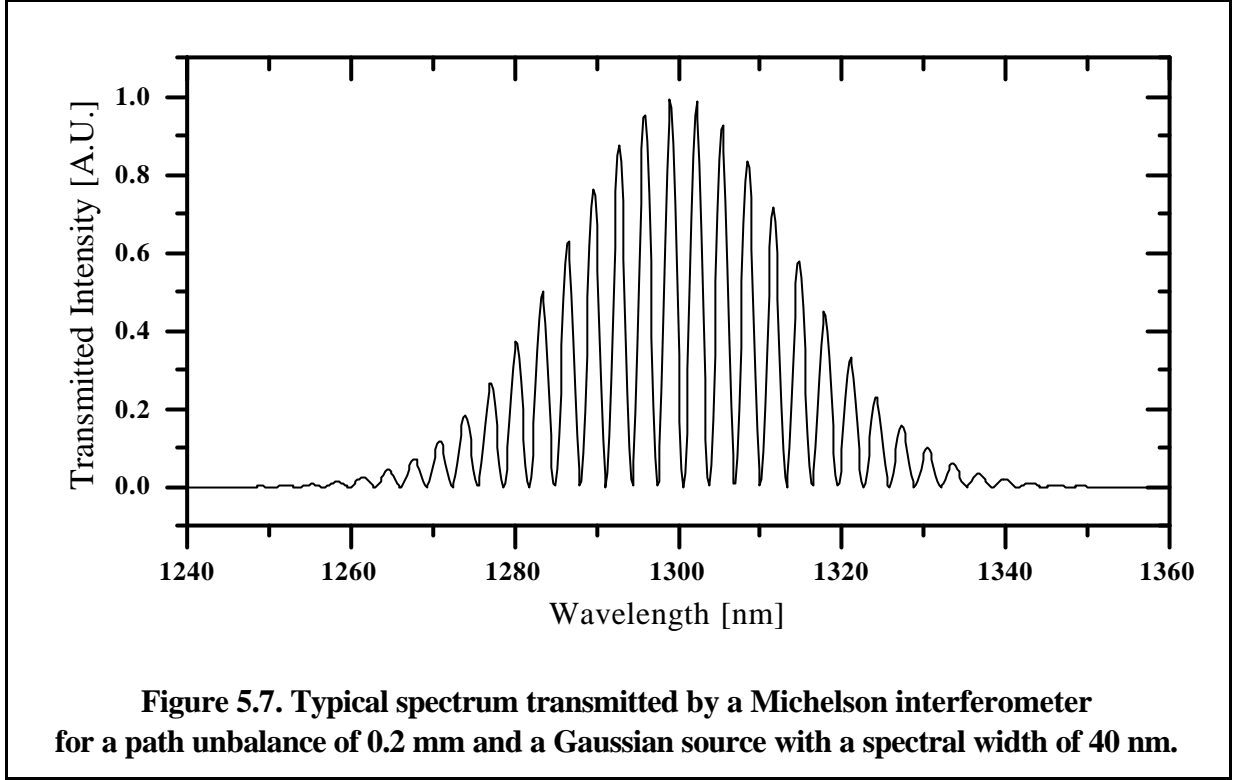
This is simply equation (10) without integration on k . This corresponds to the case of a wavelength selective detector. We see that the path unbalance ΔL_1 is encoded in the spectral content of I_1 . For a given ΔL , the transmitted spectra will have the same envelope as I_S , but will be modulated with an angular frequency $\frac{2p}{\Delta L_1}$.

At this point we have to reintroduce explicitly the Re operator. Since:

$$\text{Re}\left(e^{ix}\right) = \cos(x) = \frac{e^{ix} + e^{-ix}}{2} \quad (32)$$

equation (31) becomes:

$$(33)$$



$$I_1(k, \Delta L_1) = I_S(k) \left(E_{11}(k)^2 + E_{12}(k)^2 + E_{11}(k)E_{12}(k) \left(e^{ik\Delta L_1} + e^{-ik\Delta L_1} \right) \right)$$

Figure 5.7 shows a typical transmitted spectrum a function of the wavelength.

We have seen in the previous chapter that a Michelson interferometer can be used to analyze the spectrum of a given source. This same concept can now be applied to the measurement of I_1 and indirectly of ΔL_1 . If a second analyzing Michelson interferometer with a controllable path unbalance ΔL_2 is added after the first measurement interferometer, we obtain on the (wavelength blind) detector:

$$I_D(\Delta L_1, \Delta L_2) = \int_k I_S(k) \left(E_{21}(k)^2 + E_{22}(k)^2 + 2E_{21}(k)E_{22}(k) e^{ik\Delta L_2} \right) \left(E_{11}(k)^2 + E_{12}(k)^2 + E_{11}(k)E_{12}(k) \left(e^{ik\Delta L_1} + e^{-ik\Delta L_1} \right) \right) dk \quad (34)$$

If we, once again, define a term independent from ΔL_2 ⁴:

$$I_0(\Delta L_1) = \int_k I_S(k) \left[E_{11}^2 E_{21}^2 + E_{11}^2 E_{22}^2 + E_{12}^2 E_{21}^2 + E_{12}^2 E_{22}^2 + (E_{21}^2 + E_{22}^2) E_{11} E_{12} \left(e^{ik\Delta L_1} + e^{-ik\Delta L_1} \right) \right] dk \quad (35)$$

Where we have omitted the explicit wavelength dependence of the four reflectivity.

Equation (34) becomes:

⁴ The same could be done for ΔL_1 . The development presented here assumes that ΔL_1 is unknown and ΔL_2 can be measured and varied.

$$I_D(\Delta L_1, \Delta L_2) = I_0(\Delta L_1) + \int_k I_s(k) e^{ik\Delta L_2} \cdot \left(2(E_{11}^2 + E_{12}^2)E_{21}E_{22} + 2E_{11}E_{12}E_{21}E_{22} \left(e^{ik\Delta L_1} + e^{-ik\Delta L_1} \right) \right) dk \quad (36)$$

If we consider a source with its emission centered around k_0 we find:

$$I_D(\Delta L_1, \Delta L_2) = I_0(1 + V(\Delta L_1, \Delta L_2) e^{ik_0 \Delta L_2}) \quad (37)$$

With:

$$V(\Delta L_1, \Delta L_2) = \frac{1}{I_0(\Delta L_1)} \int_k I_s(k) e^{ik\Delta L_2} \cdot \left(2(E_{11}^2 + E_{12}^2)E_{21}E_{22} + 2E_{11}E_{12}E_{21}E_{22} \left(e^{ik\Delta L_1} + e^{-ik\Delta L_1} \right) \right) dk \quad (38)$$

The visibility function is therefore given by the Fourier transform of the product between the source power spectra and a modulation function of period $\frac{2p}{\Delta L_1}$.

Since the Fourier transform of the product of two function corresponds to the convolution of the Fourier transforms of each function and the Fourier transform of e^{ikx} is a Dirac function centered in x , we find:

$$V(\Delta L_1, \Delta L_2) = \frac{2}{I_0(\Delta L_1)} (E_{11}^2 + E_{12}^2) E_{21} E_{22} \tilde{I}_s(\Delta L_2) + \frac{2}{I_0(\Delta L_1)} E_{11} E_{12} E_{21} E_{22} (\tilde{I}_s(\Delta L_2 - \Delta L_1) + \tilde{I}_s(\Delta L_2 + \Delta L_1)) \quad (39)$$

The visibility function will therefore be composed of three *peaks* centered around 0, $+\Delta L_1$ and $-\Delta L_1$. By measuring the distance between the *central peak* and the *lateral peaks*, it is possible to obtain an absolute measurement of $|\Delta L_1|$. If the reflectivity E_{11} and E_{12} of the two arms in the measurement interferometer are equal, the central peak will have an intensity corresponding to the double of the intensity of each of the lateral peaks.

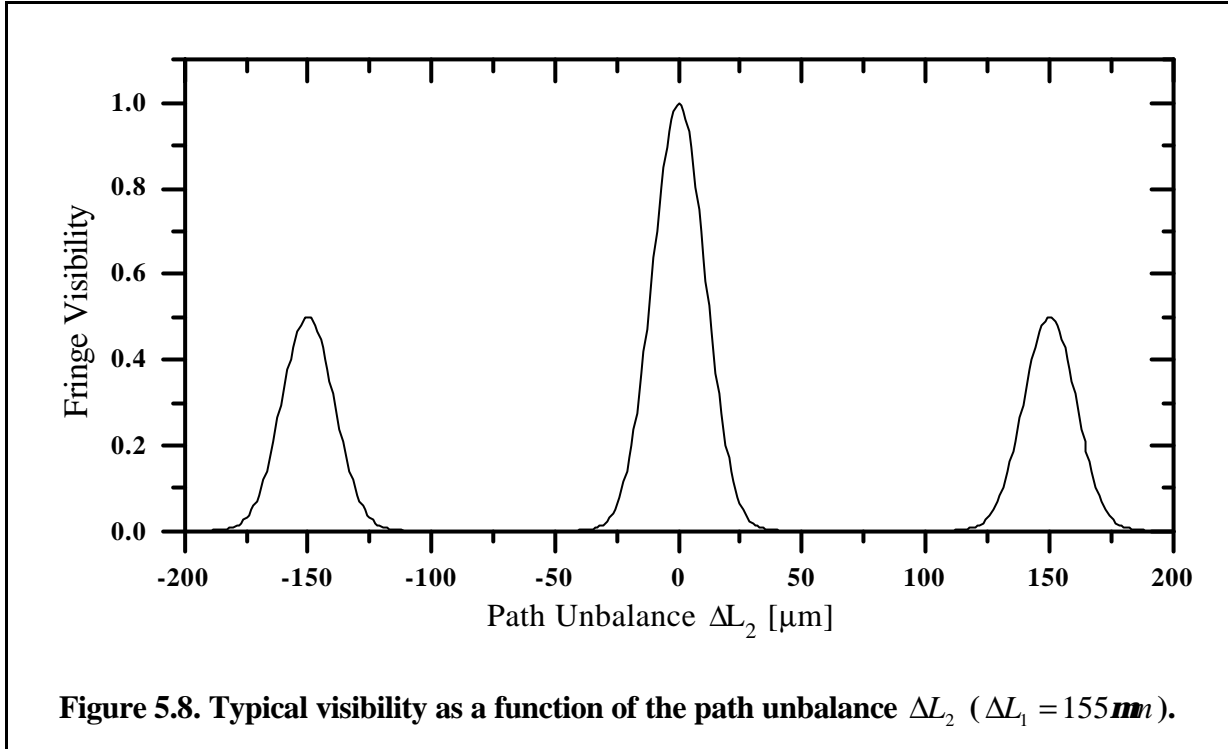


Figure 5.8 shows a typical plot of the visibility as a function of the path unbalance ΔL_2 of the analyzer.

5.4.2 Wave packets approach

In the previous paragraph we have analyzed the characteristics of the double Michelson interferometer in terms of spectral analysis. This approach is consistent with the wave-like nature of EM radiation. In this paragraph we will introduce the concept of *wave-packet*. A wave packet is a particular structure of the EM field that propagates in space. A wave-packet is characterized by its group velocity, its frequency, its length and its amplitude. It can be considered as a superposition of monochromatic waves with a stable phase relationship. If we consider, a source with spectral amplitude distribution $A_s(k)$ centered around k_0 , we obtain for the amplitude at a given point in space and time:

$$E(x, t) = \int_k A_s(k) e^{i\left(\frac{c}{n}t - x\right)k} dk \quad (40)$$

Or:

$$E(x, t) = e^{i\left(\frac{c}{n}t - x\right)k_0} \tilde{A}_s\left(\frac{c}{n}t - x\right) \quad (41)$$

This corresponds indeed to a wave packet with an envelope given by the Fourier transformation of the spectral content of the source. The packet is centered around the position $\frac{c}{n}t$ and propagates therefore with a group speed of $\frac{c}{n}$. The physical length⁵ of the non-vanishing part of this packet is the coherence length L_c of the source. This wave packet

⁵ when traveling in air.

can be considered as a non-quantized photon. A real source emitting contiguous radiation will produce a multitude of superimposed packets with no stable phase relationship between one another. Interference is therefore possible only within one and the same packet. The study of the properties of an interferometer can be reduced to the analysis of the propagation of a single packet.

Let's consider a wave packet emitted from the source at $x = 0$ and the time $t = 0$. The packet will be split by the coupler and sent towards the two measurement arms. After passing through the first interferometer with a path unbalance ΔL_1 the two packets will be recombined by the coupler. Since ΔL_1 is, in most cases, greater than L_c , the two packets will not superpose and will reach the analyzer interferometer with a relative delay of $\frac{n \Delta L_1}{c}$. The analyzer splits this packet pair again and recombines two pairs of pairs (four packets) with a relative delay of $\frac{n \Delta L_2}{c}$. The four packets will reach the detector⁶:

$$\begin{aligned}
 E_D(t) = & \cos\left(\left(\frac{c}{n}t - (L_{11} + L_{21})\right)k_0\right) \tilde{A}_s\left(\frac{c}{n}t - (L_{11} + L_{21})\right) E_{11}E_{21} + \\
 & \cos\left(\left(\frac{c}{n}t - (L_{11} + L_{22})\right)k_0\right) \tilde{A}_s\left(\frac{c}{n}t - (L_{11} + L_{22})\right) E_{11}E_{22} + \\
 & \cos\left(\left(\frac{c}{n}t - (L_{12} + L_{21})\right)k_0\right) \tilde{A}_s\left(\frac{c}{n}t - (L_{12} + L_{21})\right) E_{12}E_{21} + \\
 & \cos\left(\left(\frac{c}{n}t - (L_{12} + L_{22})\right)k_0\right) \tilde{A}_s\left(\frac{c}{n}t - (L_{12} + L_{22})\right) E_{12}E_{22}
 \end{aligned} \tag{42}$$

which records the total intensity of these four packets integrated over a time which is in general longer than the traveling time of the packets:

$$\begin{aligned}
 I_D = & \int_{t=-\infty}^{+\infty} E^2(t) dt = \\
 = & \frac{1}{2} \left(E_{11}^2 E_{21}^2 + E_{11}^2 E_{22}^2 + E_{12}^2 E_{21}^2 + E_{12}^2 E_{22}^2 \right) + \\
 & + \frac{1}{2} \left(E_{11} E_{12} E_{21}^2 + E_{11} E_{12} E_{22}^2 \right) \cos(k_0 \Delta L_1) \tilde{A} \otimes \tilde{A}(\Delta L_1) + \\
 & + \frac{1}{2} \left(E_{11}^2 E_{21} E_{22} + E_{12}^2 E_{21} E_{22} \right) \cos(k_0 \Delta L_2) \tilde{A} \otimes \tilde{A}(\Delta L_2) + \\
 & + \frac{1}{2} \left(E_{11} E_{12} E_{21} E_{22} \right) \cos(k_0 (\Delta L_1 + \Delta L_2)) \tilde{A} \otimes \tilde{A}(\Delta L_1 + \Delta L_2) + \\
 & + \frac{1}{2} \left(E_{11} E_{12} E_{21} E_{22} \right) \cos(k_0 (\Delta L_1 - \Delta L_2)) \tilde{A} \otimes \tilde{A}(\Delta L_1 - \Delta L_2)
 \end{aligned} \tag{43}$$

Since:

⁶ the Re operator has been explicitly applied.

$$\begin{aligned}
I_D &= \int_{t=-\infty}^{+\infty} \cos\left(k_0 \frac{c}{n} t - k_0 L_A\right) \cos\left(k_0 \frac{c}{n} t - k_0 L_B\right) & (44) \\
&\quad \tilde{A}\left(k_0 \frac{c}{n} t - k_0 L_A\right) \tilde{A}\left(k_0 \frac{c}{n} t - k_0 L_B\right) dt \\
&= \frac{1}{2} \cos(k_0(L_A - L_B)) \int_{t=-\infty}^{+\infty} \tilde{A}\left(k_0 \frac{c}{n} t - k_0 L_A\right) \tilde{A}\left(k_0 \frac{c}{n} t - k_0 L_B\right) dt \\
&= \frac{1}{2} \cos(k_0(L_A - L_B)) \tilde{A} \otimes \tilde{A}(L_A - L_B)
\end{aligned}$$

Equation (44) requires that \tilde{A} is a slowly varying function compared to the cosine of the same argument.

Since $A^2 = I_s$ we have (from the convolution theorem): $\tilde{A} \otimes \tilde{A}(x) = \tilde{I}_s(x)$ and (43) becomes:

$$\begin{aligned}
I_D &= \frac{1}{2} \left(E_{11}^2 E_{21}^2 + E_{11}^2 E_{22}^2 + E_{12}^2 E_{21}^2 + E_{12}^2 E_{22}^2 \right) + & (45) \\
&\quad + \frac{1}{2} \left(E_{11} E_{12} E_{21}^2 + E_{11} E_{12} E_{22}^2 \right) \cos(k_0 \Delta L_1) \tilde{I}_s(\Delta L_1) + \\
&\quad + \frac{1}{2} \left(E_{11}^2 E_{21} E_{22} + E_{12}^2 E_{21} E_{22} \right) \cos(k_0 \Delta L_2) \tilde{I}_s(\Delta L_2) + \\
&\quad + \frac{1}{2} \left(E_{11} E_{12} E_{21} E_{22} \right) \cos(k_0(\Delta L_1 + \Delta L_2)) \tilde{I}_s(\Delta L_1 + \Delta L_2) + \\
&\quad + \frac{1}{2} \left(E_{11} E_{12} E_{21} E_{22} \right) \cos(k_0(\Delta L_1 - \Delta L_2)) \tilde{I}_s(\Delta L_1 - \Delta L_2)
\end{aligned}$$

If we again consider a fixed and unknown ΔL_1 and a controllable ΔL_2 we obtain in equation (43): a first term independent of ΔL_2 , a second term also independent of ΔL_2 (and usually vanishing since $\Delta L_1 > L_c$ and therefore $\tilde{A} \otimes \tilde{A}(\Delta L_1) = 0$), a third term giving a peak centered around $\Delta L_2 = 0$ and two terms giving two peaks centered around $\Delta L_2 = \Delta L_1$ and $\Delta L_2 = -\Delta L_1$. This result is therefore equivalent to the one found with the spectral approach.

More generally, the visibility of the fringes as a function of ΔL_2 will be given by the auto-correlation function of the convolution between the visibility function of the source (i.e. the Fourier transform of the amplitude spectra) and a Dirac function centered at the position of each reflector in the first interferometer.

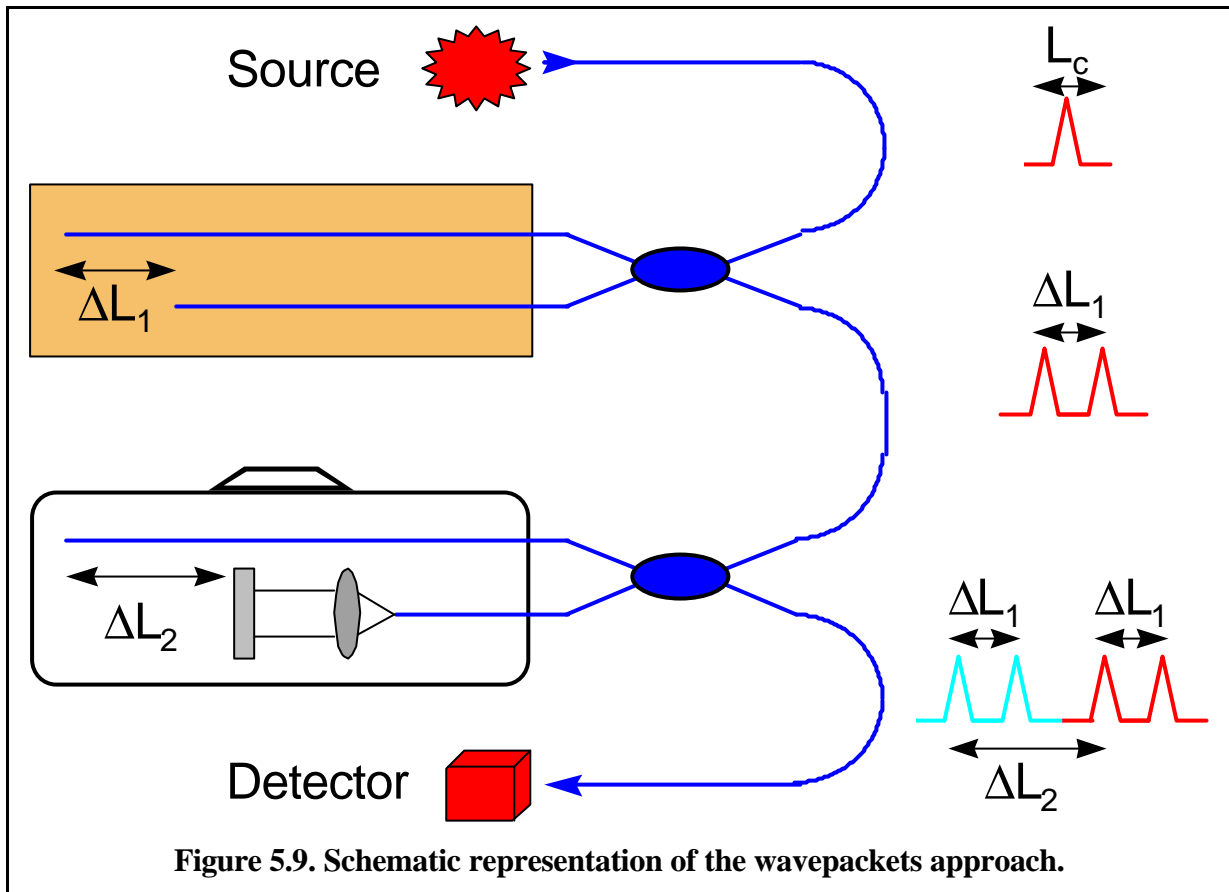


Figure 5.9 gives a schematic representation of the evolution of a wavepacket in the path matching interferometer. By varying the path unbalance in the reading unit it is possible to re-superpose the different packets split by the sensor.

The spectral approach will be useful to understand the cases where some of the components are wavelength selective (e.g. a fiber Bragg grating). The wave-packet approach will be used to discuss the cases where some of the components have an explicit time dependence (e.g. a phase modulator).

5.5 Birefringence and polarization effects

Until now we have considered the radiation propagating in the fibers as a scalar field. In reality, light is a vector field with two components or polarization states that propagate independently in the same wave-guide. We should now consider how this affects the behavior of a path matching interferometer.

The electric field at each point of a monochromatic wave propagating in a fiber can be described as:

$$\vec{E}(x, t) = \text{Re} \left(E_0 e^{i(\omega t - kx + \Phi_0)} \right) \begin{bmatrix} a \\ b \end{bmatrix} \quad (46)$$

where a and b are the complex polarization components expressed in an orthogonal base (e.g. TE/TM or left/right circular).

If we compare the electric field \vec{E}_i at the input and \vec{E}_a at the output of a fiber we can define a matrix J which transforms the input polarization vector into the output polarization vector:

$$\begin{bmatrix} a_o \\ b_o \end{bmatrix} = J \cdot \begin{bmatrix} a_i \\ b_i \end{bmatrix} \quad (47)$$

This matrix is usually known as the Jones matrix. If a wave propagates in two successive fibers the global matrix is simply given by the multiplication of the two partial matrixes.

Let's now consider the case of a birefringent fiber, i.e. a fiber with different propagation times between two polarization.

A model of the double Michelson interferometer presented in the previous paragraphs should take the following aspects into account:

- The birefringence of each of the arms in the two interferometers and in the three common-path trunks can be arbitrary.
- The input state of polarization of the source is unknown.
- The source is partially polarized.
- The source is broadband.
- The birefringence of all fibers can be wavelength dependent.

All these conditions complicate sensibly the model and a complete analysis of the obtained effects exceeds the scope of this paragraph. We will however give a simplified explanation of the effects observed in this type of double interferometer. The following simplifications are made:

- No wavelength dependence of the birefringence.
- Polarized source. With a Jones vector $\begin{bmatrix} 1 \\ 0 \end{bmatrix}$

The whole interferometer can be represented by seven Jones matrices as schematized in Figure 5.10. The central peak and the two lateral peaks are the result of different combination of the matrices and their visibility is not, in general, identical. The visibility of the interference fringes will be given by [5,6]:

$$V = V_0 \cos \mathbf{h} \quad (48)$$

Where V_0 is the visibility calculated without taking the polarization effects into account and \mathbf{h} is the angle on the Poincaré sphere between the two vectors representing the polarization states of the two interfering paths. It can be seen that for orthogonal states of polarization (SOP) the visibility can vanish completely. This phenomenon is known as polarization fading.

The central peak is given by a superposition of two distinct interferometers. The two are

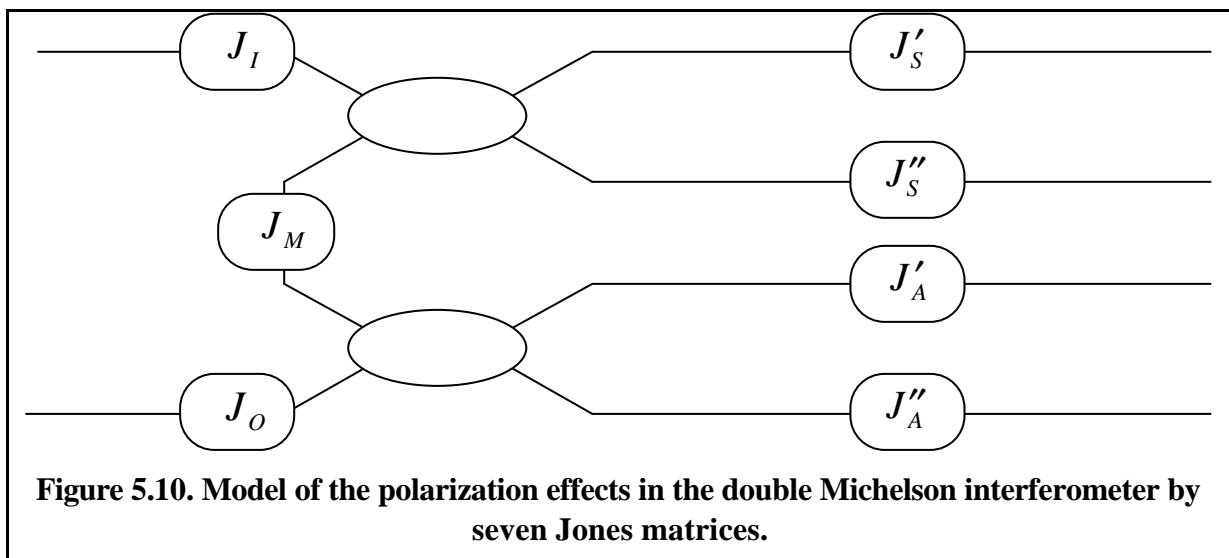


Figure 5.10. Model of the polarization effects in the double Michelson interferometer by seven Jones matrices.

distinguished by the path of the light in the first (or sensor) interferometer. If the light passes in the first arm of the first interferometer, the output SOP of the two interfering arms will be given by:

$$\begin{aligned} J^1 &= J_O J'_A J_M J'_S J_I \\ J^2 &= J_O J''_A J_M J'_S J_I \end{aligned} \quad (49)$$

If the light passes in the second arm of the sensor's interferometer we have:

$$\begin{aligned} J^1 &= J_O J'_A J_M J''_S J_I \\ J^2 &= J_O J''_A J_M J''_S J_I \end{aligned} \quad (50)$$

These two paths are distinguishable and the intensities should therefore be added. Equations (49) and (50) show that it is highly unlikely that the central peak will vanish because of polarization fading. This would mean that both equations applied to the source SOP give orthogonal states.

The two lateral peaks also correspond to different interfering paths. The first (e.g. left) peak corresponds to an interference between the SOPs described by:

$$\begin{aligned} J^1 &= J_O J'_A J_M J'_S J_I \\ J^2 &= J_O J''_A J_M J'_S J_I \end{aligned} \quad (51)$$

This corresponds to the paths going through the first arm or the second arm of the two interferometers.

The second (e.g. right) peak, by:

$$\begin{aligned} J^1 &= J_O J'_A J_M J'_S J_I \\ J^2 &= J_O J'_A J_M J''_S J_I \end{aligned} \quad (52)$$

This corresponds to the paths going through the first arm of the sensor interferometer and the second arm of the analyzer and vice versa.

For the same reason as for the central peak, it is highly unlikely that both peaks disappear at the same time. This is however possible if the analyzer does not introduce any birefringence between its two arms, for example if it is made of polarization maintaining fibers and coupler.

This shows that if all arms of the two interferometer are made with standard fibers with low and random birefringence, the central peak and at least one of the side peaks are highly likely to appear. This behavior has been observed experimentally.

If the source is partially unpolarized, another fading effect can occur. It could happen that both polarization show a good visibility but are out of phase. Since the detector is polarization blind, the incoherent sum of the two will be observed. This sum could however give a constant if the intensity maxima of one polarization correspond to the minima of the other (always as a function of the total path unbalance). This phenomena is also very unlikely to appear for random birefringence.

Finally, a strong wavelength dependence of the birefringence could lead to a peak broadening, since only parts of the source spectrum would interfere while other would fade. This phenomena was never observed (at least at 1300 nm).

5.6 Sign ambiguities

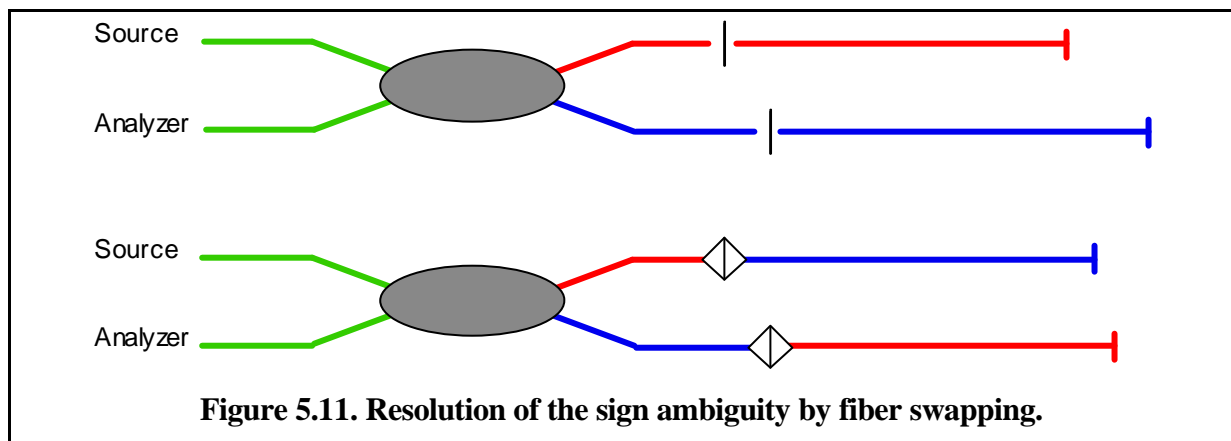
From the previous chapters it clearly appears that a path matching interferometer can measure only the absolute value of the length difference between measurement and sensing fibers. In many cases however, it is interesting to know the sign of this difference and therefore the direction of a displacement (expansion or contraction of the host structure). In some cases it is even possible that the sign of this length difference changes from one measurement to another

(peak crossing). In this case, the determination of the sign is fundamental in order to interpret the deformation correctly.

There are three approaches that can solve the sign ambiguity. The most obvious solution is to ensure that one of the fiber is and always remains longer than the other. The second requires the application of an additional and known displacement to either the reference or the measurement fiber. By observing the resulting displacement of the peaks one can reconstruct which of the fibers is longer. If the measurement fiber is longer, an expansion of the structure will result in an increase of the measured path unbalance, and vice versa. the required additional displacement could be applied, for example, by a piezoelectric coil.

The third approach is used when connectors are installed between the first coupler and the sensing fibers. The total path unbalance is in this case given by the sum of the path unbalance between the coupler and the connectors and the one between the connectors and the mirrors. If it is known which of the coupler arms is longer, it is easy to know which of the fibers in the sensor is longer. If we first measure the path unbalance normally and then swap the connectors of the reference and the measurement fibers and take another measurement, a larger value will be found when the longer fiber in the coupler is connected to the longer fiber in the sensor. In order to determine which of the fibers in the connector is longer, one can use a sensor where the length difference between the two fibers is evident (e.g. 1 cm).

Figure 5.11 presents a typical situation before and after fiber swapping.



5.7 Conclusions

In this chapter we have demonstrated that a path matching interferometer can be used to measure precisely and non-incrementally a path unbalance between two fibers. The effect of polarization were also discussed and should not be neglected since they can reduce or even destroy totally the visibility of the fringes.

5.8 Bibliography

- [1] J. W. Goodman, "Statistical Optics", Wiley, 1985
- [2] V. Gusmensoli, M. Martinelli, "Absolute measurements by low-coherence sources", Advances in Optical Fiber Sensors, Wuhan, China, October 1991
- [3] A. Koch, R. Ulrich, "Fiber optic displacement sensor with 0.02 mm resolution by white light interferometry, Sensors and Actuators A, 25-27, pp. 201-207, 1991
- [4] D. Inaudi, A. Elamari, L. Pflug, N. Gisin, J. Breguet, S. Vurpillot, "Low-coherence deformation sensors for the monitoring of civil-engineering structures", Sensor and Actuators A, 44 (1994), 125-130.
- [5] A. D. Kersey, A. Dandridge, A. B. Tveten, "Dependence of visibility on input polarization in interferometric fiber-optic sensors", Optics Letters, Vol. 13, No. 4, April 1988
- [6] A. Mabrouky, M. Gadonna and R. Le Naour, "Polarization characterization of a Mach-Zehnder interferometer", Applied Optics, Vol. 35, No, 19, July 1996

6. SOFO design and fabrication

One of the main achievements of this work was the realization of a measurement system based on low coherence interferometry. This includes both a portable and rugged reading unit as well as a series of sensors adapted to different types of structures. This section first describes the SOFO system and its evolution and then focuses on the different parts that compose it. This system can be subdivided into three main parts: sensors, reading unit and data processing. The different chapters will describe the final setup used in the SOFO system as well as the other options that were or could have been considered. The choice of each option was made according to the aim of producing a reliable system adapted to the needs of civil engineering structural monitoring. At the end of the section we analyze the performance of the system and we give some suggestions on the possible future evolution of SOFO.

The development of the SOFO measuring system was not the work of a single person. Although the ideas and concepts behind the SOFO system are mine, I have to acknowledge the invaluable contribution of the persons who worked on different practical aspects of the system¹. Charles Gilliard and Aleksander Micsiz have designed and carried out most of the electronics subsystems as well as the mechanical setup of the ruggedized reading unit, Nicoletta Casanova, Raymond Delez, Pascal Kronenberg, Annette Osa-Wyser, Ange Pontier, Xavier Rodicio, Samuel Vurpillot and the team at DIAMOND have worked with me on the development of the sensors. Samuel Vurpillot was also in charge of the elaboration of advanced algorithms for the analysis of complex results in structures instrumented with many sensors.

¹ Cited in strict alphabetical order by family name!!!

6.1 Introduction

This work aimed principally to the development and the on-site application of a measuring system adapted to the needs of civil engineering structural monitoring. It was chosen to put emphasis on the long-term monitoring of small displacements, since other well established technologies were already available for dynamic and short-term measurements (e.g. microbending sensors) and for strain measurements (e.g. fiber Bragg gratings and EFPI). As seen in the previous section, low-coherence interferometry is well suited for this application, allowing an absolute measurement with a precision which is, in principle, unaffected by time. This technique requires a fairly simple setup for the sensor itself and can therefore be brought to a large scale production at reasonable cost. The reading unit is, on the other hand, more elaborate and therefore expensive. Since the measurements are absolute, a single reading unit can be used to monitor multiple sensors and even multiple structures, redistributing its cost over thousands of measurements.

The principle of low-coherence interferometry is reasonably well known and has been extensively tested in laboratory conditions. The challenge of this work was to bring this technique outside of the laboratory and into the hostile environment found on most building sites and structures. This requirement has seriously affected many choices during the development of this system and required new solutions to known problems. The final result can be considered as unconventional when compared with similar equipment used for the characterization of integrated optics components or optical fiber links².

6.2 Requirements

The applications that are expected for the SOFO system include on one hand the replacement of conventional monitoring equipment already used in civil engineering, and on the other the development of sensors to open new measurement possibilities impossible with today's technology. The first category includes the replacement of techniques such as mechanical extensometers, vibrating strings and long electrical strain gages. The second type of sensors include long (1-2 m) and very long (2-20 m) displacement sensors for concrete, rocks and soils; sensors for curved path (tanks, reservoirs, pipelines) and embedded sensors for the geometrical monitoring of large structures (bridges, towers, tunnels).

It is not easy to define common requirements for such different applications. A deeper investigation shows that most differences refer to the sensor side of the system, while the reading unit requirements are far more uniform. We try to summarize them in the following points:

- **Resolution:** A standard mechanical extensometer offers a resolution of about 10 microns. It seems that this resolution is well suited for most situation and often exceeds the real needs. We will therefore aim to a resolution of 2 microns for the reading unit. This precision will be reduced to about 10 to 20 microns for some sensor types that are subject to additional constraints, such as temperature variations, handling (connection and disconnection), or imperfect mechanical link to the host structure. If special care is used in the fabrication and installation of the sensor, it should be possible to reach the reading unit resolution of 2 micron.

² For example the coherence domain reflectometers of Hewlett-Packard and Photonetics or the polarization mode dispersion analyzers of GAP Optique, EXFO and Photonetics.

- **Stability:** A stability of 10 microns should be guaranteed for at least 2 years. Once again, the main limit to the stability will be given by the sensor and not by the reading unit. In the sensor, the long term precision is limited by creeping effects. In the reading unit the stability is limited by the resolution of the displacement table which is always better than 10 microns, even for large temperature changes³.
- **Measurement range:** The measurement range in elongation and shortening depends obviously on the sensor length. Its upper limit is limited by the maximal path unbalance that can be compensated by the reading unit. A range of 100 mm in both directions seems adapted to most applications including soil mechanics. For displacements over this value a precision of a few microns becomes useless and other measurement techniques are certainly more adapted. For large displacements, the ultimate limit of the precision is given by the uncertainty in the elasto-optic coefficient k_{Stress} and not by the reading unit accuracy in the measurement of Δt .
- **Sensor length:** The sensors should have a length between 100 mm and 50 m. This size range does not put any restriction on the design of the reading unit itself. We will see that different types of sensors are needed to cover different length ranges. For shorter sensor lengths the resolution of 10 microns becomes insufficient and other measurement techniques⁴ are more suitable (e.g. fiber Bragg grating and EFPI sensors). Lengths over 50 m are uncommon in civil engineering since a large structure is best measured by subdividing it into shorter sub-domains.
- **Remote sensing range:** This value defines the maximal distance between the sensor and the reading unit. This distance is mainly limited by the dispersion characteristics of the fibers. The use of singlemode fibers at 1300 nm excludes both the modal and the chromatic dispersion. The system will therefore be limited by the polarization mode dispersion which is normally below $0.5 \text{ ps}/\sqrt{\text{Km}}$. If we allow three to five times increase of the peak width, it becomes possible to obtain a precise measurement with a distance of at least 1 km between the sensor and the reading unit.
- **Dynamic range:** The system should be able to measure sensors having a very low reflectivity. This allows a good security margin in the case of alteration to the sensors, such as a deterioration of the reflective mirrors, a bad splice or a dirty connector. On the other hand a good sensitivity is the first step towards a multiplexed system where the signal returned by each partial reflector pair is usually low. The Fresnel reflectivity⁵ of 4% should be considered as a typical value, but a reflectivity as low as 0.1% should be measurable without a noticeable reduction of the system performance.
- **Speed:** Since a structure can be instrumented with tens of sensors, the measurement time for each should not exceed one minute, including optical connection to the sensor and data storage. In the case of automatic measurements with no operator attendance and no manual connection, a measurement time below 10 s would be an advantage. It is clear that the shorter the measurement time the better the performance of the system. If one wants to include dynamic measurements, the speed should be increased to at least ten measurements per second, which is not without consequences on the design of the

³ According to the manufacturer specification and confirmed by the experience.

⁴ The so called “strain sensors”

⁵ The reflectivity obtained at the glass-air interfaces.

detection stage and mechanics. In this work we have decided not to explore the domain of dynamic measurements where other measurement system seem more appropriated.

- **Dimensions:** The whole system including the external PC should be transportable by a single person over short distances. This limits the weight of the reading unit to about 15-20 kg and its volume to about 50 l. Obviously, a smaller reading unit increases the comfort of the user. It was decided not to make excessive demands on the integration of the different electrical and optical components, in order to maintain the modular nature of the system and allow an easy reconfiguration and the testing of different configurations. Once the system has been tested and proved to respond well, it would be possible to increase the level of integration, especially on the side of the electronics⁶.
- **Case:** The measurement system will be used in demanding environments where a careful handling can not be guaranteed. The case housing the reading unit should therefore be rugged enough to withstand shocks and frequent movements. The reading unit should function independently of the orientation of the case, even upside-down. It is also important that the enclosure and all the connectors are waterproof allowing its use in humid environments, such as a tunnel or a foundation building yard.
- **Power supply:** The system should be independent from any external power supply and be able to run on its internal rechargeable battery. For laboratory applications and when an AC power supply is available, the system should run on 220 VAC and recharge its internal battery. It would be helpful if the system could be powered by an external DC source such as a car battery.
- **Environment:** The reading unit can be subjected to of extreme environmental conditions. It has to operate in a temperature range between -20°C and +50°C and high humidity.
- **User interface and data storage:** After using portable PCs on different building yards, it was decided that they are well suited as interface between the reading unit and the user. Some precautions have to be used when using standard laptop computers which are not waterproof⁷. The interface software should reduce to a minimum the number of operations that have to be carried out on site and store all the data for further analysis and interpretation. It is important that the operator can make sure that the measurement has been successfully carried out. The software should furthermore be able to transfer the results to other programs for deeper investigation and graphical representation.

All these requirement were kept in mind during the development of the SOFO system. We will find that it is indeed possible to produce at a reasonable cost a system responding and sometimes exceeding all these requirements.

6.3 Overview

In this paragraph, we will try to define a general block diagram that will be used as a tool to analyze different solutions and implementations of the SOFO system.

Not unlike most measurement systems, the functioning of a low-coherence interferometric system is best understood by following the evolution of the signals from the quantity to be measured (in this case a displacement) to the representation of this quantity in a digital format.

⁶ This was partially done in SOFO III and in the successive industrial version of SOFO

⁷ Waterproofed portable PC are available, however standard laptops offer adequate protection and were used in a number of field applications without a single failure.

A generic low-coherence interferometric system can be subdivided into six main functional blocks plus one extra block including additional elements:

- **Source:** The optical source creates the low-coherence radiation and injects it into an appropriate optical fiber. This subsystem also includes the current generator and possibly a cooling of the optical source itself. The optical source is physically located in the reading unit.
- **Sensor:** The sensor is installed in the structure to be monitored and encodes displacements into changes of the path unbalance ΔL_1 between a measurement and a reference fiber. If we adopt the wavelength approach to describe the system, the sensor acts as a periodic spectral filter encoding the path unbalance in the fibers into its free spectral range. The sensor subsystem includes the measurement and reference optical fibers, the external coupler, the optical connectors, the protection of the fibers and the mechanical pieces that create the mechanical contact between the measurement fiber and the host structure. The external optical coupler can be a part of the sensor itself, or can be separated from it and be reused for reading multiple sensors. In the case of remote monitoring, the sensor subsystem also includes the fibers that are used to carry the optical signals from and to the reading unit. The sensor is the subsystem that is most dependent on the specific application. Its design has to be tailored to the host structure. Different host materials (such as concrete, steel, timber, composites or glass) require different sensor setups. The length of the sensing region also influences the sensor design.
- **Analyzer:** The analyzer subsystem implements the path matching interferometer. It includes a coupler, a reference arm of fixed length and a scanning arm with a variable delay line. The analyzer can introduce a controllable path unbalance ΔL_2 between its interferometer arms. All the bulk, guided or integrated optics needed to implement the delay line, as well as the scanning device (motorized translation stage, piezo stretcher,...), are included in this subsystem. The function of the analyzer is to recombine the delayed wavepackets and allow interference to take place despite the reduced coherence length of the source. In the wavelength approach the analyzer is seen as a Fourier spectrometer resolving the periodic spectra produced by the sensor subsystem. The output signal of the analyzer subsystem is an optical intensity as a function of the path unbalance ΔL_2 . If the delay line is scanned at constant speed, the output signal will be a time dependent intensity and the scanning speed will give the proportionality factor between time and ΔL_2 . The analyzer subsystem is physically located in the reading unit.
- **Detection:** The detection stage transforms the optical intensity from the analyzer output into an electrical signal. This subsystem includes the photodiode as well as a preamplifier. The detection stage should be capable of adapting itself to variations of the average received intensity that are expected when measuring sensors with different reflectivities. It should be sensitive enough to detect a weak signal without being saturated by strong ones. This can be obtained either by changing the preamplifier gain or by implementing a feedback loop to the source current supply. The detection is also located in the reading unit.
- **Signal processing:** The signal processing unit extracts the value of ΔL_1 from the ΔL_2 dependent voltage obtained by the detection subsystem. This subsystem usually includes an analog signal processing stage, an analog to digital converter and a digital processing stage. Different demodulation approaches will lead to designs that divide differently the

processing steps between the analog and the digital parts. The signal processing subsystem can be physically split between the reading unit and the interface computer.

- **Data processing:** At this stage the data is presented to the operator and stored for further interpretation. This subsystem also gathers the results from multiple measurements at different times or on different sensors and extracts the relevant parameters useful to determine the behavior of the host structure. The data analysis part strongly depends on the application. In some cases, the evolution of the displacements of each single fiber can be sufficient to obtain meaningful information, while in other cases it is necessary to compare and combine the results of tens or hundreds of measurements on many sensors. In a complex structure, such as a bridge, it becomes impossible to analyze manually the displacement evolution of all the sensors and the data processing unit should deliver a more global behavior pattern. In the framework of the smart structure concept, the data processing unit constitutes the link between the sensors and the actuators. In the case of civil structures, the actuator could be an hydraulic jack dynamically damping excessive vibrations, or a simple red light stopping the traffic on an unsafe bridge or tunnel, or even a hard-hat team performing maintenance activities on the structure.
- **Additional elements:** Although not directly included in the data path, other elements play an important role in the measuring system. These include the power supply, the casings and the processors running the software for signal processing and data analysis. Telecommunication links or interface systems such as screens, keyboards and pointing devices are also included in this subsystem.

In certain setups, the boundaries between these subsystems are not so clear-cut. This subdivision is nevertheless helpful to organize the discussion on the development and the evolution of the SOFO system. The block diagram and the signal path are resumed in Figure 6.1.

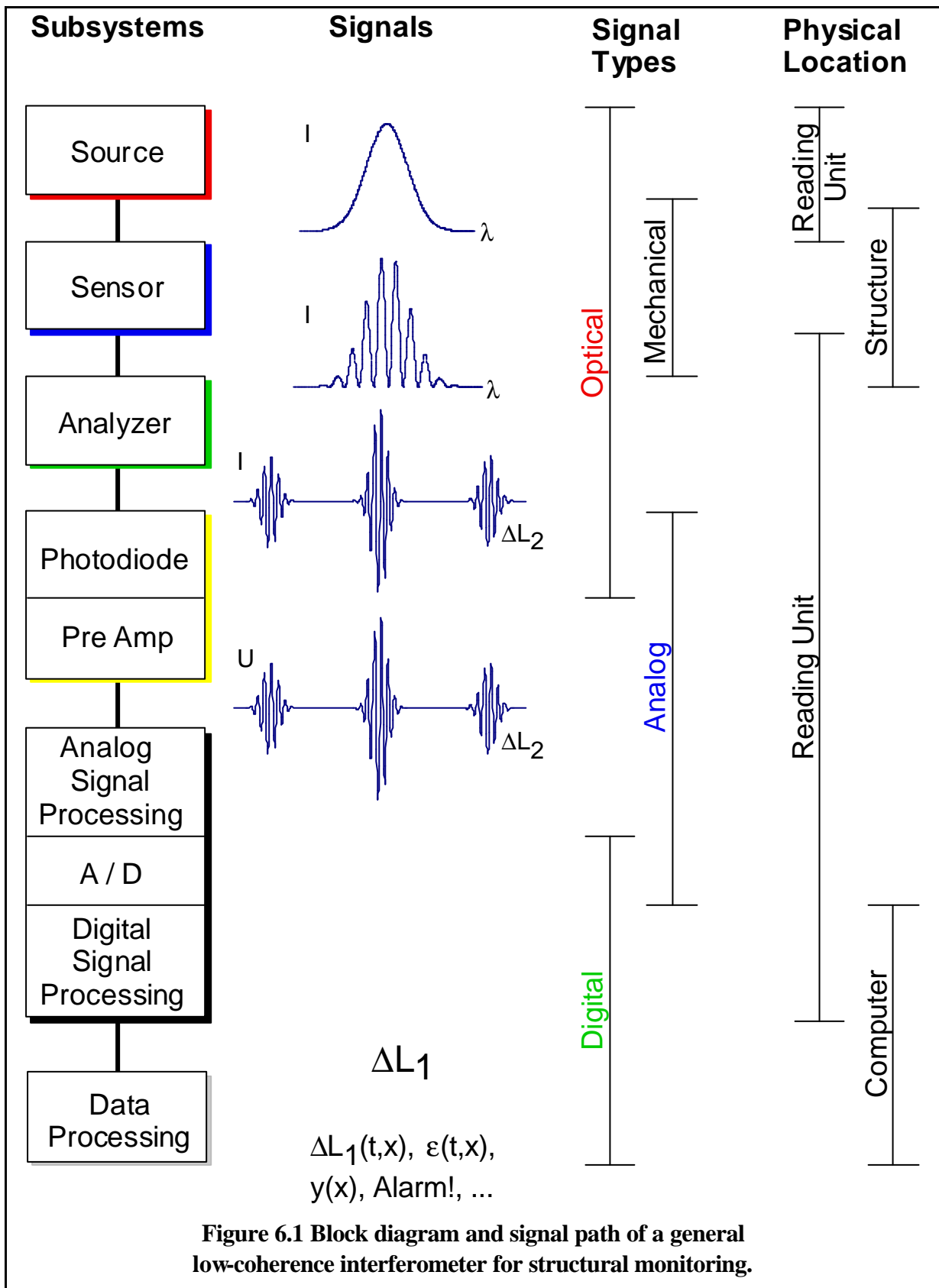


Figure 6.1 Block diagram and signal path of a general low-coherence interferometer for structural monitoring.

6.4 Evolution: the history of SOFO

Before we enter the detailed analysis of each subsystem, it is useful to give a general overview on the different system that have been realized and tested in this project. This should give the reader the feeling of how a real system appears and help him or her visualize the subsystems in a more realistic way. During this work five systems were built or used at IMAC:

	Formos	SOFO I	SOFO II	SOFO III	SOFO IV and further...
General design	L. Thévenaz R. Passy D. Inaudi	D. Inaudi	D. Inaudi	D. Inaudi	D. Inaudi
Manufacturer	GAP (Uni Geneva)	IMAC A. Micsiz	IMAC A. Micsiz	IMAC A. Micsiz	Smartec
Owner	IMAC	IMAC / LMS	IMM/ SMARTEC	IMAC/ SMARTEC	
Delivery	10.1994	3.1995	8.1995	4.1996	mid 1997
Primary function and characteristics	Feasibility tests.	First field version, improved speed. Retrofitted in 1996 to SOFO III electronics.	Field version for industrial applications Similar to SOFO I. Retrofitted in 1996 to SOFO III electronics.	Reduced size and improved sensitivity for use with partial reflectors.	Industrial version.

Table 6.1. Summary of the five generations of SOFO.

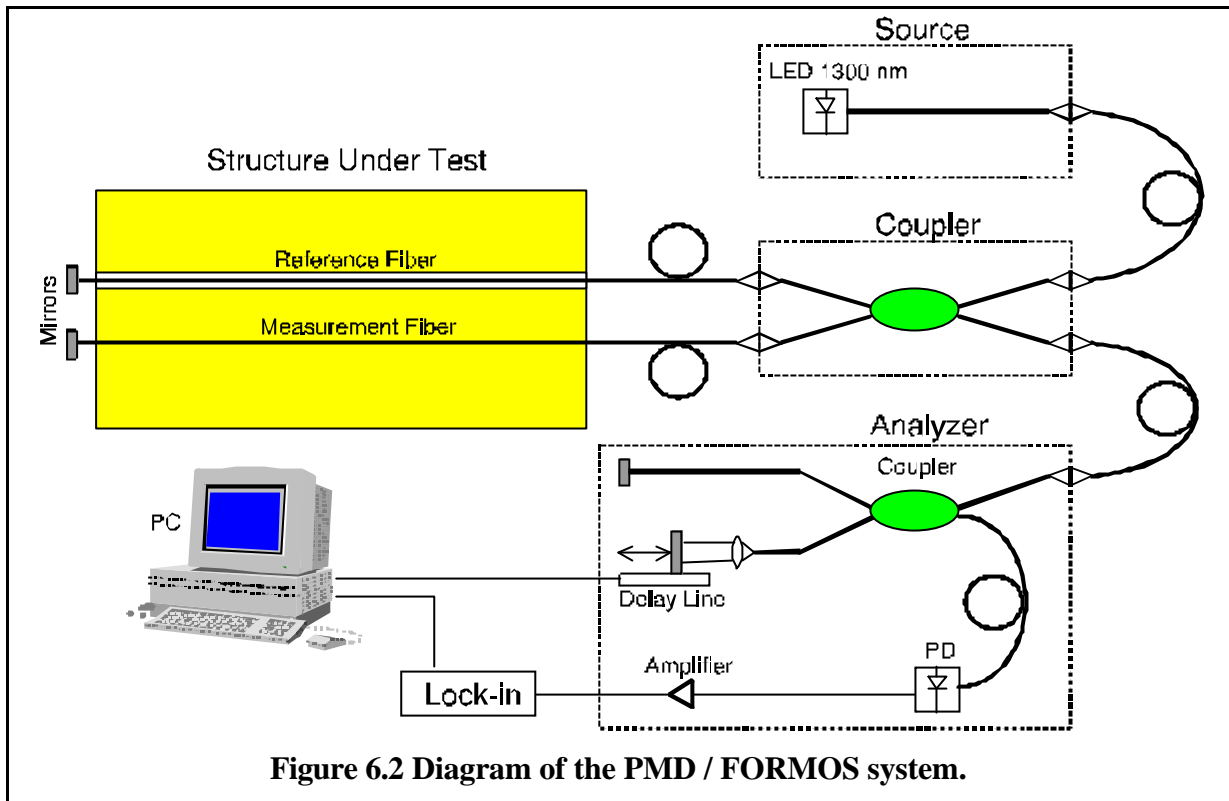


Figure 6.2 Diagram of the PMD / FORMOS system.

6.4.1 PMD / FORMOS

The feasibility tests for a low-coherence monitoring system were performed using a system originally developed by Alpatronic SA to measure the chromatic dispersion in optical fiber links and later adapted to the characterization of polarization mode dispersion (PMD) by the Group of Applied Physics (GAP) of the university of Geneva [1,2]. The FORMOS (Fiber Optic aRray for the Monitoring Of Structures) [3] was a minor evolution of the PMD system. The main novelty consisted in an extended measurement range. Figure 6.2 give a schematic representation of this system and Table 6.2 give an overview of the different subsystems.

Subsystem	Description
Source	Pigtails LED @1300 nm (or 1550 nm.)
Analyzer	Michelson interferometer. The coupler and the reference arm are fiber optic components, while the variable delay line is bulk. The mirror is scanned by a stepper motor where each step is initialized by the external PC. The scanning process is therefore very slow and the fringe frequency is typically 150 Hz. The maximal displacement of the mirror is 25 mm for the PMD system and 50 mm for FORMOS. The delay line uses a reflection off the fiber ferrule to obtain a self-stabilized setup resistant to misalignments.
Detection	Since the fringe frequency is low, the detection stage is not critical. A multimode pigtailed photodiode is used.
Signal processing	The fringes are demodulated by an asynchronous lock-in amplifier acting, in fact, as a band pass filter. The amplitude output giving the

fringe envelope is then digitized by a A/D PC card. The results are displayed and the path unbalance ΔL_1 is measured manually by moving two cursors on the screen.

Data processing	None.
Additional elements	The source, the analyzer, the lock-in amplifier and the PC are housed in four different casings which are not ruggedized nor waterproof. It would have been possible to squeeze the first three in a single case. The total weight of the system exceeds 30 kg and an AC power supply is necessary.

Table 6.2. Subsystem description of the PMD / FORMOS system.

Although the existence of a ready-made system was invaluable in testing the feasibility of low-coherence interferometric sensors, it became rapidly clear that this system was not adapted for full scale, in-field applications. Table 6.3 analyzes the performances of this system. Parameters in brackets do not meet to the requirements stated in paragraph 6.2.

Parameter	Analysis
(Resolution)	About 10 μm , limited by the manual peak analysis.
Stability	Tested successfully over more than one year.
Measurement range	The FORMOS system meets the requirements having a 50 mm displacement table.
Sensor length	This parameter does not depend on the reading unit characteristics.
Remote sensing range	Never tested, but probably sufficient. In the case of noisy interferogram the resolution is limited by the manual peak analysis.
Dynamic range	About 30 dB. The slow scanning speed is an advantage from this point of view.
(Speed)	The reading unit is very slow. A single measurement can take up to 60 minutes for a long scan.
(Dimensions)	The system exceeds both in weight and size the requirements for a transportable reading unit.
(Case)	The case is not waterproof nor rugged enough for an in-field use.
(Power supply)	Only 220 VAC power supply.
(Environment)	The system probably meets the temperature requirements, but can not withstand the humid condition found on some building sites. Because of the low fringe frequency the system is sensitive to external vibrations and shocks during the measurement.
(User interface and data storage)	The user interface is clumsy and was developed to measure the PMD. The software is written in turbo Pascal and runs under MS-DOS. The peaks can be analyzed only manually and the results have to be transferred to another system for further interpretation.



Figure 6.3 The FORMOS system.

Table 6.3. Performance of the PMD / FORMOS system.

The main drawbacks of this system reside in its slowness, in its unsuitability for field applications and in its clumsy user interface. The two last problems could have been solved, but the dramatic speed increase needed to meet the specifications calls for a complete redesign of the reading unit.

Figure 6.3 shows the FORMOS system including the control PC, the reading unit and the lock-in amplifier.

6.4.2 SOFO

Because the FORMOS system did not fulfill the needs for civil engineering applications and

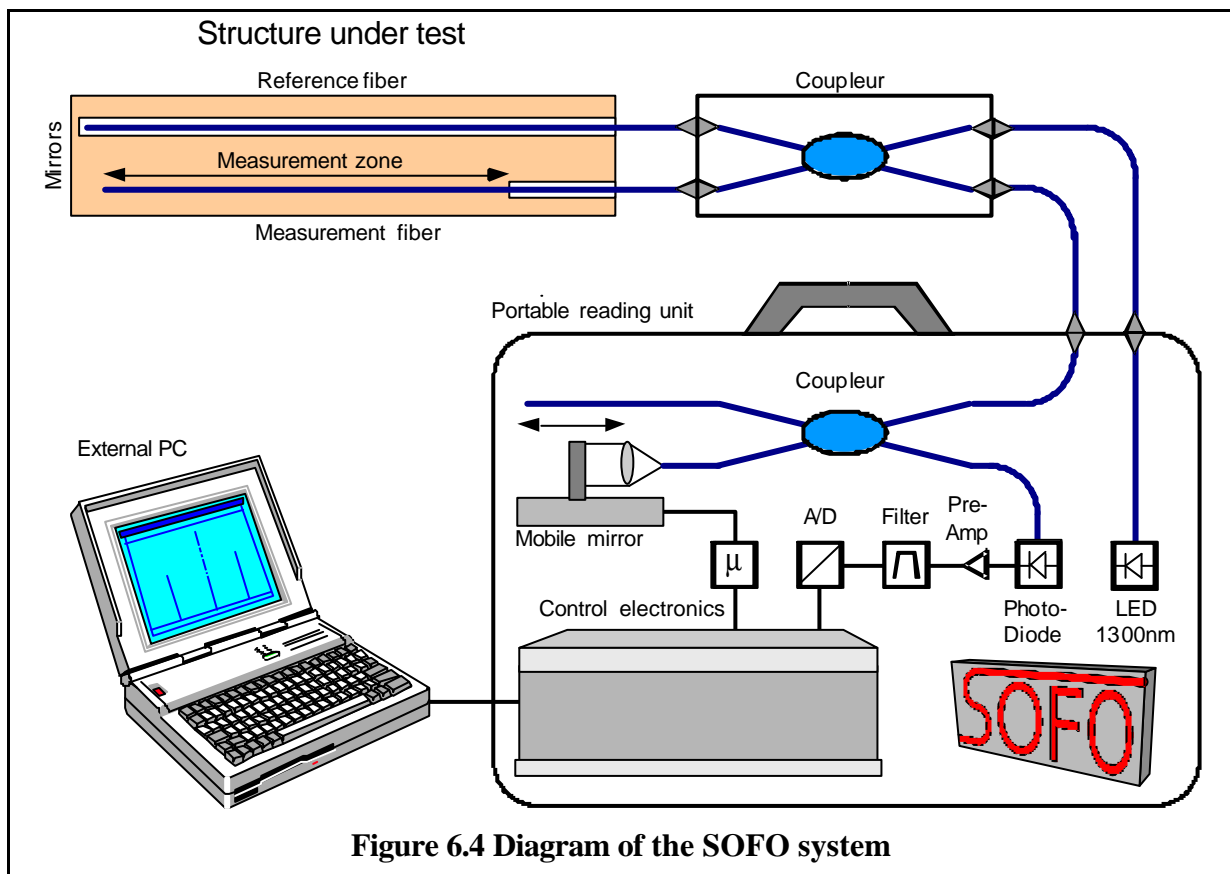


Figure 6.4 Diagram of the SOFO system

major changes would have been necessary to adapt it, it was decided to redesign at IMAC a completely new reading unit especially adapted to civil structural monitoring. The design process of this new system is described in detail in this section. This paragraph should give the reader a first overview on the system and allow a comparison with the FORMOS system. The SOFO reading unit went through different evolution phases that will be described later. In this first introduction we concentrate on the basic design concept that are common to most generation of the SOFO family.

The SOFO system [4] was entirely developed in the framework of this work. The first prototype was realized at the beginning of 1995 after six month of frantic work. The other generations followed with a six month gestation period. Until now four SOFO generations have been fabricated for internal use and for selling to external users.

Figure 6.4 give a schematic representation of this system and Table 6.4 gives an overview of the different subsystems.

Subsystem	Description
Source	Pigtailed LED @1300 nm
Analyzer	Michelson interferometer. The coupler and the reference arm are fiber optic components, while the variable delay line is bulk. The mirror is scanned by a DC motor controlled by an ad-hoc microprocessor. The motor can scan with speeds exceeding 10 mm/s. The frequency is typically 35 kHz giving a speed gain of a factor 200 compared to FORMOS. The maximal displacement of the mirror is 51 mm. The delay line uses a reflection on the fiber ferrule to obtain a self-stabilized setup resistant to misalignments. The mechanical setup holding the ferrule and the microscope objective is compact and mounted on the displacement table itself in order to reduce vibrations induced relative displacements.
Detection	A new detection has been developed to obtain both a good sensitivity and the sufficient bandwidth required by the higher fringe frequency. The photodiode has an integrated fiber connector port without multimode fiber pigtail.
Signal processing	The fringes are demodulated by a high-pass filter plus, in some setups, an integrator (to extract the envelope) The amplitude is then digitized by a A/D converter and analyzed to retain only the peak information. The results are displayed on the external computer and the peak position is analyzed automatically and saved for further analysis.
Data processing	Different modules have been realized to interpret automatically, the data produced by the SOFO system. The simpler package plots separately the evolution of the displacements for the different fibers installed in a given structure. More elaborated algorithms combine the results from different fibers and return more global behavior trends for the structure such as curvatures or vertical displacements in a bridge. These packages

can be used to represent the results in a way familiar to civil engineers.

Additional elements	The source, the analyzer, and the control electronics are housed in a ruggedized and waterproof casing. An external laptop PC also acts as the user interface. The total weight of the system is about 15-20 kg and the system works on an AC or DC power supply or on its internal rechargeable battery.
----------------------------	---

Table 6.4. Subsystem description of the SOFO system.

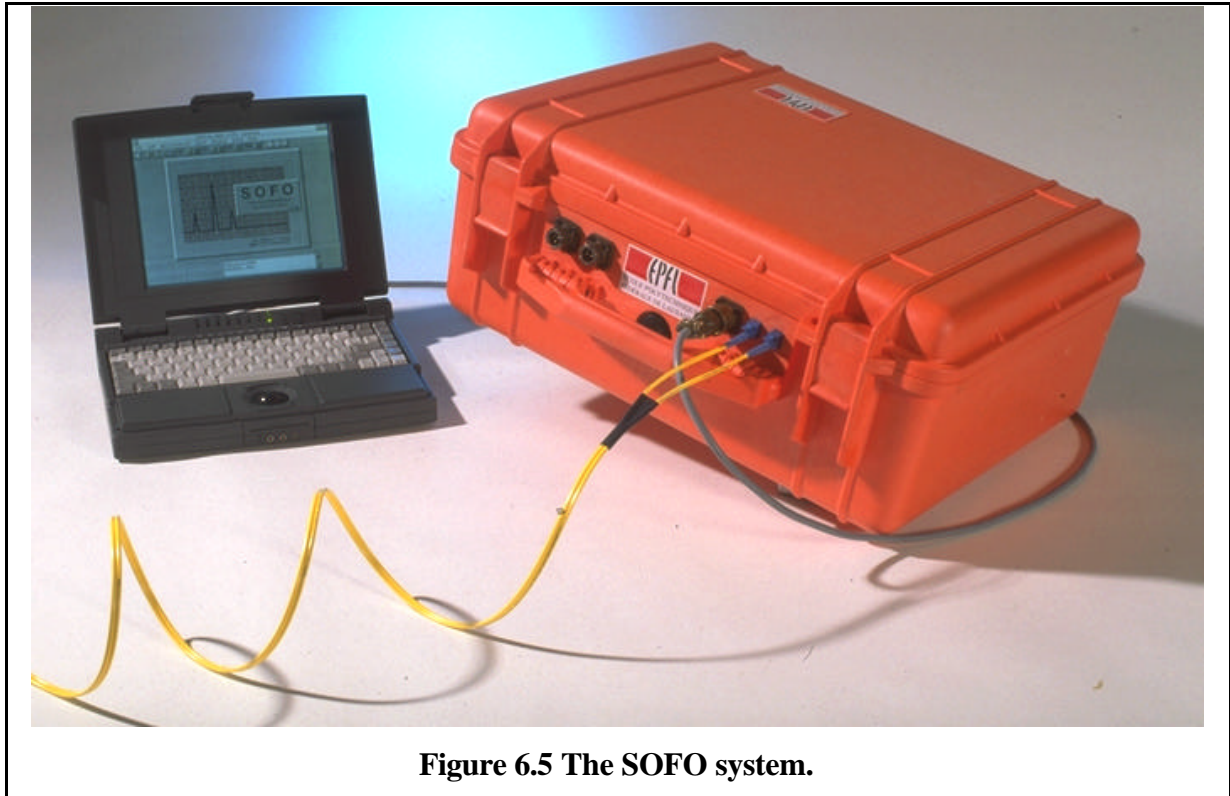
Table 6.3 analyzes the performances of this system. A more detailed discussion of the performances of SOFO will follow in chapter 6.12.

Parameter	Analysis
Resolution	The reading unit resolution is about 1 micron, thanks to the automatic peak analysis algorithm. This resolution is reduced to about 10 microns in the case of sensors with external couplers because of reconnection errors.
Stability	Tested successfully over more than one year. The stability is given by the precision of the displacement table which is guaranteed to better than 2 microns.
Measurement range	The SOFO system meets the requirements having a 50 mm displacement table.
Sensor length	This parameter does not depend on the reading unit characteristics.
Remote sensing range	Tested up to 5 km. In the case of noisy interferograms the resolution decreases slowly thanks to automatic peak analysis.
Dynamic range	About 30 dB.
Speed	10 seconds are required to perform a measurement, analyze it, save the results on the disk and having the reading unit ready for the next scan.
Dimensions	The system meets both in weight and size the requirements for a transportable reading unit. The comfort is not optimal when the reading unit has to be transported manually over large distances. In this case it is possible to install the reading unit in a backpack.
Case	The case is waterproof, rugged and adapted to in-field use.
Power supply	AC/DC external power supply or internal rechargeable battery.
Environment	The system meets the temperature and humidity conditions found on most building sites. Thanks to high fringe frequency sensing the system is particularly insensitive to external vibrations and shocks during the measurements.
User interface and data storage	The user interface runs under Windows and is adapted to both laboratory and field conditions. The software records and manages multiple measurements on many fibers and can manage large project

involving complicated measurement scheduling. The results can be exported for deeper investigation to ad-hoc external analysis packages. The software was written in Visual Basic and allows for easy reconfiguration and additions.

Table 6.5. Performance of the SOFO system.

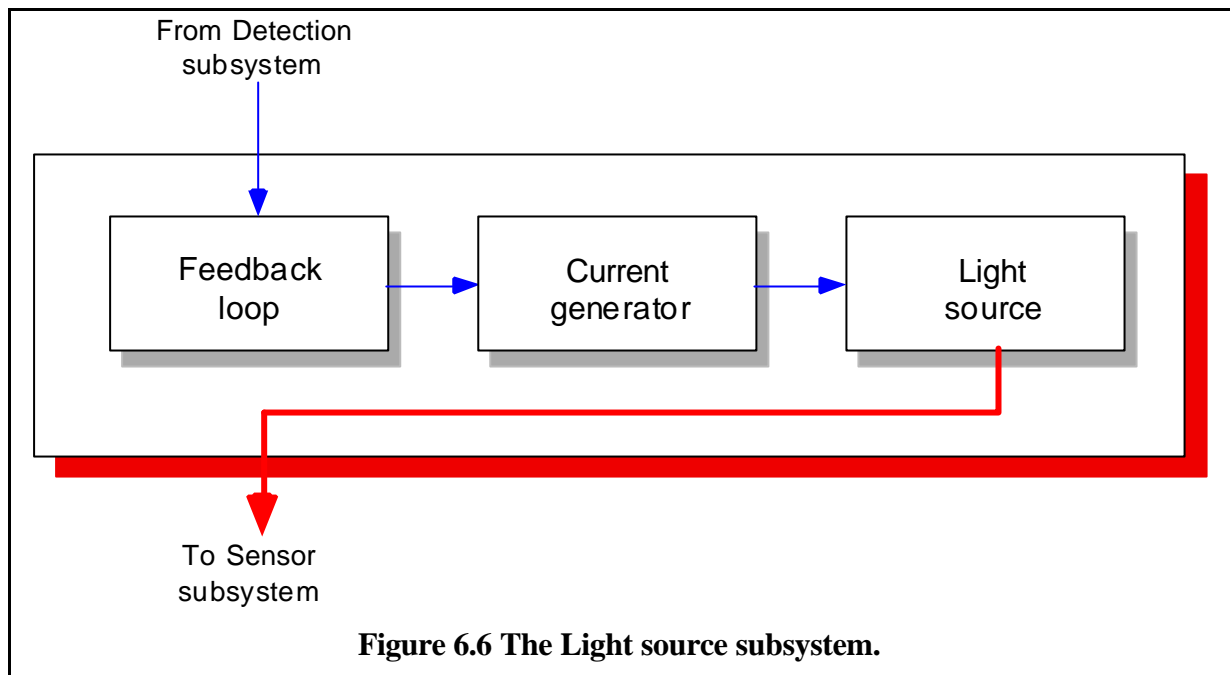
Figure 6.3 shows the SOFO system including the laptop PC, and the reading unit.



6.4.3 Industrial version of SOFO

The SOFO system is now (end 1996) evolving in an industrial product. The industrial version of the reading unit will be very similar in its setup to the SOFO systems presented in this chapter. The main innovations will reside in the 10 mm stroke of the mirror as well as in the possibility to connect multiple reading units and optical switching units to a single control PC using a serial bus. It also complies to international standards.

6.5 Light source



The light source subsystem is the first element of a low coherence measuring system. It includes the optical source itself, the electronics needed to drive it (the current source and possibly the temperature controller) and the optics needed to inject the radiation in the optical fiber. In some cases it is interesting to vary the emitted power to adjust it to the detector sensitivity. In this case a feedback loop from the detection subsystem to the source subsystem should be added.

6.5.1 Requirements

In a low coherence interferometric system the source has to meet the following requirements:

- **Central wavelength:** The emission of the source should be centered around a transmission window of optical fibers. Even if for the short distances typically found in a sensing system, the attenuation does not play a prominent role, it is interesting to work at a standard telecommunication wavelengths in order to take advantage of the large number of components available and their lower price. The three most used wavelengths are 820, 1300 and 1550 nm. The 1300 nm window is the most interesting because of the zero chromatic dispersion characteristic of optical fibers at this wavelength.
- **Emission power:** A more powerful source is an advantage since it allows the measurement of sensors with low reflectivity without increasing the detection gain and therefore reducing the noise and increasing the bandwidth of the detector. To compare the power of different sources, one should always consider the power coupled into the fiber. Some sources can have an high power but, because of the poor directivity of their emission, most of the light will not be coupled into the optical fiber.
- **Optical bandwidth:** Low-coherence interferometry requires a broadband source. We have seen that source with a large spectra will produce a narrow coherence peak and vice versa. It is therefore interesting to have a wide spectra in order to achieve a better precision in the determination of the peak center. Sources with a very wide emission band

will, on the other hand, produce such narrow coherence peaks, that the detection and analysis will become problematic. In this case the dispersion phenomena can no longer be neglected. An ideal source should produce a coherence peak one to two order of magnitude larger than the desired measurement resolution. In our case this gives:

$$\Delta l = \frac{I_0^2}{L_c} = \frac{(1.3 \text{ mm})^2}{30 \text{ mm}} \approx 50 \text{ nm} \quad (1)$$

- **Spectrum:** We have seen that the form of the coherence peaks is given by the Fourier transformation of the source spectra. In order to obtain a narrow and well defined coherence peak with the smallest possible side-peaks, it is therefore interesting to have a source with a near-Gaussian emission spectra. Lorentzian spectra are also interesting. Irregular, rectangular and multiple monochromatic spectra have to be avoided.
- **Size:** The source should possibly be small and light since it will be integrated in the portable reading unit.
- **Power requirements:** A source requiring high electrical power to function will reduce the autonomy of the reading unit. Since high electrical power usually means important heating, an high power source requires cooling, which is a major drawback.
- **Price:** The price to emission-power ratio is of course an important factor in the choice of a source.

6.5.1.1 Choice of the optical source

The three following broad-band sources can be considered for a low-coherence system [5]:

- **Thermal sources:** This type of source can deliver high power with a Gaussian spectra. The emission is not directive and most of the initial power is lost in the coupling into the optical fiber.
- **Light Emitting Diodes (LED):** Surface emitting diodes are also difficult to couple into a singlemode fiber without important losses.
- **Superluminescent Light Emitting Diodes (SLED):** This type of diode has a structure similar to the one of semiconductor lasers but the cavity effect is reduced so that the wavelength selection is much lower. The spontaneous emission produced by the recombination of an electron-hole pairs is coherently amplified while the photons travel to the device surface. The emission is therefore directive and it is possible to couple the radiation into a singlemode fiber with a good efficiency. These devices can be compact and cheap, while offering an interesting optical power output. The spectra is usually nearly Gaussian with minor ripples (ripple increases with emitted power).
- **Erbium doped fiber:** This type of source is similar to a SLED but the amplification of the spontaneous emission occurs in an optical fiber which is doped with erbium ions and optically pumped. The emission occurs in the 1550 nm window and the spectra is usually smooth but not symmetric nor Gaussian. The coherence length tends to be longer than for SLEDs. The required optical pump increases the complexity of the setup and their cost is high. The main advantage of this type of source resides in the high optical power that they can deliver.
- **Laser diodes:** Multimode laser diodes can be used alone or combined to produce low-coherence-like interference patterns [6,7]. These sources can present a very easily recognizable central fringe but tend to have side-peaks extending over large path

unbalances. This can be a problem if multiple sensors have to be multiplexed or even if the lateral peaks come to close to the central one.

Two SLED and one Erbium doped fiber source were retained as possible candidates for the SOFO system and are compared in Table 6.2.

Manufacturer	MRV	Superlum	Photonics
Model	MREDSP015/M REDSP5003	SLD-561	FiberWhite
Source type	SLED	SLED	Erbium doped fiber
Central wavelength [nm]	1300 / 1550	1300	1550
Emitted power (in the fiber) [mW]	250 / 40	500	10'000
Optical bandwidth [nm]	40	42	25
Spectrum	Gaussian	Gaussian	near Gaussian
Polarization state of the emission	partially polarized	partially polarized	depolarized
Size	1 cm ²	1 cm ²	Bulk stand-alone unit
Power requirements [mA at rated power]	80	300	
Price [SFr.]	300	2000	

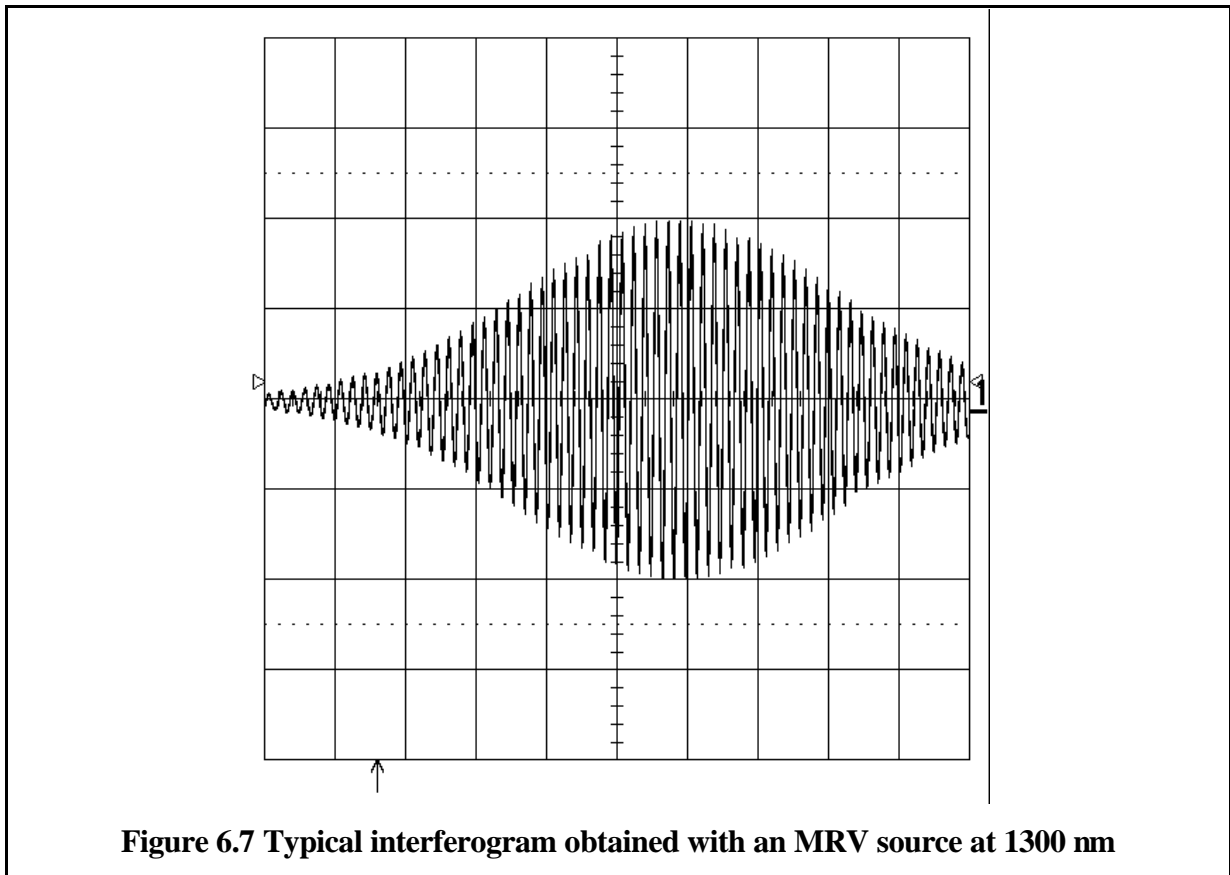
Table 6.6. Comparison between three optical sources.

The Photonics Erbium doped fiber source is delivered as a stand-alone tabletop unit and is not adapted for an integration in an instrument. A subsystem version is probably available, but the price exceeds, for the time being, the available budget. The spectrum is furthermore inferior to the one obtained by SLED sources. This type of source seems very promising for the future but at the technology does not seem mature for field application at this time.

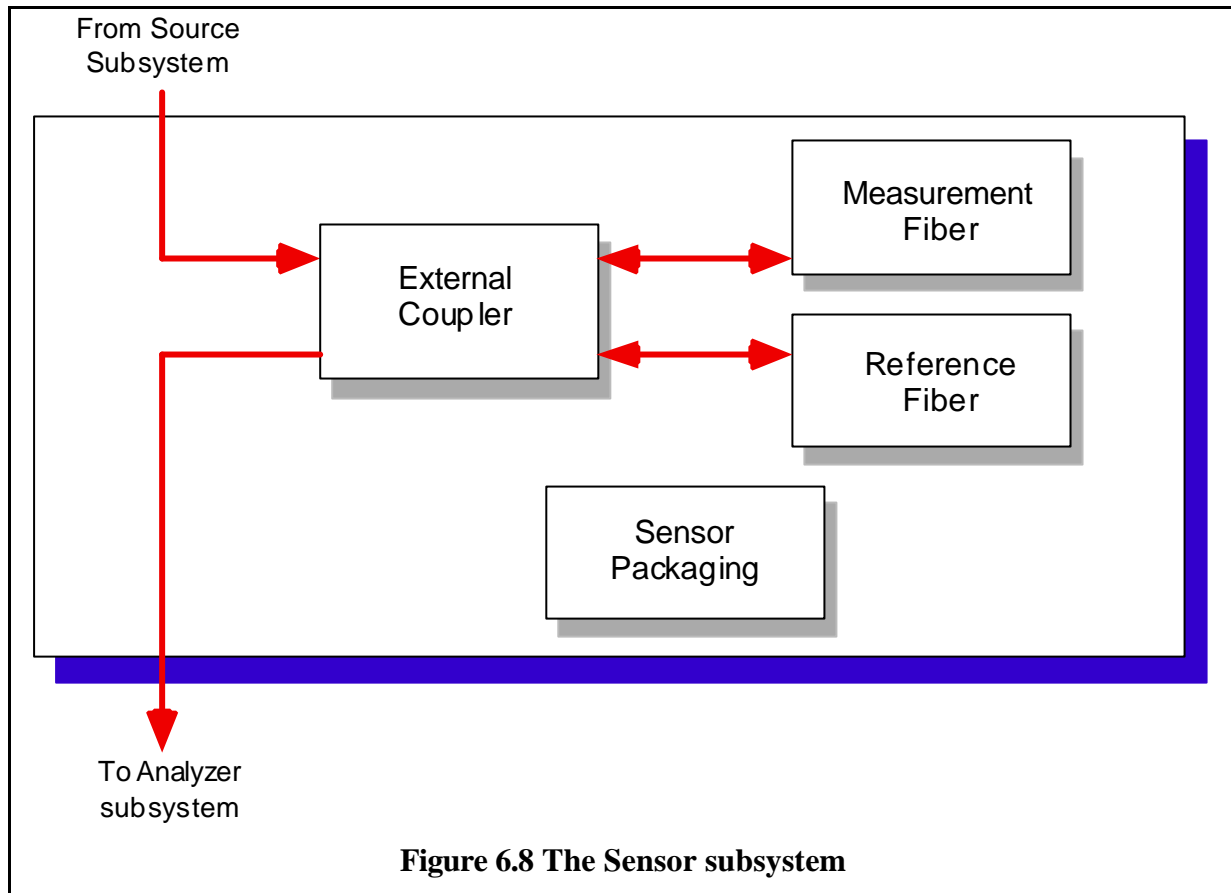
The Superlum SLED (from Superlum LTD, Moscow) has a very high optical power output but requires high currents and is quite expensive.

The MRV sources at 1300 nm (from MRV, Chatsworth, California) offer the best price/performance ratio and were therefore selected for the SOFO system. They are available in either cooled or uncooled packages and are very reliable and stable. During more than three years, we have used about ten of these sources without any failure. The emitted power of the uncooled SLEDs tends to decrease during the first minutes after turn-on because of heating. The optical output is a standard nylon buffered singlemode fiber.

Figure 6.7 shows a typical interferogram obtained with an MRV source. The envelope is almost Gaussian and the coherence length can be estimated to about 40 μm .



6.6 Sensors



The sensor subsystem is for many reasons a special case among the other subsystems and could have justified a section for itself. We have decided to present it in this section since it is an important part in the signal processing chain.

The sensor is the part of the measuring system that is installed in or on the structure and transforms displacements into a change in the path unbalance between two fibers.

Since different types of structures and different materials need specific sensors, this subsystem is the one that has to be adapted most to the particular application. Most efforts have been directed towards the development of a reliable sensor for new concrete structures, but some tests were also conducted on metallic and timber structures, as well as on existing structures where only surface installation was possible.

6.6.1 Requirements

The sensor must respond to different requirements both from the optical point of view as on its mechanical solidity and transmission of the displacements from the structure to the fiber.

- **Optical requirements:** The sensor has to encode a displacement of the structure into a change of the path unbalance between the two fiber arms of a Michelson interferometer. The easiest way to achieve that is to use one of the fibers as a measurement fiber following the structure displacement and a reference fiber independent of it. Obviously, the fibers

have to be intact and microbending must be reduced to minimize the losses and avoid the appearance of parasitic peaks.

- **Mechanical requirements:** The measurement fiber has to be in mechanical contact with the host structure. All axial displacements have to be transferred from the host structure to the fiber. Creeping effects have to be avoided since the final aim of the system are long-term measurements. The reference fiber, on the other hand, has to be completely free and independent of the deformations of the structure. The long term solidity of the fibers have to be guaranteed by avoiding any induced brittleness of the fibers due to superficial micro-cracks. The fiber coating has to be removed only when strictly necessary and only on fiber sections that are not under tension in the sensor.
- **Environmental requirements:** The sensor has to survive the construction and, if possible, the whole life-span of the structure. During the construction phases the sensor is exposed to an hostile environment and has therefore to be rugged enough to protect the fibers from external agent. Chemical aggression has to be taken into account since concrete can be particularly aggressive because of its high alkalinity. These requirements are often contrasting with the ones of the previous point. To protect the fiber one tends to isolate it from the environment by using thicker or multiple layers of coating. This has the side effect to impede the strain transmission from the structure to the fiber. Finally, the sensor must be easy to use by inexperienced persons and has to be installed rapidly without major disturbance to the building yard schedule.
- **Economical requirements:** Since the number of sensors required to monitor a large structure such as a bridge can be counted in the tens, or even in the hundreds, the price of each sensor should be kept as low as possible. It is clear that in the development phase the main cost will be given by the manpower required to fabricate the sensors in small quantities. It is interesting to develop a sensor that could be easily industrialized for a large series production at reasonable prices. The price of the fibers themselves can usually be neglected when compared to the one of connectors, pipes, mechanical pieces and so on.

6.6.2 Fiber and coating types

We have seen that our choice will be limited to singlemode fused silica fibers. The different index profiles will not be discussed in this section since they usually do not affect the mechanical properties of the fibers and standard profiles are ideal for most application and optical set-ups. The only freedom of choice will be on the fiber coating.

The coatings have the function of protecting the fiber from external agents and are usually applied on the fiber directly on the drawing tower. Additional coating can be applied later and the fibers can finally be assembled in cables. The main fiber coatings that can be considered are the standard acrylate micro-coating, the polyimide micro-coating (primary coatings), the nylon tight buffer coating and the micro tube coating (secondary coating). The micro tube is not strictly speaking a coating since the fiber is allowed to slip inside it.

Property	Acrylate coating	Polyimide coating	Nylon buffer	Micro tube coating
External diameter [mm]	250	145	900	900
Coating sequence (from inside to outside)	soft acrylate hard acrylate	polyimide	soft acrylate hard acrylate nylon	soft acrylate hard acrylate air or gel plastic
Stripping	Mechanical or chemical	chemical or thermal	thermal or mechanical	mechanical
Transmission of strain across coating	good for short times, low tensions and $T < 35^{\circ}\text{C}$	excellent	poor	very poor
Mechanical protection	very poor	very poor	moderate	moderate
Chemical protection	moderate	moderate	good	moderate
Price	low (about 0.1 SFr/m)	high (about 3 SFr/m)	moderate (about 0.5 SFr/m)	moderate

Table 6.7. Comparison between different fiber coatings

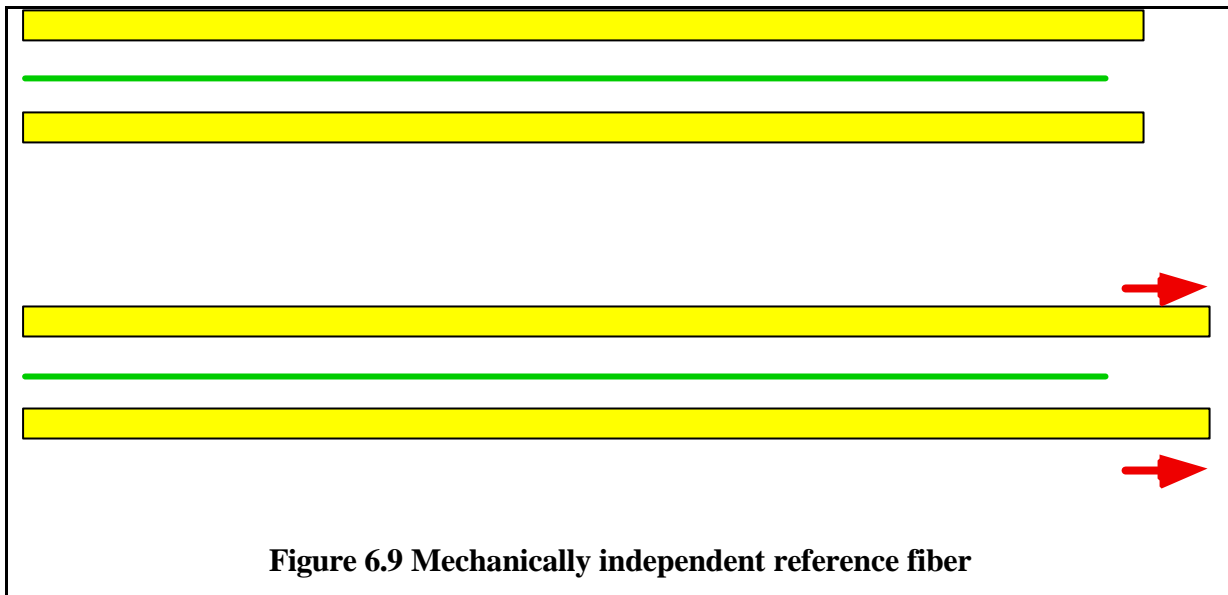
None of these coatings is sufficient to protect the fiber from direct concrete poring. In most case the fiber has to be protected with an additional packaging.

Extensive data is available on the long-term durability of optical fibers installed in telecommunication cables under small tensions [8]. If the strain of the fiber does not exceed 1%, the fiber should have a typical life of more than 40 years before a failure is likely to occur. Thermal and mechanical fatigue can also decrease the life-span of the fibers. We have successfully fatigue tested SOFO sensors for more than 18 millions cycles (corresponding to 40 years in a highway bridge) and with amplitudes typical for concrete structures.

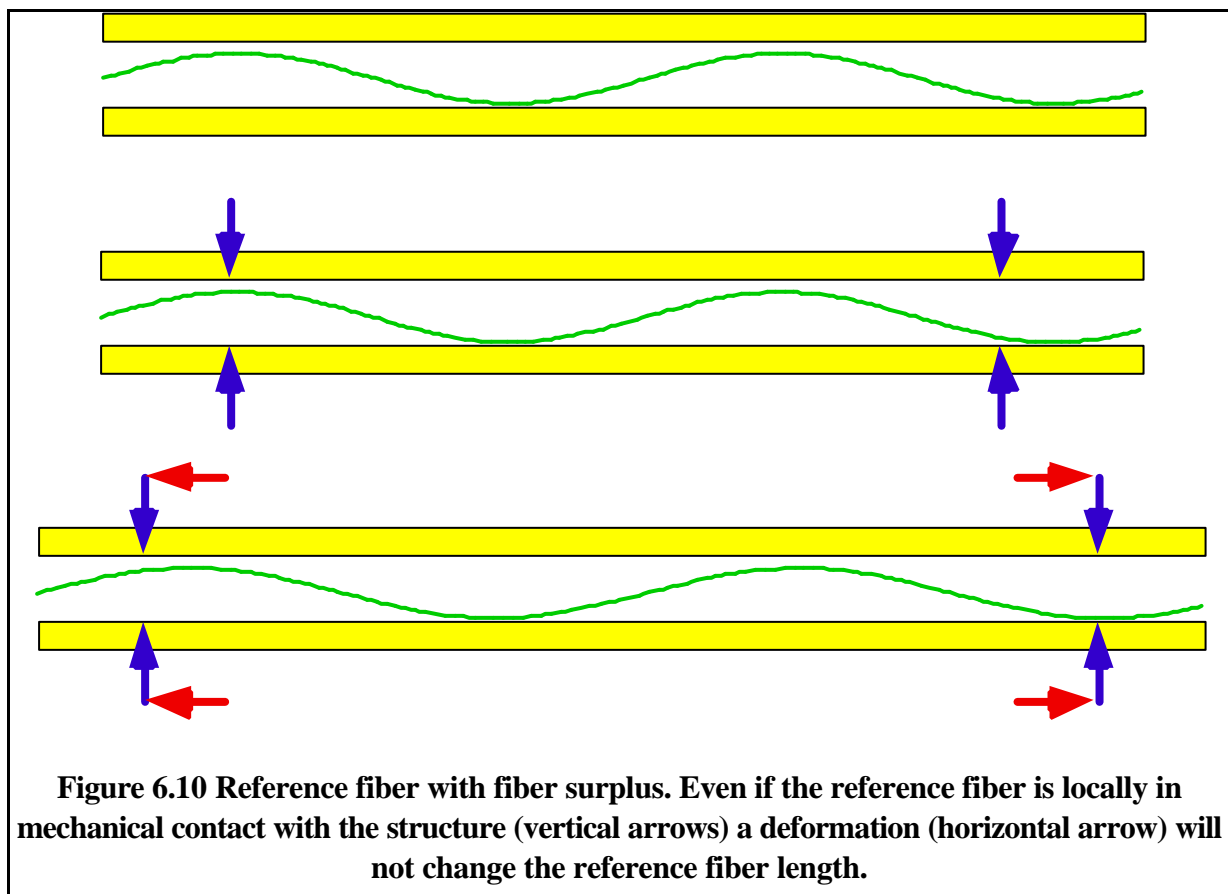
6.6.3 Reference fiber

The reference fiber constitutes the second arm of the sensing interferometer, the other being the measurement fiber. The reference fiber is supposed to be unaffected by the structure displacements and change its optical length only under the influence of temperature variations. Furthermore it is important that the measurement fiber and the reference fiber always have the same temperature locally. This will reduce the parasite sensitivities in the temperature. These requirements are satisfied by installing the reference freely inside a pipe side by side with the measurement fiber. If the measurement fiber setup is based on the local coupling principle (see below), it is even possible to install both fibers in the same pipe. The reference fiber will in this case have an extra length and will therefore remain unstressed when pre-stressing is applied to the measurement fiber. For measurement bases longer than a few meters it was, however, found that the independence of the two fibers could not be guaranteed since the fibers tend to wrap one around the other.

In order to obtain an independent reference fiber, two approaches can be imagined:



- Mechanical independence:** The reference fiber is in this case installed inside a pipe and is supposed to move freely inside it and not to change its proper length when the host structure expands or contracts. This is easier achieved by using multiple layers of concentric pipes with no mechanical contact between one another (except for friction). One example would be a fiber with its acrylate micro-coating installed inside a micro-tube which is finally contained inside a larger pipe. This type of setup has proved its efficiency in laboratory conditions, but seem less interesting for in-field applications where local bending of the pipes can not be avoided. This will increase the friction between the



different layers and ultimately transfer some external deformation to the fiber.

- **Fiber surplus:** In this case the reference fiber is installed in a pipe having an internal diameter much larger than its size and an spare fiber length is stored in the empty space. In this case, even if the reference fiber and the structure are locally in mechanical contact, a displacement of the host structure will not result in a variation of the reference fiber length. If a surplus S is stored inside the pipe, the structure can expand of the same length S without putting the reference fiber in tension as shown in Figure 6.10.

It was found that for short sensors (up to 6 m) the surplus approach was sufficient. For longer sensors or large displacements it was found that the best results would be obtained by first putting the fiber in a micro-tube and then installing this one into a large tube allowing a consistent surplus. By this means, it was typically possible to pull the external pipe up to 2% without having the fiber stretched more than 0.01%.

6.6.4 Local vs. distributed coupling

Since the measuring system responds to variations of the total optical length of the sensing fibers, two installation approaches can be followed to couple the fiber to the structure: local and distributed (or full-length) coupling. In the first case the measurement fiber is fixed to the host structure at two points and free inside a pipe in-between. In order to follow both elongation and shortening, the fiber must be pre-strained. The two attachment points will define the limits of the measurement zone. In this case the quality of the coupling between the fiber and the structure at the two attachment points will play an important role in the response of the sensor to the structure deformations.

In the case of distributed coupling the measurement fiber is attached to the structure along the whole active region. In this case the characteristics of the fiber coatings will have a strong influence on the sensitivity of the sensor.

6.6.5 Distributed coupling sensors

This type of coupling offers the advantage of an apparent simplicity, since the measurement fiber is identical over the whole active region and no special attachment points are needed. Furthermore, in most cases the fiber will respond to both elongation and shortening without the need of pre-stressing. The contact between the host material and the fiber over its whole length, introduces two potential problems that should not be neglected: transversal strains and microbending.

Since the fiber is surrounded by the host material or by the glue used to attach it to the structure, it is possible that it will be subject to transversal strain components perpendicular to the fiber axis. These components will alter the refractive index and the core diameter of the fiber and therefore induce an optical path variation. This variation will be incorrectly interpreted as a displacement in the fiber direction. The transmission of transversal strain from the structure to the fiber core depends strongly on the characteristics of the fiber coating. Soft coating reduces these effects but also increases the possibility of creeping effects in the axial direction. Different optical arrangements have been proposed in order to separate the axial and transversal components but in all cases the axial sensitivity and resolution are reduced. In the case of civil structural monitoring it is easier, in most cases to isolate the fiber in a pipe so that no transversal strain will reach the fiber (local coupling). This is not the case in other fields such as composite material monitoring, where a pipe would alter significantly the structural behavior.

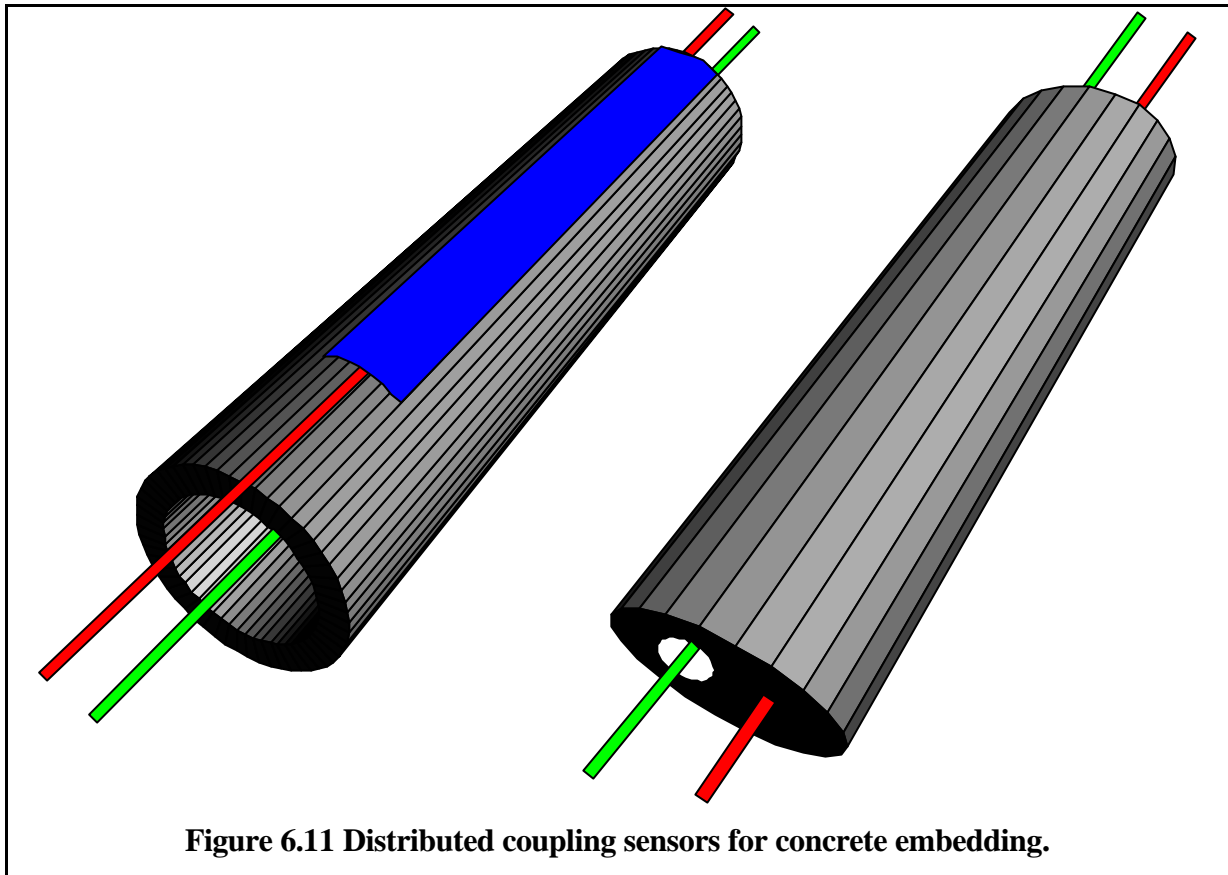


Figure 6.11 Distributed coupling sensors for concrete embedding.

The local coupling approach is nevertheless interesting in some cases since the extended coupling length allows good measurements even if the mechanical contact between the fiber and the structure is rather weak. It is furthermore possible to reduce the size of the sensor to the one of a coated fiber (the reference fiber has to be installed in a pipe in any case). This type of coupling is interesting in the case of metallic structures, where the measurement fiber can be simply glued on the surface or mortars where a nylon coated fiber can be embedded directly. It was also attempted to glue optical fibers directly on the re-bars. The survival rate was low because the fibers tended to be damaged at the re-bar crossings. Furthermore, it was difficult to prove that the presence of the fiber and of the glue on at least one eighth of the re-bar perimeter would not alter the adhesion between the re-bar and the surrounding concrete. Other tests were directed to the design of a sensor based on distributed coupling for direct embedding into concrete.

Figure 6.11 shows two possible sensor design based on this concept. The first sensor consists in a rigid pipe containing the reference fiber and with the measurement fiber attached to its surface with an adhesive tape. The rigid pipe protects the nylon coated measurement fiber from excessive bending and it was found that an high survival rate could be obtained with this type of sensor. It appears that an excellent coupling between the fiber and the structure could be achieved by this mean. The second sensor showed in Figure 6.11 consists in a custom designed cable containing the reference fiber in a empty or gel filled cavity and the measurement fiber directly surrounded by nylon. Although Cabloptic (in Cortaillod, Switzerland) would be able to manufacture such a sensor, an experimental realization was never attempted, mainly for financial reasons.

Another interesting example (see Figure 6.12) of distributed coupling was attempted with shotcrete (used mainly for tunnel casing). In this test, we have installed optical fibers with

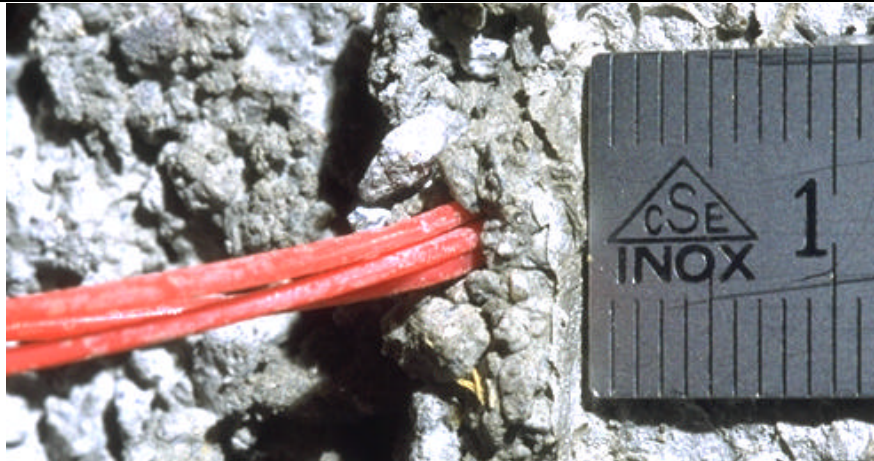


Figure 6.12 Example of distributed coupling: nylon coated fibers installed in shotcrete.

0.9 mm nylon coating in a 1 m long sample projected in real tunneling conditions. A 5 cm layer of concrete was first laid, the fibers were then placed on this soft surface. Some fibers were unprotected, while others were covered by a plastic half-pipe, a plastic profile, wood or a small re-bar. All of the 10 fiber (protected or not) survived the projection of a second 4 cm layer of concrete. The increase in the scattering losses was small and the microbending induced back-signal was at least -15 dB from the transmitted signal. By providing external reference fibers of the same length measurements could be performed normally.

In all these cases the perpendicular strain component seems not to play an important role and measurements could be performed without the need of special correction. This type of coupling presents some other drawbacks that have led us to concentrate on local coupling. The first resides in the difficulty to separate the active from the passive region inside the structure. The measurement fiber should become free at the interface between these two regions. This means that it should enter a pipe at this point and this increases the complexity of the setup. Most designs, even if they appear simple at first, turned out to be of difficult application in real structure and the fabrication of the sensors often proved tricky and tedious. Furthermore, the possibility of creeping between the fiber and the structure in the axial direction has not been addressed in the case of long-term measurements.

6.6.6 Local Coupling sensors

In this type of setup, the measurement fiber is attached to the structure at the extremities of the active region and pre-stressed between these two points. The fiber is contained in a pipe over its whole length, free in the passive regions and stressed in the active region. In this case the main problem to be solved is the realization of a reliable mechanical coupling between the fiber and the mechanical piece used to anchor it to the structure.

Since all the efforts are transmitted from the structure to the fiber at the two anchorage points, the fiber has to be bonded to the anchorage points in a very rigid way. Besides the strains due to the structure deformations, these points have to react to the forces produced by the necessary pre-stressing of the measurement fiber.

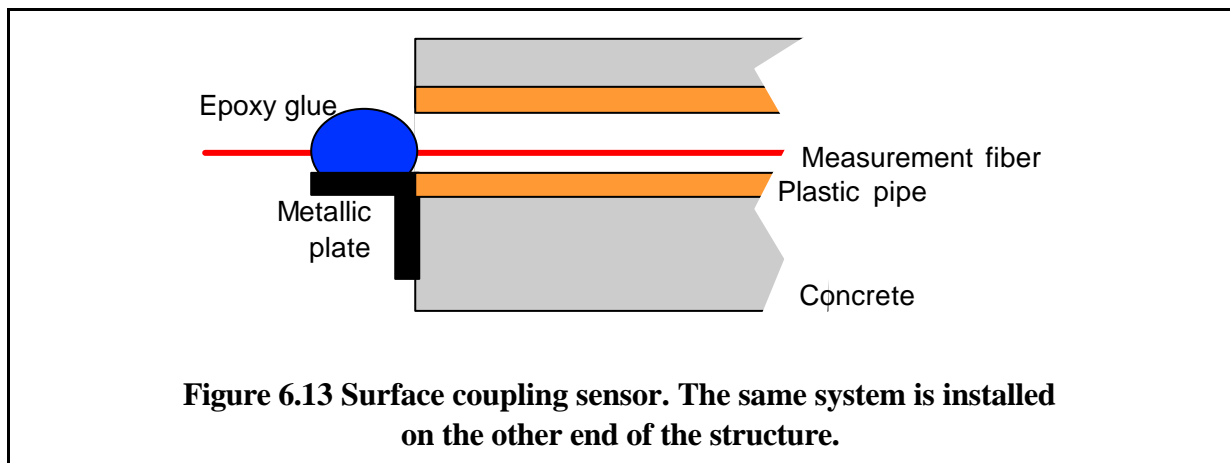
It was found that epoxy glues were well suited to obtain the necessary rigidity and immunity from creeping effects. Gluing on the acrylate micro-coating was sufficient for short term measurements with fiber elongation under 0.5% and for temperatures below 30°C during the whole experiment. For long-term measurements, high tensions or temperatures above 30°C

(such as the one found during the setting process in concrete) it is necessary to remove locally the acrylate micro-coating in order to glue directly on the glass and avoid creeping problems. The mechanical stripping of the micro-coating induces a fragilization of the fiber itself and this increases the chances of sensor failure after a short period. Two solutions are possible to avoid this problem: chemical removal of the coating or use of polyimide coating. In the first case the acrylate coating is removed by attacking it with an acid (sulfuric acid) or a solvent (dichloromethane). A fiber stripped chemically maintains almost the same strength as a coated fiber. However, any contact of the unprotected fiber region with a sharp edge would increase the failure probability in a dramatic way. This makes the chemical stripping particularly unattractive for large-scale applications, since very complicated procedures should be developed in order to conserve the mechanical strength of the uncoated fiber during the whole sensor assembly process. The use of polyimide coated fibers makes the stripping process unnecessary, since the strains are easily transmitted through this thin and hard coating. No creeping is expected for this type of coating even at temperature up to 300°C. The main drawbacks of this type of coating resides in its high price and in the necessity to strip the fiber mechanically to mount a splice or a chemical mirror. These components are installed in fiber regions that are not under permanent tension. This reduces the possibility of a failure due to a fragilization of the fiber during its manipulation.

The following chapters present the evolution of the local coupling sensors for the SOFO system from their first application to its industrial production.

6.6.6.1 Surface coupling

The first application of the low-coherence interferometer to the monitoring of civil structures, was the measurement of the free shrinkage of a 20 m x 5 m x 0.5 m concrete slab [9,10]. The variation of its length were monitored over a period of more than one year. In this case most sensors were installed a few days after concrete pouring, inside different pipes that had been installed empty in the re-bar cage. The measurement fibers were nylon coated. The buffer coating was removed thermally with hot air, while the acrylate micro-coating was removed chemically with dichloromethane. The fibers were thereafter glued to a metallic plate screwed on the surface at the two ends of the concrete slab (see Figure 6.13). A pre stress of about 0.5% was given to the measurement fibers.



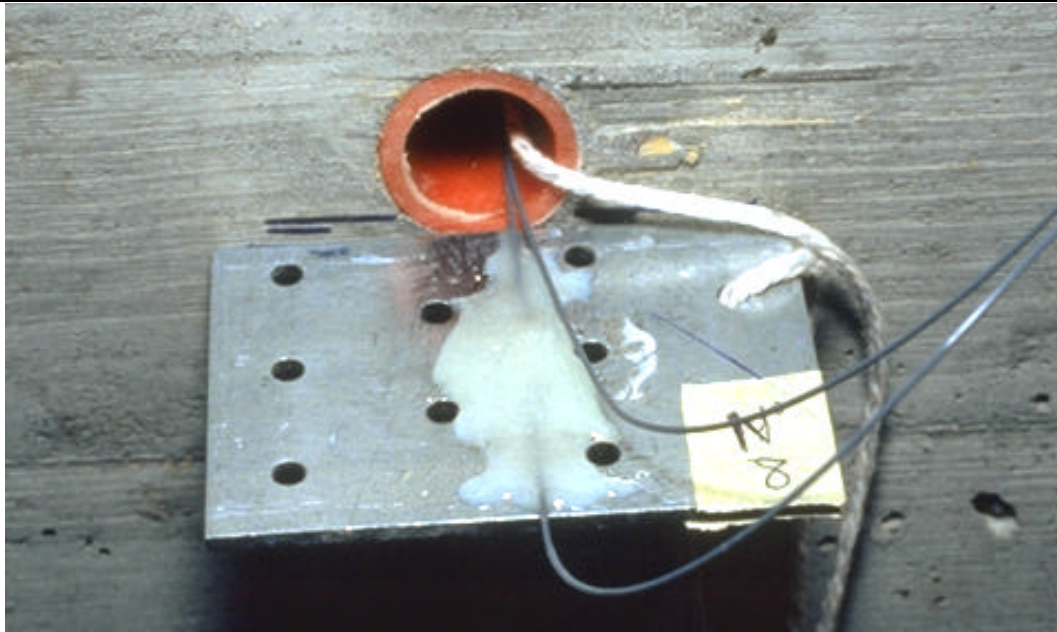


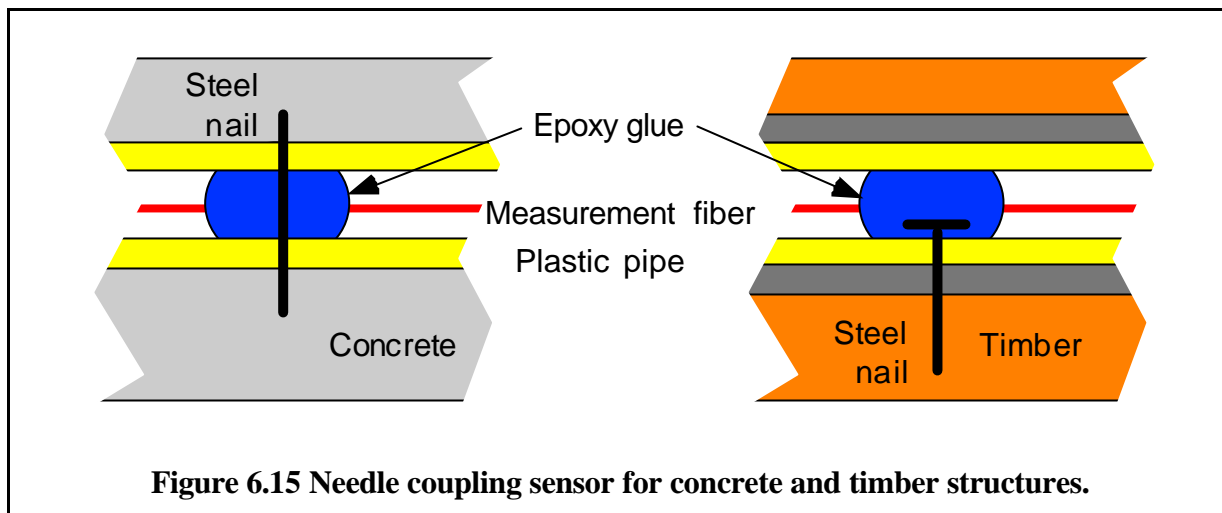
Figure 6.14 An example of surface coupling sensor.

From the point of view of the measurements this setup proved very effective and it was possible to obtain reliable measurements over two years without any noticeable creeping effect. This setup presents different drawbacks from the point of view of the installation procedure. First, since the fibers can be installed only after removal to the formwork, it is impossible to measure the displacements occurring during the first days after concreting. Furthermore, the installation is very time-consuming and a large-scale application of this technique would be impossible. Finally, the system was very fragile and many fibers broke outside the structure because of careless manipulation. This problem could have been solved by protecting the fiber outputs inside a box. The main drawback of this setup is that only the whole structure length can be monitored. In real structures this would be an intolerable limitation.

Figure 6.14 shows an example of surface coupling. The free reference fiber is also visible.

6.6.6.2 Needle coupling

After the first feasibility tests using the surface coupling setup, it became clear that it was necessary to develop a stand-alone sensor that could be easily installed in the re-bar cage before concreting. The first realization of this new concept was tested in a mixed timber-concrete structure and the fibers were installed in both materials with an analogous setup [11]. The measurement fiber is protected along its whole length by a plastic pipe. The fixation points are realized by piercing the pipe with steel nails at the location of the anchorage points (see Figure 6.15). Epoxy glue is then injected around the nail through the pipe wall. Once hardened, the glue realizes (with the nail) the desired mechanical contact between the fiber and the structure. The necessary pre-stressing of the fiber is applied while installing the sensor in re-bar cage by pulling on the two nails. This type of sensor is very simple in its manufacture and the installation needs only a few minutes for each sensor. The only delicate operation is the pre-stressing of the sensor in the re-bar cage.

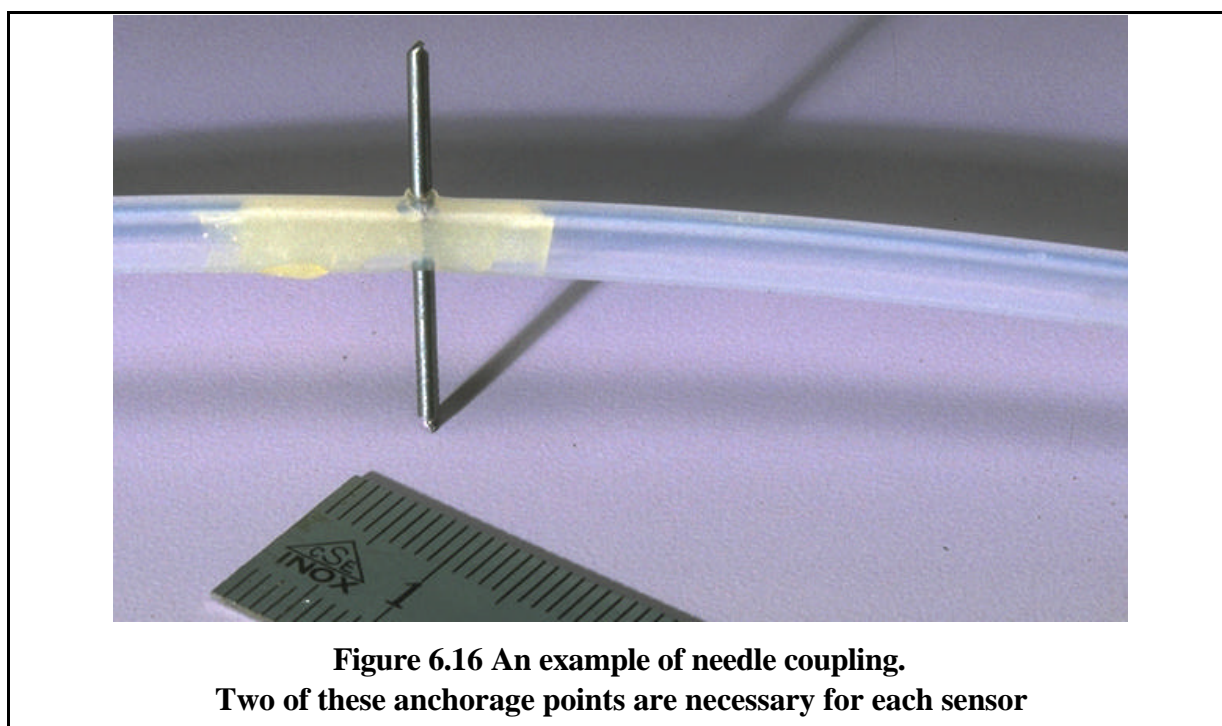


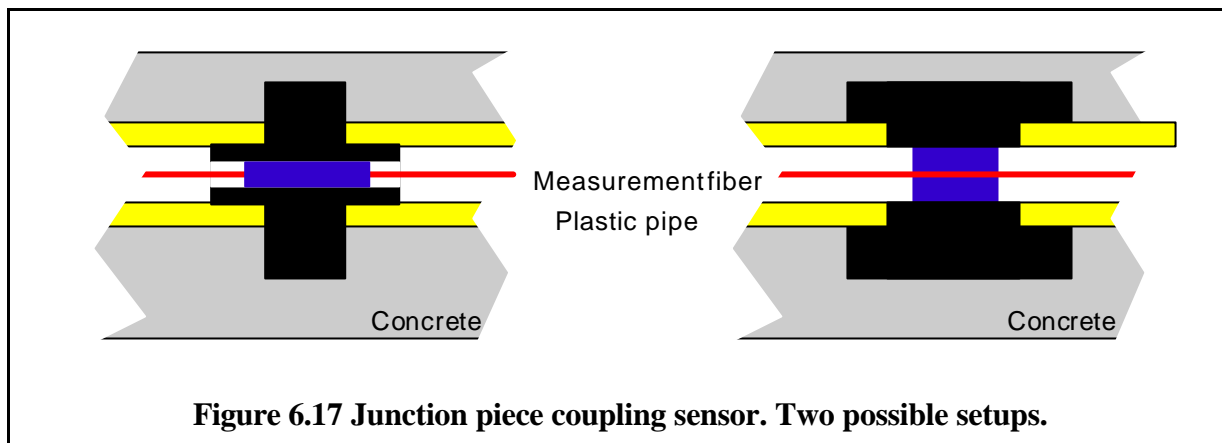
The main problem with this sensor is that the efforts have to be transferred to the fiber through the acrylate micro-coating. This is not a concern for short-term measurements, but leads to problems for long-term measurements or when the structure temperature rises above 35°C. At this temperature, the viscosity of the inner acrylate coating is drastically reduced and creeping occurs at a high rate. It would be possible to remove the coating at the fixation points before putting the fiber in the pipe, but this would increase the complexity of the sensor fabrication. The use of a polyimide coated fiber solves this problem and was later tested experimentally on a timber beam.

Figure 6.16 shows an example of needle coupling for installation in concrete. The reference fiber would be contained in a separate pipe.

6.6.6.3 Junction piece coupling (VSL, IBAP, EDF)

Two main problems were addressed in the design of this new generation of sensors. On one hand it was wished to obtain a better mechanical coupling than the one realized with the steel





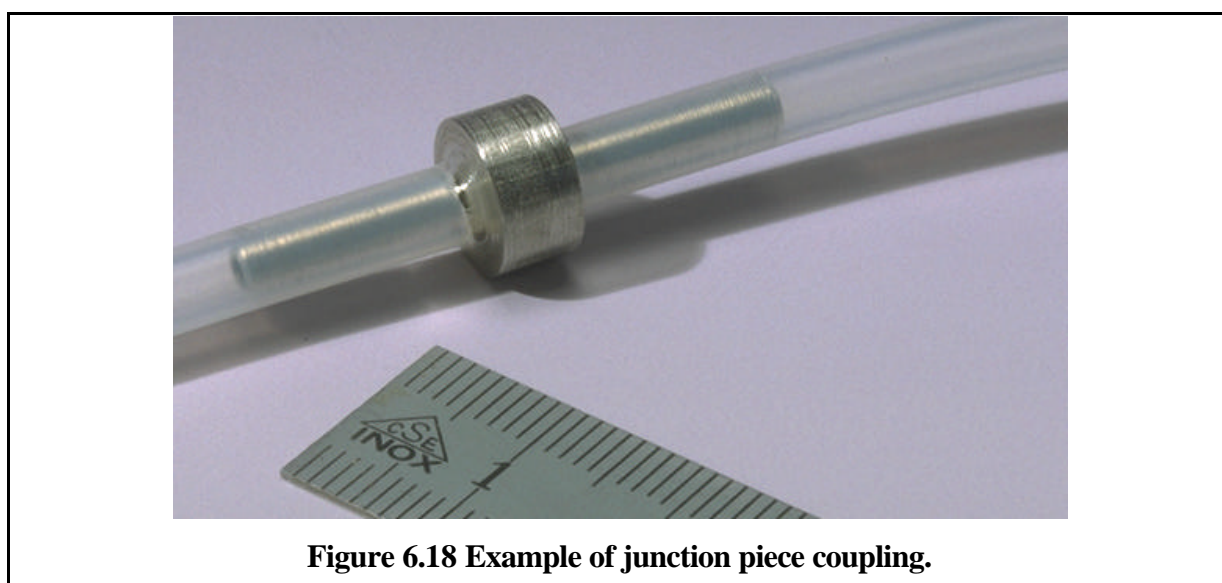
nail and gain access to the fiber in order to strip the coating easier. On the other hand it seemed important to pre-stress the measurement fiber at the manufacturing stage and not at installation. These problems were solved designing custom mechanic pieces that act as fixation points for the fiber and at the same time as junctions between two pipes [12]. Examples of such pieces are given in Figure 6.17 and Figure 6.19.

At first it was attempted to strip the micro-coating mechanically at the location of the two fixation points. This rendered fragile the fibers that failed after a few days under tension. This problem could have been solved with chemical stripping at the expense of a increased complication in the fabrication procedure. At that time it was decided to direct the research in towards polyimide coated fibers.

In a successive variation on the same theme, both fibers were installed in the same pipe and glued onto a half-moon shaped mechanical piece. This allowed gluing the polyimide coated fibers from the side. The sensor was then completed by closing the mechanical pieces with a second half-moon piece and pre-tensioning the sensor by letting the pipe slip inside one of the junction pieces and then blocking it with a ring. This sensor has been successfully tested on a number of applications and proved very easy to install into a new structure (without delay to the building yard schedule) or on the surface of an existing structure.

Figure 6.19 shows a detail of the junction pieces used in this setup.

6.6.6.4 Industrialization of the sensor



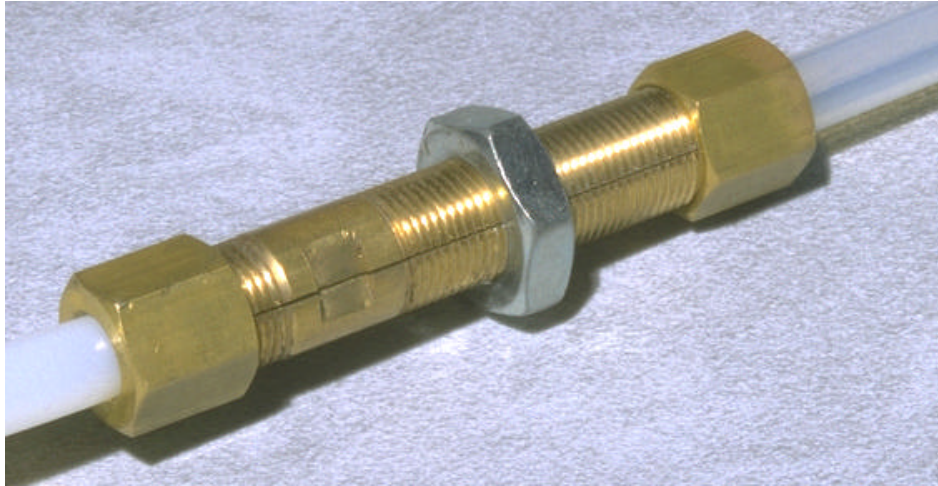


Figure 6.19 Junction piece sensor.

After fabricating a few tens of junction piece sensors it became clear that they were indeed well adapted to the needs of civil engineering monitoring. Fabrication required about six hours for a batch of six sensors. This process proved to be rather tedious and attempts were made to teach non-engineers to build the sensor. In order to install hundred of these sensors in a structure without needing months to assemble them, it was necessary to find an industrial partner interested and capable of re-engineering the sensors to bring supplies to large quantity production. The connector manufacturer DIAMOND SA in Losone (Switzerland) was the ideal partner for this task. After a few months of intense collaboration, it was possible to transfer the knowledge accumulated at IMAC over more than three years installing sensors in concrete to DIAMOND and combine it with the industrial experience of this company in the domain of connector production.

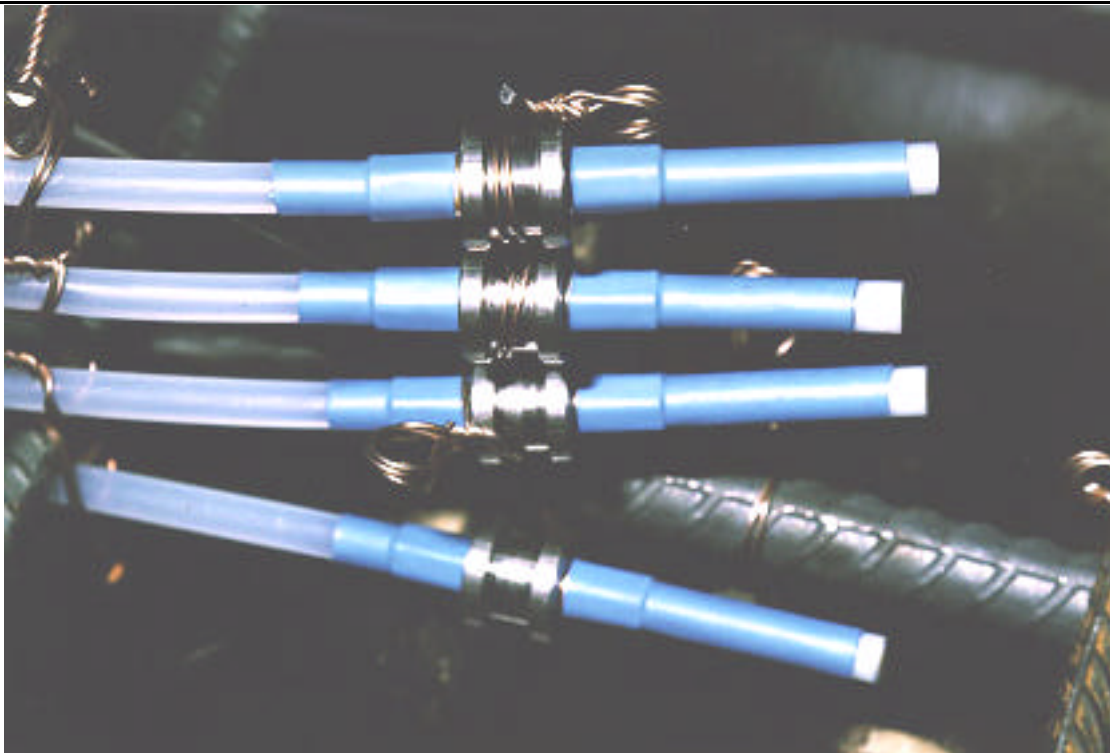


Figure 6.20 The IMAC-DIAMOND sensor.

The result is the sensor shown in Figure 6.20. This sensor has now been used in many different applications both embedded in concrete or mounted on the surface of existing structures [13], and is now commercialized by SMARTEC SA..

6.6.7 Mirrors

The light has to be reflected back at the ends of both the measurement and the reference fibers. This required the installation of reflectors at the end of both fibers. This can be obtained by one of the following ways:

6.6.7.1 Fresnel mirrors

If the fiber is cleaved, a reflection of about 4% is obtained because of the refractive index change between glass and air. This reflection is sufficient to perform a measurement. The reflection will drop almost to zero if a dust particle deposits or humidity condenses on the end-facet. This type of reflection is therefore useful only when the end facet is accessible and serviceable, i.e. only in laboratory conditions.

6.6.7.2 Mechanical mirrors

If a ferrule or a connector is installed at the fiber end and a polished ferrule is positioned in physical contact in front of it, a good reflection of up to 100% can be achieved. This reflector is bulky, expensive and possibly subject to corrosion. An improvement consist in adhering a gold leaf to the polished end-facet of the ferule. Reflection up to -1 dB can be obtained that way. This type of reflector has been used in early versions of the DIAMOND sensors.

6.6.7.3 Chemical mirrors

The easiest way to produce an highly reflective mirror on the end of a fiber is to deposit silver on its cleaved end-facet. The following procedure will produce such a mirror:

1. Cleave the fiber at the right length.
2. Add one part of solution A to one part of solution B in a clean pot.
3. Mix the two until the solutions becomes clear.
4. Immerse the fibers and add one part of solution C.
5. Wait about 30 min or until the back-reflected signal ceases to increase.
6. Let the silver coating dry and protect it.

The composition of the solutions is the following:

Solution A: 1 dl H₂O (distilled water) + 3 g AgNO₃ (silver nitrate).

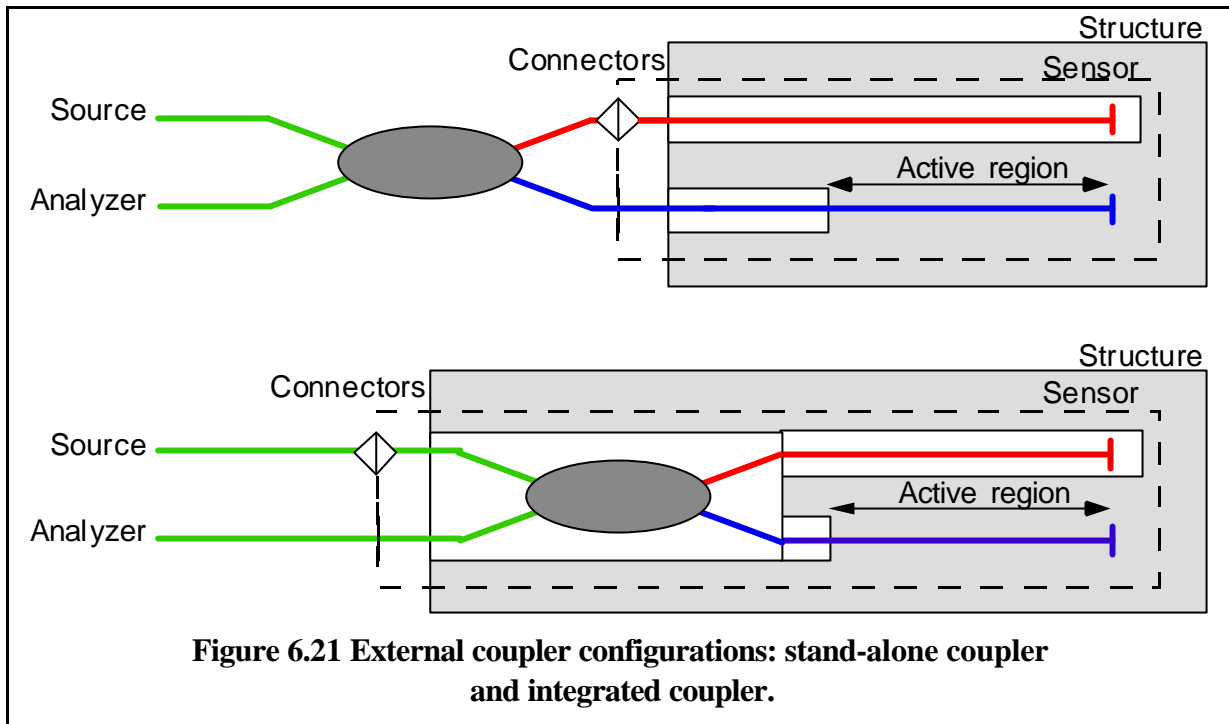
Solution B: 0.25 dl NH₃ (ammonia: 24%) + 0.75 dl H₂O + 4 g KOH (potassium hydroxide).

Solution C: 1 dl H₂O + 15 g Glucose.

The mirrors produced in this way have proved to be stable of many years. Furthermore the size of the fiber end is not increased (except for the mirror protection) and the cost of this type of mirror is negligible.

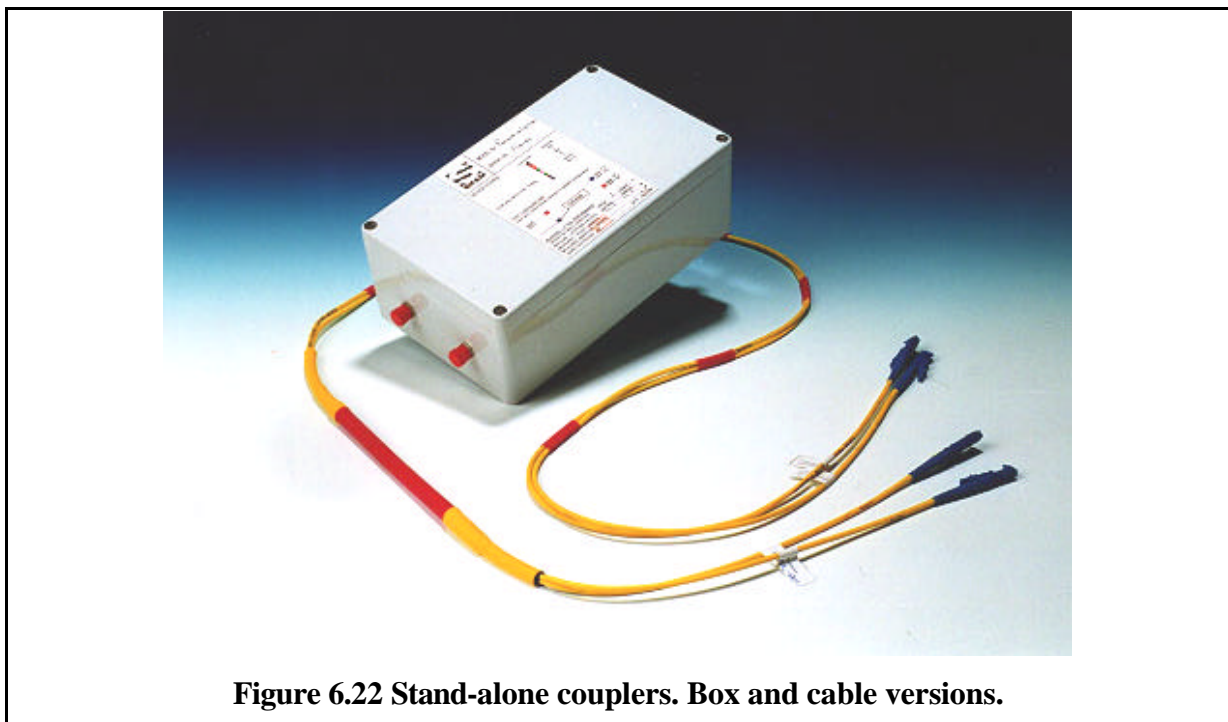
6.6.8 External optical coupler

The external optical coupler divides the optical power produced by the source and directs it towards the measurement and reference fiber. Once the light reflected at the two fiber ends, this coupler recombines the beams and directs them towards the analyzer (half of the reflected light is, in fact, sent back to the source and therefore lost). The path unbalance that will be



measured by the analyzer corresponds to the difference of optical length between the two interferometer arms, i.e. the optical length difference between the coupler and the two mirrors. This is an important point to be considered when connectors are present between the coupler and the sensor. In this case if another coupler is used, the measurements will be affected. It is possible to characterize the delay introduced by each coupler and compensate for it in at the data processing stage.

The packaging of the coupler can be realized in different ways. In some case it is interesting to use the same external coupler for different sensors. This results in a reduction of the sensor cost, since a coupler costs about 50-100 SFr. When an higher precision is required or when



the sensor is very distant from the analyzer, it is useful to install an external coupler in each sensor, as close as possible to the sensing region.

6.6.8.1 Stand-alone coupler

The stand-alone coupler is either contained in a small box or integrated into the optical duplex cable coming from the reading unit. The measurement and reference arms have to be clearly identified in order to avoid any possible inversion that will lead to incorrect measurements. The box version is used when the sensors are terminated in a connector bundle. The cable version is more useful when the sensors are terminated by mating adapters mounted in a connection box.

6.6.8.2 Integrated coupler

In this case the coupler is integrated into the sensor package. This avoids any connection and disconnection in the active region and therefore improves the accuracy of the measurement. The main drawback of this configuration is in the increased sensor price. When a coupler is installed in the sensor it is possible to connect the sensor to the reading unit via a single fiber. This produces a loss of 6 dB but halves the cost of all connectors, mating adapters and fiber cables, which offsets the increased cost of the sensor. By using an optical circulator it would even be possible to obtain the same power efficiency as with the two fibers. Displacement precision down to a micron were obtained in field conditions with such sensors. Another problem resides in the fact that it becomes impossible to determine the sign of the path unbalance by inversion of the coupler connection (see paragraph 5.6). This problem is solved if one of the fibers, usually the reference fiber, is clearly longer than the other and no sign inversion is possible even for the maximal expected displacement of the host structure.

6.6.9 Optical connectors

Since multiple sensors can be measured by the same reading unit, optical connectors are required in order to plug the sensors one after the other. Most singlemode connectors used in the telecom industry are optically well suited for this application. However these connectors will be used in the very dusty and demanding environment of a building yard. After using 3M's FC/PC connectors for about two years, it became evident that these connectors, although well suited for laboratory conditions, were too sensitive to dust for in-field applications. At that time, DIAMOND was delivering its first E2000 connectors (Figure 6.23) that seemed better suited for this type of application. These connectors feature an integrated dust cap that closes

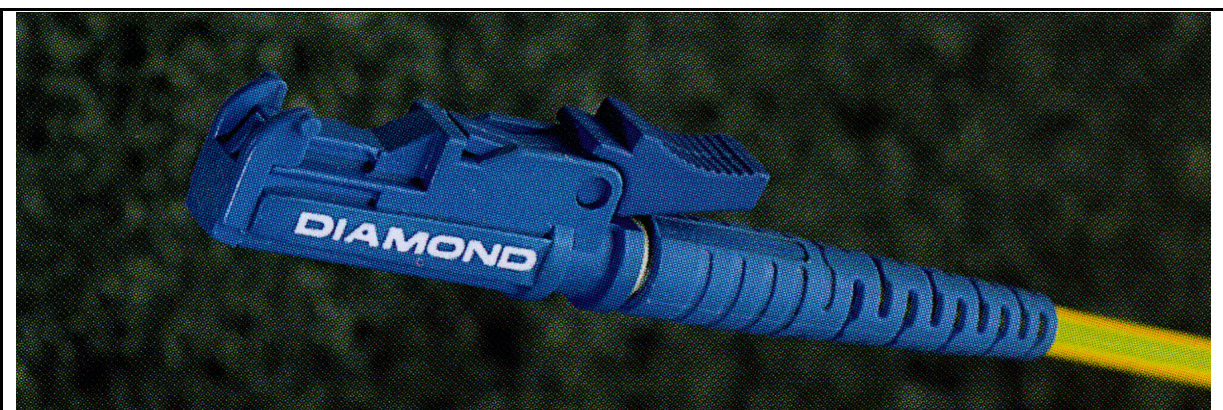


Figure 6.23 DIAMOND E2000 connector with integrated dust cap.

automatically when removing the connector from its mating adapter. Furthermore, the mechanical connection is rapid and unlike the 3M system requires no time consuming screwing and unscrewing. These connectors are factory mounted and present excellent optical properties, including low insertion losses ($<0.3\text{dB}$) and good repeatability.

6.6.10 Optical cables

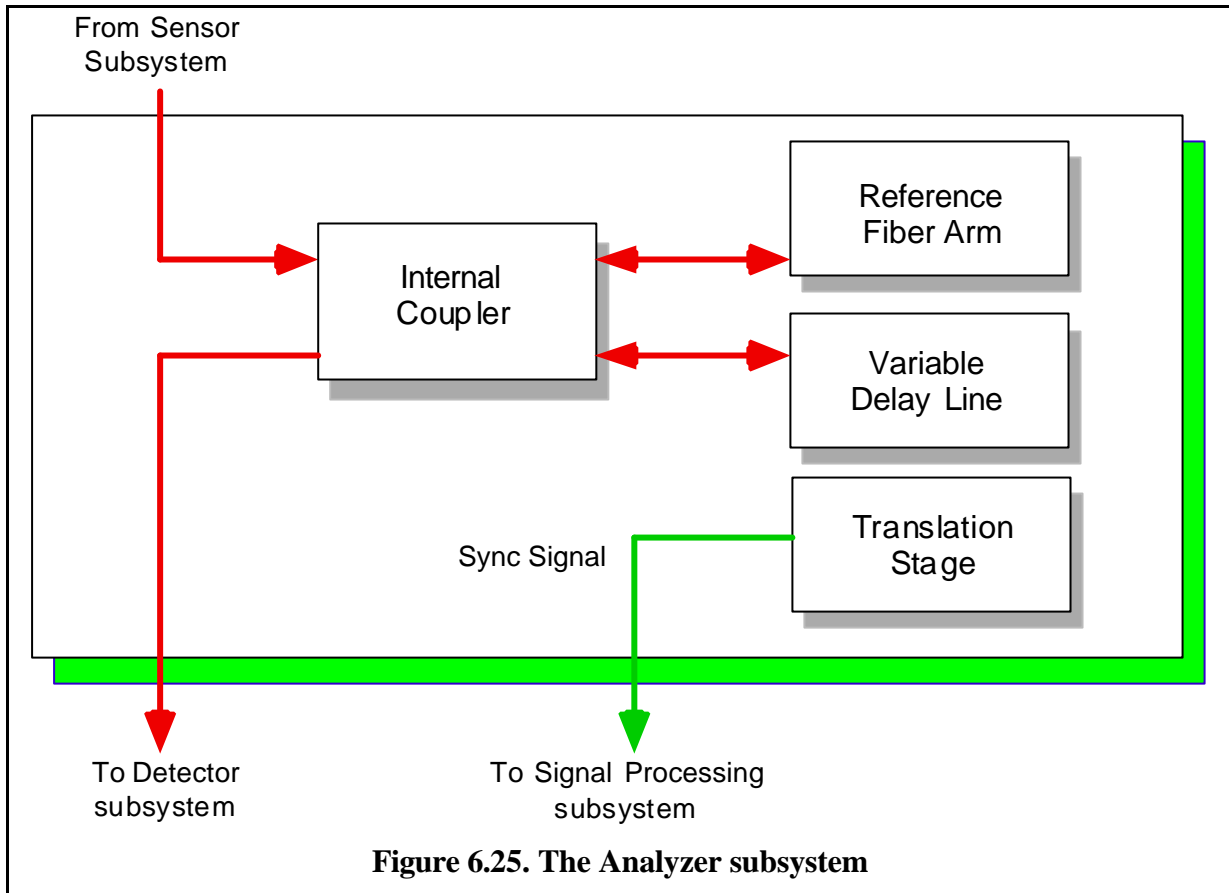
In many cases the sensor is placed in an inaccessible region of the structure and the optical fibers have to be routed to a common access point where the reading unit can be easily connected. In these cases it is necessary to install optical cables between the sensor and the reading unit. According to the two configurations presented in Figure 6.21, the cable can be installed either between the active region and the coupler (i.e. in the active region) or between the coupler and the reading unit (i.e. in the passive region). In the second case, an external coupler is necessary for each sensor.

As a general rule, if the optical cable is installed in the active region, the fibers must be contained in micro-tubes inside the cables and the tight buffered fibers have to be avoided. Furthermore, the cable should not be moved, unrolled or displaced between the measurements or a dramatic decrease in the accuracy will result. In the case of structures that are constructed in different phases, where the installation of the optical fiber wiring has to precede in parallel with the construction progress two alternatives are possible. Either each sensor is provided with its own coupler and the cable is installed in the passive region, or a measurement is performed immediately before and after each cable displacement and the errors are then corrected at the data processing stage. If the cable is installed in the passive region no correction or special procedures are needed and nylon buffered cables can be used. These considerations point to the fact that for most field applications the use of integrated couplers is preferable. We will see in the following section on multiplexing that partial reflectors can overcome some of these limitations. Where connection between different cables are necessary, a small plastic or metallic box will protect the connectors and the mating adapters (see Figure 6.24).



Figure 6.24 Connection box with mating adapters.

6.7 Analyzer



The function of analyzer subsystem is to introduce a well controlled path unbalance between its two arms in order to compensate the unknown path unbalance between the two arms of the sensor. In this sense the analyzer is the optical equivalent of a resistive Whetstone's bridge. In the spectral approach the analyzer is seen as a Michelson interferometer performing a Fourier analysis of the incoming spectra.

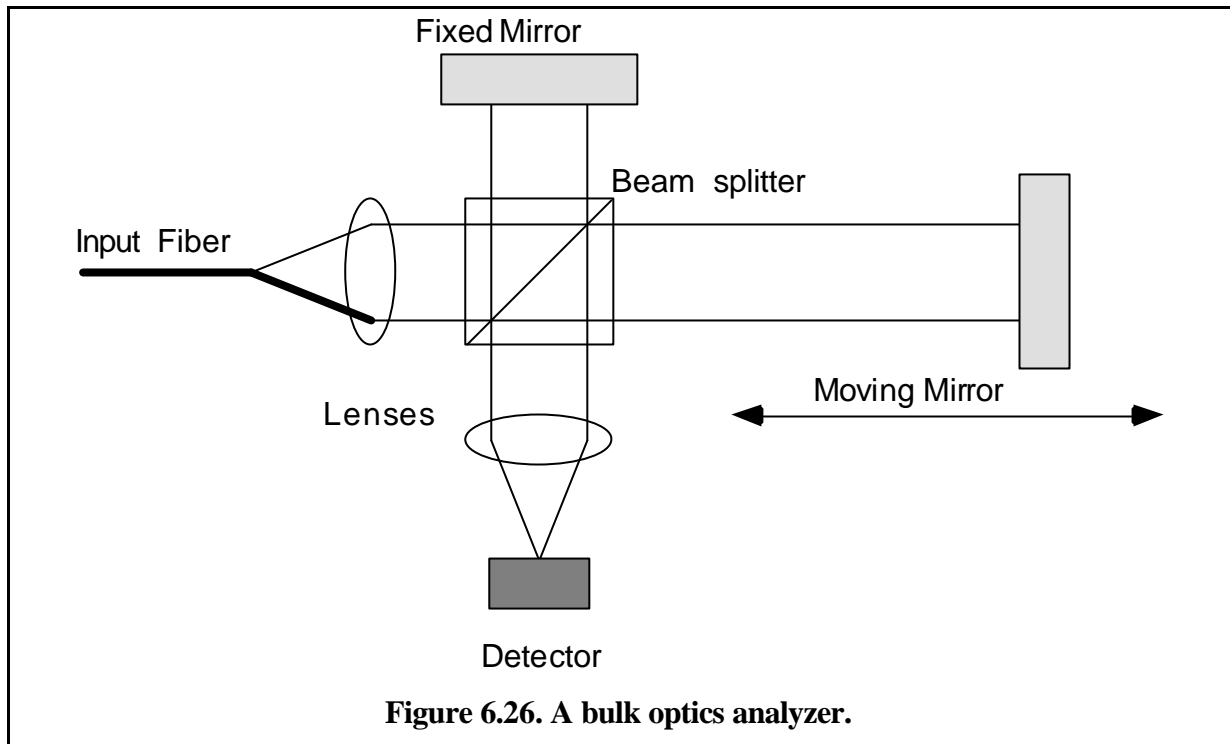
The analyzer subsystem consists in a beam splitter, one fixed-length arm and a variable delay line on its second arm. The mechanical and electrical components necessary to operate the delay line are also part of this subsystem.

6.7.1 Optical setup

Many realizations of the delay line are possible with different combinations of bulk and fiber components. In all cases it is required that the delay line is able to introduce path unbalances up to at least 200 mm (one way).

6.7.1.1 Bulk optics setups

The delay line can be realized fully with bulk optics. In this case the light is uncoupled from the incoming fiber and split by hand of a cube beam-splitter. The two resulting beams are reflected by two mirrors and recombined by the beam-splitter. The detector (possibly with additional focusing optics) is placed at the second output of this interferometer. In a first possible configuration one of mirror is fixed and the other mobile, while in a second one both mirrors move in a push-pull fashion. Corner-cubes can be used instead of the mirrors to achieve a

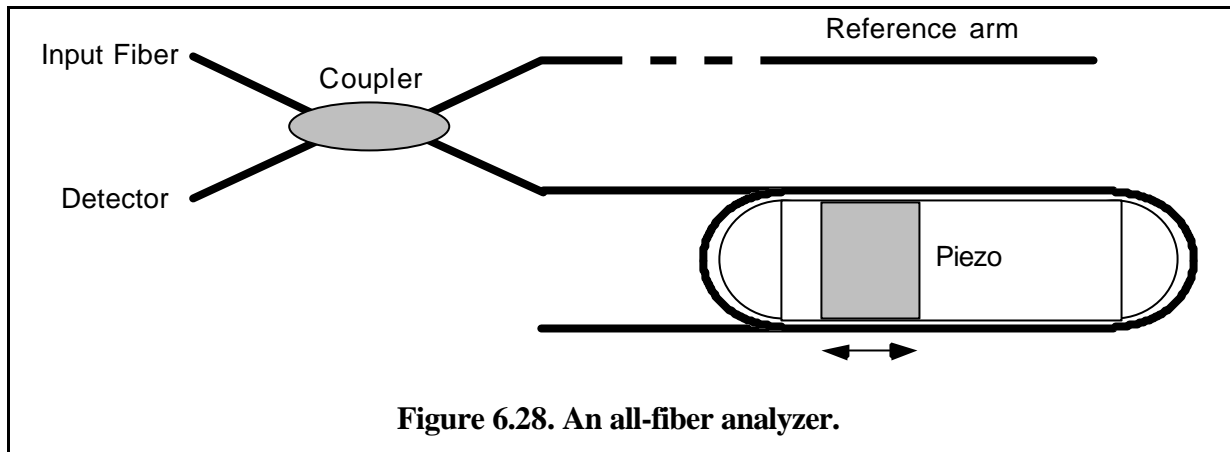


better insensitivity to misalignments. Figure 6.26 shows an example of this type of setup. Since the index of refraction of air is only weakly temperature dependent, it is possible to control the exact amount of path unbalance introduced in this interferometer by mechanically measuring or controlling the mirror displacements.

Other bulk optics setups without moving parts have been proposed. Most are based on wedges that compensate for the path unbalance and linear CCD elements as detectors [14,15]. These setups can be brought to dynamic systems since the measurement time is only limited by the read-out time of the CCD. These setups can unfortunately not introduce large path unbalances as the one required for the SOFO system. Even if this were possible it would require a linear CCD with more than 50'000 elements in order to guarantee the necessary resolution. Furthermore, since the incoming light is spread over the whole CCD length, only a small fraction of it will be used in the regions where interference actually takes place. This points to a very inefficient use of the already small intensity available.

6.7.1.2 All fiber setups

In an all-fiber setup both interferometer arms are constituted by optical fibers. One of these fibers is stretched to introduce the desired path unbalance. If one wants to introduce an equivalent path unbalance in air of 20 mm (one way) it will have to stretch the fiber by about 9 mm (two ways). If we want to limit the stress in this fiber to 1% this means that the fiber needs to be about 10 m long. This means that the fiber will have to be wrapped around appropriate supports and be pulled by a piezoelectric element (see Figure 6.28). Since the index of refraction of the fiber, its elastic coefficient as well as the response function of the piezoelectric element are temperature dependent and non-linear, it will be necessary to measure the introduced path unbalance by another mean. This can be done by injecting, by means of a wavelength selective coupler, an highly coherent beam at a different and well defined wavelength and count its interference fringes. To obtain the necessary wavelength stability it would be necessary to use a bulky gas laser eliminating the size advantage of this setup.



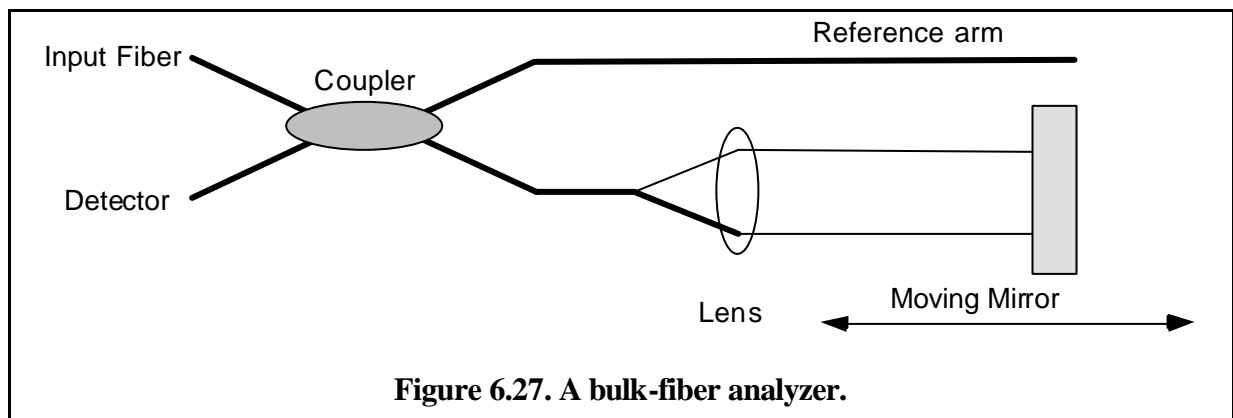
6.7.1.3 Bulk - fiber setups

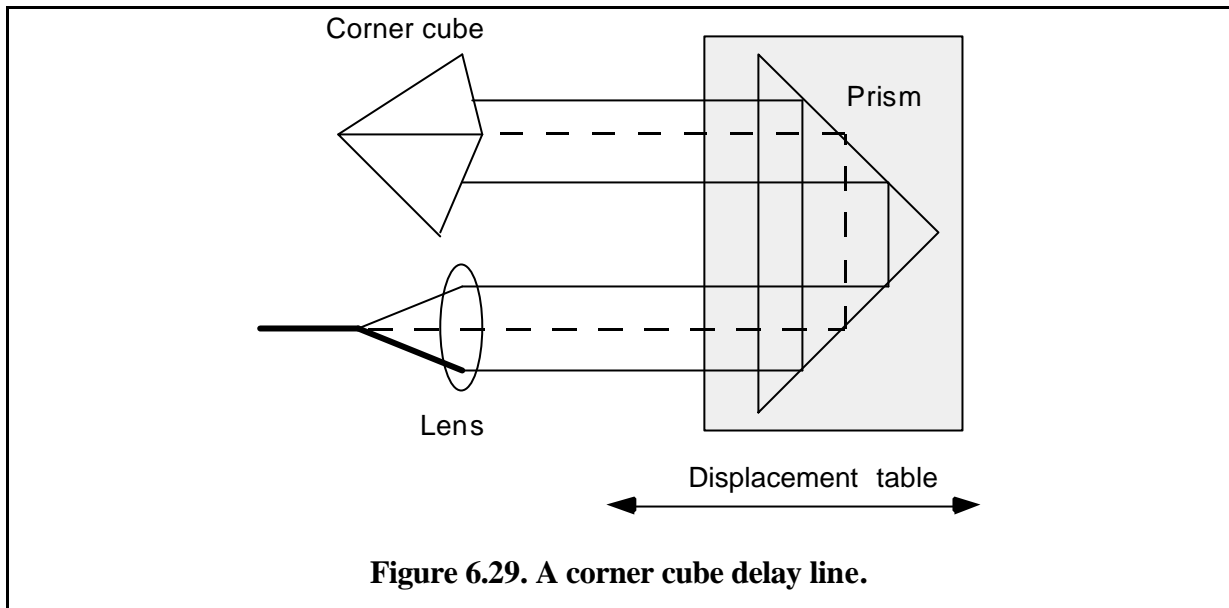
In this mixed setup the beam-splitter and the reference arm are realized with fiber components and only the delay line uses bulk optics. This reduces the size and weight of the setup while conserving the interesting properties of an in-air delay line. Figure 6.27 shows a typical bulk-fiber analyzer.

This setup was retained for the SOFO system because it can introduce large path unbalances without the need of an optical measurement of the path unbalance.

6.7.2 Beam Collimator

If we now restrict our choice to the hybrid bulk-fiber combination it will be necessary to define the best setup for the bulk delay line. The first part that need to be designed is the beam collimator that extracts and re-couples the light from and to the fiber. This can be obtained using a grin lens [16], a micro lens or a microscope objective. Since the light will travel in some cases more than 300 mm before being coupled back into the fiber, it is necessary to have a particularly well collimated and aberration-free beam. This is difficult to obtain with a grin- or micro-lens particularly for broadband spectra like the ones used in this setup. As a microscope objective we have selected a component manufactured by EALING with a focal length of 16 mm a numerical aperture of 0.4 and a working distance of 9mm. The large working distance greatly simplifies the alignment of the setup. The numeral aperture is much larger then the one of the fiber so that only the central part of the lens aperture will be used (except in the case of the double-path setup, see below). This objective also possesses antireflective coatings optimized for IR operation.

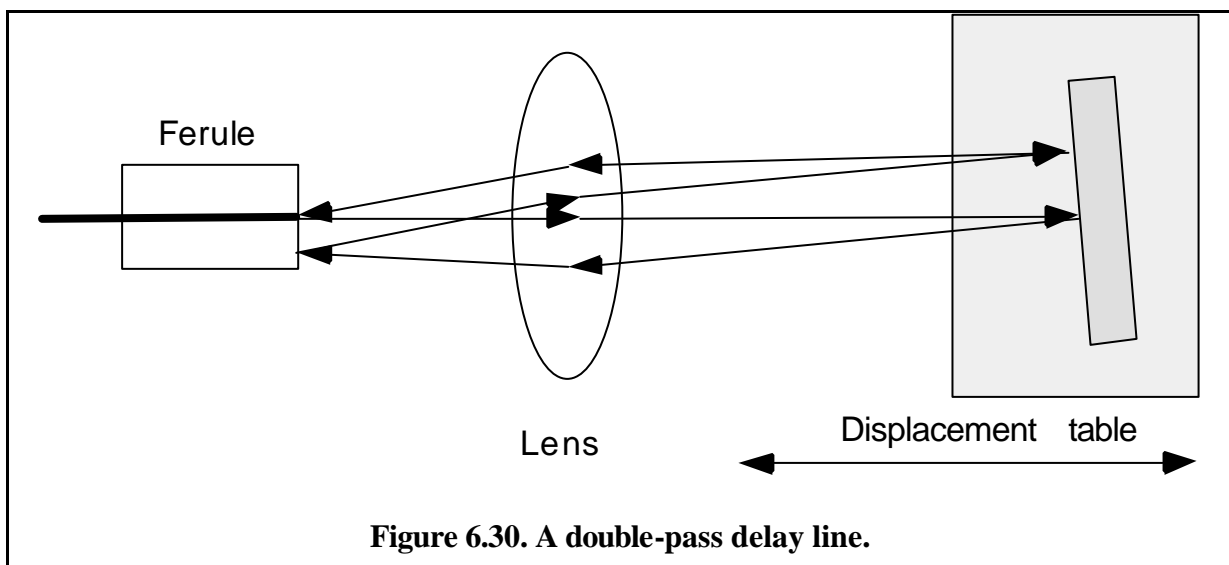




6.7.3 Reflector

The light has to be reflected back to the objective by a movable reflector. This can either be a mirror or an hollow corner-cube. Three configurations are possible:

- **Single-pass mirror:** In the simplest configuration, a mirror reflects the light back parallel to the incoming light, so that it will be recouped directly into the fiber core after passing once again through the objective. This setup is very sensitive to the misalignments that can occur between the fiber, the objective and the mirror. This also place high requirements on the straightness and wobble of the translation stage. It seems therefore impossible to design a portable system based on this setup.
- **Corner-cube:** In this case the mirror is replaced by a corner-cube that reflects the light back in the same direction as the incident light. It is even possible to fold the setup in order to double the maximum path unbalance obtainable with a given translation range. This type of setup offers good stability and was adopted in the coherence-domain reflectometer produced by Hewlett-Packard and Photonetics.
- **Mirror with double-pass:** This amazingly simple setup allows the stability typical of



corner-cube reflectors with the simplicity of the single mirror setup. The light is collimated as usual by the objective but the mirror is now set to be slightly misaligned. The light is therefore reflected and focused to a point on the same plane as the fiber surface but at a certain distance from the fiber core. If the fiber is mounted inside a polished reflecting ferule, the light will be reflected back again to the objective and will travel one more time to the mirror and back. Since the fiber core and the focal point after one round-trip are conjugated points with respect to the objective, it is relatively easy to see that after two round-trips the light will always be focused back to the fiber core. This will happen for each mirror angle, each fiber-objective alignment and each mirror position, provided that the focus point falls on the reflective ferule and all rays stay inside the pupil of the objective. The fact that the light is entirely focused back to the fiber core does not mean that the efficiency of this system is 100%. In fact, the light will arrive on the fiber core with an angle respect to the normal to the fiber surface. This will produce a loss since some of the light will be coupled into cladding modes and lost. The next paragraph will give a more detailed description of this setup. All SOFO setups have used the double-pass setup.

6.7.3.1 Double-pass delay line

In order to explain rigorously the functional principle of the double-pass delay line we will follow the path of a light ray exiting the fiber through the two round-trips. We will approximate the system paraxially and calculate at each interface the position and angle of the beam respect to the objective axis (defining the optical axis of the whole system). We will also suppose that all beams remain in the same plane as shown in Figure 6.30. Finally, the objective will be approximated by a thin lens.

To follow the path of the light ray through the system we will use the matrix method. The lateral position and angle to the optical axis are expressed in vector form:

$$r = \begin{bmatrix} \mathbf{a} \\ x_0 \end{bmatrix} \quad (2)$$

where \mathbf{a} is the angle (in radiant) and y the lateral position.

The action of a thin lens is taken into account by multiplying the input vector with the refraction matrix:

$$A(f) = \begin{bmatrix} 1 & -1/f \\ 0 & 1 \end{bmatrix} \quad (3)$$

where f is the focal length of the lens.

A free path in air is represented by the transfer matrix:

$$T(L) = \begin{bmatrix} 1 & 0 \\ L & 1 \end{bmatrix} \quad (4)$$

where d is the distance traveled in air.

The tilted mirror changes the angle of propagation and can be taken into account by adding the vector:

$$M(\mathbf{b}) = \begin{bmatrix} 2\mathbf{b} \\ 0 \end{bmatrix} \quad (5)$$

where \mathbf{b} is the angle between the optical axis and the mirror normal.

After one round-trip, the vector r will be transformed into a vector r' . This is obtained by multiplication of the refraction and transfer matrices and addition of the mirror vector:

$$r' = T(f) \cdot A(f) \cdot T(d) \cdot \left[\left[T(d) \cdot A(f) \cdot T(f) \cdot r \right] + M(\mathbf{b}) \right] \quad (6)$$

or:

$$r' = \begin{bmatrix} -\frac{2x_0}{f} + 2\mathbf{b} - \mathbf{a} + \frac{2dx_0}{f^2} - \frac{2d\mathbf{b}}{f} \\ 2\mathbf{b}f - x_0 \end{bmatrix} \quad (7)$$

The focal point after one round-trip will therefore be located at a distance from the fiber center of:

$$y = 2\mathbf{b}f - 2x_0 \quad (8)$$

If this distance is inferior to the fiber radius, the light will be coupled into the fiber cladding. Otherwise it will reflect on the fiber ferule and start a new round-trip.

If the ferule has a focal length f_f , the vector will transform in a vector r'' :

$$r'' = \begin{bmatrix} -\frac{2x_0}{f} + 2\mathbf{b} - \mathbf{a} + \frac{2dx_0}{f^2} - \frac{2d\mathbf{b}}{f} - \frac{2\mathbf{b}f}{f_f} + \frac{x_0}{f_f} \\ 2\mathbf{b}f - x_0 \end{bmatrix} \quad (9)$$

We can now use this vector as a new input vector and substitute it into (7) and therefore propagate it once again through the optical system. After this second round-trip we finally obtain:

$$r''' = \begin{bmatrix} -4\mathbf{b} + \frac{4x_0}{f} - \frac{4dx_0}{f^2} + \frac{4d\mathbf{b}}{f} + \frac{2\mathbf{b}f}{f_f} - \frac{x_0}{f_f} \\ x_0 \end{bmatrix} \quad (10)$$

Where we have assumed $\mathbf{a} = 0$, i.e. the fiber surface perpendicular to the optical axis. Equation (10) shows that the beam is indeed focused back to the fiber core. The incidence angle will vary depending on the position and angle of the mirror, the relative position of the fiber and the objective and the focal length of the objective and the ferule.

To obtain the coupling efficiency of the system we now have to calculate the overlapping integral between the admission cone of the fiber and the tilted cone of the back-focused light. Both (Gaussian) cones will have the same center (the fiber core) and aperture (the numerical aperture of the fiber) but will be at an angle as expressed by the first term in equation (10). The overlapping function will be a Gaussian function of the ratio between the numerical aperture of the fiber and the angle between the two cones.

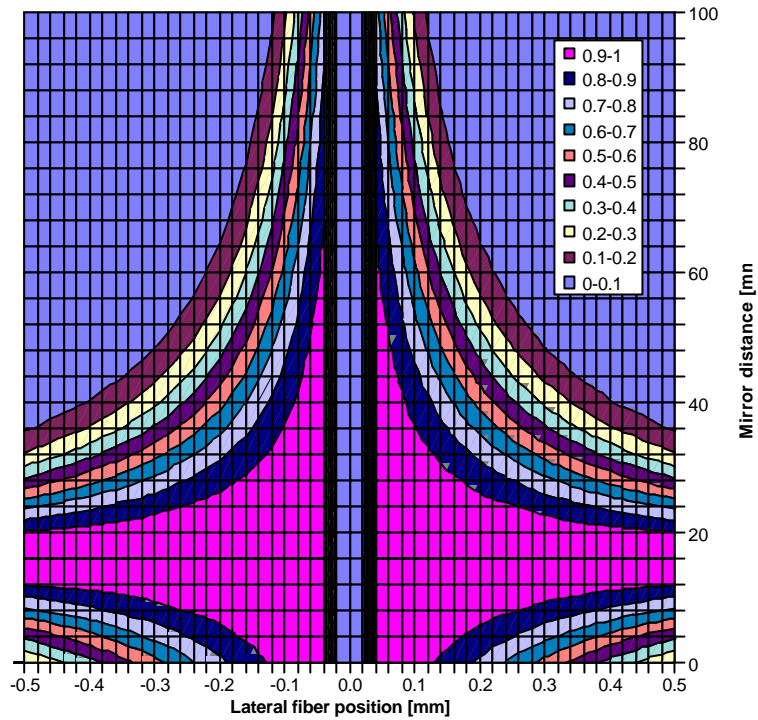


Figure 6.31. Theoretical back-coupling efficiency as a function of mirror and fiber position. Flat ferule and un-tilted mirror. Objective focal: 16 mm. Numerical aperture of the fiber: 0.1.

In Figure 6.31 we represent the back-coupled power as a function of the objective to mirror distance and the lateral displacement of the fiber core to the objective axis. The focal length of the objective is set to 16 mm and the numerical aperture of the fiber to 0.1. The ferrule is assumed as flat and the mirror tilt is zero. The vertical zone with zero coupling (blind region) is the result of focusing on the fiber after one round-trip instead than on the ferule. It is interesting to notice that for a mirror distance equal to the focal length of the objective (in this case 16 mm) the coupling is perfect for all lateral displacements.

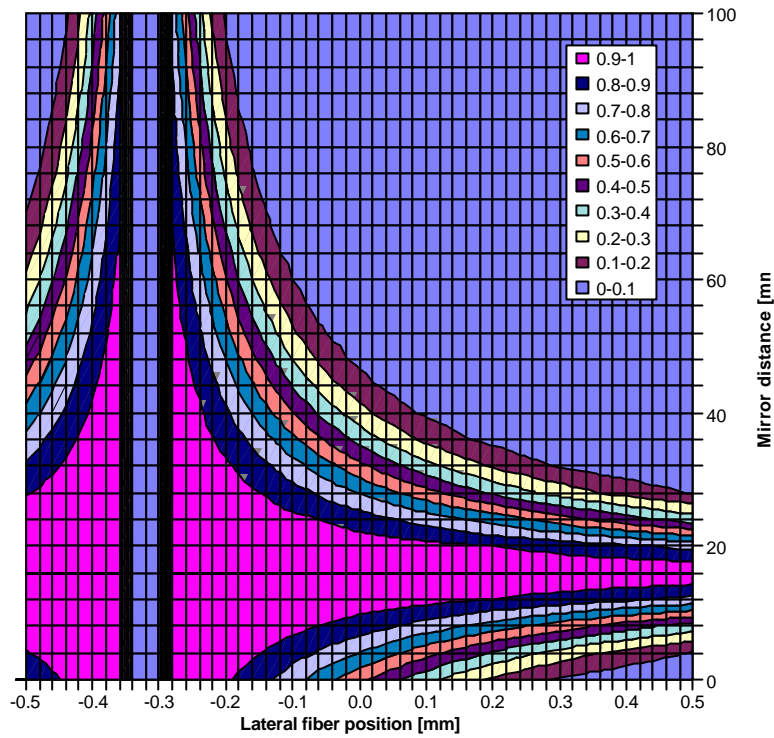


Figure 6.32. Theoretical back-coupling efficiency as a function of mirror and fiber position. Flat ferule and mirror tilted by 0.02 rad. Objective focal: 16 mm. Numerical aperture of the fiber: 0.1.

Figure 6.32 shows the same situation but with the mirror tilted by 0.02 radiant. The blind region is now displaced laterally by a distance equal to the product of the tilt with the focal length of the objective. In this case: $0.02 \cdot 16\text{mm} = 0.32\text{mm}$.

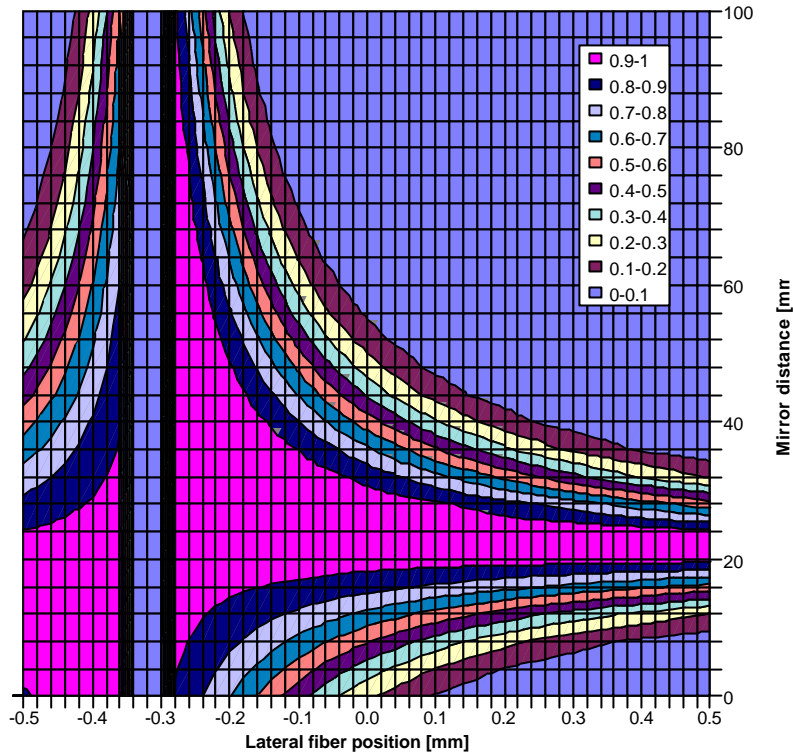


Figure 6.33. Theoretical back-coupling efficiency as a function of mirror and fiber position. Ferule with -15 focal length and mirror tilted by 0.02 rad. Objective focal: 16 mm. Numerical aperture of the fiber: 0.1.

Figure 6.33 shows the same situation but with a ferule focal length of -15 mm typical of a polished ferule. The picture is now radically different in the sense that the maximal coupling for a given mirror position is no longer placed in the blind region. This allows for adjustment of the fiber position just slightly to the side of the blind region and then obtain almost perfect coupling over an extended mirror distance range. In the example of Figure 6.33, if the fiber is aligned at -0.25 mm from the optical axis, it is possible to obtain a coupling efficiency above 90% over mirror distances between 10 mm and 70 mm. This covers more than the required range of 50 mm.

This behavior was verified experimentally. Coupling up to more than 50% have been realized with this setup. Taking into account the losses due to two reflections on the mirror, one on the ferule, four passes through the objective and the two Fresnel reflections at the fiber-air and air-fiber interface, this result is remarkably consistent.

All these results are based on the assumption that the fiber surface is placed exactly at the focal plane of the objective. The ferule to objective distance is indeed critical and has to be controlled precisely in order to obtain a good coupling.

All FORMOS and SOFO systems used this setup. The importance of the curvature of the ferule was realized only recently⁸. All systems needed to be aligned after fabrication but no further manipulation was required for the rest of their life, even in the case of long transport by

⁸ The intuitive approach used at the time of the FORMOS and early SOFO systems pointed to the realization of a ferule as flat as possible!

car or rough manipulation. Of course all the degrees of freedom of the ferule respect to the objective have to be blocked after the ideal alignment is found.

During the alignment procedure, the ferule has to be moved in both lateral directions and longitudinally with respect to the objective. In the FORMOS system and in the first SOFO system, the three degrees of freedom were distributed between the objective (the two lateral translations) and the ferule (the longitudinal translation). The final SOFO system and its industrial version relied on a miniaturized XYZ translation stage⁹ supporting the ferule and a fixed objective.

6.7.4 Translation stage

The translation stage carries the mirror and moves it in order to obtain the desired path unbalance. The translation stage is also used to measure this path unbalance and therefore influences directly the measurement precision. To obtain the required resolution and precision of about one micron, the translation stage also has to move and measure its position with this resolution. Furthermore, it is interesting to keep a constant mirror angle (\mathbf{b}) during the whole scan so that the light beam will always be focused at the same spot on the ferule. This allows the choice of a good reflecting spot during the alignment procedures. This means that the translation stage has to move wobble free. Since the optical setup is auto stabilized, most precision translation stages will fulfill these basic requirements. In the different versions of the SOFO we used translation stages from Microcontrole, Aerotech and Anorad. All had a maximal displacement of at least 50 mm but varied largely in size and weight.

A motor drive is used to move the translation stage back and forth. Two basic types of motor are available: step and DC. The stepper motor turns at a given angle for each impulse received from its controller. By counting the impulses and knowing the gear de-multiplication and screw-pitch it is easy to calculate the displacement of the table. The FORMOS system used a stepper motor with a displacement of 0.1 microns per impulse. The main drawback of this motor is in its relative slowness compared to the DC motor and in the speed variations of the mirror at each step. This last problem can be overcome using sinusoidal impulses instead of square-waves normally produced by basic controllers. This complicates considerably the control electronics.

A DC motor is driven directly by a continuous voltage and moves at a speed roughly proportional to it. The speed and angular position of the motor are measured by an optical encoder attached to the motor axis. The encoder signals are treated by an appropriate controller that adjusts the motor voltage to obtain the desired speed and/or position. This type of motor was used on all SOFO systems and resulted in a speed gain of about 200 times compared to the FORMOS system.

In some laboratory experiments a translation stage from Physics Instruments with DC drive was also used. The following table resumes the characteristics of the different translation stages used in the different systems.

⁹ About the size of a couple of sugar cubes.

	PMD / FORMOS	SOFO I-III	SOFO IV
Manufacturer	Microcontrole	Aerotech	Anorad
Motor type	step	DC	DC
Scan range [mm]	30 / 50	50	100
Scan speed [mm/s]	0.05	12	12
Mechanical resolution [microns]	0.1	1	0.5
Size [mm × mm × mm]	300 x 100 x 65	360 x 100 x 57	34 x 6 x 45
Weight [kg]	ca. 3	2.5	2

Table 6.8. Comparison between different translation stages.

6.7.5 Coupler

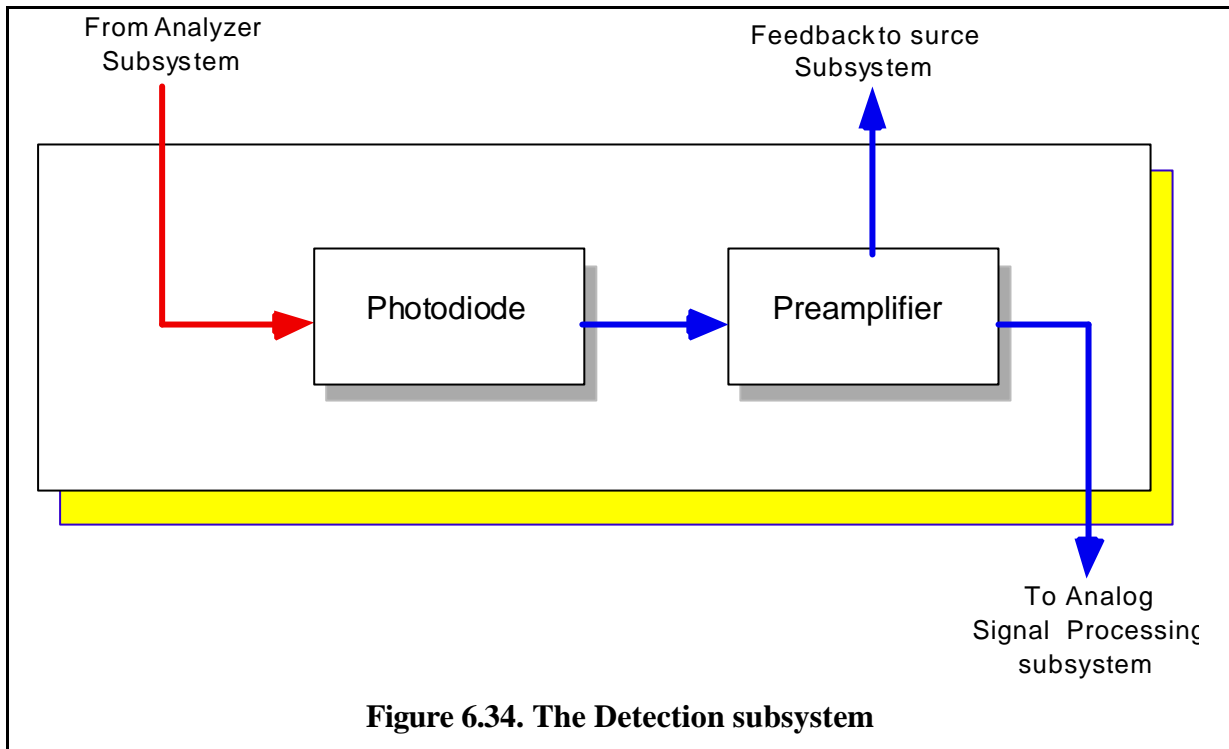
A 50:50 wavelength flattened coupler for 1300 nm and 1550 nm was used in most systems. Although most measurements are performed at 1300 nm it is interesting to keep the possibility of using the other wavelength for particular experiments.

All fibers are either with the acrylate primary coating or with an additional micro-tube protection.

6.7.6 Reference arm

The reference arm is simply one of the coupler arms ended by a silver mirror (see 6.6.7). The length of the reference arm is calculated so that the interferometer is balanced at about 1/5 of the displacement table range. Since it is difficult to calculate exactly the optical path length inside the objective, the final cut position was obtained by cutting at a longer position and then observing the position of the central fringes (this can be done using just the Fresnel reflection at the reference fiber end facet). Knowing the index of refraction of air and glass and remembering that the light passes twice through the delay line, it is easy to obtain the required correction length and cleave the fiber once again.

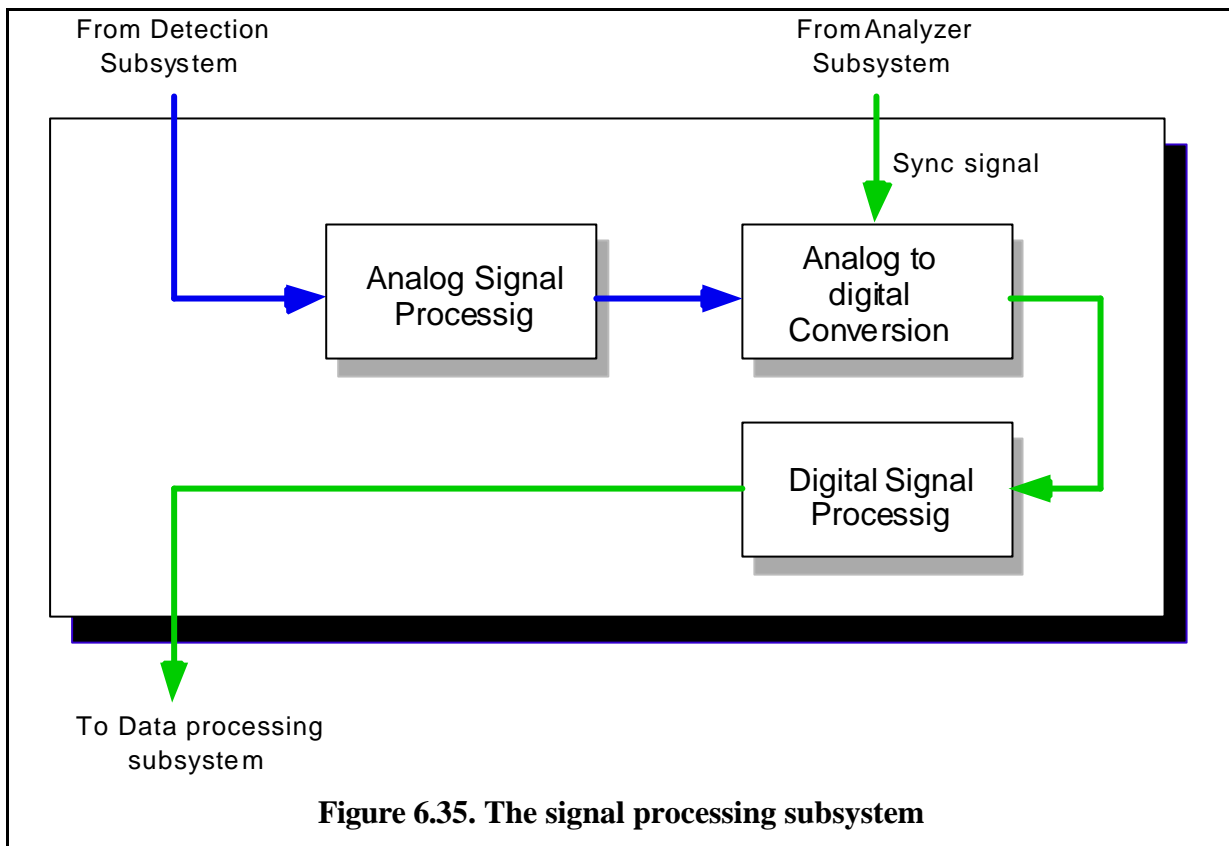
6.8 Detection



The detection subsystem transforms the optical signal into a proportional electrical signal. It is usually composed of a photodiode and a trans-impedance preamplifier. The photodiode transforms the incoming photon flux into a current. The preamplifier converts this current into a voltage and amplifies it to a convenient value. Since the optical power at the source is low and only a small fraction of it contributes to the interference fringes, it is important to select a detection stage that introduces the smallest possible noise. The ultimate noise limit is given by the Shot noise that accounts for the statistical particle nature of light (only an integer number of photons can be detected). There is a trade-off between the speed of a detector and its sensitivity.

In the FORMOS system it was relatively easy to obtain low-noise operation, since the fringe frequency was only about 150 Hz. In the SOFO system this frequency was increased to 30 kHz and, when using partial reflectors, the available light intensity was further reduced. After attempting to build a suitable receiver from a photodiode and a operational amplifier, it was decided to rely on a commercial component produced by New Focus (model 2011). This lowered the noise floor by almost an order of magnitude, down to $1\text{pW}/\sqrt{\text{Hz}}$. This unit can work at different gains and even includes low- and high-pass filters with variable cutting frequency. The price of this element (about 1200 SFr.) is justified by the important increase in detector sensitivity.

6.9 Signal processing



The signal processing subsystem analyzes the analog signal and extracts the peak information. It first acts as a demodulator at the fringe frequency and extracts the fringe envelope. This corresponds to measuring the fringe visibility as a function of the mirror position. It then calculates the peak position and transfers it to the data processing subsystem.

These operations can be subdivided in a number of ways between analog and digital signal processing with an A/D converter in-between. The Analog to digital converter will be triggered by the sync signal coming from the translation stage. If this signal is not at the right frequency, it is possible to multiply and/or divide it with a phase-locked-loop (PLL) circuit.

A few different demodulation schemes have been tested in the different versions of the SOFO system:

6.9.1 Lock-in amplifier

The FORMOS system relied to a lock-in amplifier to extract the fringe contrast. The lock-in reference signal was generated synthetically at a frequency equal to the expected frequency of the fringes. The two-channel lock-in was set up to give the phase and the modulus of the signal and this later was digitized synchronously to the step motor signal. Although this is not the way a lock-in is supposed to work (the reference should have a constant phase relationship to the signal) this setup acts in fact as a narrow-band filter and allows the detection of very weak signals. Against this solution speaks the price of this device and the fact that it can work only at

low signal frequencies (up to 10 kHz) and with slowly varying envelopes. The lock-in used in the FORMOS system was a Stanford Research model SR530.

6.9.2 Analog envelope extraction

In the first SOFO systems it was attempted to emulate the lock-in function with a simpler and faster electronic circuit consisting in an high-pass filter (6 dB/Oct at 10 kHz) followed by a crest-holding circuit. This first cut the negative part of the signal and then charged a capacity with the instantaneous voltage. The capacity was then discharged through a resistance that determined the time-constant of the system. This simple system works remarkably well for low-noise signals. Having no frequency discrimination, it tends to integrate the noise with the signal and make fringes with low contrast disappear into the noise floor. It would have been possible to improve the performances to this system by using a narrow-band filter centered around the fringe frequency instead of the simple high-pass filter. This last solution was never attempted experimentally. The analog envelope extraction circuit was used in SOFO I and II.

6.9.3 All digital processing

Instead of extracting the envelope with an analog circuit, it is possible to perform the same operation numerically after the A/D conversion of the modulated fringe signal. In order to represent the signal unambiguously, the Shannon theorem requires the sampling frequency to be at least double the highest frequency component of the signal. The limit frequency of the signal for a given sampling rate is called the Nynquist frequency. If a signal at a frequency higher than the Nynquist frequency is present, under-sampling will produce an aliasing of this signal. We will see that under certain conditions the aliased signal contains the same envelope information as the original signal.

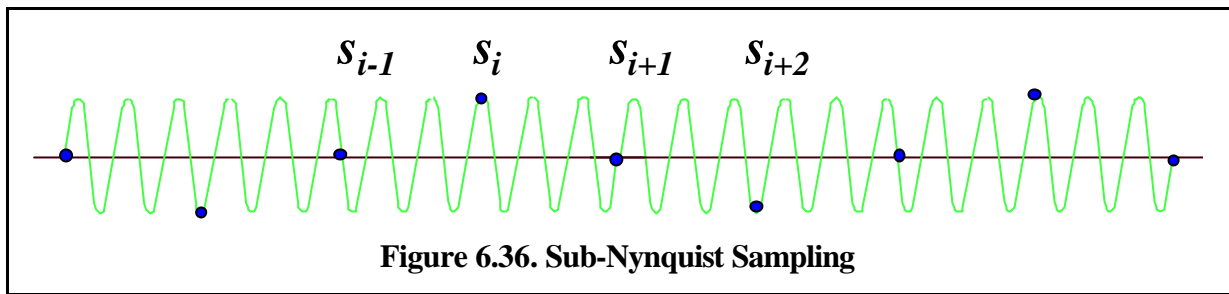
6.9.3.1 Nynquist sampling

The Shannon theorem requires the conversion of at least two samples for each interference fringe. Three samples per fringe allow a comfortable detection of the fringe contrast for each relative phase between the signal and the sampling. The signal has three unknowns (mean intensity, contrast and phase). With three measurement per fringe it is possible to extract all three unknown and particularly the contrast that is interesting in our case. This method is known as a three sample phase stepping algorithm. Each sample will have a phase difference of 120° from the precedent and successive one. Four sample algorithms are also popular since the mathematical transformation take a simpler form. In this case the phase-step will be 90° .

In the double-pass delay-line configuration, a fringe will correspond to a displacement of $\frac{1.3\text{mm}}{4} = 0.325\text{mm}$. If the mirror scans over 50 mm and three samples are required for each

fringe, a total of $4 \frac{50000}{0.325} \cong 620'000$ samples will be required to represent the signal conveniently. The transmission and analysis such a large amount of data is time-consuming and it would be interesting to reduce the sampling rate by at least an order of magnitude.

6.9.3.2 Sub-Nyquist sampling



If the signal is under-sampled it will appear as having a frequency much lower than the real one [17]. Since in our case we have an a-priori knowledge of the signal frequency, aliasing is not a problem. The phase-step will in this case be larger than 180° . It is easy to see that when the residual phase, obtained by subtracting the maximal possible number of \mathbf{p} 's, corresponds to $-\mathbf{p}/2$ or $+\mathbf{p}/2$, the signal can be treated by the same four-sample algorithm. Figure 6.36 shows an example of under-sampling with a residual phase of $-\mathbf{p}/2$. Provided that the contrast varies slowly compared to the fringe period, the calculation of the contrast will give the same result as for the Nyquist-sampled signal.

Figure 6.37 shows the residual phase at 1300 and 1550 nm as a function of the mirror displacement between successive samples. At 0.9 microns we obtain a residual phase of about 270° at 1300 nm and about 90° at 1550 nm. This step was therefore retained for the SOFO system. For a scan range of 50 mm it will be necessary to acquire about 55000 samples. This is a gain of an order of magnitude compared to the Nyquist case.

For this step, four successive samples will give the intensities:

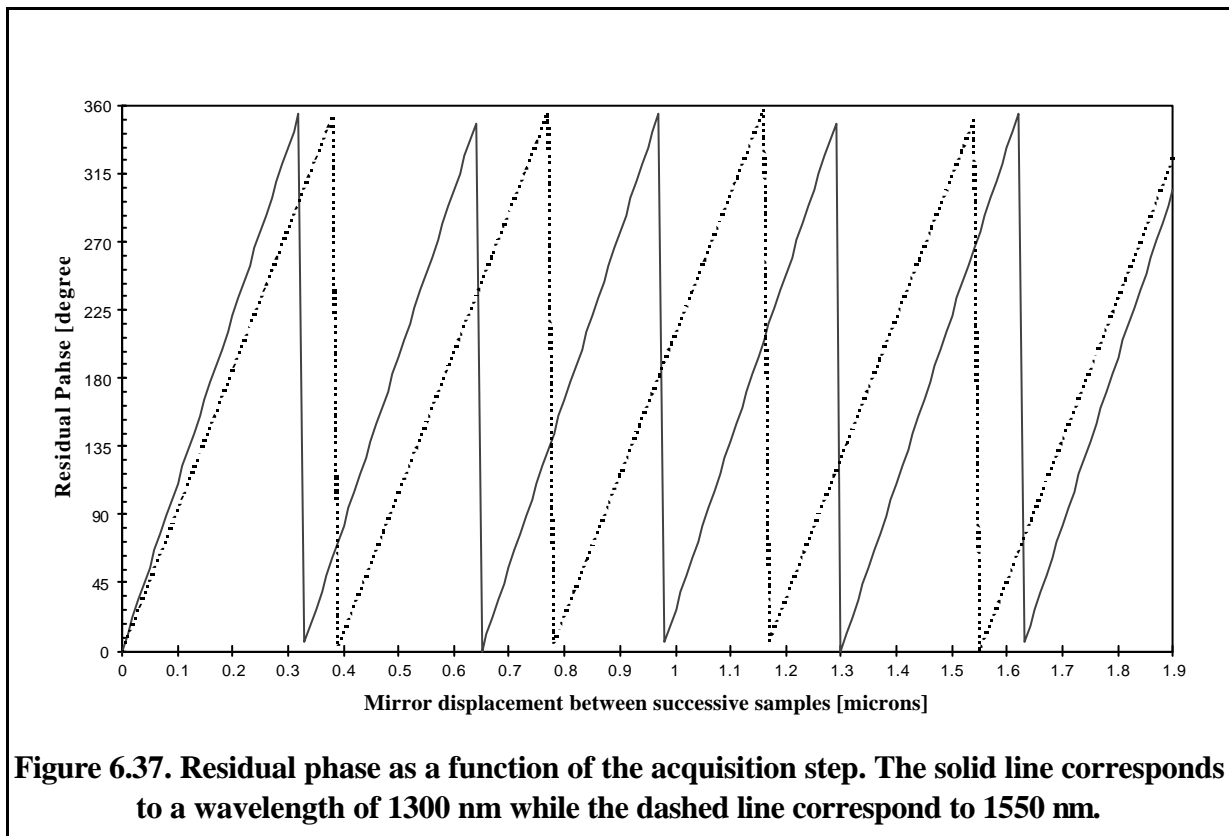


Figure 6.37. Residual phase as a function of the acquisition step. The solid line corresponds to a wavelength of 1300 nm while the dashed line corresponds to 1550 nm.

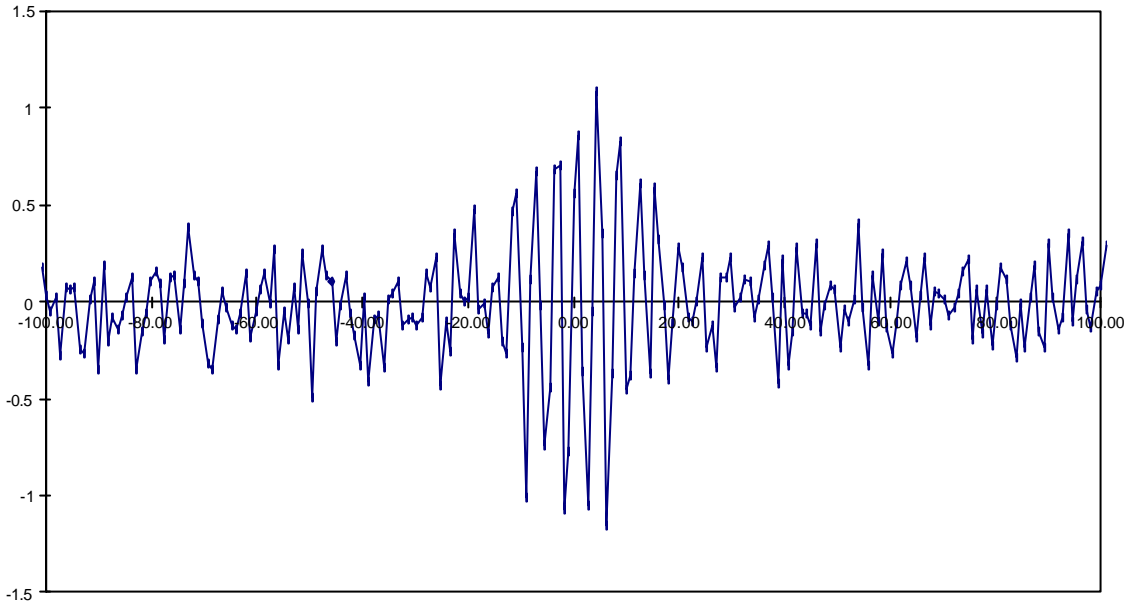


Figure 6.38. Sampled noisy signal intensity as a function of the mirror position [mm].

$$I_i = I(V \cos(\mathbf{j}_0)) \quad (11)$$

$$I_{i+1} = I(V \cos(\mathbf{j}_0 + 2n\mathbf{p} \pm \frac{1}{2}\mathbf{p})) = I(V \cos(\mathbf{j}_0 \pm \frac{1}{2}\mathbf{p}))$$

$$I_{i+2} = I(V \cos(\mathbf{j}_0 + 4n\mathbf{p} \pm \mathbf{p})) = I(V \cos(\mathbf{j}_0 \pm \mathbf{p}))$$

$$I_{i+3} = I(V \cos(\mathbf{j}_0 + 6n\mathbf{p} \pm \frac{3}{2}\mathbf{p})) = I(V \cos(\mathbf{j}_0 \pm \frac{3}{2}\mathbf{p}))$$

with the minus sign for 1300 nm and the plus sign for 1550 nm and $n=2$ in both cases. The contrast V can be easily calculated (for 1300 and 1550 nm) as:

$$V_i = \sqrt{-(I_i I_{i+2} + I_{i+1} I_{i+3})} \quad (12)$$

In the case of a noisy signal it is possible that the expression under the square root will be negative. In this case we will assume a zero contrast:

$$V_i = \begin{cases} \sqrt{-(I_i I_{i+2} + I_{i+1} I_{i+3})} & \text{if } (I_i I_{i+2} + I_{i+1} I_{i+3}) < 0 \\ 0 & \text{if } (I_i I_{i+2} + I_{i+1} I_{i+3}) > 0 \end{cases} \quad (13)$$

Figure 6.38 shows a sampled signal with a signal to noise ratio of about 5.

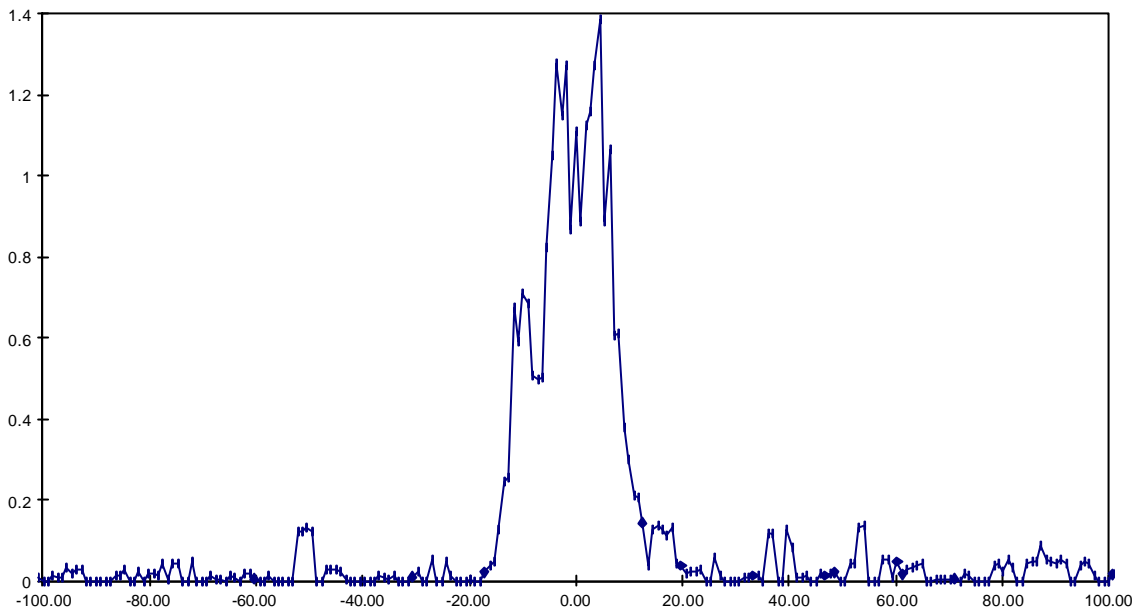
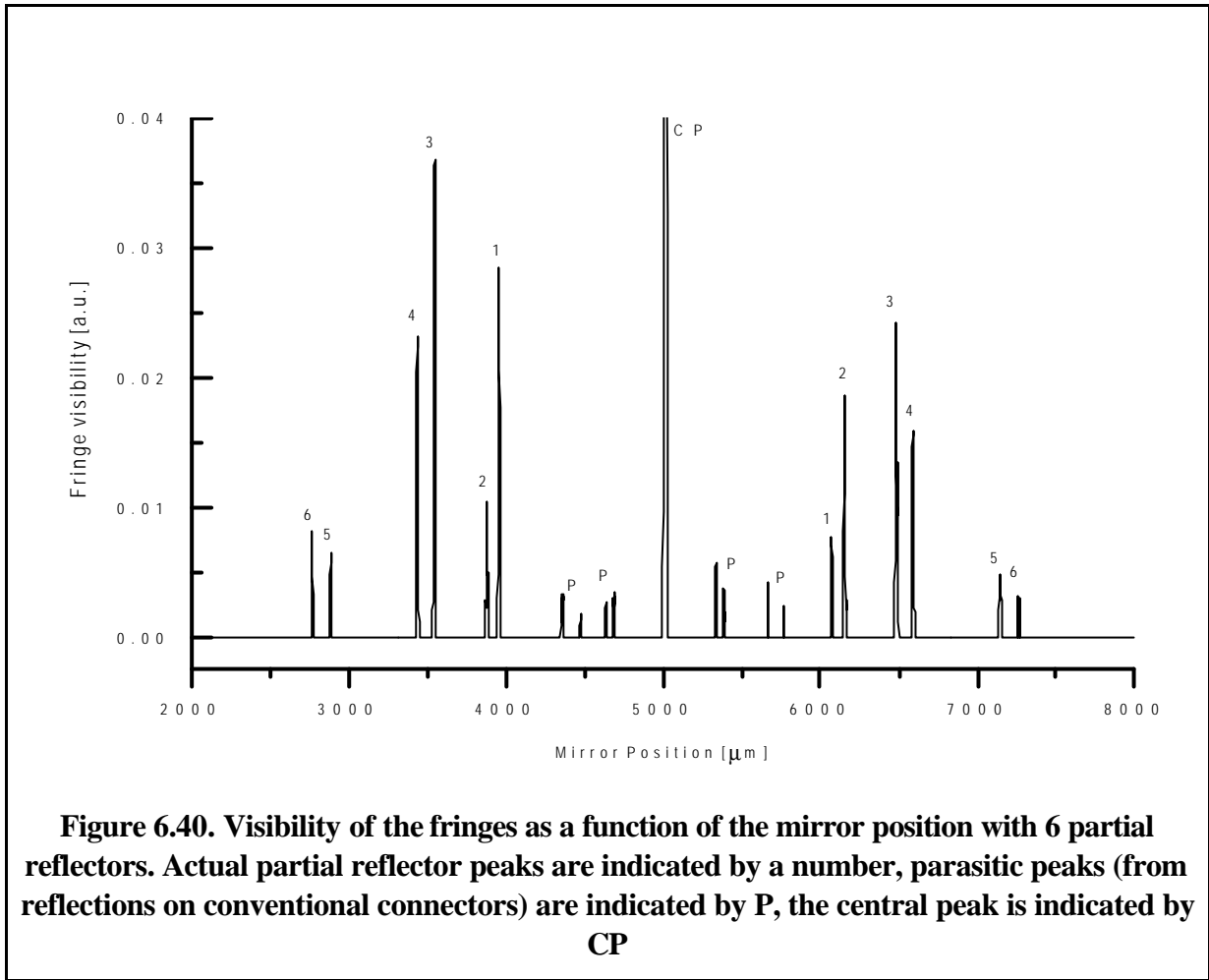


Figure 6.39. Contrast of the signal in Figure 6.38 as a function of the mirror position [mm].

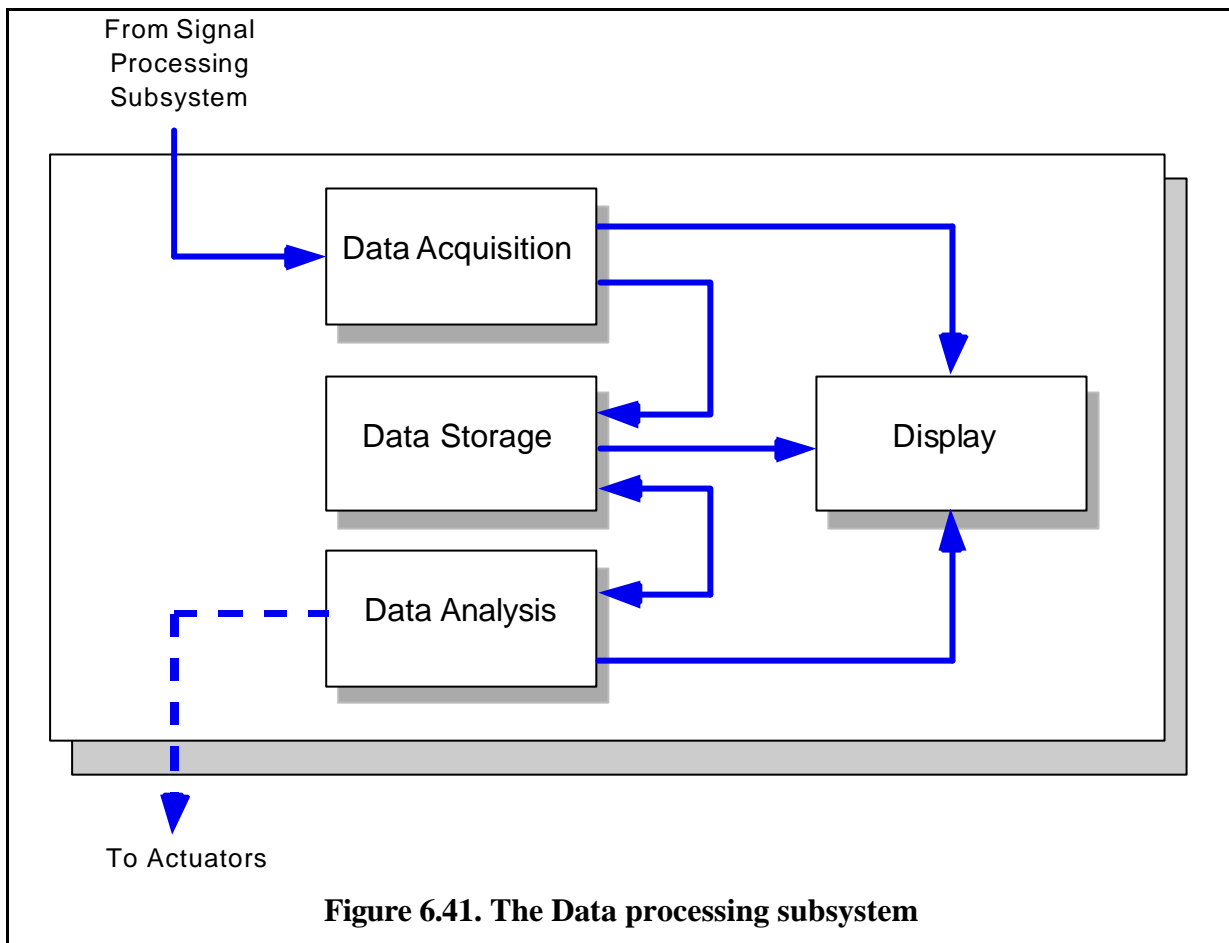
Figure 6.39 shows the same data after calculating the contrast with equation (13). The peak at the center of the graph is clearly retrieved. After an adequate smoothing and thresholding it is possible to calculate the center of gravity of this peak with a precision of better than one sample or an equivalent deformation of about 1 micron. Once the signal is thresholded and one peak isolated the center of gravity X_c is given by:

$$X_c = \frac{\sum x I(x)}{\sum I(x)} \quad (14)$$



A typical experimental scan with 6 peaks from 6 partial reflector pairs (see the section on multiplexing) is shown in Figure 6.40.

6.10 Data processing and interface



In a typical structure, tens of sensors are installed and measured many times, either manually or automatically. For each measurement the signal processing subsystem returns a series of peaks. The data processing subsystem has to analyze, store and represent graphically this data. This subsystem is implemented at the software level and is physically located in the PC that controls the reading unit. The software performs two basic functions: data acquisition and data analysis. In the acquisition phase the measurements are performed on different sensors and stored for further analysis by specialized data analysis packets. The acquisition software is therefore universal, while the analysis software depends on the application. There would be, for example, different software for data analysis on bridges and dams.

6.10.1 Acquisition software

This software is used as interface between the user and the reading unit during the measurement sessions. It should connect the appropriate sensor or ask the operator to do so, perform a measurement, store and display the results. It should also store additional data that could be useful at the data analysis stage such as the date and time, the DC intensity detected on the photodiode or any other user defined parameter (load level, temperature, ...). The acquisition software has evolved with the reading unit. The development of these software packages took a lot of time and it is unfortunately difficult to do justice of this work and

describe their functioning on a written page. The interested reader is encouraged to test these software packages. These are the main acquisition software programs that have been written or used:

6.10.1.1 FORMOS

The FORMOS system used a software written by Rogerio Passy at GAP (University of Geneva) in Turbo Pascal under MS-DOS and oriented to the measurement of the polarization mode dispersion. It can display the fringe visibility as a function of the mirror position. The user had then to recognize the peaks and manually move a cursor to measure their distance. This was inaccurate and time consuming. Furthermore, the results had to be recorded separately, usually in hand-written form.

6.10.1.2 SOFO / SOFO 95

The SOFO software was written in Visual Basic under Windows 3.11 and later ported to Windows95 (SOFO95). This software was a great improvement over the clumsy FORMOS software. It would semi-automatically recognize the peaks and calculate their center of gravity. The results were stored in individual files and collected in a history file that could be read by Excel or another data analysis software. The user could define a sequence of measurements and the program would prompt for the sensor connection when needed. The main drawback of this software was the lack of a coherent data storage. The information about the deformation evolution was scattered in many files that sometimes went out of synchronization. Furthermore, it was impossible to see the evolution of the displacements right after a measurement. This is useful to verify the correct functioning of a sensor.

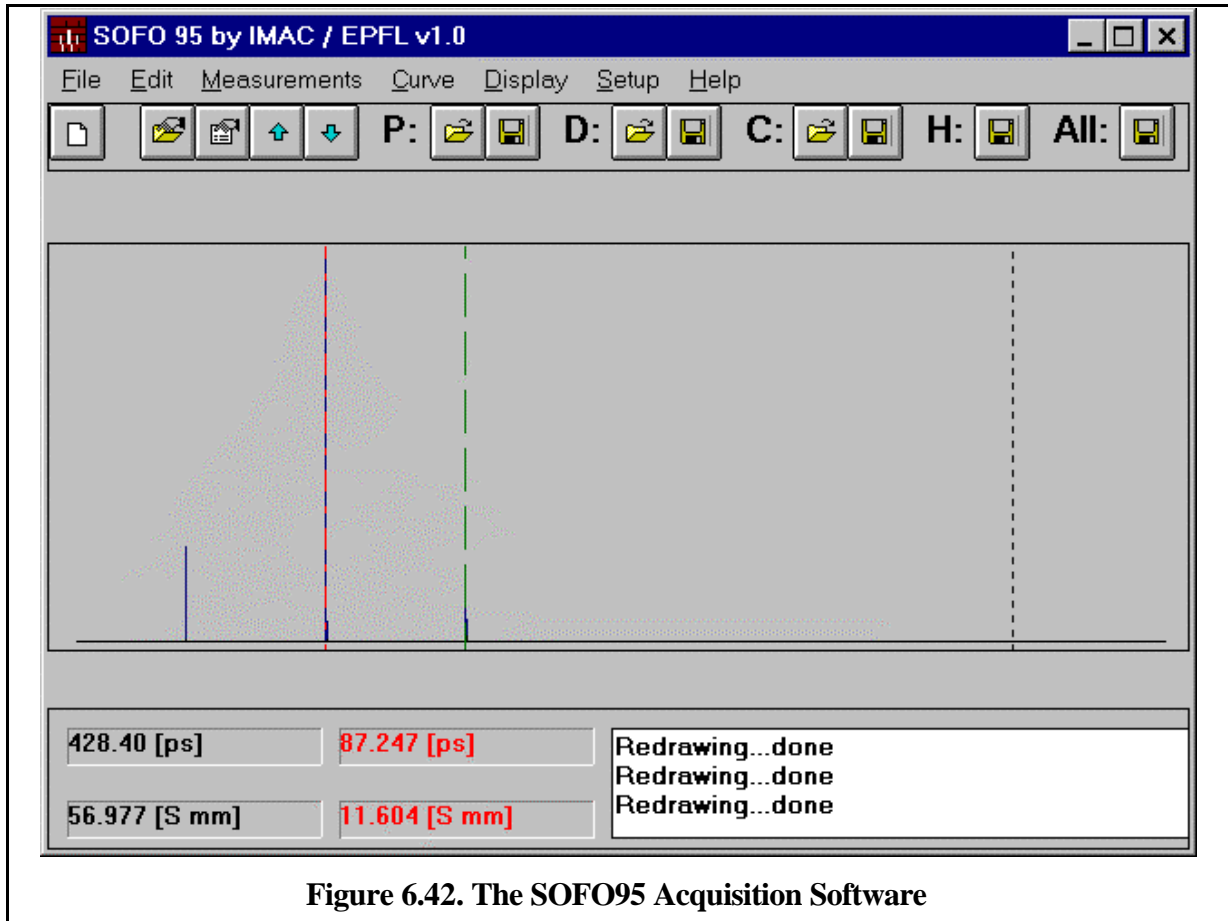


Figure 6.42. The SOFO95 Acquisition Software

6.10.1.3 SOFO DB

The SOFO DB software is the natural evolution of SOFO 95. It was also written in Visual Basic for Windows 95 and Windows NT. Its main characteristic resides in that all the data concerning a single project and structure, are stored in a single database file. The information is organized in a number of tables. The most important tables are:

- **Project table:** Contains a single record holding general information about the project such as the project name and description, its creation date and the numerical value of the fiber constants .
- **Sensor table:** Stores information about each sensor (or sensor chain). This includes the sensor name and description, its total length and indication on how to connect the sensor (manually, or via an optical switch) and about the presence of an integrated coupler.
- **Campaign table:** Holds information about every measurement campaign. A campaign is a set of measurements that are performed on the structure at the same time, load, temperature and so on. This comprises the campaign name and description, the date and time the campaign was started, the name of the operator, and a description on the A/D signals¹⁰ and user data¹¹.
- **Measurement table:** Stores single measurements on one sensor (or sensor chain). The stored fields include the measurement name and description, the date and time, the acquisition step and the serial number of the reading unit, the number of data points after thresholding, the position of the central peak, the voltages measured on the A/D channels, the DC component of the photodiode voltage, the voltage of the internal battery, the internal temperature of the reading unit and a Boolean field indicating whether the result of this measurement should be disregarded during data analysis¹².
- **Peak definition table:** This table contains a description of each peak that appears for a given sensor. If the sensor is a single sensor, only one peak definition is used. If the sensor is a partial reflector chain or any other multiplexing setup that gives rise to multiple peaks, one peak definition will be provided for each sensor in the chain. Stored information include the peak name, the active length of the sensor producing the peak, the sensor's serial number and two Boolean fields indicating if the reference fiber is longer than the measurement one and whether the peak is a parasite peak and holds no information.
- **Peak table:** Contains the position and area of a peak for a given measurement and peak definition. Also stores a flag indicating that the measurement should be disregarded.

The software also stores so called agendas that contain instruction on the sequence and timing of measurement. An agenda can either execute automatically using optical switches or semi-automatically by asking the operator for manual connection of each sensor or sensor chain.

After a measurement, the software tries to identify the peaks that were present in the previous measurements and shows the results of the scan to the user so that they can be compared to the previous ones. It can also show the evolution of the position of every peak to allow an easy check of the good functioning of the sensor.

¹⁰ These signals are used to measure external parameters such as the load of an hydraulic jack. Any apparatus that gives a voltage as output can be measured.

¹¹ This data is entered manually by the operator when a direct measurement is not possible. Examples are the load state of the structure or the elongation imposed with a manual translation stage.

¹² It is useful to also store "bad" measurements. Sometimes they hold precious information that becomes interesting later.

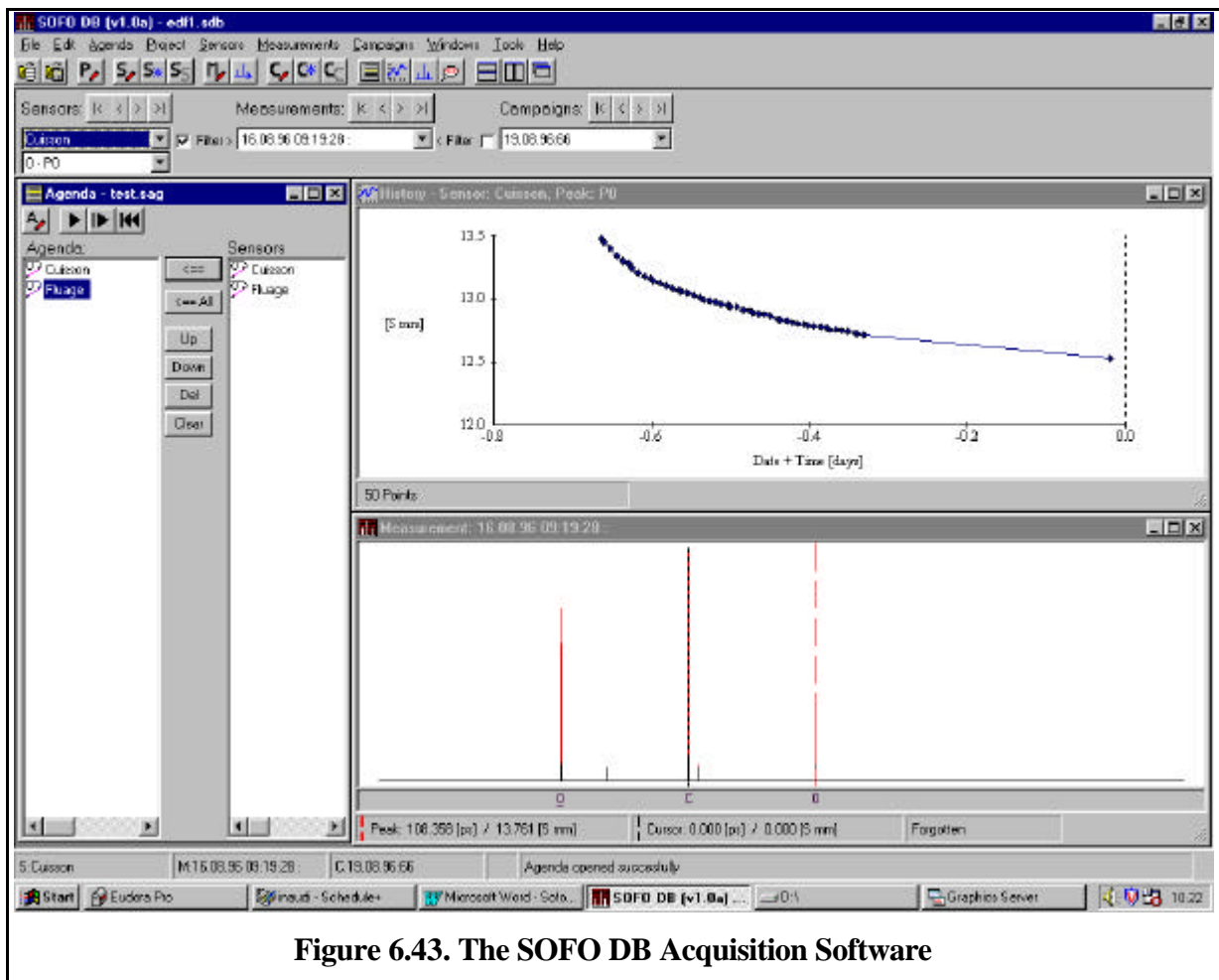


Figure 6.43. The SOFO DB Acquisition Software

This software can work with all generations of the SOFO system (but not with the FORMOS system). It can even address multiple reading units connected to a single PC.

The user interface (see Figure 6.43. The SOFO DB Acquisition Software) allows for an easy and quick navigation between sensors, measurements and sessions. It is adapted for both laboratory and field use and allows a good overview of the results before further analysis is conducted with advanced software packages.

6.10.2 Data analysis Software

The data analysis packages interpret the data stored by the acquisition software in the database¹³. Some of these packages are of general use and can be used with each type of structure, while others are aimed to a precise structure of structure type¹⁴. Examples of such tools are:

- **Displacement evolution analysis:** This general purpose package extracts the results concerning a single sensor and displays them as a function of time or load. The data can then be exported to other software packages, like spreadsheets or other graphical tools for adequate representation.
- **Curvature:** In beams, slabs, vaults and domes, it is possible to measure the local curvature and the position of the neutral axis by measuring the deformations on the tensile and

¹³ Samuel Vurpillot is working on his Ph.D. developing such analysis tools.

¹⁴ For example bridges, dams and tunnels require different analysis packages

compressive sides of a given element. In many cases, the evolution of the curvature can give interesting indication on the state of the structure. For example, a beam which is locally cracked will tend to concentrate its curvature at the location of the cracks. Furthermore, by double integration of the curvature function, it is possible to retrieve the displacements perpendicular to the fibers direction. This is particularly interesting since in many cases the engineers are interested in deformation that are at a right angle to the natural direction in which the fiber sensors are installed¹⁵.

- **Feedback to finite element programs:** Nowadays most structures are modeled by FE software. It would be interesting to feed the data measured on the structure once constructed back to these programs. By doing so it will be possible to gain further insight into the properties of a given type of structure and eventually improve its design. This method known as “design by testing” is expected to generate more efficient structures, thus reducing their cost and improving their reliability and safety.

6.10.3 Outlook: Smart Civil Structures

We have already analyzed the first two building block of a smart structure: sensors and data processing. The missing link to close the loop is an array of actuators that, driven by the data processing stage, act back on the structure. The sensors would then measure the result of this action, feed the data to the processor and so on. Smart structure are already used in other engineering fields including aerospace and naval structures. They allow vibration and noise control in rotor-blades and hopefully flap-free airplane wings that change their shape using integrated piezoelectric actuators.

Some smart civil structures already exist. A few skyscrapers are actively damped against wind and seismic loads with heavy weights installed on rails on high levels and moved by hydraulic jacks. Other civil structures could benefit from such active damping: think of a suspension bridge with variable stiffness that could avoid resonance conditions. Besides dynamic control which is for the time being out of reach for the SOFO system, other structures could benefit from a slower response. For example, the post-stressing cables of a concrete bridge could be re-tensioned to compensate for concrete creep, the water flow could be altered to change the shape of a dam or cold water could be circulated in the beams supporting an high-rise building to compensate for deformation induced by differential heating (due to direct sunshine or fire). Other more traditional ways of acting on a structure, like a construction team makings repairs can also be considered, in a broader definition, as actuators.

¹⁵ For example: in a bridge fibers are installed horizontally, but vertical displacement are more interesting. In a tunnel the fibers are placed tangentially to the vault, but measurement of radial deformation is required. In a dam the fibers are installed in the plane of the wall but displacements perpendicular to it have to be measured.

6.11 Additional elements

Outside the information path, other elements play an important role in the proper functioning of the SOFO system.

6.11.1 Internal processor

The reading unit needs some internal processing power to perform its tasks like scanning the mirror and converting signals¹⁶.

- **Embedded PC:** The first SOFO systems relies on an internal PC card. The electronics cards controlling the mirror movements and data acquisition were housed on separate cards on the same PC bus. This allows a great flexibility and modularity of the system but increases considerably its size and power consumption.
- **Acquisition Card:** SOFO III is based on a National Instruments acquisition board linked to the PC via a parallel link and disposing an embedded processor controlling both acquisition and communication with the PC.
- **Micro-controller:** The industrial version of SOFO relies on a micro-controller for all its functions. The communication link disposes its independent processor.

6.11.2 Communication links

The reading unit has to communicate with the external PC this can be realized in a number of ways:

- **Serial RS232, RS485:** Serial links offer relatively small bandwidth but offer long distance links with unshielded cables. The first SOFO system communicates with the external PC by an RS232 link. RS485 is used in the industrial version of SOFO and offers higher speeds and the possibility of connecting multiple devices on a bus link.
- **Parallel:** The National instrument card communicates with the PC via the parallel port. This speeds the connection considerably by reduces the maximal distance between the reading unit and the PC to only one meter.
- **IEEE488 - GPIB:** This is the standard of communication between laboratory devices. It offers a good speed, relatively short link distances and the possibility to connect many devices. This type of link was never used in a SOFO system.
- **Network:** A direct network connection (for example Ethernet) would allow both high speed, long distance and multiple units communication. A network connection will be available as an option on the industrial version of SOFO.

The following table compares these communication links.

¹⁶ The FORMOS system relied entirely on the external PC for its processing power. This was one of the main causes of its exasperating slowness.

	Serial RS232/485	IEEE488 GPIB	Parallel Centronics	Network Ethernet
Bandwidth [Kbytes/s]	10 / 20	up to 1'000	500	up to 10'000
Maximum link distance [m]	>100	10	1	50 unlimited with repeaters
Number of devices	1 / 32	32	1	unlimited

Table 6.9. Comparison between different communication links.

6.11.3 Power supplies

The reading unit need its power supply. Since it is designed to work on building yard conditions or on existing structures where power supply is either unavailable or unreliable, the reading unit has to dispose of its own power source, for example a battery. The FORMOS system was only powered with 220 VAC and thus not adapted to field operation. All SOFO systems can be powered with an internal rechargeable battery, an external 12 VDC supply (for example a car battery) or a 220/110 VAC supply that also recharges the batteries. The autonomy of the battery should be at least one work-day, or 8 hours plus 500 measurements. Recharging should take at most one night.

6.11.4 Case and connectors

The casing of the system should be rugged, waterproof and easily visible. It should at least be transportable over short distances by a single person. For the SOFO system we have selected a very rugged plastic case orange in color (see Figure 6.44). All internal elements are fixed to a base plate and can be removed rapidly from the case for inspection or substitution. This case

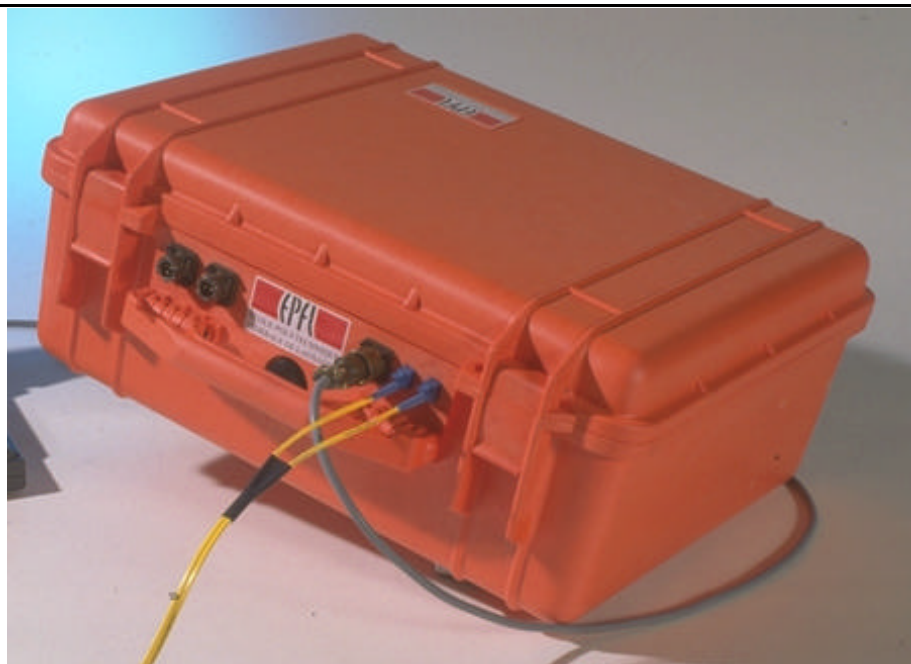


Figure 6.44. The SOFO casing.

performed well in adverse condition, for example being laid in mud or under heavy rain and snowfall.

Electrical and optical connectors should offer a good protection against water and shocks. While waterproof electrical connectors are easy to find, no fiber optic connector offers perfect protection against water and dust. DIAMOND E2000 connectors offer adequate protection against the agents found on a typical building yard, even if regular cleaning remains necessary.

6.12 Performances

The following paragraphs analyze the performances of SOFO III, the last system build at IMAC under my design, under laboratory conditions. The performances of the industrial version (SOFO IV) build, also under my design, by SMARTEC SA are practically equivalent. The behavior of such a system is better understood by looking at the performances it is capable of in real field applications as shown in section 8.

6.12.1 Reading unit precision

To quantify the precision of the reading unit alone we used an external Fabry-Perot interferometer with the far mirror supported by a piezoelectric element controlled by a strain gage with a rated resolution of 0.1 microns. The setup is shown in Figure 6.45. The reflections on the fiber surface and on the mirror give rise to two peaks in the coherence diagram. The distance between the two peaks was monitored as a function of the piezo movements.

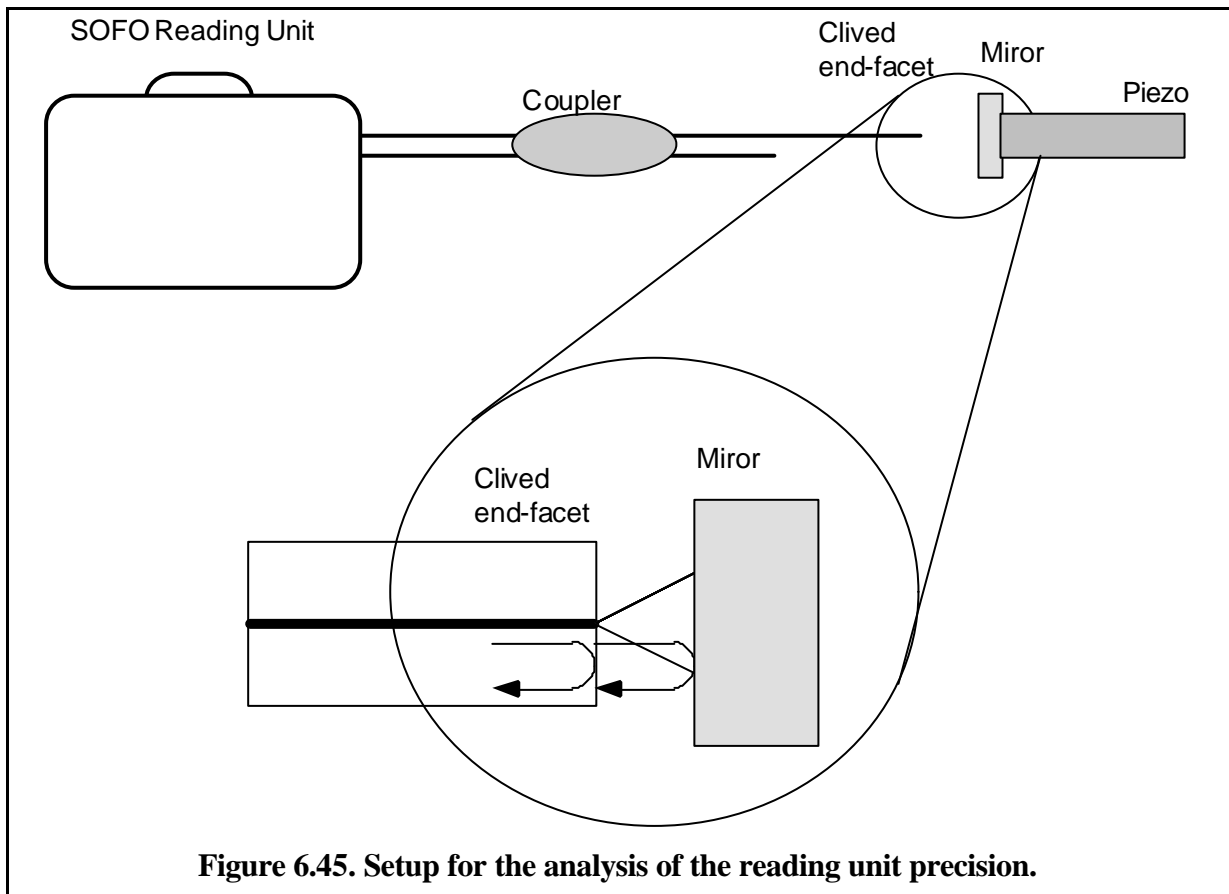
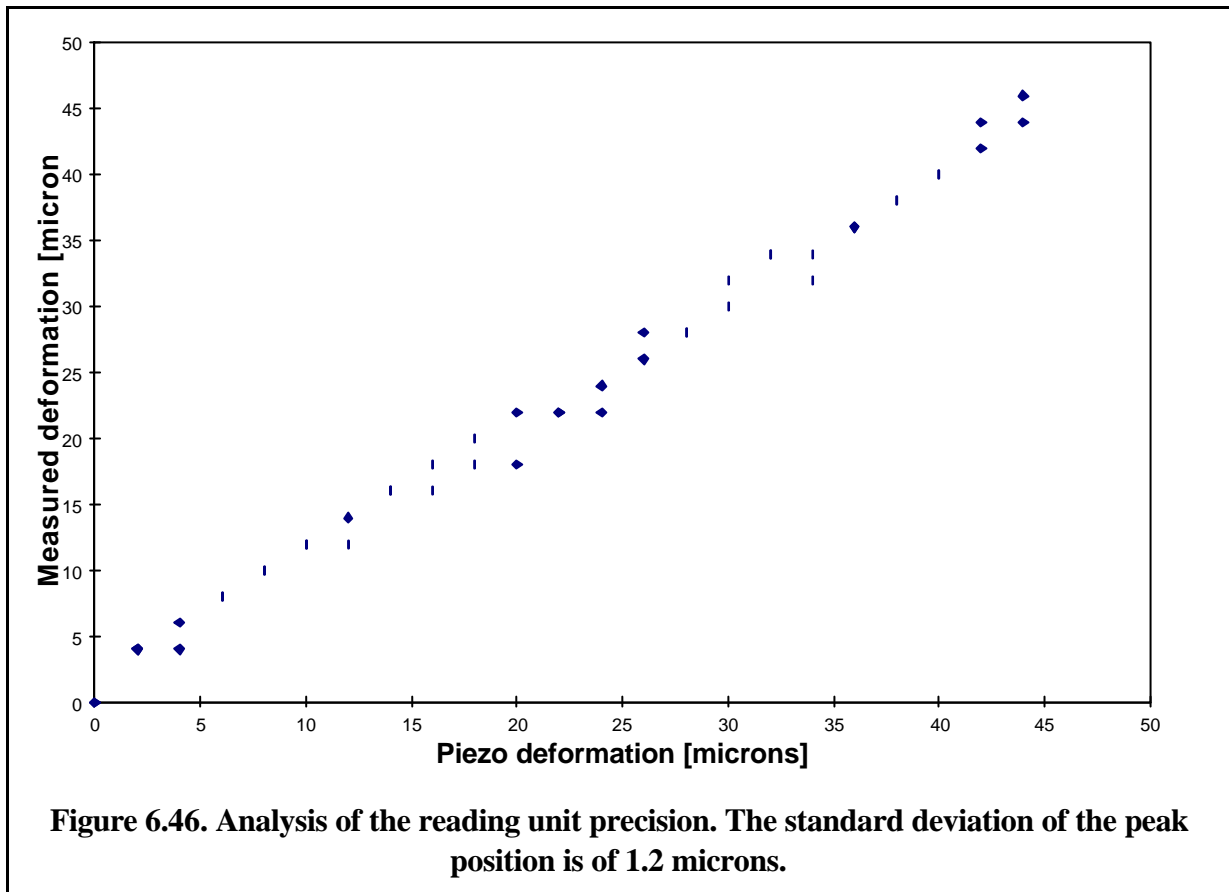


Figure 6.45. Setup for the analysis of the reading unit precision.



The result shown in shows a good linearity with a standard deviation of only 1.2 microns. This is a remarkable result since the equivalent resolution of the encoder is only 2 microns and the center of gravity of the peaks was calculated with this precision. This points to the fact that it would be possible to increase the resolution even further with a more precise encoder. This experiment tests only the resolution over short deformations. The precision for longer path unbalances will be limited by the linearity of the translation stage. In the units we have used this is guaranteed to better than 4 microns.

6.12.2 Sensor accuracy

The sensor accuracy depends on many parameters like the variations of temperature, the integration or not of the coupler into the sensor and on whether the passive region is manipulated between measurements (for example to connect the sensor). Finally the accuracy for large displacements is limited by the precision in the determination of the elasto-optic coefficient k_{stress} . In laboratory tests it was possible to obtain an accuracy of about 0.1% for deformations up to 8 cm. The resolution in field tests was found to be about 20 microns if the coupler was disconnected from the sensor between the measurements and about 2 microns for sensors with integrated coupler.

6.12.3 Stability

The long-term stability of the system is limited by the stability of the translation stage. The manufacturer guarantees a stability of about 4 microns. During long term measurements on stable or well known structures, it was found that a stability of the order of 10-20 microns

over periods as long as one year could be deduced from the measurements. Sensors with integrated coupler should reach a stability of the order of 5 microns over the same period.

6.12.4 Remote sensing capability

The system was tested with a passive region of up to 5 km in length. The light travels therefore for more than 10 km between the source and the detector. No degradation of the signals was observed for this length of fiber. Since the measurement are performed at 1300 nm, the chromatic dispersion is negligible. For longer length (unusual for most civil structures) the polarization mode dispersion could become observable and gradually degrade the measurement precision by introducing a spreading or even splitting of the peaks.

6.13 Outlook

With its industrialization, the SOFO system has reached its forth generation and a considerable maturity. The technology behind the reading unit and the sensors if now well known and mastered. The system has been used successfully in a variety of field and laboratory applications. The system has proved its reliability and is well adapted to civil applications. Further developments of the system include the automatic multiplexing of the sensors (as discussed in the next section) and the remote monitoring of the structures. In this case the system would be installed permanently inside or near the structure. The SOFO system would permanently gather information about the structural behavior, issue warnings if problems are detected and respond to remote calls allowing the downloading of the relevant parameters to a remote and centralized site.

6.14 Bibliography

- [1] L. Thévenaz, J.-P. Pellaux, N. Gisin, J.-P. Von der Weid "Birefringence Measurements in Fibers Without Polarizer", *Journal of Lightwave technology*, Vol.7, No. 8, August 1989, pp. 1207-1212
- [2] N. Gisin, J.-P. Von der Weid, J.-P. Pellaux "Polarization Mode Dispersion of Short and Long Single-mode Fibers", *Journal of Lightwave technology*, Vol.9, No. 7, July 1991, pp. 821-827
- [3] D. Inaudi, A. Elamari, L. Pflug, N. Gisin, J. Breguet, S. Vurpillot, "Low-coherence deformation sensors for the monitoring of civil-engineering structures", *Sensor and Actuators A*, 44 (1994), 125-130.
- [4] D. Inaudi, L. Vulliet, L. Pflug, S. Vurpillot, A. Wyser, "Low-coherence interferometry for the monitoring of underground works", 1995 North American Conference on Smart Structures and Materials, San Diego February 1995, Volume 2444, 171-178.
- [5] V. Gusmensoli, M. Martinelli, "Absolute measurements by low-coherence sources", *Advances in Optical Fiber Sensors*, Wuhan, China, October 1991
- [6] Y. J. Rao, Y. N. Ning, D. A. Jackson "Synthesized Source for White-light sensing system", *Optics letters*, Vol. 18, No 6, March 1993, pp. 462-464
- [7] Y. N. Ning, K. T. V. Grattan, B. T. Mergitt, A. W. Palmer "Characteristics of laser diodes for interferometric use", *Applied optics*, Vol. 28, No. 17, September 1989, pp. 3657-3661.
- [8] *Fiber Optics Reliability: Benign and Adverse Environments IV* (1990), SPIE vol. 1366

- [9] D. Inaudi, A. Elamari, L. Pflug, N. Gisin, J. Breguet, S. Vurpillot, "Low-coherence deformation sensors for the monitoring of civil-engineering structures", *Sensor and Actuators A*, 44 (1994), 125-130.
- [10] A. Elamari, D. Inaudi, J. Breguet, L. Pflug, N. Gisin, S. Vurpillot, "Low Coherence Fiber Optic Sensors for Structural Monitoring", *Structural Engineering International*, Volume 5, Number 1, 43-47
- [11] D. Inaudi, A. Elamari, S. Vurpillot, "Low-coherence interferometry for the monitoring of civil engineering structures", *Second European Conference on Smart Structures and Materials*, Glasgow October 1994, SPIE Volume 2361, 216-219.
- [12] S. Vurpillot, D. Inaudi, P. Mivelaz, "Low-coherence interferometry for the monitoring of concrete structures", *European Symposium on Optics for Environmental and Public Safety*, Munich June 1995, SPIE Volume 2507, 35-44
- [13] D. Inaudi, S. Vurpillot, Nicoletta Casanova, Annette Osa-Wyser, "Development and field test of deformation sensors for concrete embedding", *Smart Structures and materials*, San Diego February 1996, SPIE Volume 2721-16.
- [14] S. Chen, B. T. Mergitt, A. J. Rogers "Novel electronic Scanner for Coherence Multiplexing in a Quasi-distributed Pressure Sensor", *Electronics letters*, Vol. 26, No. 17, August 1990, pp. 1367-1369
- [15] S. Chen, A. J. Rogers, B. T. Mergitt "Electronically Scanned Optical-Fiber Young's White-light interferometer", *Optics Letters*, Vol. 16, No. 10, May 1991, pp. 761-763.
- [16] A. Koch, R. Ulrich "Fiber-optic Displacement Sensor with 0.02 μm Resolution by White-light Interferometry", *Sensors and Actuators A*, 25-27 (1991), 201-207
- [17] P. de Groth, L. Deck "Three-dimensional imaging by sub-Nyquist sampling of white-light Interferograms", *Optics Letters*, Vol. 18, No. 17, September 1993, pp. 1462-1464.

7. Multiplexing

In a typical civil structure such as a bridge, tens or even hundreds of sensors have to be installed and measured. In the previous sections we have seen how to measure a single sensor and obtain information about the deformations at a particular point in the structure. In order to measure a larger number of sensors it is possible to manually connect each sensor one after the other. This is made possible by the absolute nature of low-coherence interferometry: no permanent connection is necessary between the sensor and the reading unit. This ‘manual multiplexing’ is especially adapted for the long-term monitoring of structures that require only occasional measurements (for example once a month or once a year). When measurements are required more often, manual multiplexing becomes a tedious task and an automatic procedure has to be established.

Another major drawback in the manual multiplexing scheme, is the need of one or two lead-out fibers for each sensor. For a large number of sensors this can result in an important number of cables running from the sensors to the reading unit that can sometimes be placed at a large distance from one another. If a larger number of sensors could be connected to the reading unit by a reduced number of fibers, this would simplify the sensor network and its installation and reduce the costs of the passive fibers and the relative connectors.

In this section we will explore different multiplexing techniques that address both automatic measurement of a large number of sensors and the reduction of the lead-out wires.

7.1 Introduction

The goal of any multiplexing architecture, is to connect a number of sensors to a single reading unit. These sensor can be addressed either simultaneously or sequentially. No manual intervention should be necessary.

In the case of low-coherence interferometry, the multiplexing schemes can be subdivided into two broad categories: lateral (parallel) and longitudinal (serial) multiplexing. In the lateral multiplexing configuration, the sensors remain identical to the ones used in the single sensor configuration, but the passive regions are organized into a star or tree configuration that converges to the reading unit. In the case of longitudinal multiplexing, the sensors are chained one after the other and provided with partial reflectors that act as semi-reflective mirrors and allow the discrimination of the deformations occurring in each of the so obtained sensor sections. In many cases, the optimum performance will be obtained by mixing these two approaches.

Figure 7.1 presents the different techniques that will be discussed in this section.

Multiplexing				
Lateral Multiplexing <i>(7.2)</i>	Longitudinal Multiplexing <i>(7.3)</i>			
	Coherence Multiplexing <i>(7.3.1)</i>	Peak Identification		
		Peak Form and Position <i>(7.3.2)</i>	Peak Identification <i>(7.3.3)</i>	
			Intensity Modulation	Phase Modulation
Optical Switching <i>(7.2.1)</i>	Coherence multiplexing <i>(7.3.1)</i>	Fiber Bragg Gratings <i>(7.3.2.1)</i>	Phase Shifting <i>(7.3.3.1)</i>	Phase Pulses <i>(7.3.3.2)</i>
Electrical switching <i>(7.2.2)</i>		Etalons <i>(7.3.2.2)</i>		Pseudo-random phase steps <i>(7.3.3.3)</i>
Multi-channel delay coils <i>(7.2.3)</i>		Intensity <i>(7.3.2.3)</i>		Single-pass <i>(7.3.3.4)</i>
Coherence multiplexing <i>(7.2.4)</i>		Dispersion <i>(7.3.2.4)</i>		Double-pass <i>(7.3.3.5)</i>
Wavelength multiplexing <i>(7.2.5)</i>				Chirped modulation <i>(7.3.3.6)</i>

Figure 7.1. Multiplexing techniques. The corresponding paragraph numbers are indicated in italics.

7.2 Lateral multiplexing

Lateral multiplexing consists in arranging a number of single sensors in a star or tree configuration. The sensors are then addressed either simultaneously or sequentially. Some means has to be provided in order to discriminate between the measurements from different sensors.

7.2.1 Optical switching

Optical switching is the most obvious way to address the lateral multiplexing problem. The optical switch simply replaces the human operator and connects the different sensors sequentially or according to a pre-established program. Optical switches can be used either in the $2 \times N$ configuration or in the $1 \times N$ configuration if each sensor is provided with an integrated coupler. Both configurations are schematized in Figure 7.2. Optical switching is a form of time division multiplexing (TDM) and a separate scan is required for each of the switch's channels.

Optical switches are available commercially in both configurations and with up to 100 channels. The price per channel presently exceeds the cost of a sensor, making optical switching interesting only in two special cases. First, when automatic and unattended measurements are necessary over a limited amount of time. In this case the investment for the

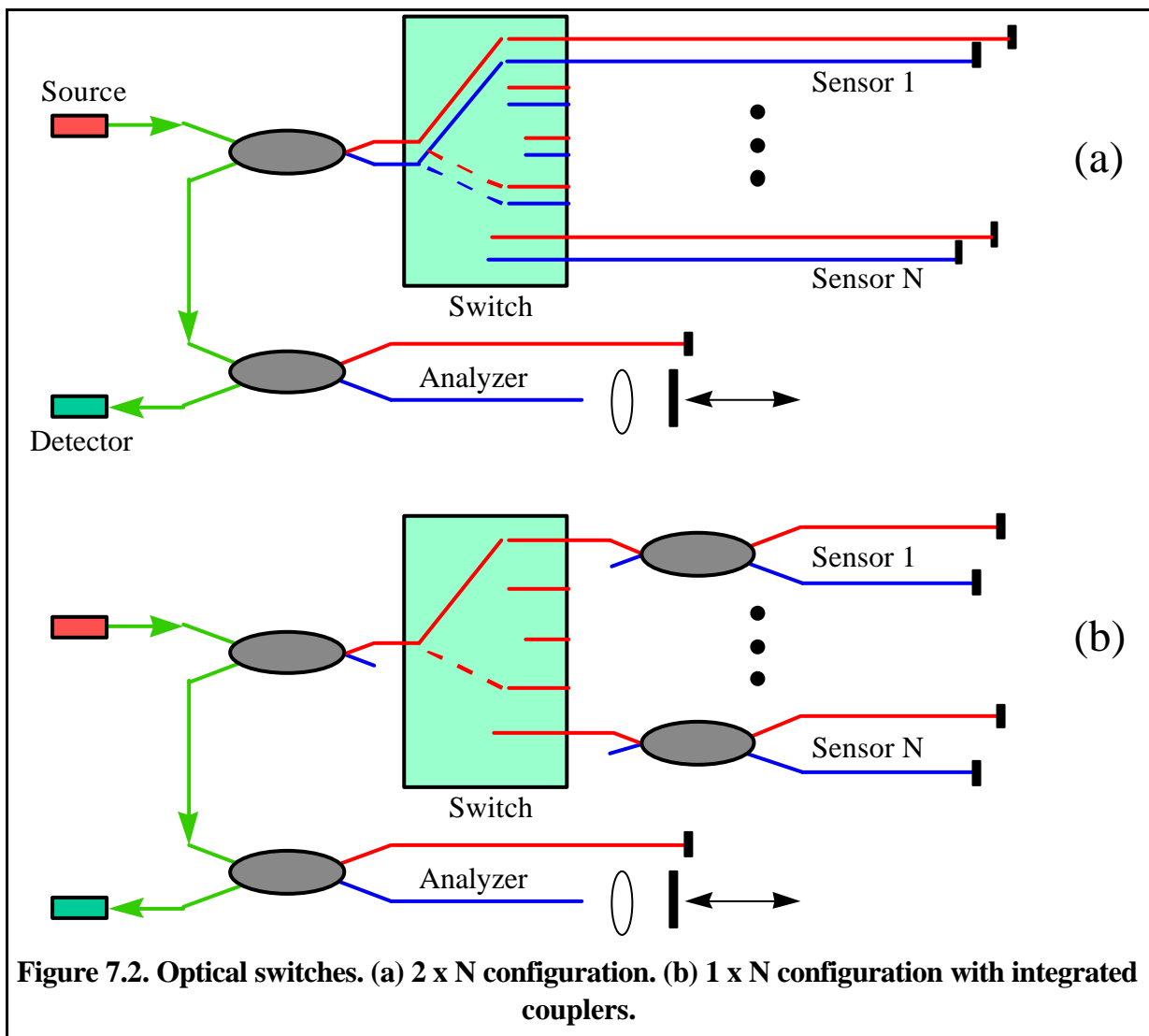


Figure 7.2. Optical switches. (a) $2 \times N$ configuration. (b) $1 \times N$ configuration with integrated couplers.

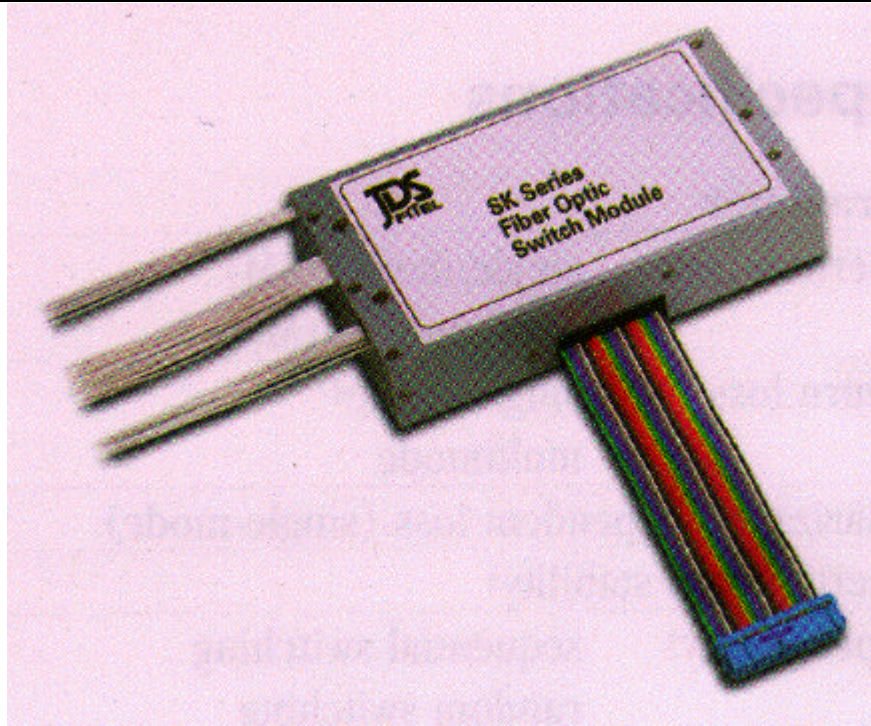


Figure 7.3. A 2 x20 Optical switch.

optical switch can be divided by reusing it on other structures. The second case include structures with a long distance between the sensor and the analyzer. By placing the optical switch near the sensors and operating it remotely it is possible to greatly reduce the number of expensive optical cables and connections. The price of these components is however destined to drop, optical switches being a key component of multimedia services like video-on-demand¹ and more generally fiber-to-the-home.

A portable, rugged, and battery powered optical switch was realized in the 2 x 20 configuration by using a commercial mechanical switch from JDS (Canada). This switch presents typical losses in the order of 0.4 dB. The round-trip losses are therefore of about 0.8 dB plus an additional 6 dB loss if the switch is used in the 1 x 20 configuration with a coupler in each sensor and a single lead-out wire. Figure 7.3 shows the realization of this switch.

¹ Each TV viewer can choose from a large palette of films available on a remote server and can browse through them like on a conventional VCR.

7.2.2 Electrical switching

Electrical switching can be implemented by using a number of sources or detectors that are addressed in sequence. The light from the different sensors is then combined by a passive $1 \times N$ coupler and sent toward the analyzer (see Figure 7.4). This solution is presently cheaper than optical switching. However the power budget is inferior due to the presence of the lossy $1 \times N$ coupler. Furthermore the multiple sources or detectors have either to sit near the sensors or additional cabling is required. Electrical switching is also a form of time division multiplexing (TDM), a mirror scan is required for each source/sensor. If, instead, the sources are frequency modulated at different frequencies well above the fringe frequency, it is possible to demodulate them separately with a single scan. This would be a form of frequency division multiplexing (FDM).

7.2.3 Multi-channel delay coils.

An extreme form of lateral multiplexing consists in realizing N completely independent tandem interferometers. This configuration allows the simultaneous measurement of all channel but increases the cost significantly. Furthermore, this configuration does not reduce the number of optical connection between the sensors and the reading units. Since the most expensive components are those found in the delay line and in particular the microscope objective and the translation stage, it would be interesting to create N independent channels using the same optics and mirror scanner. This might be possible by combining a number of fibers into a single ferrule (see Figure 7.5). Since the double-pass delay line couples the light back to the fiber independently from the relative position of the fiber and the objective, the light from each of the fibers will be coupled back to the same fiber. However, as we have seen in the previous section, the coupling efficiency decreases rapidly when the fiber is moved from its ideal position. This is due to the mismatch between the acceptance cone of the fiber and the light cone coming back from the delay line after the two round-trips.

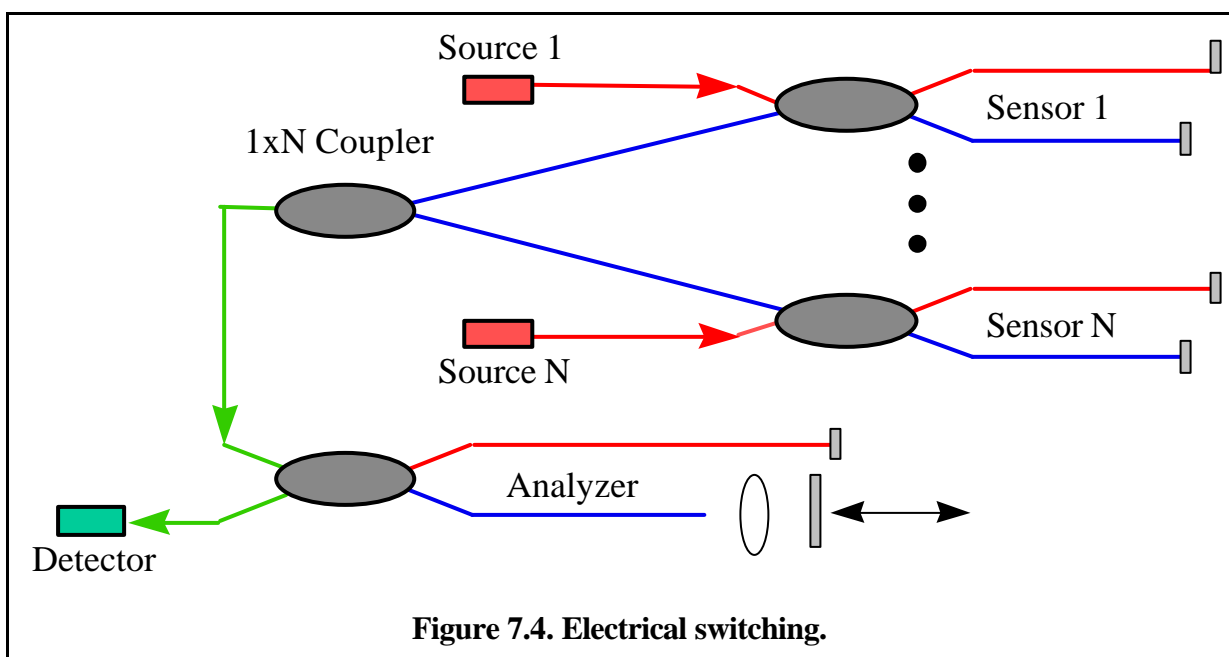
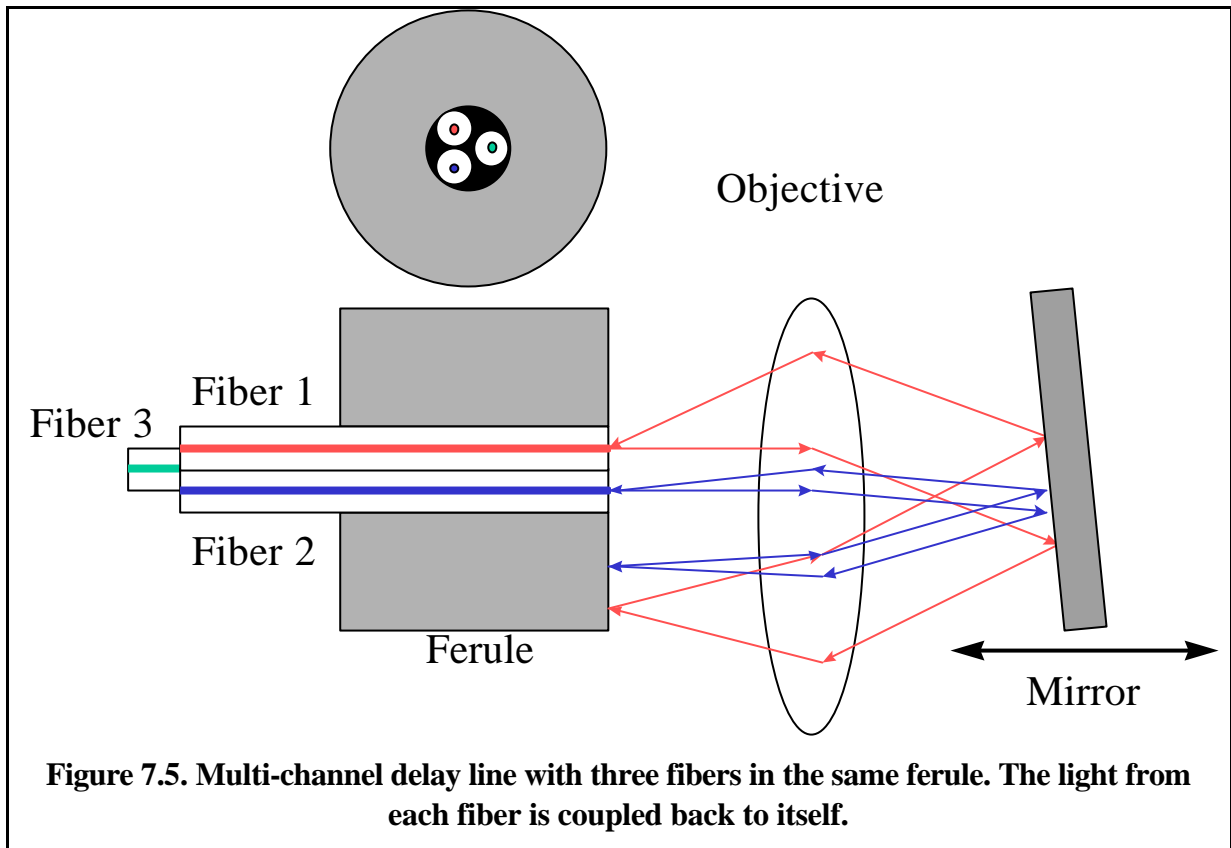


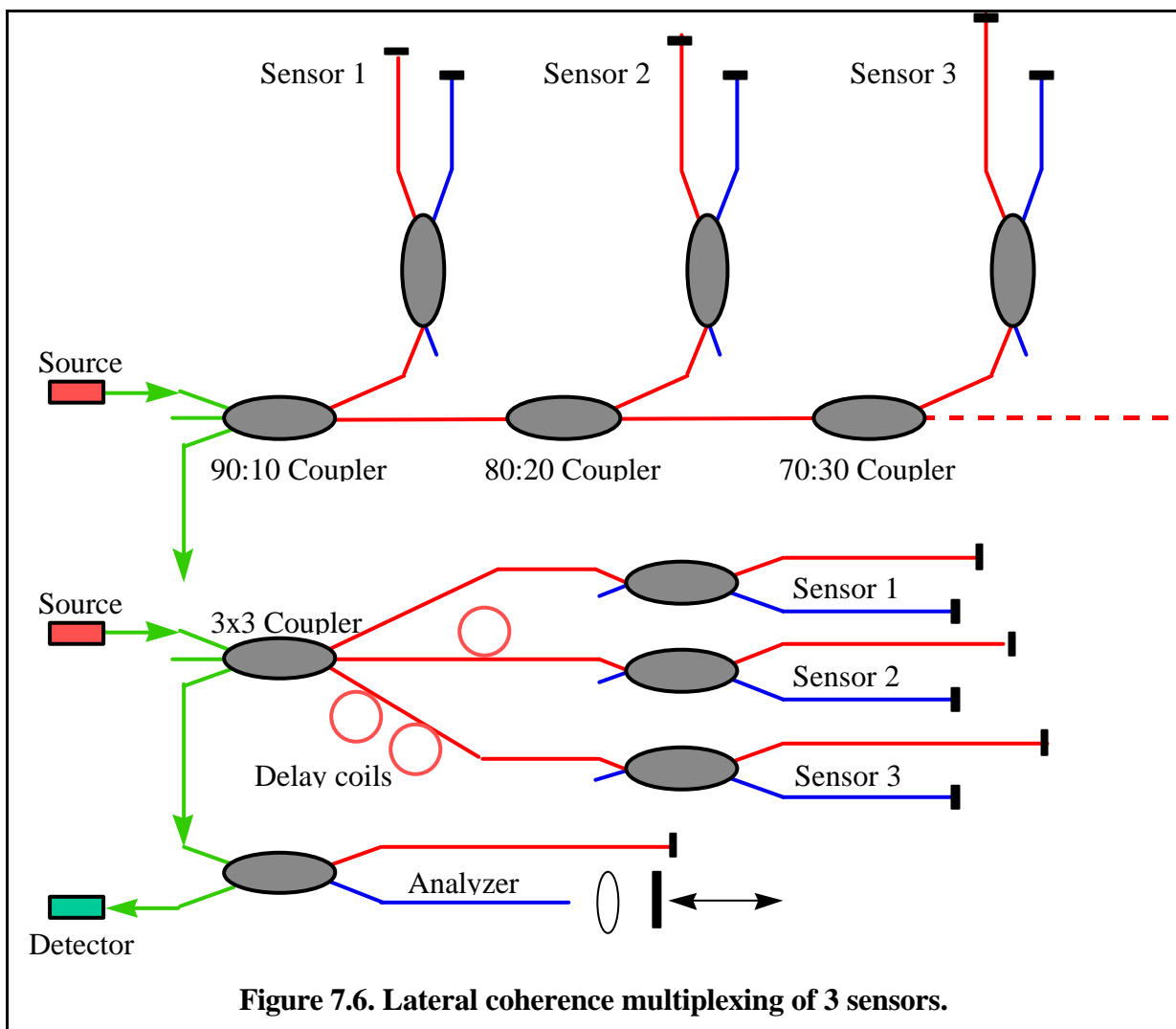
Figure 7.4. Electrical switching.



The theoretical model shows that it is possible to obtain a relatively good back-coupling for up to 7 fibers arranged in a single ferrule. Experimental tests with a ferrule with three fibers showed disappointing results because the fibers core were not parallel nor perpendicular to the fiber surface. A more careful assembly of the ferrule should give better results. All the fibers would then be measured with a single mirror scan.

7.2.4 Coherence multiplexing

Coherence multiplexing is a very simple and effective way to multiplex a reduced number of sensor laterally. This setup uses additional couplers between the reading unit and the sensors. Additional delay coils should be added to avoid cross-interference between fibers in different sensors as shown in Figure 7.6. If N sensors are connected to a single $2 \times 2N$ coupler or to a cascaded coupler structure (as in the example of Figure 7.6), the signal will be N^2 times weaker than the one returned from a single sensor ($2N$ weaker in the bus configuration). Three sensors will therefore return a signal about 10 dB weaker than the best possible signal. This can easily be accommodated by the dynamic range of the reading unit. All sensors will be measured simultaneously with a single scan.



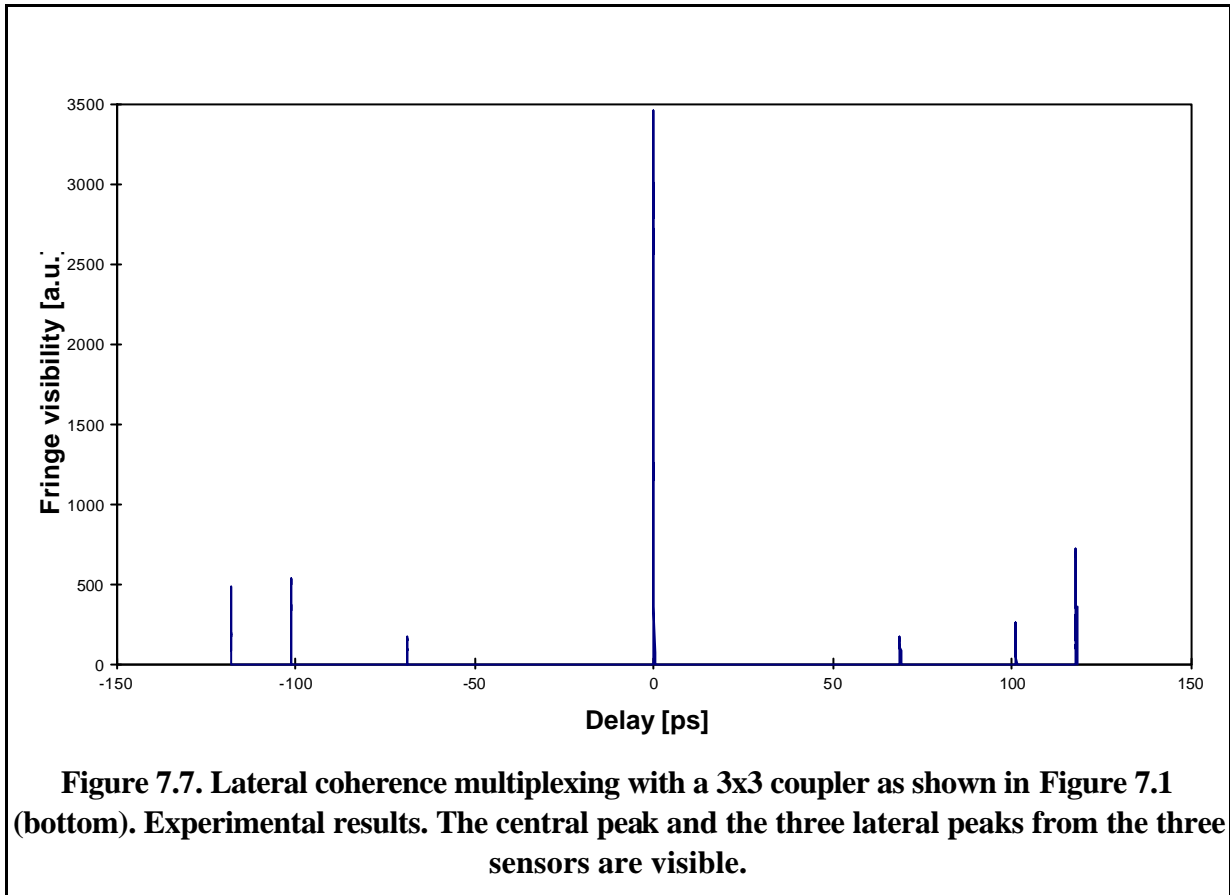
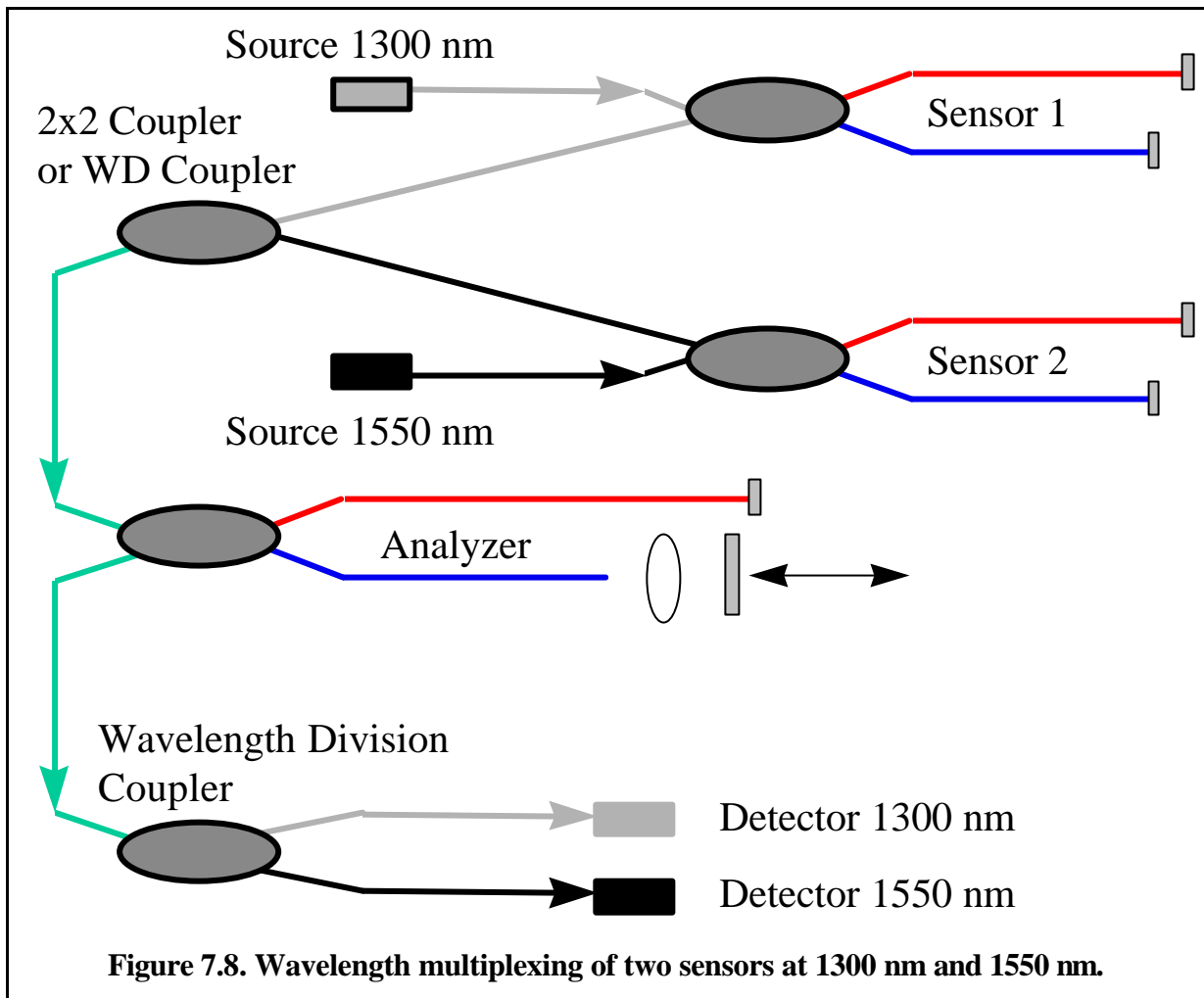


Figure 7.7 shows a sample scan obtained by this technique. The advantage of using sensors with integrated couplers resides in the fact that the peaks will appear in the coherence diagram in the same position as when the sensors are measured separately. This greatly simplifies the peak recognition. It is possible to manufacture the sensors so that their peaks will appear evenly spaced in the coherence diagram. In order to avoid peak crossings the spacing should be greater than the maximal expected deformation.



7.2.5 Wavelength multiplexing

Different sensors can be illuminated with different wavelengths that can be separated optically before the detection stage or digitally after sampling of the interferogram. Since the measurement principle requires the use of a broad-band source, it is not possible to pack a large number of wavelength into the optical windows of silica fibers. It is however possible to mix 1300 nm and 1550 nm emissions from two sources and separate them with a wavelength division coupler as shown in Figure 7.8. With current WDM components it would probably permit 4 or 6 wavelengths. If another wavelength division multiplexer is used as mixer after the sensors, no significant decrease of the signal compared to the one from a single sensor should result. The sensors will be measured simultaneously.

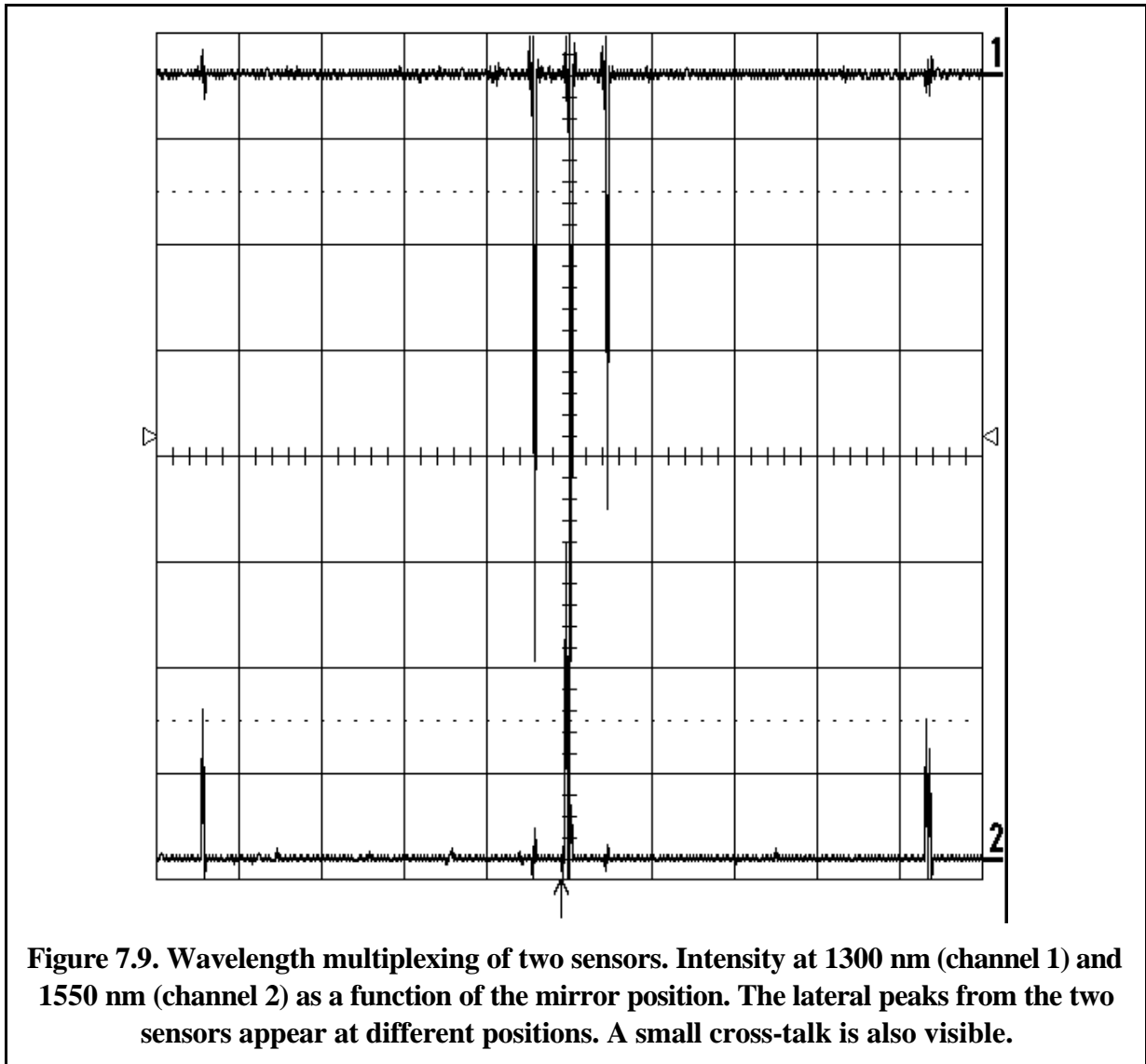
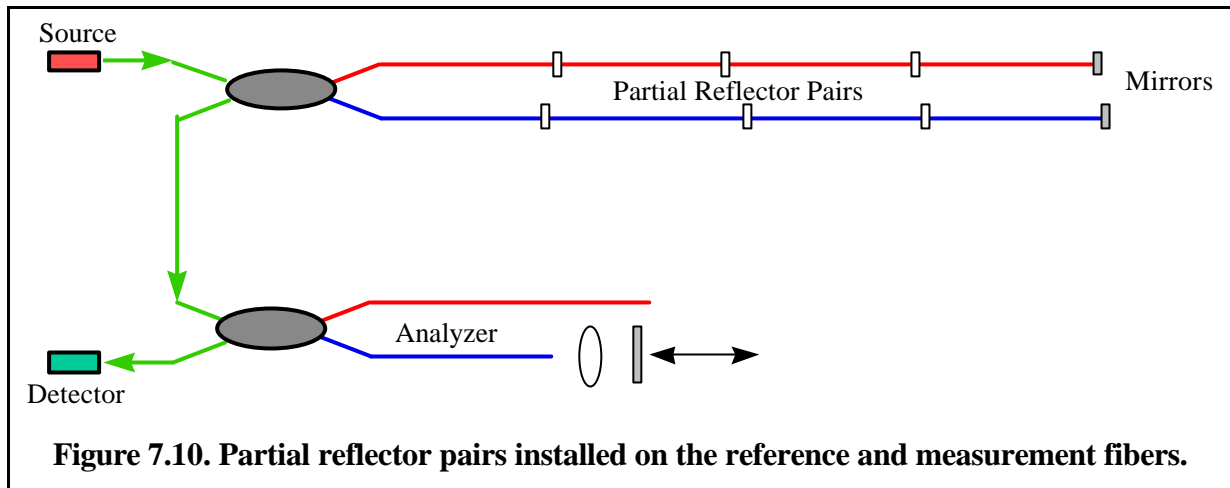


Figure 7.9 shows an experimental result using this technique to multiplex two sensors. The little cross-talk is due to the imperfect wavelength separation of the WD coupler.

7.3 Longitudinal multiplexing

In the previous paragraphs we have seen that lateral multiplexing offers only a limited potential and implies, in most passive forms, an important power loss. The only setup with a good power performance is optical switching that requires expensive components.

Many applications in civil engineering monitoring require the measurement of successive sections along the same line. Examples include the monitoring of geostuctures like tunnels, piles, anchorage and dam foundations, as well as bridges by using the curvature monitoring algorithms. In these cases it is interesting to subdivide the active length of the sensor into a number of sub-sections that can be measured separately. This is achieved by introducing partial reflector pairs on both the reference and the measurement fibers, as shown in Figure 7.10. Each partial reflector will act as a semi-transparent mirror and will reflect a small amount of light back to the analyzer. Each of the reflector pairs will therefore produce a peak in the coherence diagram. The movements of each peak will be proportional to the deformation undergone by the whole sensor between the coupler and the corresponding partial reflector



pair. By monitoring the distance between two peaks corresponding to two successive reflector pairs, it is possible to retrieve the deformation undergone by the particular section delimited by the two partial reflector pairs. We will see in 7.5.1 that the use of partial reflectors allows an optimal use of the available power. Furthermore, multiple sensors chains can be multiplexed as described in the previous paragraphs and produce mixed configuration as described in 7.4. The main problem with this configuration consists in the fact that an ambiguity exists between the physical order of the reflectors in the sensor chain and the order of the corresponding peaks in the coherence diagram. The following paragraphs will present different techniques that can be used to resolve this ambiguity. These fall into three main categories. In the first case, coherence multiplexing, the peak order is established during the fabrication of the sensor chains and the peaks are not allowed to cross. This means that the distance between the peaks is chosen to be large enough to accommodate the largest expected deformation of the structure sections. In the second case the peaks are recognized by their form. The form of the peaks can be altered by changing the spectral reflectivity of the partial reflectors, by using multiple reflectors or using the natural dispersion of the fibers. In the third case the reflector pairs are identified by their physical location in the chain. All the techniques in this category rely on a direct or indirect measurement of the time of flight required to reach a given partial reflector and come back to the analyzer.

7.3.1 Coherence multiplexing

This is the simplest form of longitudinal multiplexing [1,2]. It uses exactly the same analyzer as in the case of single sensors, but the sensor is now provided with partial reflectors. Since the reflectivity of these reflectors is typically one to two orders of magnitude lower than the one of a perfect mirror, the detection stage of the analyzer has to be adapted in order to increase its dynamic range.

Since no other mean of identification is available the relation between the spatial position of the reflectors and the order in which they appear in the coherence diagram has to be established once and for all. The most obvious way to achieve this consists in ensuring that either the reference or the measurement fiber are always longer than the other in each sensor section. This will ensure that the peaks will appear in the coherence diagram in the same order as in the sensor chain. This can be realized easily at the fabrication stage. It is furthermore necessary to ensure that one of the fibers remains longer than the other even for the maximal expected deformation. Finally, the maximal length difference between two partial reflectors (which occurs for the last pair) should not exceed the scanning range of the mirror in the analyzer. If, for example, the mirror is able to compensate deformations up to 50 mm, each of 5 section could be allowed to measure a deformation of ± 5 mm without peak crossing. If the structure is expected to undergo deformations of 1 mm/m the length of each section will be limited to 5 m. Figure 7.11 shows an example of the coherence diagram obtained from a chain with 6 partial reflector pairs. This measurement was obtained with a standard SOFO III analyzer and using DIAMOND air-gap connectors as partial reflectors.

This configuration offers the evident advantage of requiring a minimum number of components and can therefore be seen as the natural evolution of the single-sensor configuration. The main drawback resides in the necessity to subdivide the scanning range of the analyzer's mirror into separate sections for each sensor in the chain. This is due to the fact that peak crossings can not be allowed and limits either the length or the number of sections or the maximal allowed deformation.

7.3.2 Peak recognition: peak form

If we want to allocate the whole scanning range to each of the partial reflectors, it becomes necessary to identify each peak in a unique way and correlate it unambiguously to a given partial reflector pair. A first possibility to achieve this is by changing the form of each peak. It

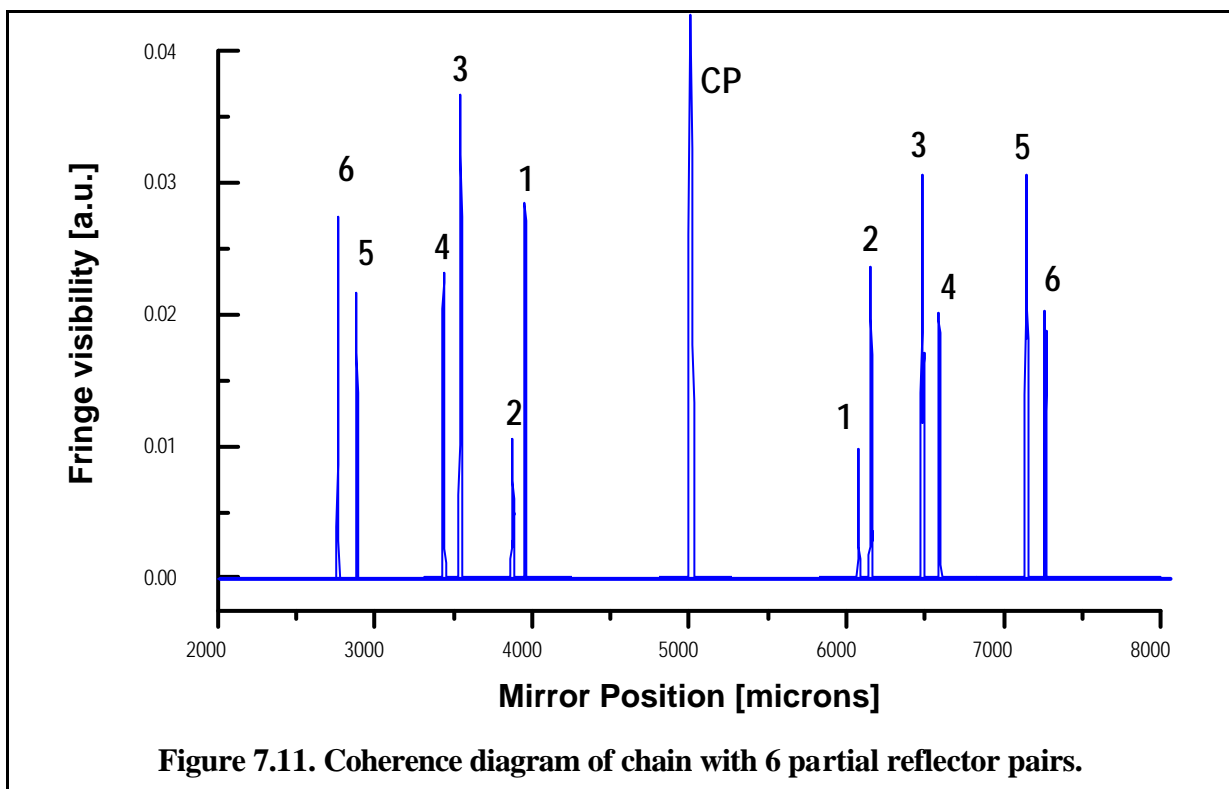


Figure 7.11. Coherence diagram of chain with 6 partial reflector pairs.

will then be possible to distinguish the peaks even after peak crossings. In the next paragraphs we will explore a few methods to change the peak's form. In all cases it will be possible to distinguish between the peaks, even after peak crossings, by calculating the correlation function between two successive measurements. Depending on the method chosen it will even be possible to recognize partially or totally superposed peaks.

7.3.2.1 Broadband fiber Bragg gratings

Fiber Bragg gratings are local and periodic alteration of the refraction index of the fiber core produced by side exposure with UV light. Conventional fiber Bragg gratings are able to reflect at a specific wavelength corresponding to the grating periodicity and transmit the rest of the incoming spectrum [3,4,5]. The typical coherence length of the light reflected by a fiber Bragg grating is of the order of a few mm to 1 cm. If used as partial reflectors in a chain this would produce peaks of this width (see Figure 7.12). Furthermore the two gratings in each pair should have matching spectral characteristics or no interference will be possible and no lateral peak will appear. These two restrictions are intolerable for most practical applications.

It is possible to obtain fiber Bragg grating pairs that reflect a broader spectrum and have therefore a shorter coherence length and better spectral overlapping. This can be done by either reducing the physical length of the grating (the coherence length of the reflected light being roughly proportional to the physical length of the grating) or by using chirped gratings with a variable periodicity. The first method produces gratings with low reflectivity whereas the chirped gratings can reflect a significant amount of light over a broad wavelength range.

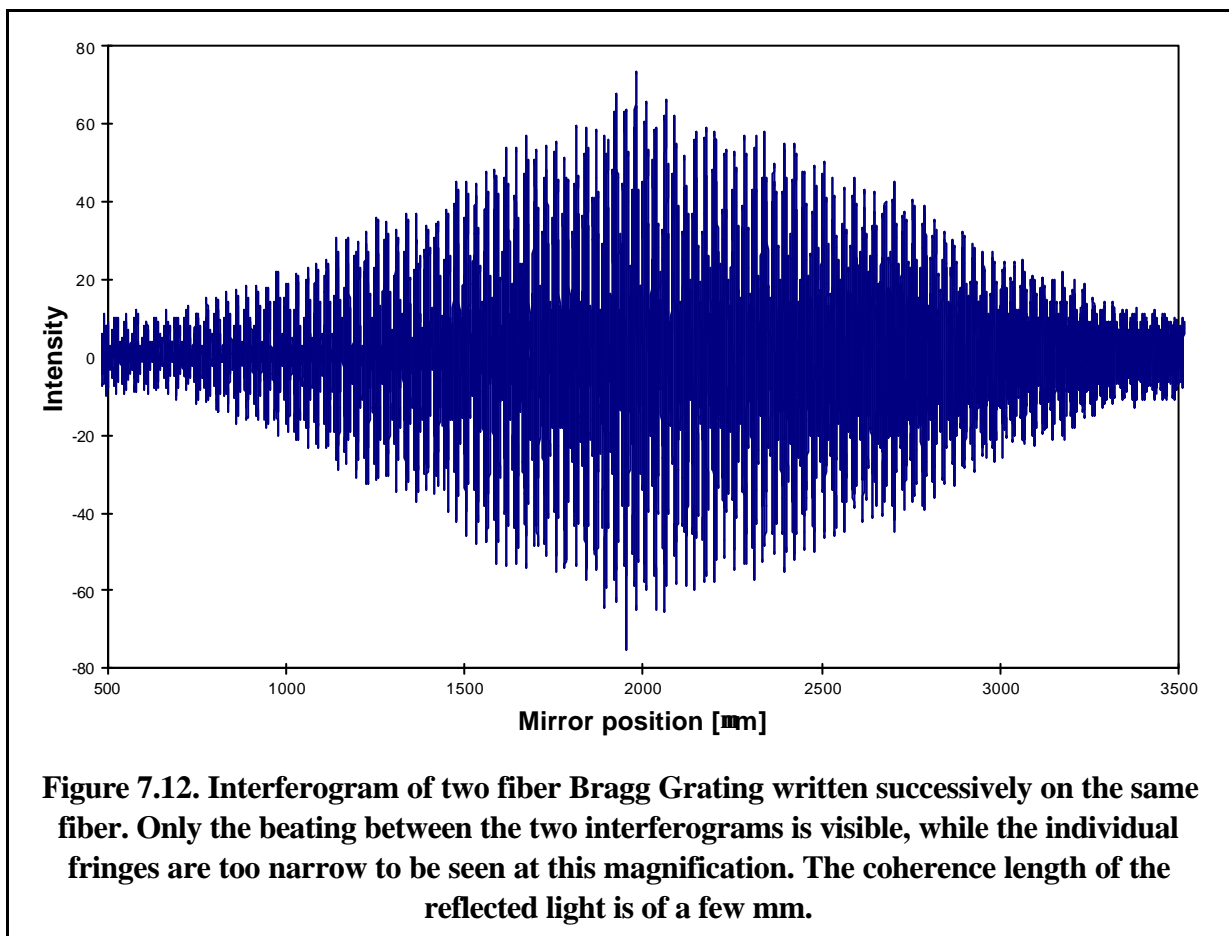


Figure 7.12. Interferogram of two fiber Bragg Grating written successively on the same fiber. Only the beating between the two interferograms is visible, while the individual fringes are too narrow to be seen at this magnification. The coherence length of the reflected light is of a few mm.

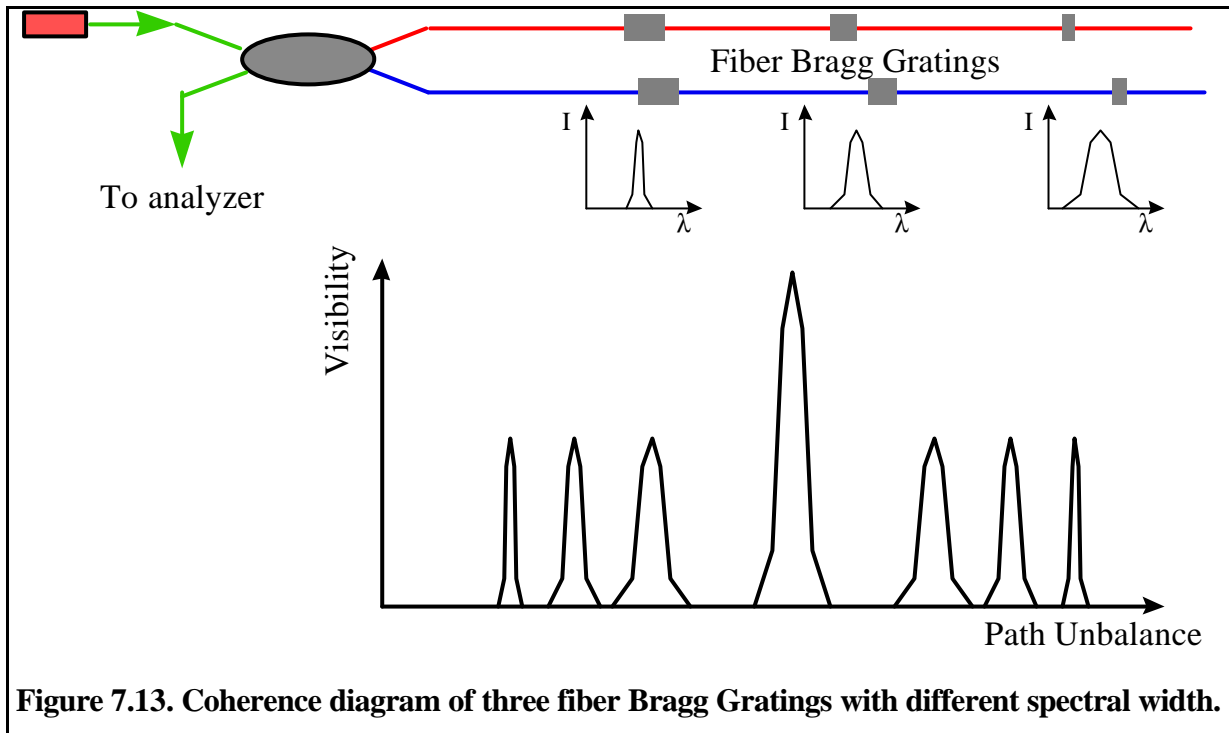
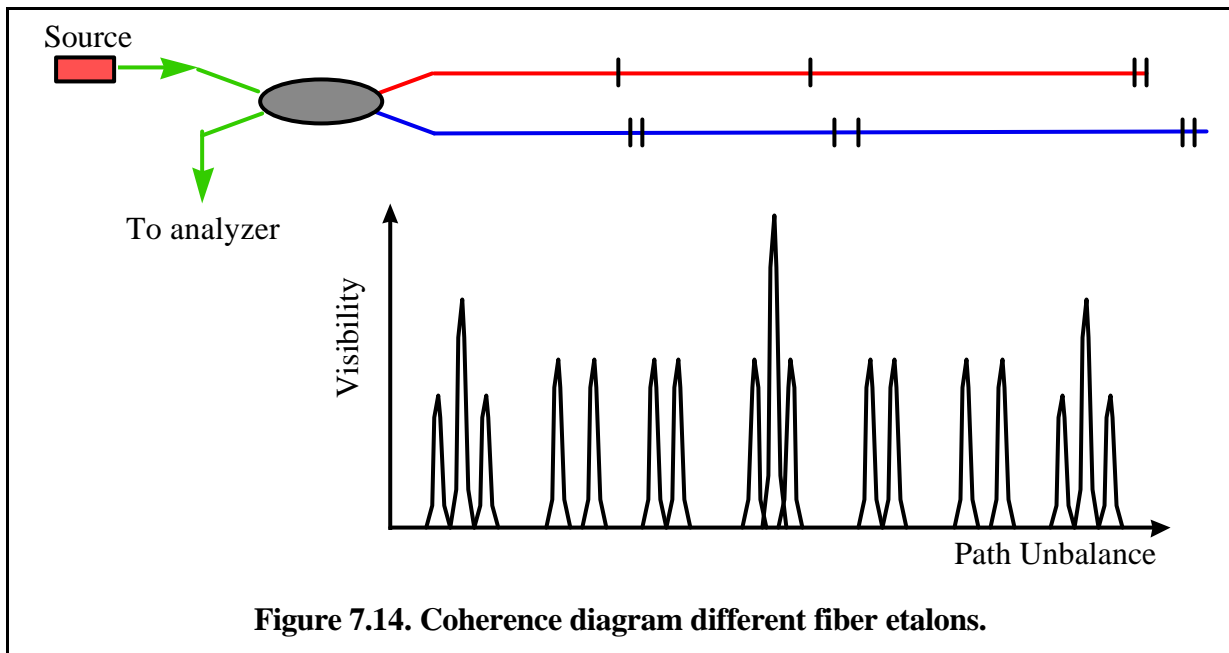


Figure 7.13. Coherence diagram of three fiber Bragg Gratings with different spectral width.

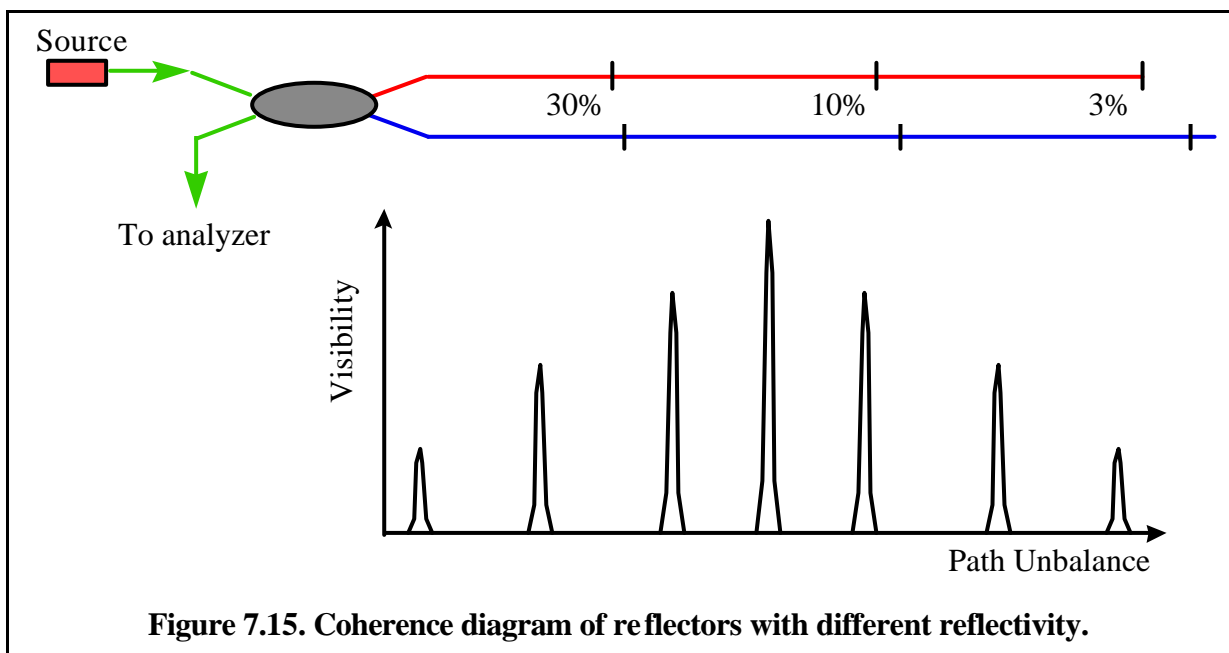
If the grating pairs in a sensor chain all have different spectral characteristics, i.e. different spectral width and/or different center wavelength, they will appear in the coherence diagram with different width (inversely proportional to the spectral width as schematized in Figure 7.13) and with different fringe periodicity. This will allow an identification of the reflectors. By combining appropriate chirping and grating modulation depth, a procedure called apodization [6], it is possible to obtain peaks of almost any wished form. It is however to be noticed that the narrowest possible peak will always be determined by the source spectral width. All peaks obtained with fiber Bragg gratings will therefore be brighter than the peaks obtained by a conventional broadband reflector. Any strain gradient induced to the Bragg grating region will alter its spectral response. The reflectors should therefore be screened from such effects, for example by installing them in unstrained regions between adjacent sensors. A major drawback of this technique resides in the currently high price of commercial fiber Bragg gratings.

7.3.2.2 Etalons



If instead of using a single reflector, we use two or more closely spaced reflectors, two or more peaks will appear in the coherence diagram. Since these peaks will move together it will be easy to recognize them. The encoding of the peaks can be achieved either by changing the distance or the number of reflectors. The distance between the reflectors should be at least of the order of magnitude of the coherence length, so that the form of the peaks is altered significantly. An example of such setup is shown in Figure 7.14. Each of the reflectors can be fabricated by any of the procedures described in paragraph 7.5. Extrinsic Fabry-Perot etalons usually present relatively high losses and it is therefore difficult to multiplex a large number of these devices on the same line.

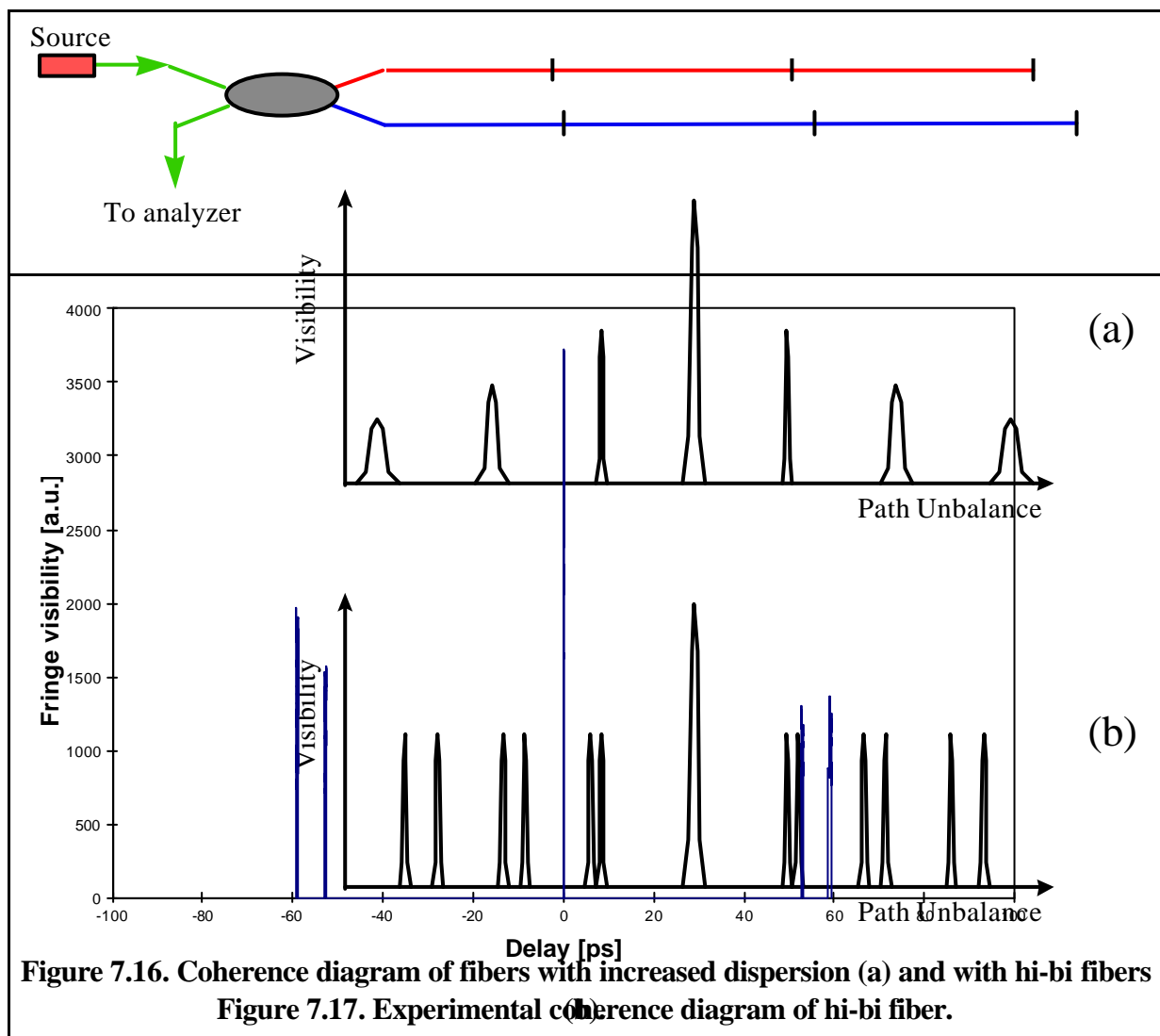
7.3.2.3 Intensity

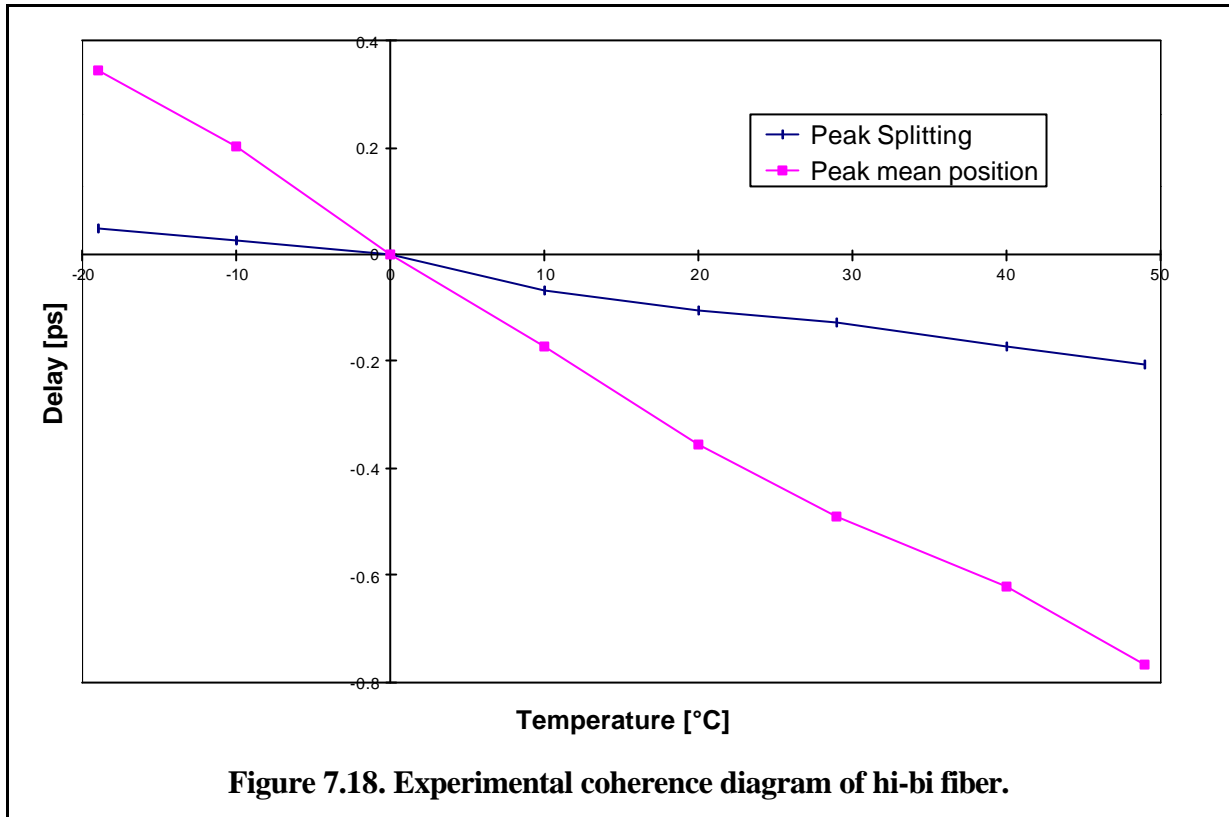


If the reflectors have different reflectivity (taking into account the losses due to all reflectors appearing before in the chain) the peaks will have different heights in the coherence diagram. This would allow an identification of the peaks by their height. Unfortunately, other parameters influence the peak height, including the birefringence state of the fibers and the connector losses. This means of identification is therefore less robust than the precedent ones and would require large reflectivity differences between the reflector pairs (limiting the number of reflectors) or require birefringence compensation (complicating the setup). A setup based on intensity discrimination is shown in Figure 7.15.

7.3.2.4 Dispersion: peak broadening or splitting

With increasing distance from the source, the peaks have a natural tendency to broaden due to dispersive phenomena including chromatic dispersion, polarization dispersion (especially in hi-bi fibers) [7] and modal dispersion (in multimode fibers). These effects can be used to indirectly measure the distance between the reflector that produces a given peak and the analyzer. In order to make the broadening visible even for the short fiber length typically involved in these kind of sensors, special fibers with particular index profiles should be used. Hi-bi fibers will produce splitted peaks where the splitting will be proportional to the fiber length [8]. Both cases are depicted in Figure 7.16.





An experimental test of this setup was realized using a 3M polarization maintaining fiber at 1300 nm with a beat-length of 1.6 mm. One of the arms of the sensor's interferometers was made of the hi-bi fiber while a standard fiber was used in the other arm. For a 1.87 m long fiber pair it was indeed found a peak splitting of 6.4 ps as shown in Figure 7.17. In general, the peak splitting will be given by:

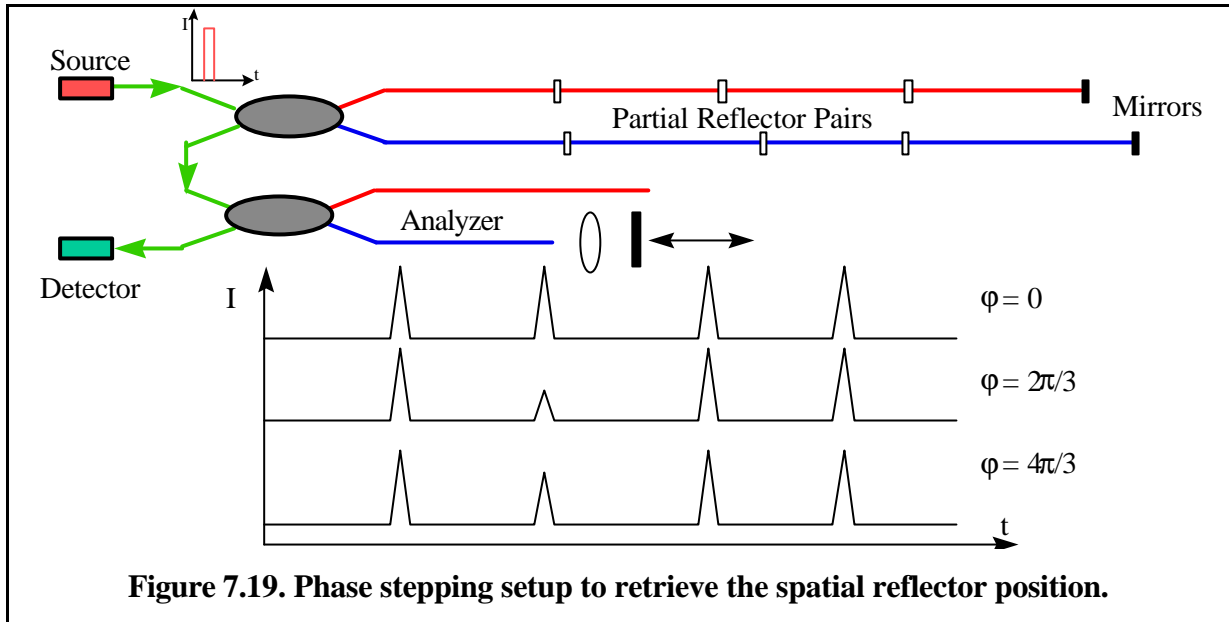
$$\Delta t = \frac{2L \lambda}{L_B c} \quad (1)$$

Were:

- L is the fiber length,
- λ is the center source wavelength,
- L_B is the fiber beat length and
- c is the vacuum speed of light.

If both fibers are subject to the same temperature variations (as in the case of a sensor using the hi-bi as a reference fiber and a standard fiber as the measurement fiber) a parasitic dependence in the temperature could result from the different thermal expansion coefficients and the different temperature dependencies of the refractive indexes between the two fibers. Furthermore the peak splitting will also be temperature dependent allowing the independent measurement of deformation and integrated temperature using only two fibers [9].

Figure 7.18 Shows the temperature dependence of the peak position (mean position of the two peaks) and peak splitting as a function of the temperature. A linear regression on the two curves gives $k_{MT} = -0.0089 \frac{ps}{^\circ C m}$ for the mean position and $k_{ST} = -0.0020 \frac{ps}{^\circ C m}$ for the peak splitting. It is therefore possible to retrieve the deformation and the temperature variations from the measurement of the peak mean position ΔM (strain and temperature dependent) and the



splitting ΔS (only temperature dependent since the hi-bi fiber is unstrained). This can be expressed in the form of the following matrix:

$$\begin{pmatrix} \Delta L \\ \Delta T \end{pmatrix} = \begin{pmatrix} k_{stress} & -k_{MT} \\ 0 & k_{ST} \end{pmatrix} \begin{pmatrix} \Delta M \\ \Delta S \end{pmatrix} \quad (2)$$

where k_{stress} is the usual stress coefficient as defined in paragraph 4.3.2. This matrix is fairly well conditioned and small errors in the measurements and in the matrix coefficients will not lead to major errors in the measurement of the length and (to a lesser extent) of the temperature.

With the current resolution of the SOFO reading unit of about 0.01 ps it is possible to retrieve the temperature variations with a resolution of 4.8°C.m. The error in the temperature compensation of the deformation measurement (due to the uncertainty in the temperature measurement) will be of 5.47μm. For comparison, the temperature dependence of the deformation measurement in a sensor with two identical fibers is of about 0.5 μm/(°C.m) (see paragraph 4.3.5). For integrated temperature variations of more than 10°C.m, using hi-bi fibers will result in a better integrated strain accuracy. Sensors of this type could be chained like usual SOFO sensors using appropriate partial reflectors. It should be noted that all fibers in the reference arm should be of hi-bi type with the fast and slow axis aligned. Otherwise, additional peaks from cross-coupled modes will appear.

7.3.3 Reflector recognition: spatial position

All solutions proposed in the previous paragraphs in order to identify the peaks require the partial reflectors to be different from one another. To keep the manufacturing of the partial reflectors simple, it would be interesting to have a series of identical reflectors and discriminate them from their spatial position. This can be done by measuring, either directly or indirectly, the time required by the light to reach the reflector and come back to the coupler. The next paragraphs will explore some possible setups to realize such a round-trip time measurement.

7.3.3.1 Intensity pulses with phase shifting

If instead of being continuous, the source is modulated in short intensity pulses, the detector will also receive a series of pulses: one for each source pulse and each reflector. If the pulses are shorter than the distance between the reflectors but longer than the path imbalance between each reflector pair, interference will be possible between pulses reflected by a pair but the pulses from different reflector pairs in the chain will not overlap. This corresponds to substituting the source and the detector with an OTDR (optical time domain reflectometer) with a broadband source and a resolution of better than the distance between the reflectors (see Figure 7.19).

If we observe the OTDR trace as a function of the path imbalance in the analyzer, it will remain identical for all mirror positions that do not correspond to a peak in the coherence diagram. However, when the mirror is positioned at a location that compensates for the path imbalance of a given reflector pair, the peak in the OTDR trace corresponding to the physical position of this reflector will show large intensity variations for small mirror displacements. This is the result of the interference made possible by the path compensation operated by the mirror. If the mirror is moved in such a way to produce evenly spaced phase steps (for example at $2\pi/3$ for the three samples phase stepping algorithm) it is possible to retrieve the fringe visibility as a function of the OTDR delay. This allows the unambiguous correlation between the reflector position and its associated peak in the coherence diagram. To achieve the desired resolution and sensitivity, long integration times are necessary. Since the process has to be repeated for each mirror position, the time required to read the whole sensor chain might become discouraging.

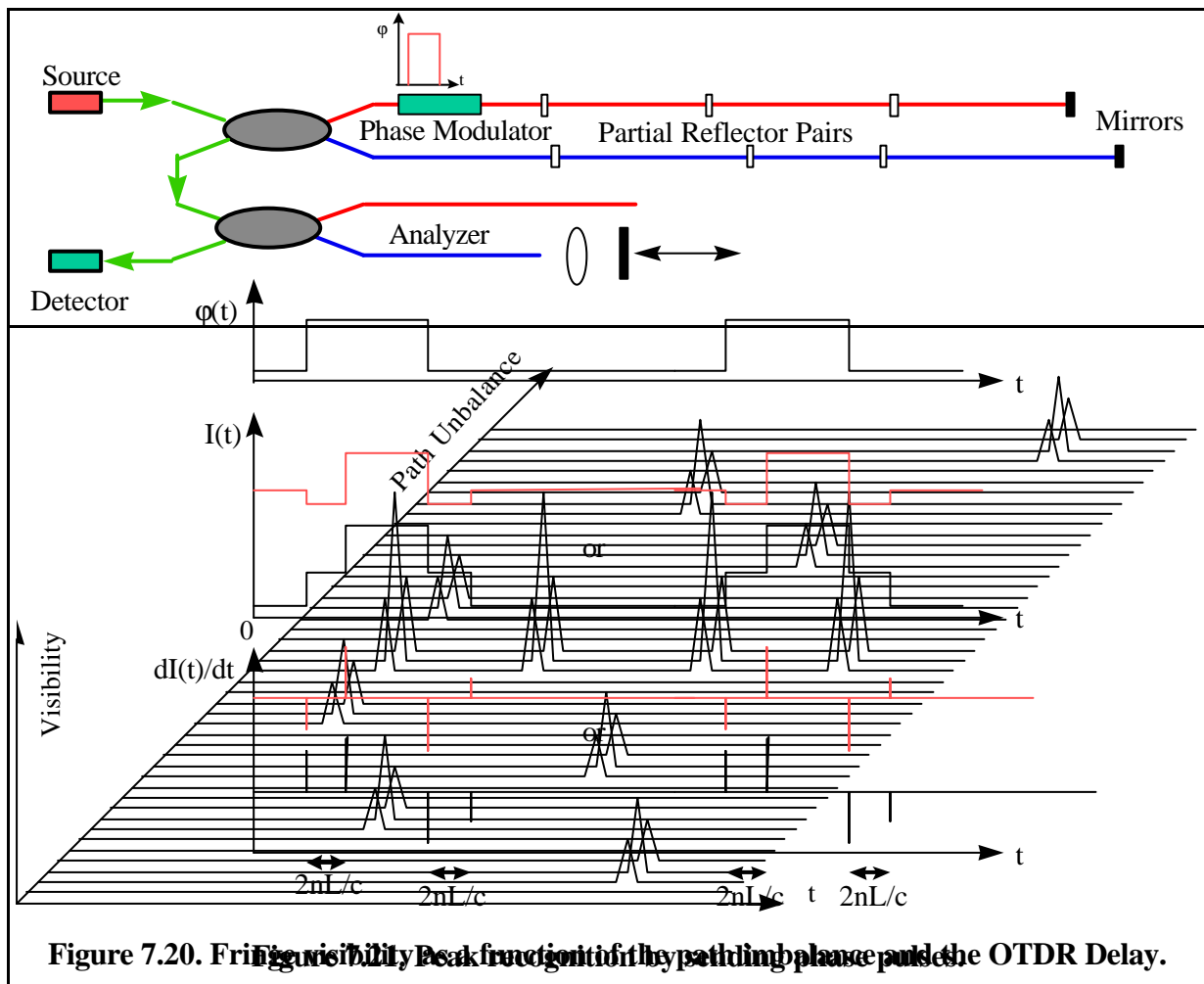
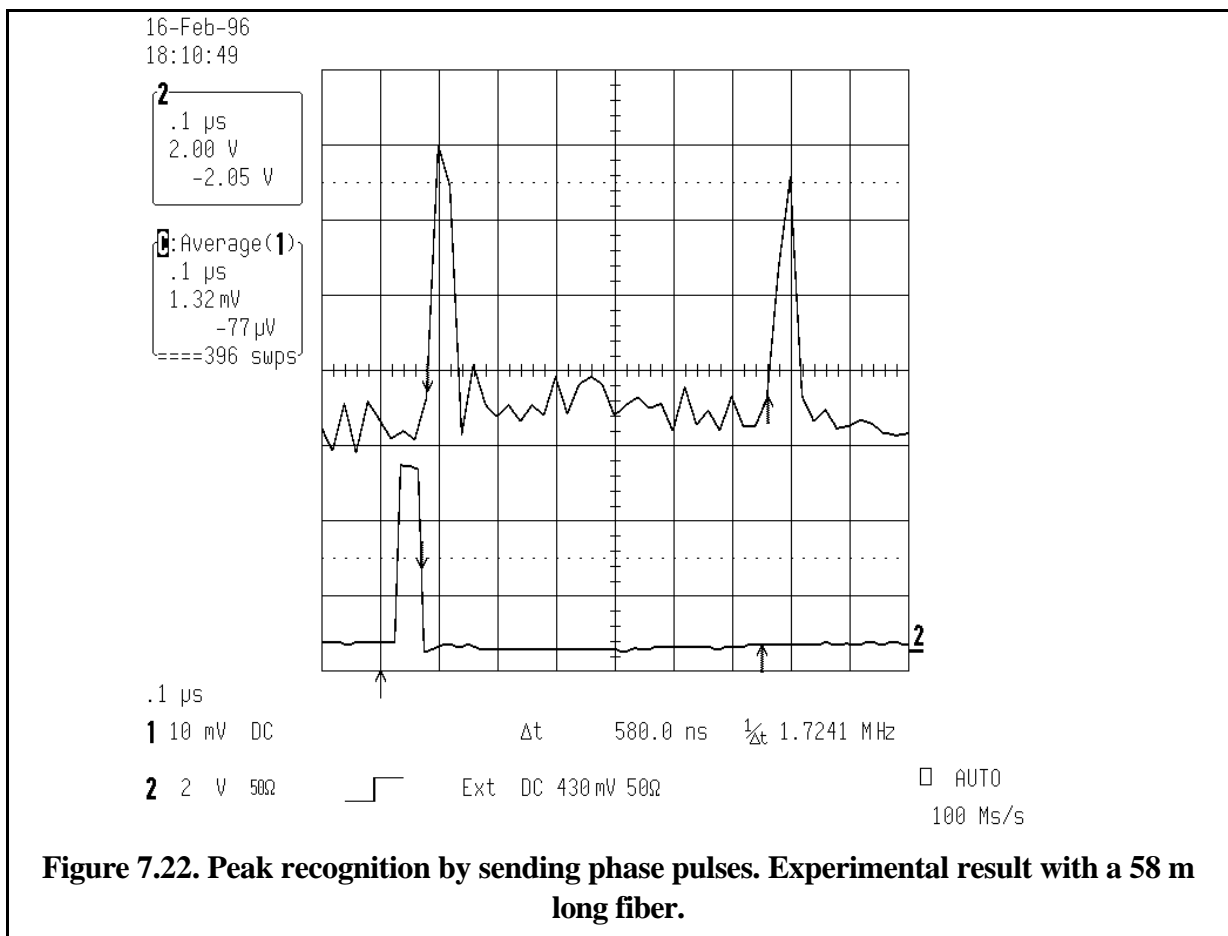


Figure 7.20. Fringe visibility peak function of the path imbalance pulse as the OTDR Delay.

7.3.3.2 Phase pulses

The main drawback in sending intensity pulses as proposed in the previous paragraph, resides in the fact that an intensity pulse is returned from each reflector and a phase stepping algorithm is required in order to establish which peak is modulating. If a phase modulator is instead added in one of the sensing arms (see Figure 7.21), it is possible to send 'phase pulses' to the sensor chain. Only when the analyzer compensates exactly the path imbalance of one of the reflector pair and interference can take place, the phase pulse will be transformed into a detectable intensity pulse returned only by the tuned reflector. If, for example, the phase is risen from 0 to π and the analyzer is tuned to a reflector positioned 1 m from the phase modulator, two successive intensity changes will be detected with an interval of 10 ns. The first variation corresponds to the introduction of a total phase of π : the light would have traveled through the modulator in its low-state on its way to the reflector and in its high-state on its way back. The second variation takes the intensity back to its original value since the light would have traveled twice through the modulator in its high-state and have accumulated a total phase of $2\pi=0$. The two intensity variations will be spaced by $2nL/c$, where n is the index of refraction, c the vacuum speed of light and L the distance between the phase modulator and the reflector.

Another possibility to implement this novel setup is by sending true phase pulses composed of closely spaced rises and falls of the phase. If this phase pulse is shorter than the distance between the phase modulator and the reflector, two intensity pulses will be observed on the photodiode. An example of this type of measurement is given in Figure 7.22. In this case the fiber length was 58 m. This setup should be able to separate successive reflectors separated



by a few meters.

7.3.3.3 Pseudo random phase steps

The results obtained with phase pulses seem promising, however this technique makes a very poor use of the already reduced available power. The information about the reflector's position is contained only in a small fraction of the total time, during the rises and falls of the phase modulator. Most of the time is spent waiting for a peak to return from the most distant reflector. It would be interesting to superpose the send and receive processes, so that the available power can be used in a more efficient way. This is possible by using, instead of the pulse modulation, a so called pseudo-random-bit-stream or PRBS [10] to modulate the phase. PRBS are composed by a stream of binary values (in our case 0's and π 's) that have a non-vanishing auto-correlation function only in zero. If this signal is applied to the phase modulator, the returned signal will present an auto-correlation function with peaks in zero and $\pm 2nL/c$. This type of signal processing can increase the duty-cycle to 100% from a mere 0.1% typically found for a pulsed modulation. The optical setup remains the same as in Figure 7.21. This technique has often been used to improve the performances of OTDR where the PRBS is used to modulate the source amplitude. To our best knowledge this technique has never been applied to phase modulation for sensing applications.

7.3.3.4 Single-pass phase modulation

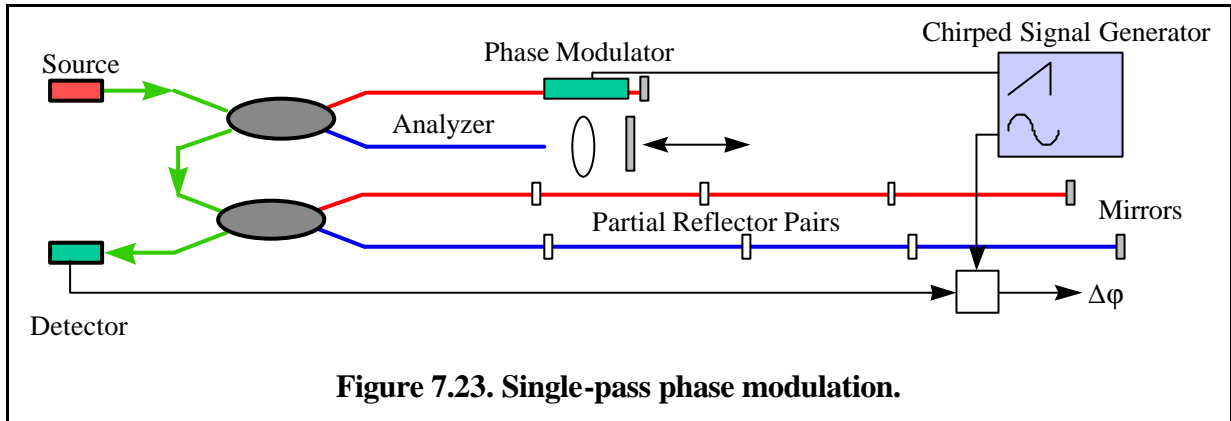


Figure 7.23. Single-pass phase modulation.

If light is first let trough the analyzer with one of its arms provided with a phase modulator driven by a saw-tooth signal and then through the sensor chain (see Figure 7.23), the detector will receive an intensity of the type:

$$I = I_0 + v \cos \mathbf{j}(t) \quad (3)$$

$$\mathbf{j}(t) = \mathbf{j}_0 + \mathbf{j}_M$$

$$\mathbf{j}_0 = 2\mathbf{p} \frac{n|2\Delta L_1 - 2\Delta L_2|}{l}$$

$$\mathbf{j}_M = 2\mathbf{p} f \left(t - \frac{2nL}{c} \right)$$

The phase difference $\Delta \mathbf{j}$ between the modulation signal and the detector signal can be measured precisely with a lock-in amplifier or a phase-meter and gives:

$$\Delta \mathbf{j} = 2\mathbf{p} \frac{n|2\Delta L_1 - 2\Delta L_2|}{l} + 2\mathbf{p} f \frac{2nL}{c} \quad (4)$$

By taking the derivative of $\Delta\mathbf{j}$ with respect to the modulation frequency f we can eliminate the influence of \mathbf{j}_0 :

$$\frac{d(\Delta\mathbf{j})}{df} = 2\mathbf{p} \frac{2nL}{c} \quad (5)$$

and therefore find:

$$L = \frac{c}{4\mathbf{p}n} \frac{d(\Delta\mathbf{j})}{df} \quad (6)$$

This gives a mean of measuring the distance L to the reflector pair that is tuned to the analyzer. The main advantage of this setup consists in the passive nature of the sensor chain, while the phase modulator is confined inside the reading unit. The main drawback consists in the fact that the phase \mathbf{j}_0 has to remain constant during the whole measurement. This might prove difficult in field applications where temperature drift changes this phase relatively fast.

7.3.3.5 Double-pass phase modulation

In the previous paragraphs we have seen that phase pulses work thanks to the fact that some photons find a different state of the phase modulator on their way to or from the reflector array. This phenomena can be used in another interesting way by using a periodic phase modulation in which the phase respects the condition:

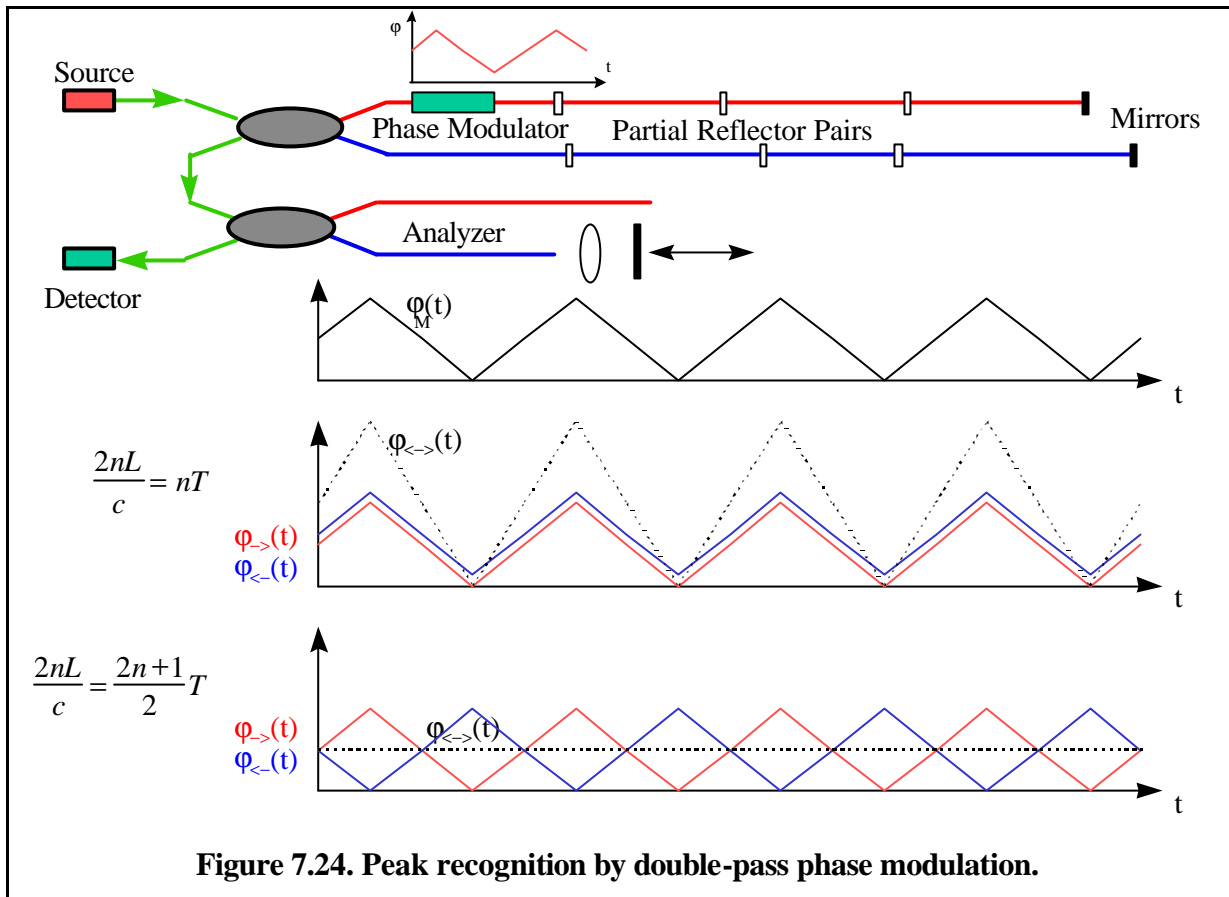
$$\mathbf{j}_M\left(t + \frac{T}{2}\right) = -\mathbf{j}_M(t) \quad (7)$$

Where T is the period of the modulation signal.

It can be seen that if the round-trip time from the modulator to the reflector is an odd multiple of the signal's half period the light will experience a zero total phase shift at any time and have therefore no modulation. If however the round-trip time corresponds to an even multiple of the signal's half period, the intensity will be modulated according to:

$$\cos(2\mathbf{j}_M(t)) \quad (8)$$

where the continuous component and the visibility of the interference pattern have been ignored.



By changing the signal frequency it will therefore be possible to find a succession of values where the intensity modulation reaches a maximum or vanishes. This novel setup is schematized in Figure 7.24. The configuration has the advantage of transforming a difficult time or phase measurement into a simpler amplitude measurement. Furthermore we will show that the residual phase \mathbf{j}_0 in the balanced interferometers has only a minor influence in the modulation amplitude.

We will now analyze in more detail two interesting cases: sinusoidal and squared phase modulation.

- **Sinusoidal modulation.**

The phase modulation is set to:

$$\mathbf{j}_M(t) = \frac{a}{2} \cos(\mathbf{w}t) \tag{9}$$

With:

$$\mathbf{w} = 2\mathbf{p}f = \frac{2\mathbf{p}}{T} \tag{10}$$

The total phase seen by a photon during one round-trip will be:

$$\begin{aligned} \mathbf{j}_{\leftarrow\rightarrow}(t) &= \frac{a}{2} \cos(\mathbf{w}t) + \frac{a}{2} \cos(\mathbf{w}(t - \Delta)) = & (11) \\ &= a \cos \frac{\mathbf{w}(2t - \Delta)}{2} \cos \frac{\mathbf{w}\Delta}{2} = \\ &= a \cos \frac{\mathbf{w}\Delta}{2} \sin \frac{\mathbf{w}t'}{2} \end{aligned}$$

Where:

$$t' = t - \frac{\Delta}{2} - \frac{\mathbf{p}}{2\mathbf{w}} \quad (12)$$

and:

$$\Delta = \frac{2nL}{c} \quad (13)$$

and L is the distance between the phase modulator and the partial reflector pair to which the analyzer is tuned.

The modulated component of the detector's signal will be given by:

$$F = \cos(\mathbf{j}_0 + \mathbf{j}_{<->}(t)) \quad (14)$$

Where \mathbf{j}_0 is the phase in the un-perturbed tandem interferometer. To quantify the modulation we calculate its RMS value:

$$A = \sqrt{\langle (F - \langle F \rangle)^2 \rangle} = \sqrt{\langle F^2 \rangle - \langle F \rangle^2} = \sqrt{f \int_0^{1/f} F^2 dt - \left(f \int_0^{1/f} F dt \right)^2} \quad (15)$$

Furthermore:

$$\langle F \rangle = f \int_0^{1/f} \cos(\mathbf{j}_0 + z \sin \mathbf{w}t) dt \quad (16)$$

where:

$$z = a \cos \frac{\mathbf{w}\Delta}{2} \quad (17)$$

Separating the cosine of the sum into a sum of products gives:

$$\langle F \rangle = f \int_0^{1/f} \cos \mathbf{j}_0 \cos(z \sin \mathbf{w}t) dt - f \int_0^{1/f} \sin \mathbf{j}_0 \sin(z \sin \mathbf{w}t) dt \quad (18)$$

The second integral vanishes because its argument is an odd function of the integrand and we integrate over one period.

So finally we obtain:

$$\langle F \rangle = \frac{1}{2\mathbf{p}} \int_{-p}^{+p} \cos \mathbf{j}_0 \cos(z \sin \mathbf{q}) d\mathbf{q} = \cos \mathbf{j}_0 J_0(z) \quad (19)$$

Where $J_0(z)$ is the Bessel function of zero order of z .

Similarly:

$$\langle F^2 \rangle = f \int_0^{1/f} \cos^2(\mathbf{j}_0 + z \sin \mathbf{w}t) dt \quad (20)$$

and:

$$\begin{aligned} \langle F^2 \rangle &= \frac{1}{2} + \frac{f}{2} \int_0^{1/f} \cos(2\mathbf{j}_0 + 2z \sin \mathbf{w}t) dt = \\ &= \frac{1}{2} + \frac{f}{2} \int_0^{1/f} \cos 2\mathbf{j}_0 \cos(2z \sin \mathbf{w}t) dt + 0 = \\ &= \frac{1}{2} + \frac{\cos 2\mathbf{j}_0}{2} J_0(2z) \end{aligned} \quad (21)$$

And finally:

$$A(z, \mathbf{j}_0) = \sqrt{\frac{1}{2} + \frac{\cos(2\mathbf{j}_0)}{2} J_0(2Z) - \left(\cos(\mathbf{j}_0) J_0(z) \right)^2} \quad (22)$$

It has to be reminded that z is a function of a and \mathbf{D} (see equation (17)).

Since the interesting parameter to be studied is the quotient between the round-trip time and the phase periodicity we define:

$$x = \frac{2fnL}{c} = \frac{\Delta}{T} \tag{23}$$

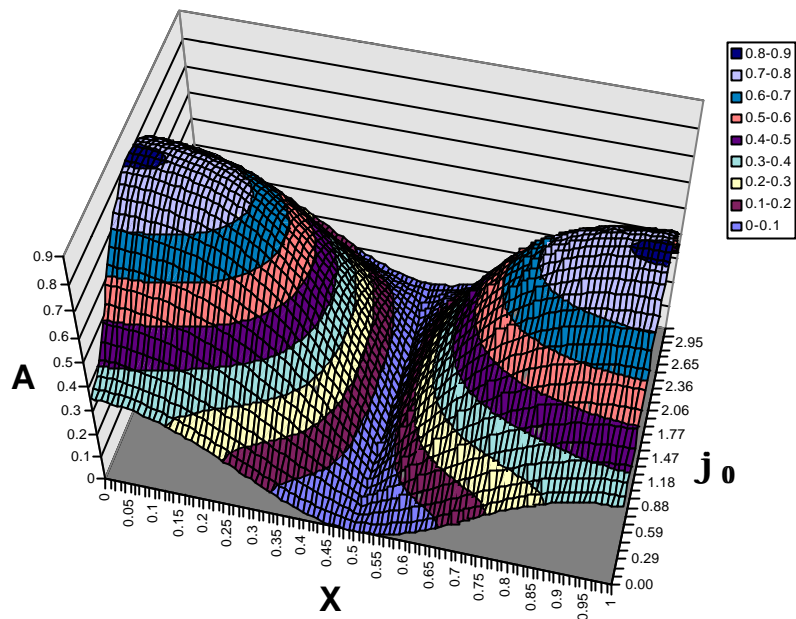


Figure 7.25. Modulation as a function of x and the initial phase j_0 . Sinusoidal modulation, $a = P/2$.

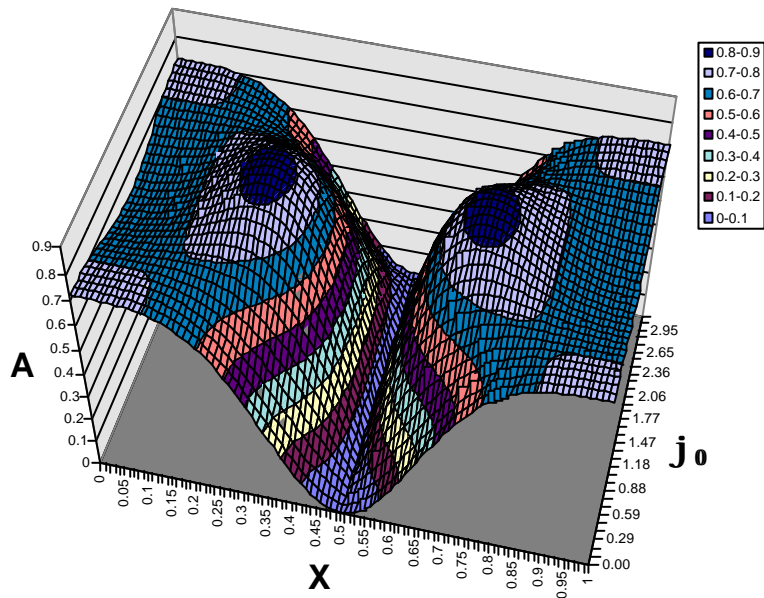


Figure 7.26. Modulation as a function of x and the initial phase j_0 . Sinusoidal modulation, $a = P$.

We first consider A as a function of x and j_0 . Figure 7.25 shows the result for $a = P/2$. Figure 7.26 shows the same for $a = P$.

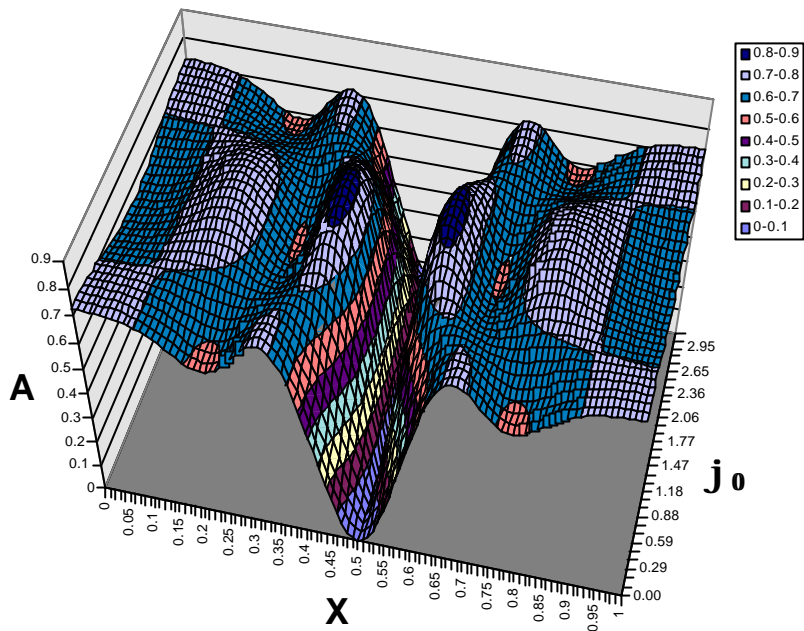


Figure 7.27. Modulation as a function of x and the initial phase j_0 . Sinusoidal modulation, $a = 2p$.

Figure 7.25 shows the same for $a = 2p$.

In all cases the modulation A vanishes, as expected, for a round-trip time corresponding to one half period of the phase modulation function (i.e. for $x=0.5$). The modulation A is obviously periodic in x and j_0 , so only the first period is shown.

Since the initial phase \mathbf{j}_0 is not known and fluctuates with time, it is interesting to integrate over all values of \mathbf{j}_0 . This can not be done analytically, but Figure 7.28 shows the numerical result of this integration. It is evident that the notch at $x=0.5$ becomes increasingly narrow with increasing phase modulation amplitude.

An experimental realization of this novel technique was realized with a United Technologies phase modulator, a 50MHz HP signal generator, a 100 MHz New Focus photodiode and using an electrical spectrum analyzer and a digital storage oscilloscope to analyze the photodiode signal at the modulation frequency.

First, a 60 m long fiber with total mirrors was tested. Figure 7.29 shows the measured modulation (in logarithmic scale) as a function of the modulator's frequency. A modulation amplitude of $a = \mathbf{p}/2$ was used. The signal at each frequency was integrated over a few seconds and \mathbf{j}_0 was intentionally perturbed (by touching the sensor fibers) to obtain a fair integration over all its possible values. As expected, minima are found at 0.83 MHz and all odd multiples of this frequency.

In general the minima will appear at:

$$F_M = \frac{c}{4nL} N \quad N \in \{1,3,5,7,\dots\} \quad (24)$$

At frequencies above 15 MHz the signal decreases because of bandwidth limitations in the electronics used to drive the experiment.

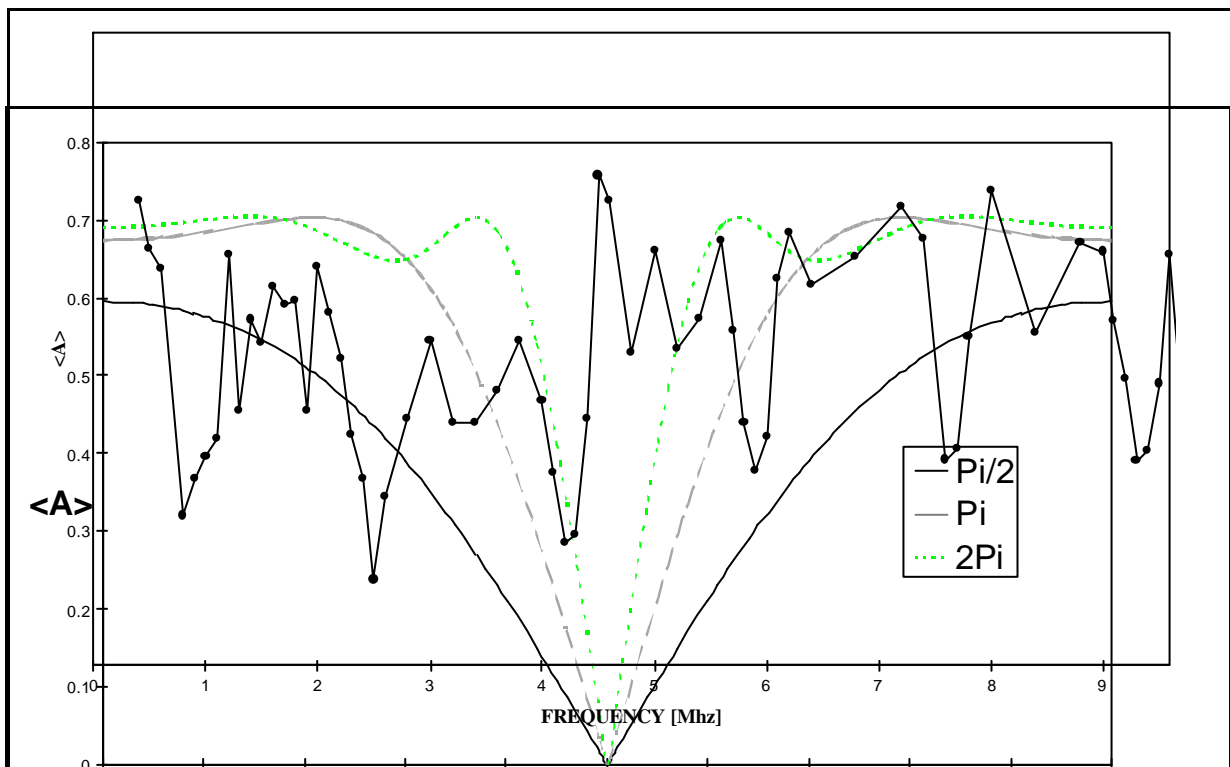
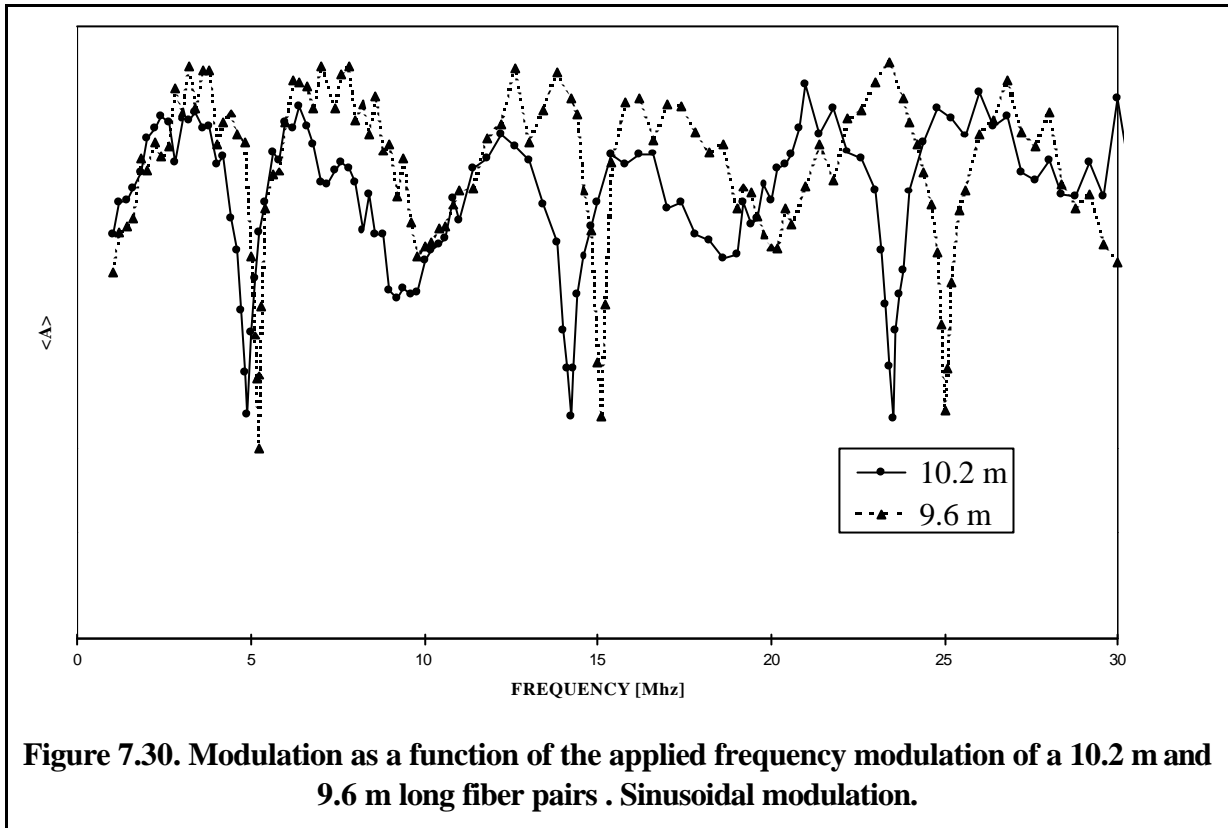


Figure 7.29. Modulation as a function of the applied frequency modulation of a 60 m long fiber pair. Sinusoidal modulation.

Figure 7.28. Modulation as a function of x , after numerical integration over the initial phase \mathbf{j}_0 . Sinusoidal modulation, $a = \mathbf{p}/2, \mathbf{p}, 2\mathbf{p}$.

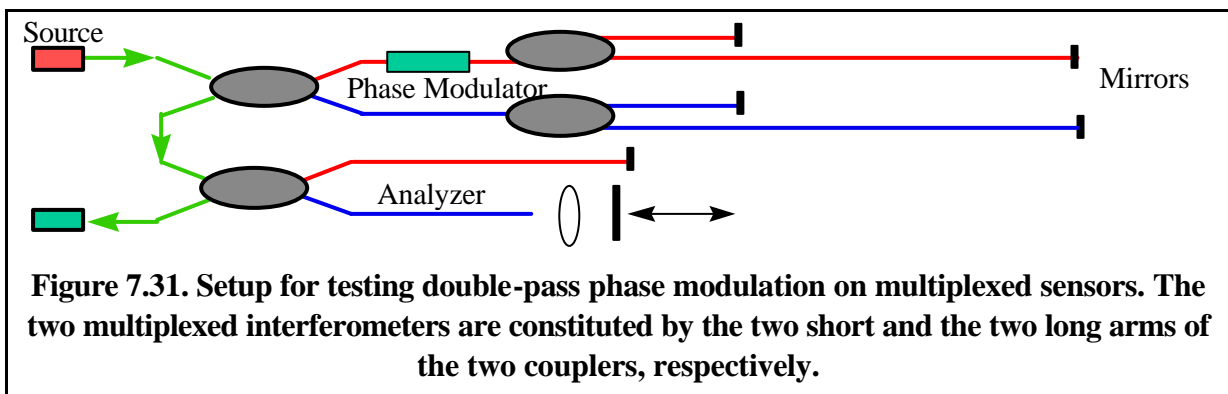


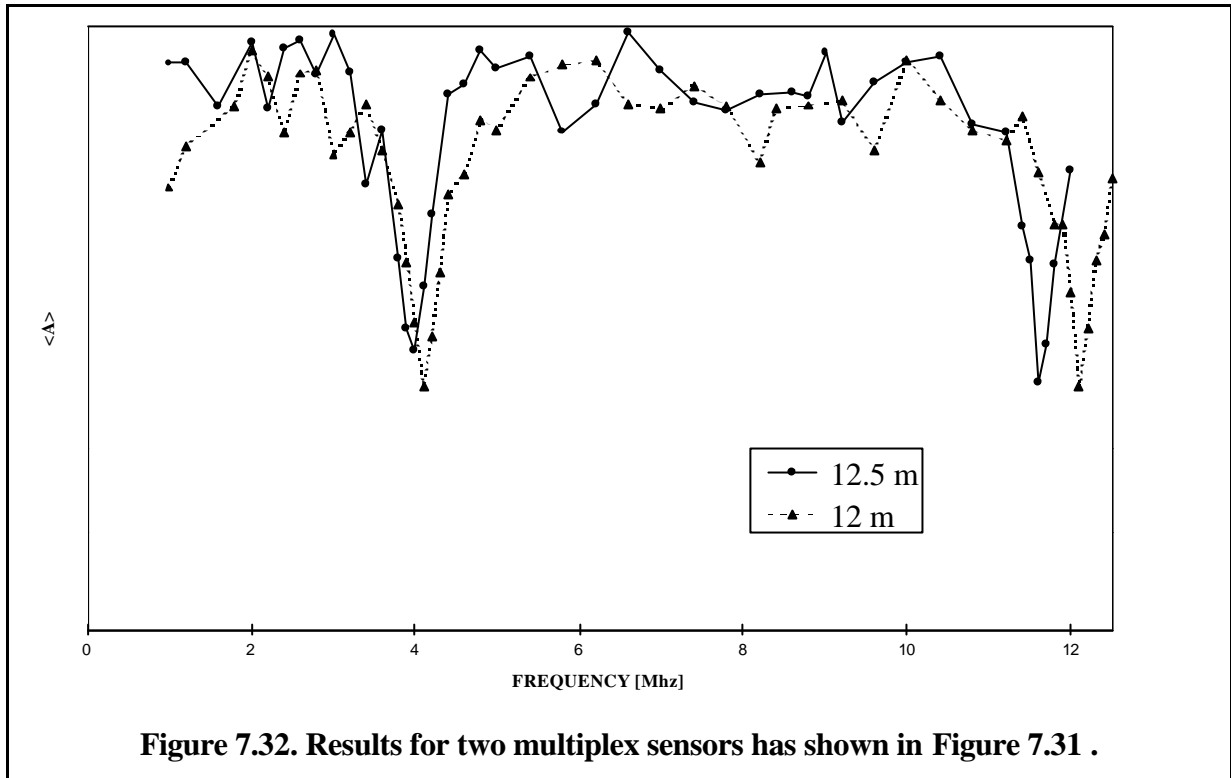
In another experiment 60 cm were cut from both the reference and the measurement fibers that were initially 10.2 m long. In Figure 7.30, a clear shift towards higher frequencies is clearly visible. It was possible to detect cuts down to a few centimeters. In general and with the simple experimental setup used, we can conclude that the length precision of this method is of about 2-4% of the fiber length for fibers longer than 5m. For shorter fibers, the current bandwidth limitation makes it impossible to observe even the first minima.

- **Multiplexing.**

To test the feasibility of this method to implement in-line multiplexing an experiment with two sensors was conducted. On both the reference and the measurement arm, a coupler was installed with a short and long arm terminated by a mirror. This corresponds to two in-line reflectors with about 25% reflectivity. Since the path imbalance between the two long and the two short fibers is not the same it was possible to tune the analyzer on each of the two side-peaks in the coherence diagram and measure the associated fiber length.

Figure 7.32 shows the result for a length difference of 0.5 m between the two fiber pairs. It





has to be noted that contrary to the results shown in Figure 7.30, in this case the two curves are obtained on the same sensor chain by simply moving the analyzer's mirror to compensate the path imbalance of one or the other reflector pair. However, an extension of this method to in-line coherence multiplexing requires a five to tenfold increase in the source power.

- **Rectangular modulation.**

We consider now a rectangular modulation of the type²:

$$\mathbf{j}_M(t) = \begin{cases} 0 & \text{if } T \in [0, T/2[\\ a & \text{if } T \in [T/2, T[\end{cases} \quad (25)$$

During one period of the phase modulation the photons will experience a phase modulation of either 0, a or 2a depending on the time and on the relation between the round-trip time and the modulation period. We indicate these states as 1, 2 and 3. The normalized probability P_i of phase being in the state i is given by:

$$P_i = \begin{cases} 1/2 - x & \text{if } i = 0 \\ 2x & \text{if } i = 1 \\ 1/2 - x & \text{if } i = 2 \end{cases} \quad (26)$$

The intensity found on the photodiode (again excluding the continuous component) will be:

$$F_i = \begin{cases} \cos(\mathbf{j}_0) & \text{if } i = 0 \\ \cos(\mathbf{j}_0 + a) & \text{if } i = 1 \\ \cos(\mathbf{j}_0 + 2a) & \text{if } i = 2 \end{cases} \quad (27)$$

Furthermore:

² This does not strictly satisfy equation (7) but is equivalent to a modulation of $\pm a/2$ and an increase of \mathbf{j}_0 by $a/2$

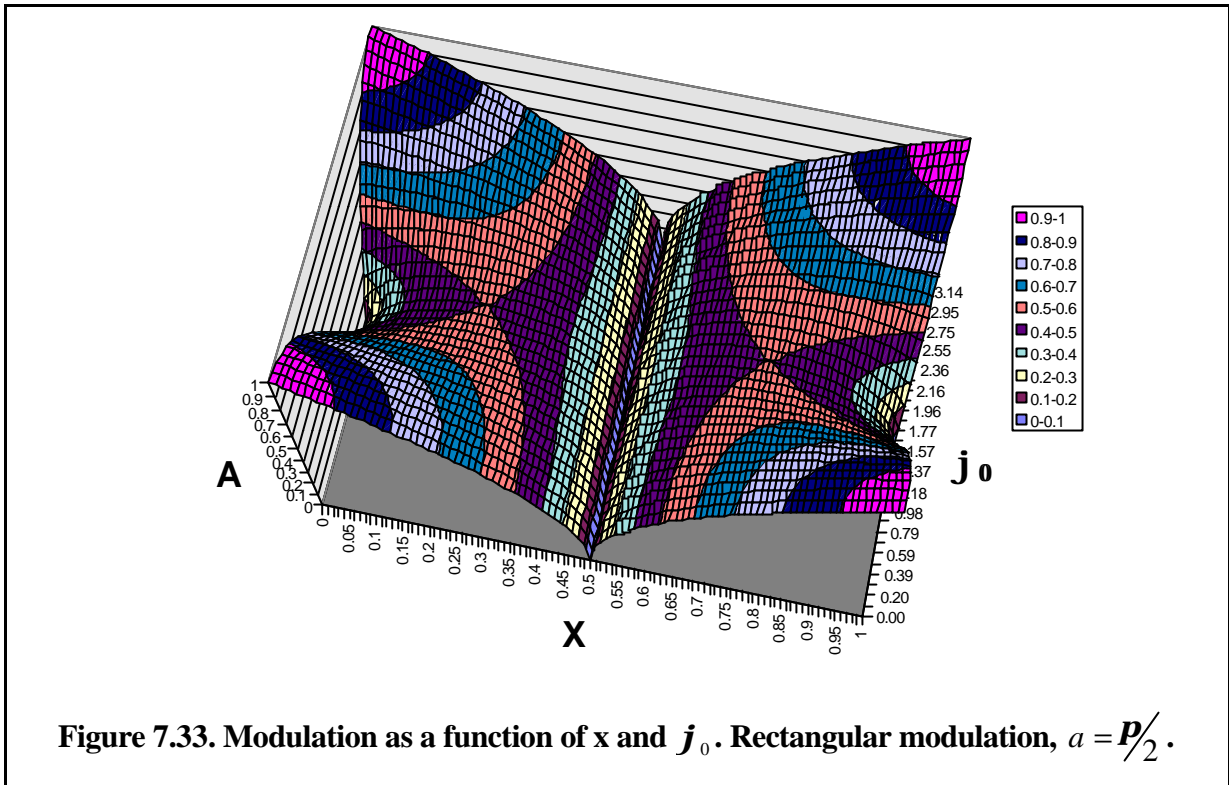


Figure 7.33. Modulation as a function of x and j_0 . Rectangular modulation, $a = \mathbf{p}/2$.

$$\langle F \rangle = \sum_i P_i F_i \quad (28)$$

$$\langle F^2 \rangle = \sum_i P_i F_i^2$$

Which gives:

$$\langle F \rangle = (1/2 - x) (\cos j_0 + \cos(j_0 + 2a)) + 2x \cos(j_0 + a) \quad (29)$$

$$\langle F^2 \rangle = (1/2 - x) (\cos^2 j_0 + \cos^2(j_0 + 2a)) + 2x \cos^2(j_0 + a)$$

As usual the modulation is given by:

$$A = \sqrt{\langle (F - \langle F \rangle)^2 \rangle} = \sqrt{\langle F^2 \rangle - \langle F \rangle^2} \quad (30)$$

We spare the reader³ the tedious general algebraic calculation of the modulation A. For the simplest case $a = \mathbf{p}$ we obtain:

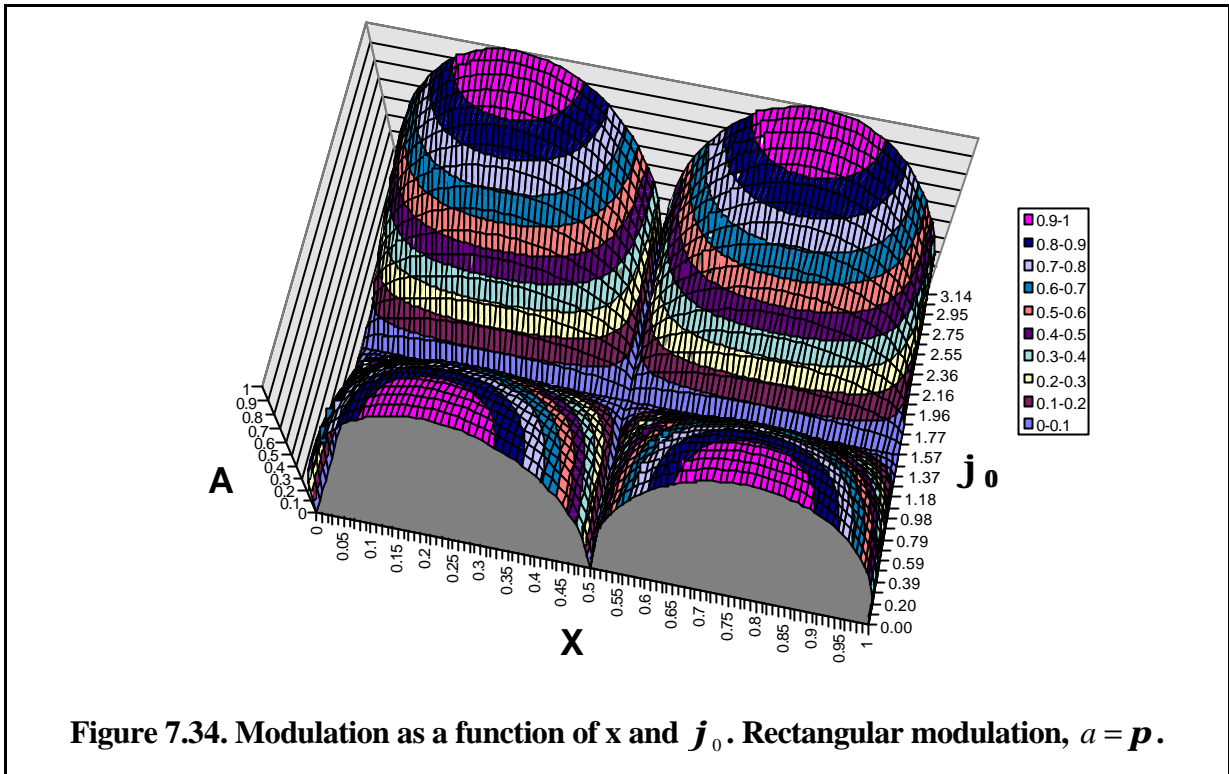
$$A = \sqrt{(8x - 16x^2) \cos^2(j_0)} \quad (31)$$

We first consider A as a function of x and j_0 . Figure 7.33 shows the result for $a = \mathbf{p}/2$.

Error! Reference source not found. shows the same for $a = \mathbf{p}$. The case $a = 2\mathbf{p}$ has no interest since no modulation would result. Higher amplitudes can be mapped to the $[0, 2\pi]$ interval.

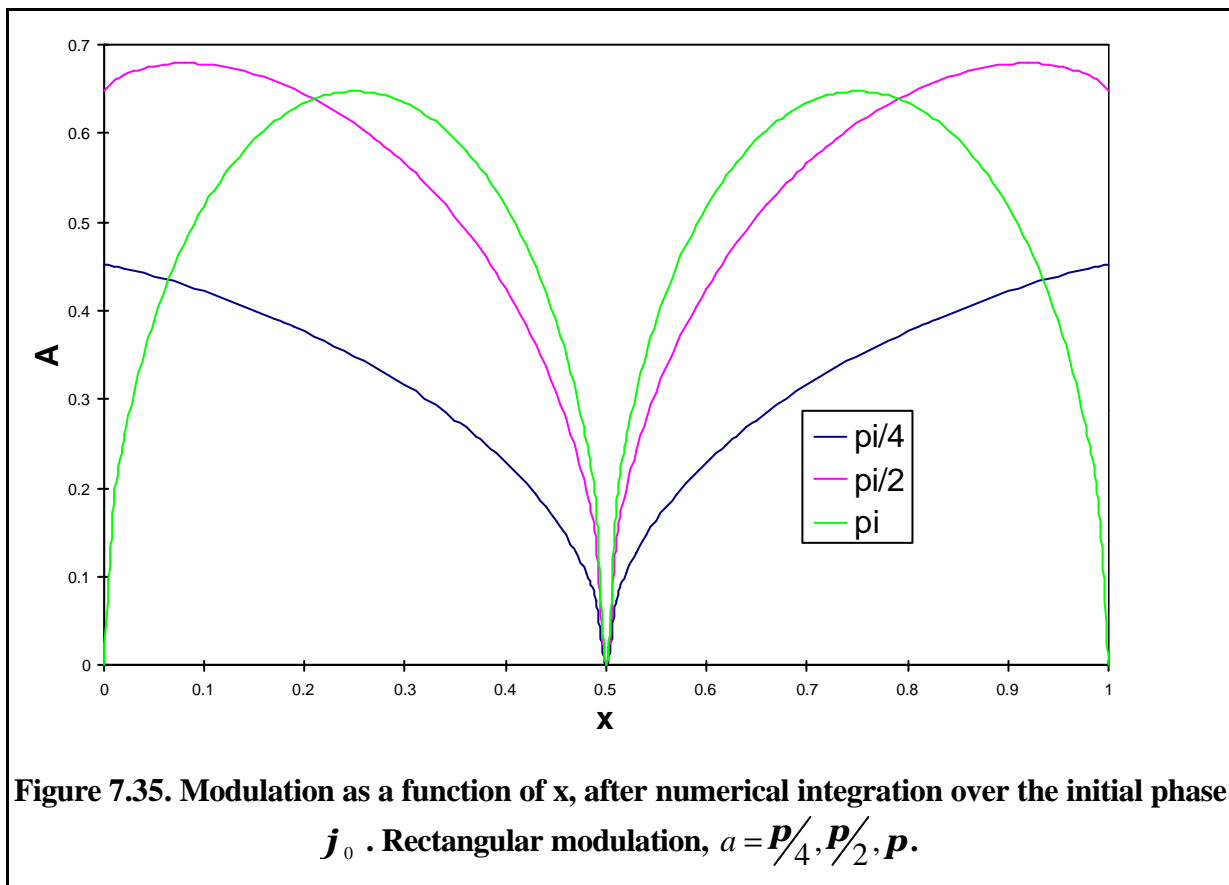
In all the cases, the modulation A vanishes as expected for a round-trip time corresponding to half period of the phase modulation function (i.e. for $x=0.5$) just as in the case of sinusoidal modulation. Interestingly, for a modulation amplitude of $a = \mathbf{p}$ other minima are found at the

³ And the writer...

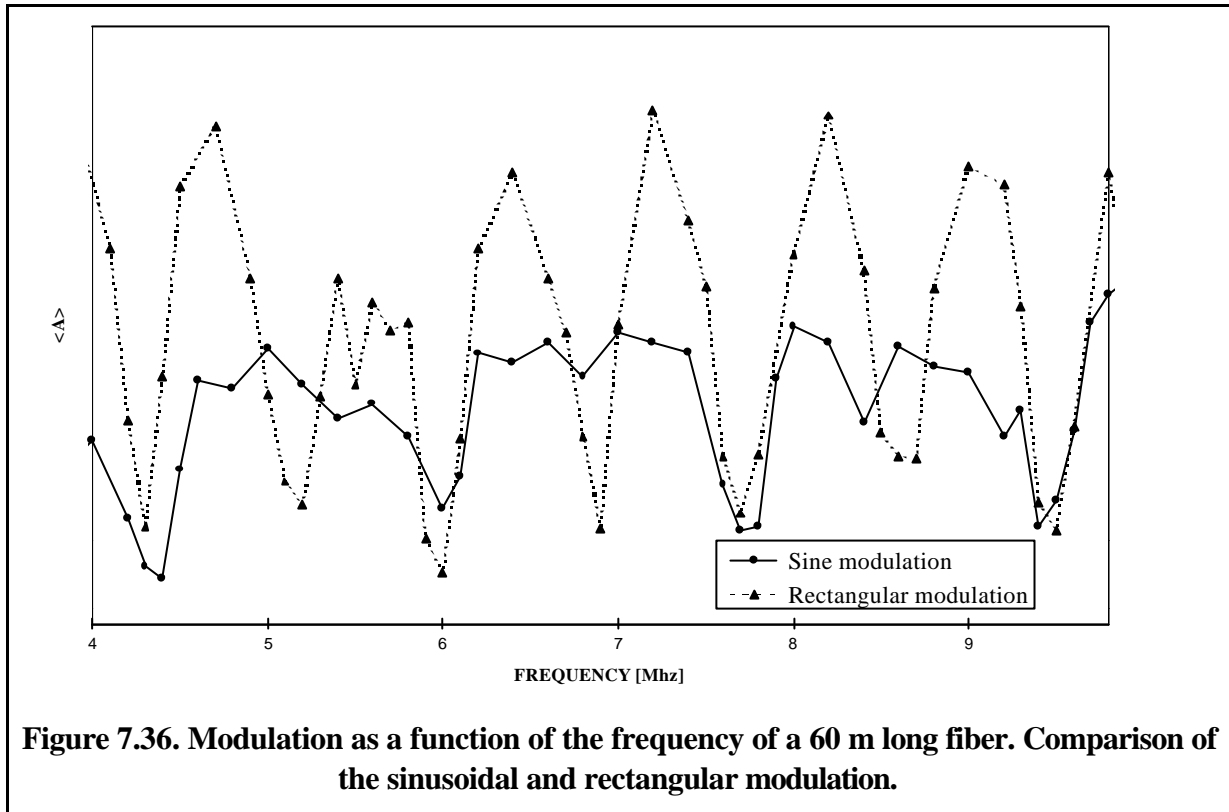


even multiples of the signal period. At these points the light undergoes a phase modulation of two times the amplitude of the modulation signal.

However two times p equals zero in terms of phase modulation. An undesired feature obtained for $a = p$ is the vanishing of the signal modulation for $j_0 = p/2$.



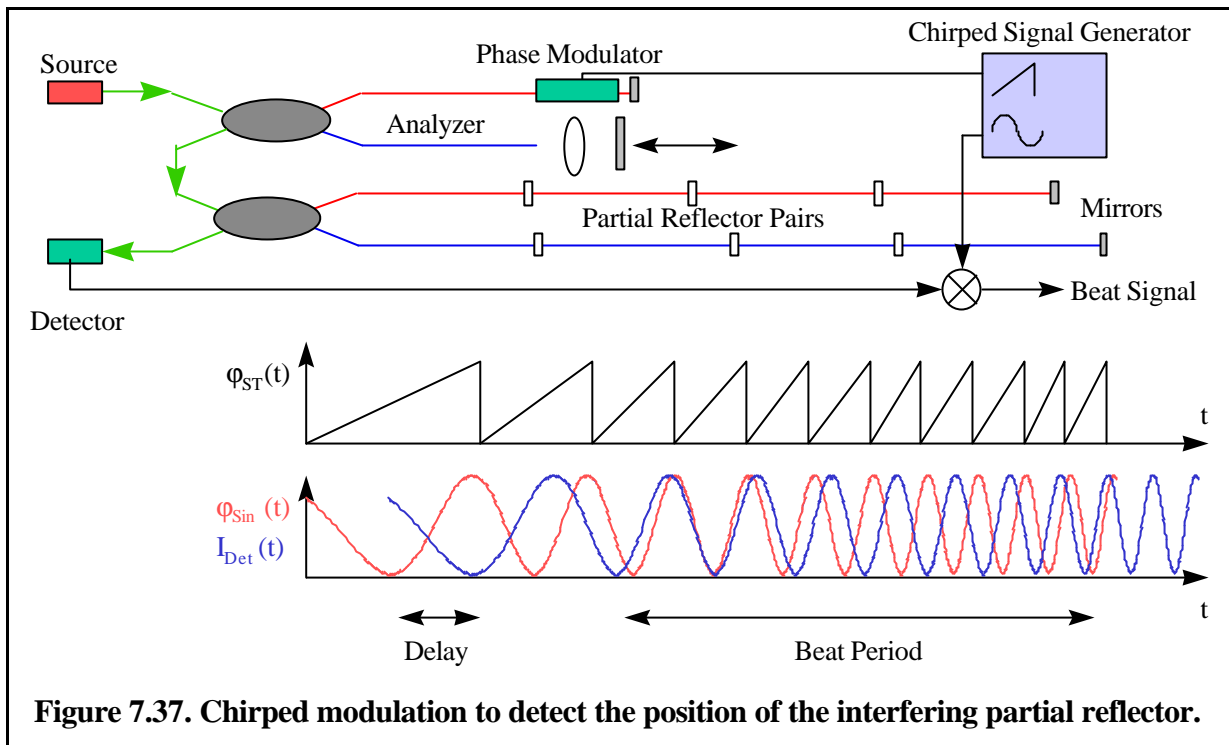
Once again, it is interesting to integrate over all values of \mathbf{j}_0 . This is shown in Figure 7.35. It is evident that the notch at $x=0.5$ becomes increasingly narrow with increasing phase modulation



amplitude. This figure shows again the period doubling for $a = \mathbf{p}$.

With the same experimental setup as in the case of the sinusoidal modulation, we tested the rectangular signals. Figure 7.36 compares the results obtained with the sinusoidal and the rectangular modulation for the same 60 m long fiber and confirm the expected period doubling

7.3.3.6 Chirped phase modulation



One last method is available to measure the time of flight of the light through the interferometer. If the phase is modulated in a single pass, for example the reference arm of the analyzer, see (Figure 7.37) with a chirped saw-tooth signal of 2π amplitude, the signal on the photo-detector will have a chirped sinusoidal modulation. The two chirps will however have a delay proportional to the round-trip time to the partial reflector pair to which the analyzer is tuned. If the signal generator that produces the saw-tooth signal can also produce a sinusoidal signal with the same instantaneous frequency and phase, it is possible to let this signal and the detected one beat by multiplying the two.

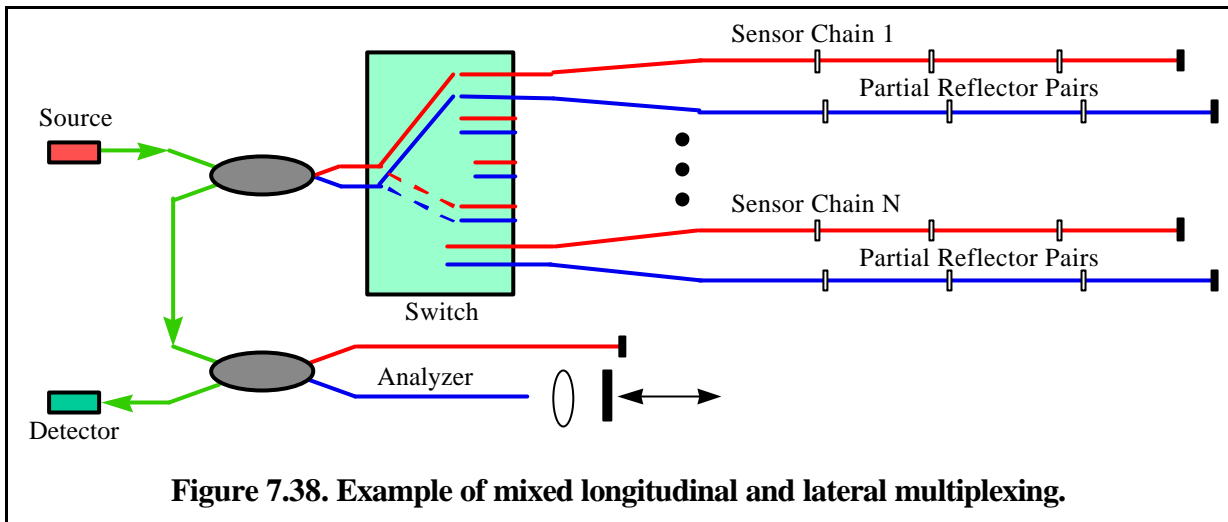
The beat frequency is given by:

$$f_{Beat} = \frac{2nL}{c} \frac{df_{Mod}}{dt} \quad (32)$$

The beat frequency is therefore proportional to the distance L between the modulator and the reflectors and to the chirp rate. The main advantage of this setup consists in the passive nature of the sensor chain.

7.4 Mixed multiplexing

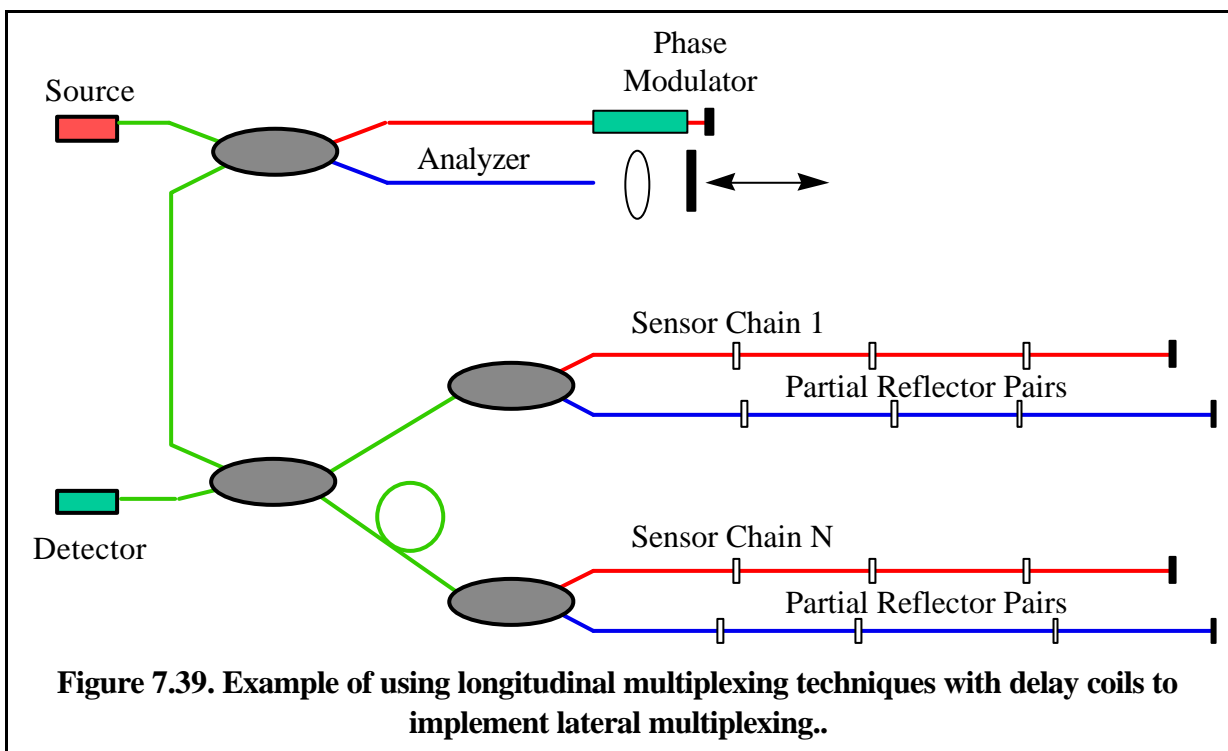
To increase even further the number of sensors that can be multiplexed or to allow a better flexibility in the sensor's layout, it is possible to combine lateral and longitudinal multiplexing into mixed setups.



The most obvious way to combine the two architectures is by laterally multiplexing longitudinally multiplexed sensor chains. Figure 7.38 shows a combination of optical switching with longitudinal coherence multiplexing. Other possible combinations include lateral wavelength division multiplexing with longitudinal coherence multiplexing or lateral multi-channel delay lines with longitudinally multiplexed broadband fiber Bragg gratings. Longitudinal multiplexing techniques can also be used to implement lateral multiplexing architectures. By adding appropriate delay coils it is possible to let parallel sensors appear to the reading unit as if arranged in a single chain. An example of such a setup using, for example, chirped modulation is shown in Figure 7.39. Many other combinations are possible and could present an interest for a particular application.

7.5 Partial reflector manufacturing

Many of the techniques presented in the previous paragraphs require the installation of partial



reflectors on both the reference and the measurement fibers. In the next paragraphs we will explore some alternatives to manufacture these reflectors and calculate the optimum reflectivity for a chain with a given length.

7.5.1 Reflector's optimization

The light intensity injected by the source in the fiber line should be distributed homogeneously among the different sensors. Since the available power will decrease towards the end of the chain it is interesting to adapt the reflection and transmission properties of the sensors to their position in the chain. On the other hand, the use of different reflectors increases the complexity and reduces the flexibility of the system. Reflectors with constant characteristics are therefore much more interesting. These sensors can also be addressed from both sides of the chain introducing an interesting redundancy factor in the case of failures.

7.5.1.1 Identical reflectors

If all reflectors have the same power reflection R and transmission T coefficients (with $R+T \leq 1$) the intensity returned by the i^{th} reflector will be given by:

$$I_i = T^{(i-1)}R \quad (33)$$

The intensity will therefore decrease with increasing i . If the T is sufficiently high (which means a low R) the difference between these intensities can however be reduced and kept inside the dynamic range of the reading unit. It is easy to see that even if the measurements are performed in reflection, it is the transmission coefficient that mostly influences the final signals. The losses, given by $1-R-T$ have obviously to be reduced to a minimum. Figure 7.40 compares the returned intensity as a function of the reflector's order for different reflection coefficients. The chains with high reflectivity show much larger differences between the power returned by the different reflectors in the chain. A reflectivity of about 4% seems a good

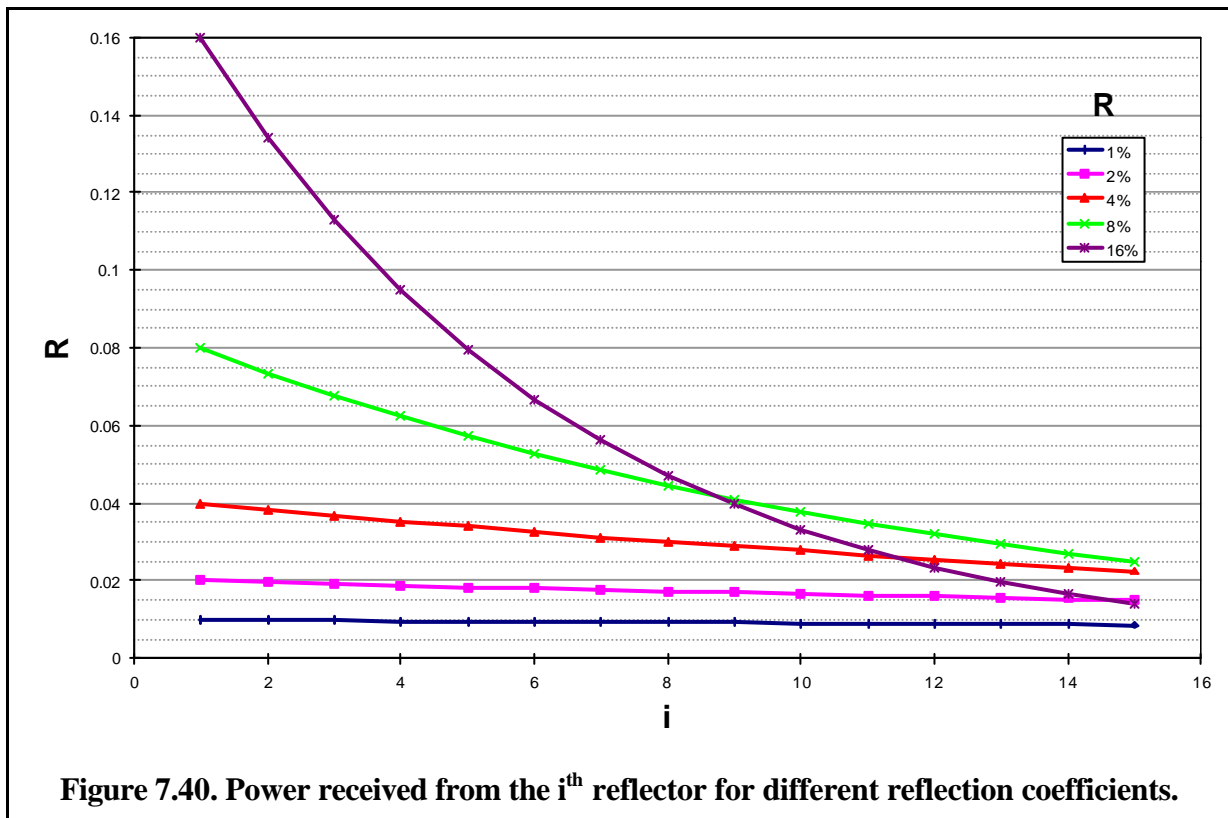


Figure 7.40. Power received from the i^{th} reflector for different reflection coefficients.

compromise between the returned power and the homogeneity of the signals for chains of about ten reflectors. Losses up to 5% do not alter this picture significantly.

7.5.1.2 Non-identical reflectors

If we have the possibility to control the reflection and transmission coefficient of each reflector, it becomes possible to obtain the same intensity from each reflector pair. For a system with N reflectors with constant losses L, the transmission coefficient T_i will be given by:

$$T_N = 0 \quad (34)$$

$$R_N = 1$$

$$T_i = \frac{-1 + \sqrt{1 + 4R_{i+1}(1-L)}}{2R_{i+1}}$$

$$R_i = 1 - T_i$$

If the losses are instead proportional to the reflection coefficient:

$$L_i = k R_i \quad (35)$$

The ideal transmission and reflection coefficients become:

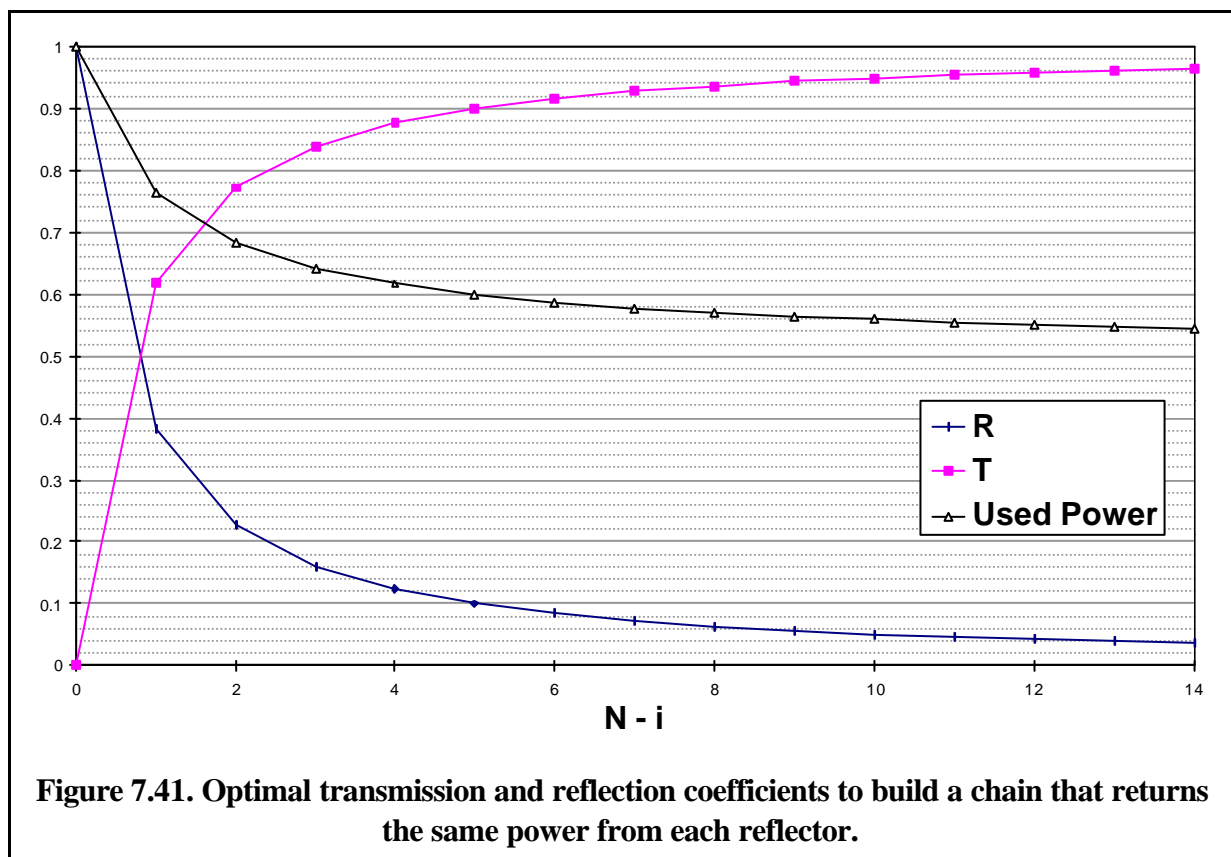
$$T_N = 0 \quad (36)$$

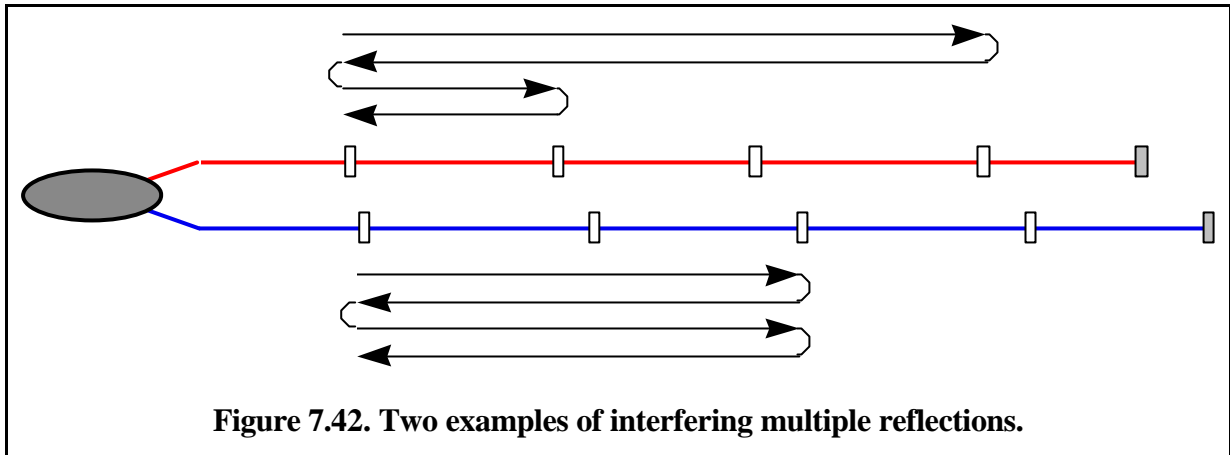
$$R_N = 1$$

$$T_i = \frac{-1 + \sqrt{1 + 4R_{i+1}(1+k)}}{2R_{i+1}(1+k)}$$

$$R_i = 1 - T_i$$

This shows that the reflection coefficients have to be tailored to the position of the reflectors in the chain. In this case the reading unit does not need to have an extended dynamic range since





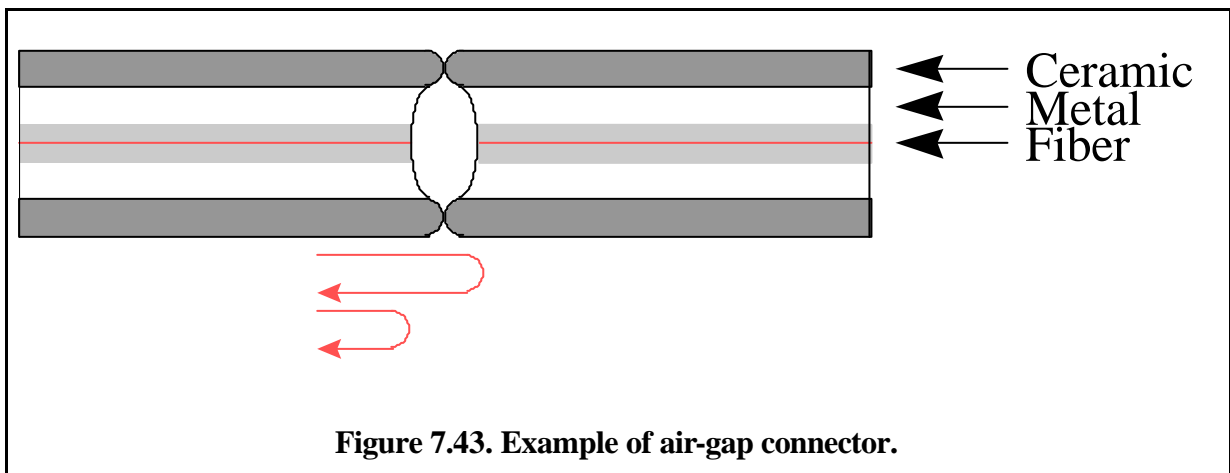
the signals from the different sensors will have a comparable intensity. The signal returned by each sensor will however decrease with increasing N , so an high detection sensitivity is still interesting. Figure 7.41 shows the optimal transmission and reflection coefficients for a chain terminated by a perfect reflector and no losses. The used power corresponds to the total power returned by the reflectors with a single reflection. For a large number of reflectors, about half of the power is returned after multiple reflections.

7.5.1.3 Multiple reflections

Besides the interesting reflections produced by each partial reflector, other parasite signals will reach the reading unit. These are produced by the multiple reflections between the different reflectors. For example, a photon could be reflected by the 4th reflector then by the 1st and finally by the 2nd. It is wished that the intensity of these parasite reflections is far lower than the one of the useful reflections.

In the case of identical reflectors, the intensity of the first-order multiply reflected signals will contain a term in R^3 . Since we have seen that R will be in general quite low (typically a few percent) this term will be negligible. If the reflectors are non identical this term can however become important, since for the last reflectors in the chain R will approach 1. A possible solution would be given by the overall reduction of the R 's by a factor K . This will reduce the interesting intensities by a factor K and the first-order parasite reflections by a factor K^3 .

7.5.2 Air-gap connectors



By using connectors with an air gap of a few microns between the two fiber surfaces it is possible to obtain a reflection of a few percents. The exact amount of this reflection can not be controlled and can change with time. This type of reflector has a certain wavelength selectivity, because of the interference between the reflection from the two glass-air interfaces. However because the source is broadband, this effects partially cancel and the range of reflectivity that can be obtained is narrower than for a coherent source. Furthermore, because the two reflection have a path difference far smaller than the coherence length of the source (typically 30 microns) the reflector can be seen as localized in a single point. Typical reflection are of about 5% and the transmission of 85%. The losses are therefore relatively low. The main advantage of this type of reflectors resides in the flexibility it offers. It is possible to add each displacement sensor one at a time and observe the appearance of the new coherence peak. It also allows a modular design of the sensor. It is possible to add new sections at successive times. This is especially useful in the case of structures that are constructed in phases, typically concrete structures like long span bridges.

In all experiments we used air-gap connectors manufactured by DIAMOND SA. We have found an average reflectivity of 5% and a power transmission coefficient of 85% at 1300 nm. Table 7.1 summarizes the received power from a number of reflectors between 1 and 10 as

Number of reflectors	Reflectivity	Reflectivity [%]	Required sensitivity [dB]
1	R	0.0500	-13.0
2	T ² R	0.0361	-14.4
3	T ⁴ R	0.0261	-15.8
4	T ⁶ R	0.0189	-17.2
5	T ⁸ R	0.0136	-18.7
6	T ¹⁰ R	0.0098	-20.1
7	T ¹² R	0.0071	-21.5
8	T ¹⁴ R	0.0051	-22.9
9	T ¹⁶ R	0.0037	-24.3
10	T ¹⁸ R	0.0027	-25.7

Table 7.1. Reflectivity as a function of the reflector order for DIAMOND air-gap connectors.

well as the necessary reading unit sensitivity. With a sensitivity of -20 dB typical of a standard SOFO reading unit, it should be possible to read 6 reflectors. If the sensitivity is pushed down to -25 dB, 10 reflectors should be visible.

7.5.3 Etalons

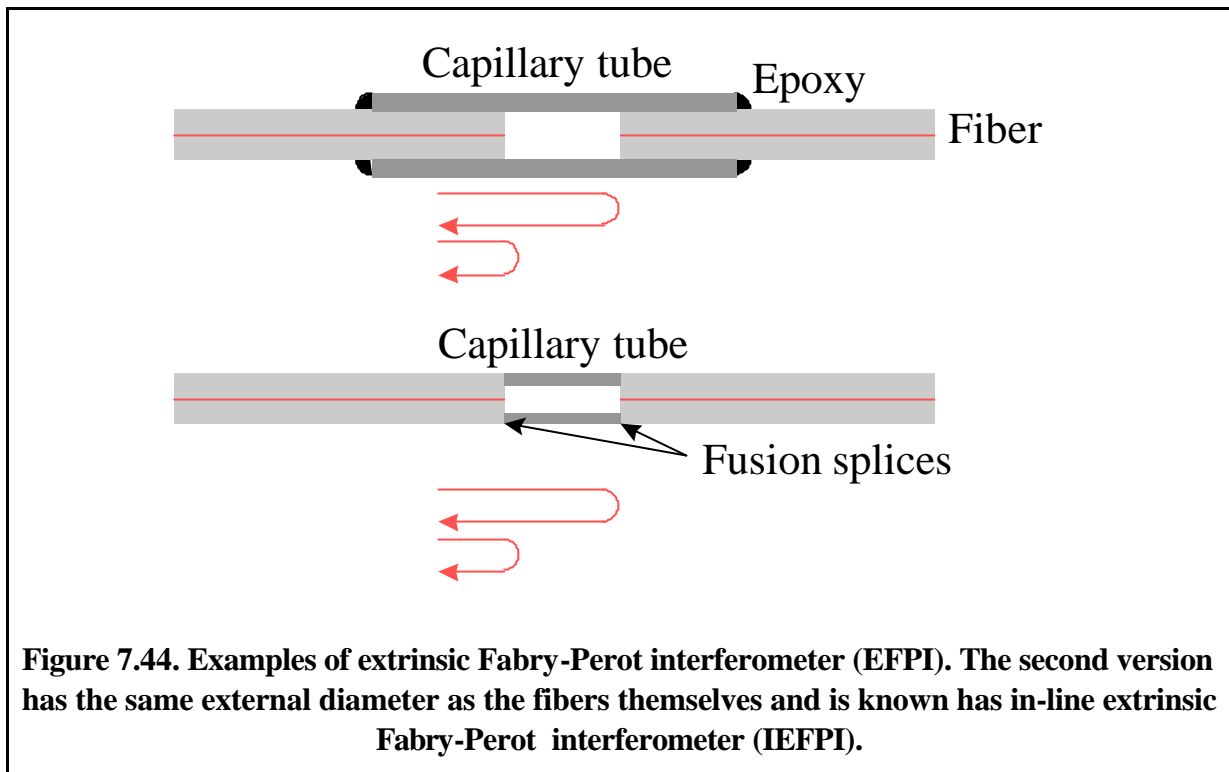


Figure 7.44. Examples of extrinsic Fabry-Perot interferometer (EFPI). The second version has the same external diameter as the fibers themselves and is known as in-line extrinsic Fabry-Perot interferometer (IEFPI).

Etalons are similar to air-gap connectors but have the two fibers permanently assembled at a fixed distance. Etalons can be realized in dimensions slightly larger than the fiber or even of the same size as the fiber itself [11] as shown in Figure 7.44. Etalons can also be made cheaper than air-gap connectors and are more adapted to applications with space constraints. They lack the flexibility of air-gap connectors that allow the separate characterization of each sensor section.

7.5.4 Bubble reflectors, bad splices

Bad mechanical or fusion splices offer another opportunity to obtain partial reflectors. In this case it is partially possible to control the reflection by adjusting the cleave angle of one or both fibers. These reflectors tend however to have higher losses and are therefore suited only for chains with only a few reflectors. Furthermore, it is necessary to add extra connectors to expand the sensor chain.

A few bubble reflectors manufactured by Ericsson (Sweden) were tested. These specimens showed a reflectivity between -17 and -25 dB. The losses were of a few dB. Even for a single bubble pair the resulting signal was much weaker than from a Fresnel reflection or an air-gap connector. Because of the high losses it was impossible to chain more than two partial reflection pairs. The only advantage of this type of reflector resides in its size which is not larger than the fiber diameter. This can be useful for applications in composite materials. In this case, broad-band Bragg gratings seem however to offer a better solution.

7.5.5 Broadband fiber Bragg gratings

By using short or chirped fiber Bragg gratings it is possible to obtain a broadband reflector. Short gratings usually have a lower reflectivity but are easier to fabricate and can be written in

the fiber directly on the drawing tower. Chirped grating can reach higher reflectivity but are more difficult to produce. Since these grating can be a few millimeters long, it should be investigated how the phase (i.e. the virtual position of the reflection within the grating) changes when a strain or a temperature variation occurs. Losses are usually very low. These reflectors offer a good latitude in the choice of the values for the reflectivity and could be used to produce chains with equivalent reflectivity from all sensors. The size of the reflector is reduced to the one of the fiber itself, an advantage in applications with size constraints like composite panel monitoring. They lack however the flexibility of air-gap connectors.

7.5.6 Photo-induced Fresnel reflectors

By exposing the fiber core to UV radiation over a short length, it is possible to obtain a local index variation and therefore a partial reflector. This technique offers low reflection coefficients and the losses are usually high [12].

7.5.7 Modal reflectors, index profiles mismatch

A last possibility to obtain a partial reflector is to splice together fibers with different modal characteristics, e.g. with different core diameter and/or index. Short section of multimode fiber can also be used without introducing a modal dispersion since only the fundamental mode will be excited. This kind of reflector usually has very low reflectivity since the index mismatches involved are small. If the losses can be kept low and a highly sensitive reading unit is available, these reflectors could be used to multiplex tens of sensors.

7.6 Conclusions

In this section we have examined many possibilities to multiplex low-coherence sensors. No single solution can be considered the best for all types of applications and budgets. When lateral multiplexing between a large number of sensors is required, optical switching appears to be the only solution despite the currently high price per channel. For a reduced number of sensors, other techniques and in particular the use of passive couplers and delay coils are simpler and cheaper. When longitudinal multiplexing is required, the expected deformations are small and the sensors relatively short (as for example in a concrete structure), simple coherence multiplexing is by far the best solution. It requires only minor modifications to both the sensors and the reading unit compared to the single sensor setup. In the case of long sensors and large deformations (typical of geomechanics) peak crossings have to be allowed and more complex demodulation schemes are required. The solutions that recognize the peaks by their form do not require major modification to the reading unit but need tailored partial reflectors. This reduces the flexibility of the system (different sections of a chain cannot be exchanged) and could lead to precision losses due to the inevitable peak broadening. On the other end, methods based on the direct or indirect measurement of the time of flight, can use identical reflectors but require high-speed electronics. Besides increasing the complexity and the cost of the reading unit, high-speed electronics also bring a sensible increase in the noise, especially at the level of the photodiode and preamplifier. This reduces drastically the number of reflectors that can be multiplexed along the same line for a give source power. High-power sources are available but their price and power consumption discourages their use in a portable reading unit. The ideal solution to multiplex sensors in-line and allowing peak crossing has still to be found. For the time being a simple solution could consist in extending the stroke of the mirror in the variable delay line of the analyzer.

7.7 Bibliography

- [1] D. Inaudi, "Coherence multiplexing of in-line displacement and temperature sensors", *Opt. Eng.*, Vol. 34, Nr. 7, July 1995
- [2] D. Inaudi, S. Vurpillot, S. Lloret, "In-line coherence multiplexing of displacement sensors: a fiber optic extensometer", *Smart Structures and materials*, San Diego February 1996, SPIE Volume 2718-28.
- [3] G. Meltz, W. W. Morey, W. H. Glenn "Formation of fiber Bragg gratings in optical fibers by a transverse holographic method", *Optics letters*, 14, 1989, p 823
- [4] W. W. Morey, J. R. Dunphy, G. Meltz, "Multiplexing fiber Bragg Grating sensors", *SPIE Vol. 1586*, p.261
- [5] A. D. Kersey, M. J. Marrone, "Nested interferometric sensors utilizing Bragg grating reflectors", *OFS11, Sapporo*, May 1996, p. 618
- [6] A. D. Kersey, M. A. Davis, T. Tsai "fiber optic Bragg grating sensor with direct reflectometric interrogation", *OFS11, Sapporo*, May 1996, p. 634
- [7] J.-P. Von der Weid, L. Thévenaz, J.-P. Pellaux, "Interferometer measurements of chromatic dispersion and polarization mode dispersion in highly birefringent singlemode fibers", *Electr. Lett.*, vol. 23, pp. 151-152, 1987
- [8] L. Thévenaz, J.-P. Pellaux, N. Gisin, J.-P. Von der Weid, "Birefringence measurements in fibers without polarizer", *Journal of Lightwave technology*, Vol. 7, No. 8, august 1989.
- [9] D. G. Luke, R. McBride, P. Lloyd, J. G. Burnett, A. H. Greenaway, J. D. C. Jones, "Strain and temperature measurement in composite-embedded highly-birefringent optical fiber using mean and differential group delay", *OFS 11, Sapporo*, may 1996, p. 200.
- [10] A. S. Subdo, "An optical time domain reflectometer with low power InGaAsP diode lasers", *IEEE J. of Lightwave technology*, LT-1, 616-618, 1983
- [11] J. S. Sirkis, D. D. Brennan, M. A. Putman, T. A. Berkoff, A. D. Kersey and E. J. Friebele, "In-line fiber étalon for strain measurement", *Optics Letters*, Vol. 18, No. 22, pp. 1973-1975, 1993
- [12] J. A. Green et al. "Photoinduced Fresnel reflectors for point-wise and distributed sensing applications" *Smart Structures and Materials 95*, S. Diego, SPIE vol. 2444, p 64

8. Applications

Practical tests were necessary to check the theoretical development. So during this work many applications were realized using the SOFO system. These applications have always been the center of the SOFO project and have given invaluable feed-back to the design of the sensors, reading unit and software. Many interesting, but sometimes frustrating, properties of optical fibers and their interaction with coatings and glues, would never have been discovered in laboratory conditions. The reading unit was improved according to the needs of the end-users. The software has gone through an evolution driven by the need of a more convivial interface, both during the measurement sessions as back in the office where the raw data is analyzed.

At some points, the field applications were so numerous that they monopolized the activity of the whole SOFO team and the results were sometime analyzed only much later. This sometimes led to the repetition of the same errors in different experiments, that could have been avoided by analyzing more carefully the results after each test. As the team expanded, I was allowed to take a certain distance from the applications and concentrate more on the reading unit and software. Nevertheless, the field applications have remained the part of this project that gives me the biggest satisfactions, more than compensating the small occasional disappointments. By working with many passionate people, I have learned a lot on civil engineering and construction materials. I would like to thank all these persons, that will be cited with each application, for bearing with me and with occasional childhood problems of the SOFO system.

This section is intended to give an overview of the applications in which the SOFO system was applied and tested. The main results are only briefly reminded with emphasis on their consequences on the evolution of the SOFO system. The reader interested in a deeper analysis of the results from the point of view of civil engineering or material science, will consult the cited literature.

8.1 Holographic table

- **Date:** beginning of 1993.
- **Location:** IMM, Lugano-Grancia
- **People involved:** Daniele Inaudi, Adil Elamari, Samuel Vurpillot
- **Sponsors:** CERS/CTI¹, IMM², Passera + Pedretti, CABLOPTIC
- **Short description of the experiment:** Measurement of the deformations of a 20 m x 5 m x 0.5 m concrete slab concreted indoors (see Figure 8.1). This slab would later be supported on air cushions and became one of the largest holographic tables in the world.



Figure 8.1. The holographic table before concreting. The orange pipes would later contain the optical fibers.

The sensors were placed parallel to the longer side of the slab and installed with the surface coupling approach. Some other sensors relied on distributed coupling approach, being mounted on the outside of plastic pipes. The measurements were conducted daily during the first month and during pre-stressing and about monthly for the next two years. This table is still measured with the SOFO system annually.

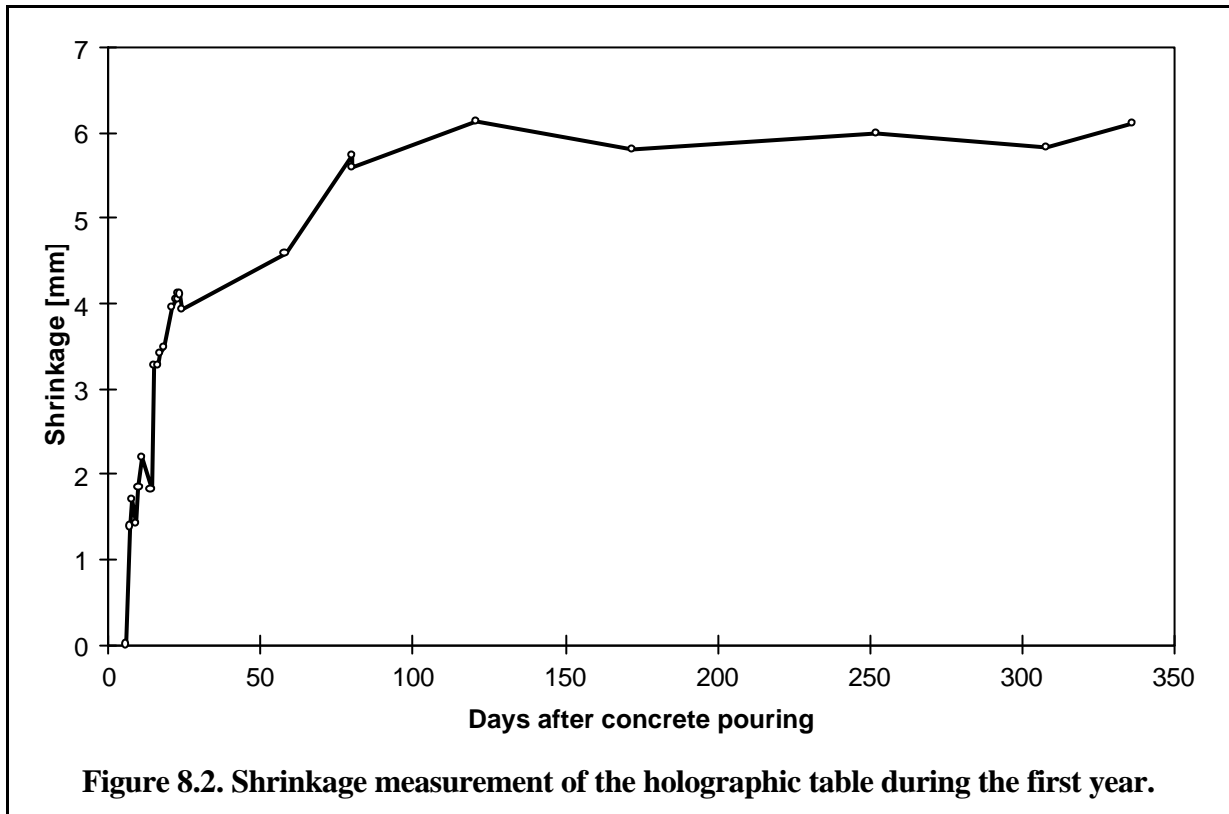
- **Main results for the SOFO system:** First application of the FORMOS system³. The feasibility of such measurements was proved. The stability of the system was tested over more than two years. It was learned that nylon coated fibers introduce a parasite sensitivity in the temperature, that could be accounted for thanks to the 250 electrical temperature sensors that were also placed in the slab. It was demonstrated that chemically stripped fibers could survive under tension and without creeping effects for many years.

¹ Commission pour l'Encouragement de la Recherche Scientifique, now renamed CTI: Commission pour la Technique et l'Innovation.

² Istituto di Meccanica dei Materiali. Institute for Materials Mechanics

³ At that time it was not yet called like this.

- **Main results:** Measurement of the slab deformation over two years. It was possible to first follow the shrinkage of the slab and then its seasonal length variations due to temperature change. The results were compared with numerical simulations. It was verified



that painting a concrete structure reduces significantly its shrinkage rate.

- **Bibliography:**

- "Construction of a 100-tonns holographic table", L. Pflug, M. Pedretti, Practical holography VII: Imaging and materials, San Jose 1993, SPIE Volume 1914, 50-54
- "Low-coherence deformation sensors for the monitoring of civil-engineering structures", D. Inaudi, A. Elamari, L. Pflug, N. Gisin, J. Breguet, S. Vurpillot, Sensor and Actuators A, 44 (1994), 125-130.
- "Low Coherence Fiber Optic Sensors for Structural Monitoring", A. Elamari, D. Inaudi, J. Breguet, L. Pflug, N. Gisin, S. Vurpillot, Structural Engineering International, Volume 5, Number 1, 43-47

8.2 High performance concrete tendon

- **Date:** end of 1993.
- **Location:** Hall ISS, EPFL, Lausanne
- **People involved:** Daniele Inaudi, Samuel Vurpillot, Pierre Mivelaz (IBAP-EPFL).
- **Sponsors:** CERS/CTI, CABLOPTIC, EDF⁴, Bouygues, Sika
- **Short description of the experiment:** Measurement of the deformations of a 5 x 1 x 0,5 m concrete tendon subject to pure traction loading (see Figure 8.3). This experiment was designed to test the waterproofing characteristics of different types of concrete. The SOFO

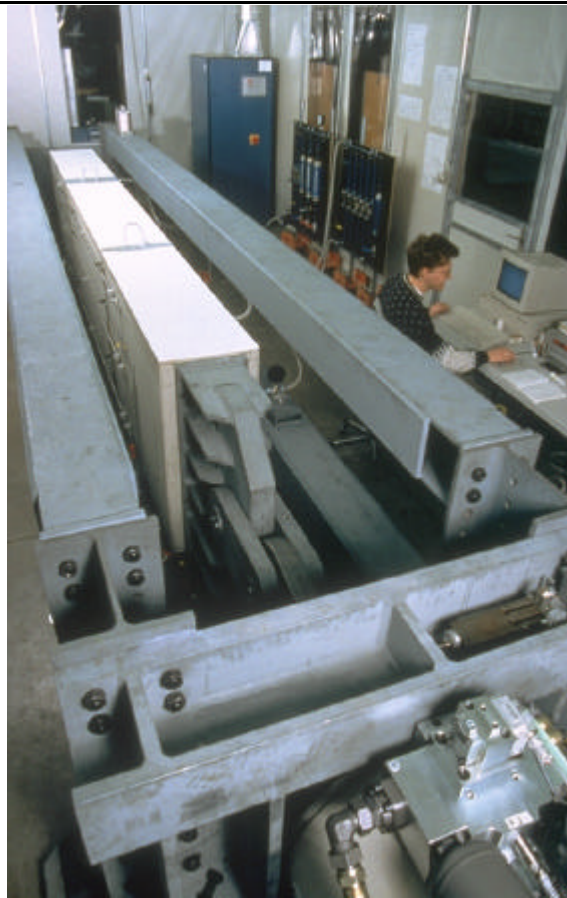
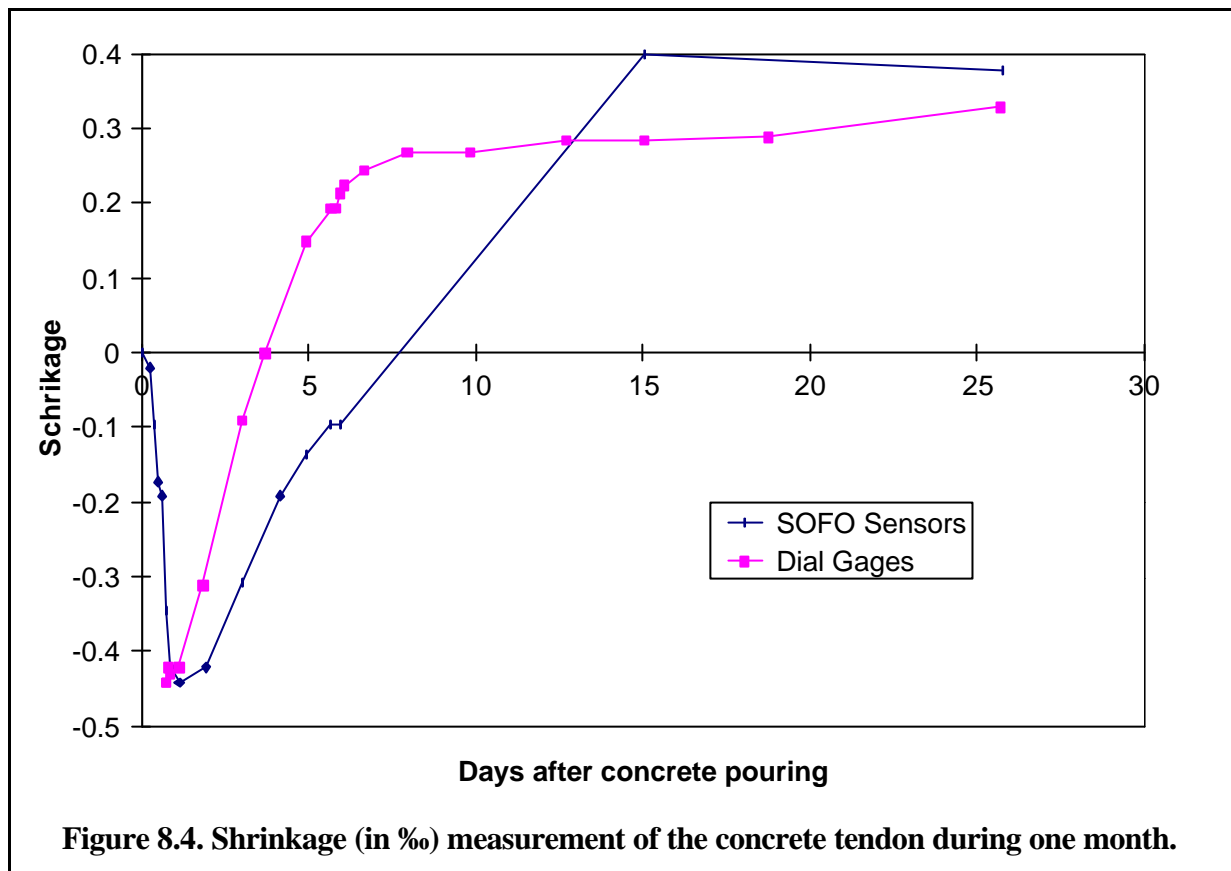


Figure 8.3. High performance concrete slab during pulling test.

system measured the shrinkage of the three central meters of the elements during the first month after pouring and during the traction test. The sensors were of the needle coupling type and a few of the external pipe distributed coupling type. Fifteen centimeter long sensors with junction piece coupling also measured the crack's width evolution inside the element.

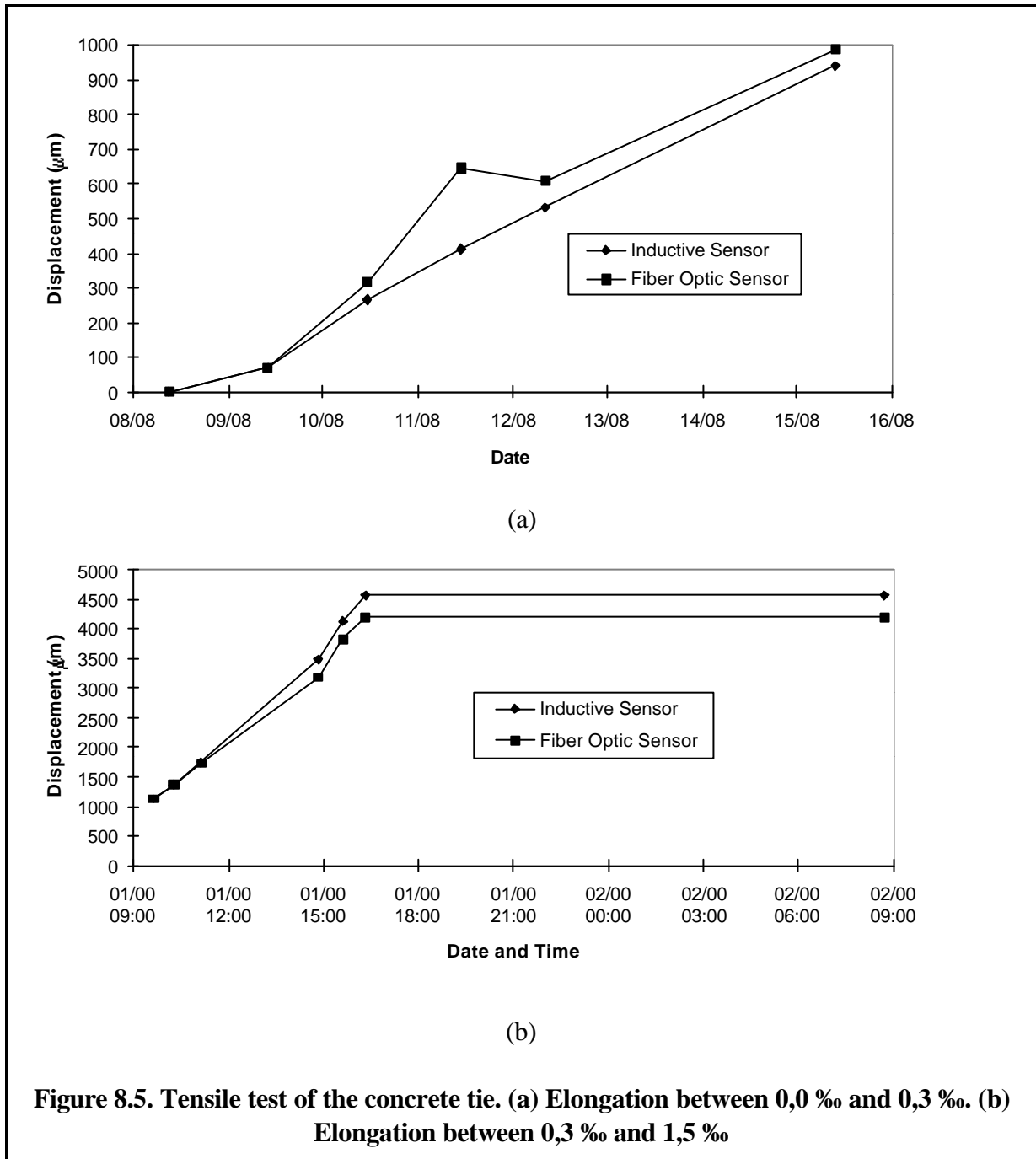
⁴ Electricité De France

- **Main results for the SOFO system:** This test allowed for the first time the comparison between the results obtained by the SOFO system with those of standard measuring systems. During the first month the reference were dial gages mounted on the outside of the



beam. During the traction tests, the deformation were monitored with external inductive sensors and the crack openings with omega strain gauges. It was found that the needle sensors suffered from creeping during concrete setting. This pointed to the fact that creeping was initiated at temperatures above 35°C. The results during the traction tests proved the good precision and resolution of the SOFO system. For the first time, self-contained sensors were used. The necessary pre-straining was given during installation in the rebar cage. A good survival rate was found.

- **Main results:** The shrinkage results proved interesting, especially in the thermal expansion region that could not be measured with the dial gages. A delay was found between the surface and the inner shrinkage (see Figure 8.4). During the pulling test it was possible to



follow the crack propagation through the element. These was probably the first reported measurement of crack openings inside a concrete element.

- **Bibliography:**

- "Low-coherence interferometry for the monitoring of concrete structures", S. Vurpillot, D. Inaudi, P. Mivelaz, European Symposium on Optics for Environmental and Public Safety, Munich June 1995, SPIE Volume 2507, 35-44

8.3 Timber-concrete slab

- **Date:** beginning of 1994
- **Location:** Hall IBOIS, EPFL, Lausanne
- **People involved:** Daniele Inaudi, Samuel Vurpillot, Reto Emery (IBOIS-EPFL).
- **Sponsors:** CERS/CTI, CABLOPTIC, Hilti
- **Short description of the experiment:** Measurement of the internal deformations of a 13 x 1 x 0,4 m mixed timber-concrete slab subject to four-point bending (see Figure 8.6). This experiment was designed to test the cohesion between timber and concrete. The SOFO

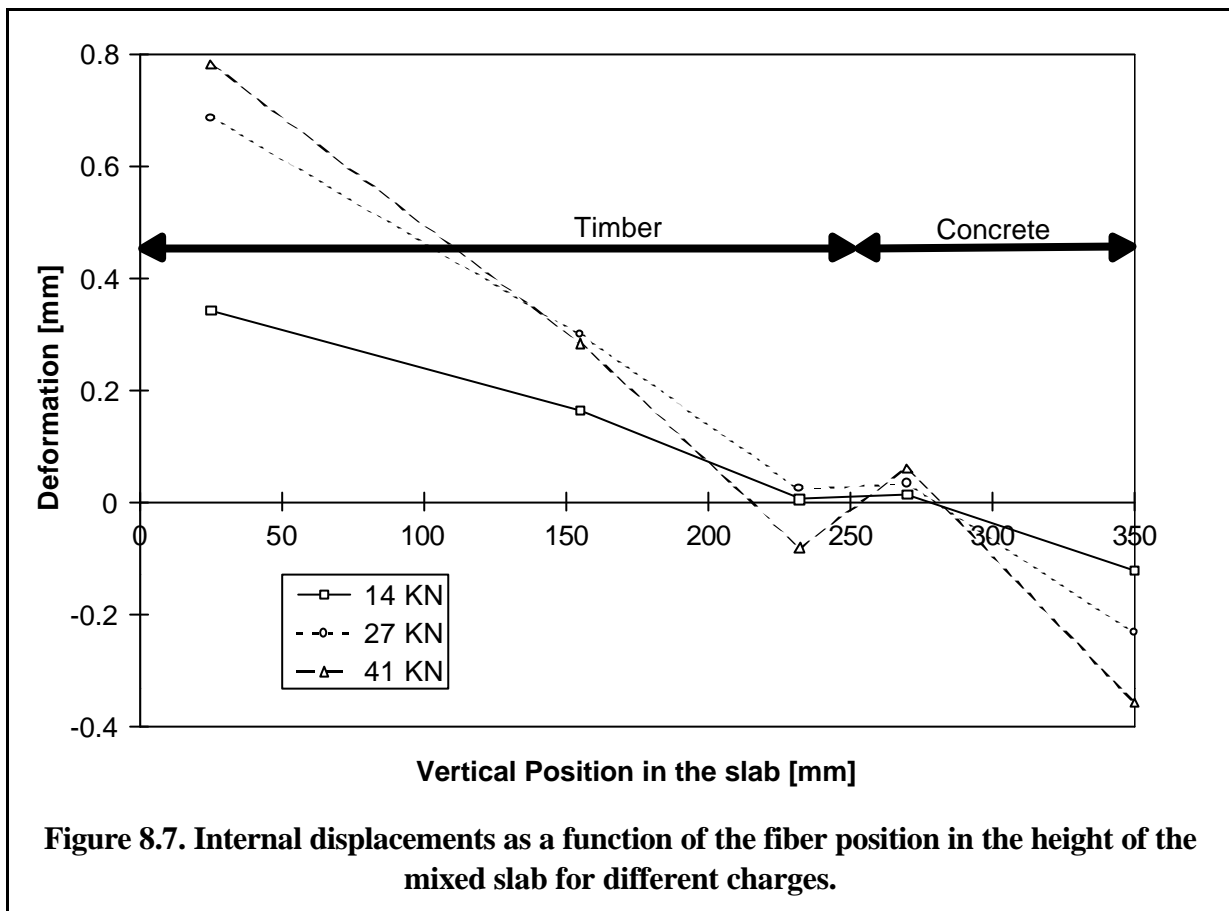


Figure 8.6. Mixed timber-concrete slab.

system measured the deformations on the four central meters of the slab at 6 different height (3 in timber and 3 in concrete) during the load test. The sensors were of the needle coupling type. The sensors for the wood parts were installed into machined grooves before assembly of the four timber beams.

- **Main results for the SOFO system:** This test used sensors very similar to those of the high performance concrete tendon. Being a short term test, the creep effect were not a concern. After the final test, some of the needles coupling in concrete were exposed and the creeping of the acrylate coating confirmed visually. The sensors installed into the timber part proved the feasibility of internal deformation measurements in this material by fiber sensors. These sensors did not suffer from any creep because they were not subject to temperature above 30°C.

- **Main results:** It was possible to retrieve the vertical internal distribution of strains and confirm the good cohesion between timber and concrete⁵. The typical Z shaped strain diagram (see Figure 8.7) can be observed at high loads, indicating that the two materials



are starting to slip mutually. This type of mixed construction is supposed to bring important cost benefits over all-concrete slabs of the same load-bearing capabilities.

- **Bibliography:**

- "Low-coherence interferometry for the monitoring of civil engineering structures", D. Inaudi, A. Elamari, S. Vurpillot, Second European Conference on Smart Structures and Materials, Glasgow October 1994, SPIE Volume 2361, 216-219.
- "SOFO Surveillance d'ouvrages par senseurs à fibres optiques", D. Inaudi, S. Vurpillot, IAS Ingénieurs et Architectes Suisses, No. 26, Décembre 1995

⁵ Thanks to vertical metallic connectors between the two materials and large transversals grooves into timber.

8.4 Steel-concrete slab

- **Date:** mid 1994
- **Location:** Hall ISS, EPFL, Lausanne
- **People involved:** Samuel Vurpillot, Daniele Inaudi, Cristophe Meister (ICOM), Nicola Dassetto (ICOM)
- **Sponsors:** CERS/CTI, CABLOPTIC
- **Short description of the experiment:** Measurement of the deformations of a 14 x 2 m mixed steel-concrete slab on three supports subject to distributed loading (see Figure 8.8). The SOFO system measured the internal deformations of the concrete part at different



Figure 8.8. Mixed steel-concrete slab. The fiber sensors exiting concrete are visible in the foreground. The usefulness of the SOFO sensors outside the elastic domain of the structure is clearly demonstrated by this picture.

locations during shrinkage and load test. The sensors were of the needle coupling type and presented important creep during the shrinkage phase but gave useful results during the load tests. Other sensors were glued directly on the upper and lower flange of the I-beams supporting the deck. These sensors were glued along their whole length realizing a distributed coupling sensor. Attempts were made to glue nylon coated fibers directly on the rebars. Although preliminary results in a loading machine gave excellent results⁶, three out of four such sensors didn't survive the installation into the rebar cage and concrete pouring. It is probable that the workman walking on the rebars during concrete pour, did either

⁶ We even discovered a flaw in the calibration procedure of this press, after the initial results seemed to indicate a malfunctioning of the fiber sensors.

damage the fibers directly or make the rebars turn and thus brake the fiber at the crossings with others rebar.

- **Main results for the SOFO system:** This test used for the concrete part sensors very similar to those of the high performance concrete tendon and the timber-concrete slab. These sensors did suffer from shrinkage because they were subject to temperature above 30°C during concrete setting. Unfortunately, this creep was attributed incorrectly to the glue rather than the fiber coating and the same error was than repeated on the partially retained wall experiment (see below). The sensors installed directly on the I-beams proved very reliable. However the long measurement basis is in this case unnecessary since steel is an homogeneous materiel and local sensors (like strain gages) give more precise data about the material's behavior. This type of sensors would be interesting for geometrical measurements, were a more global measurement is required. The installation of fibers directly on the rebars proved tedious and the survival rate was low. Furthermore, the results of the only surviving sensors were practically identical to those of the closely placed concrete sensor, indicating that either the rebar-concrete connection remained perfect even after severe cracking or that the fiber sensors resulted to be better connected to concrete than to steel. During the load test, the inadequate measuring speed to the FORMOS system became evident. It was impossible to measure all installed sensors at a convenient rate.
- **Bibliography:**
 - “Etude expérimentale du comportement d’une poutre mixte fléchie”, G. Couchmon, N. Dassetto, C. Meister, rapport d’essai ICOM 332, May 1996.

8.5 Partially retained concrete walls

- **Date:** end of 1994
- **Location:** IMM, Lugano-Grancia
- **People involved:** Daniele Inaudi, Samuel Vurpillot, Nicoletta Casanova, Simone Bassi (IMM).
- **Sponsors:** CERS/CTI, IMM, Passera + Pedretti, CABLOPTIC.
- **Short description of the experiment:** Measurement of the internal deformations of four 3 x 1 x 0.25 m reinforced-concrete walls concreted on massive concrete bases in order to impede shrinkage at the bottom of the walls (see Figure 8.9). The SOFO system was



Figure 8.9. Formwork and rebars of the reinforced concrete walls. The white sensor bundles are also visible.

supposed to measure the internal deformations of the concrete part at different heights in the wall during shrinkage.

- **Main results for the SOFO system:** The sensors were of the needle coupling type and presented important creep during the shrinkage phase. This time, the problem was correctly recognized to be at the level of the fiber coating. The needle coupling sensor using acrylate coated fibers was abandoned after this experiment and re-introduced later using polyimide coatings. In this experiment we learned the hard way that it is unwise to install a large number of identical sensors in a structures (at least while in the development phase). A small flaw in the design can lead to failure of most sensors. This experiment showed however the possibility and necessity to fabricate the sensors routinely in a batch process and by people with low training. This led to the collaboration with DIAMOND on the industrialization of the sensors.
- **Main results:** The optical fiber sensors gave almost no useful results because of the creeping problem. Some interesting curves were obtained with fiber optic temperature

sensors based on differential measurements between two free fibers, one acrylate coated, the other nylon coated. These results should have been compared with data recorded by electrical temperature sensors also installed in the walls. The relevant data from these sensors was however lost due to a hard-drive failure⁷. IMM was able to obtain useful information on the behavior of the different concrete mixes used in this experiment, thanks to superficial measurements by mechanical dial gages.

⁷ It really looks like the guardian angel who helped our project in other situations before and after this experiment, was taking a couple of days off...

8.6 Tendons

- **Date:** 1994-1995
- **Location:** Val Rovana (TI)
- **People involved:** Daniele Inaudi, Samuel Vurpillot, Nicoletta Casanova.
- **Sponsors:** CERS/CTI, IMM, Passera + Pedretti, VSL, Injectosond, CABLOPTIC.
- **Short description of the experiment:** Measurement of the rock movement in an unstable slope. Feasibility of the installation of fiber optic sensors into anchorage cables (see Figure



Figure 8.10. Tendons before and after installation in the concrete pillars. The optical fiber sensor and its anchorage point is visible in the first picture.

8.10). The optical fibers were installed along the steel tendons and exited through an unused hole in the tendon head. The sensors were manufactured with the junction piece approach and were up to 30 m long.

- **Main results for the SOFO system:** This interesting experiment showed the possibility of installing fiber optic sensors in the demanding environment of a tendon. More than half of the fibers survived the assembly of the cable, its installation and grouting as well as its tensioning. Most failures were due to deliberate cutting of the fibers after cable injection due to insufficient instruction to the workmen. The measurement fibers were put into tension after the cables using mechanical pieces similar to those retaining the steel tendons. Due to the long sensor length, the mechanical independence of the reference fiber from the

measurement fiber could not be guaranteed since the two (and sometimes four) fibers installed in the same pipe tended to wrap around one another. Although no meaningful displacement measurement was possible, this experiment is considered a success and shows that tendon monitoring is feasible using the SOFO system.

- **Bibliography:**

- "Low-coherence interferometry for the monitoring of underground works", D. Inaudi, L. Vulliet, L. Pflug, S. Vurpillot, A. Wyser, 1995 North American Conference on Smart Structures and Materials, San Diego February 1995, Volume 2444, 171-178

8.7 Vertical displacement measurements: Timber beam

- **Date:** 1994-1996
- **Location:** Hall IMAC - EPFL
- **People involved:** Samuel Vurpillot, Daniele Inaudi, Antonio Scano, Pascal Kronenberg.
- **Sponsors:** CERS/CTI, DIAMOND, CABLOPTIC.
- **Short description of the experiment:** Measurement of the vertical displacement of a 6 m long timber beam on two or three supports by double integration of the mean local

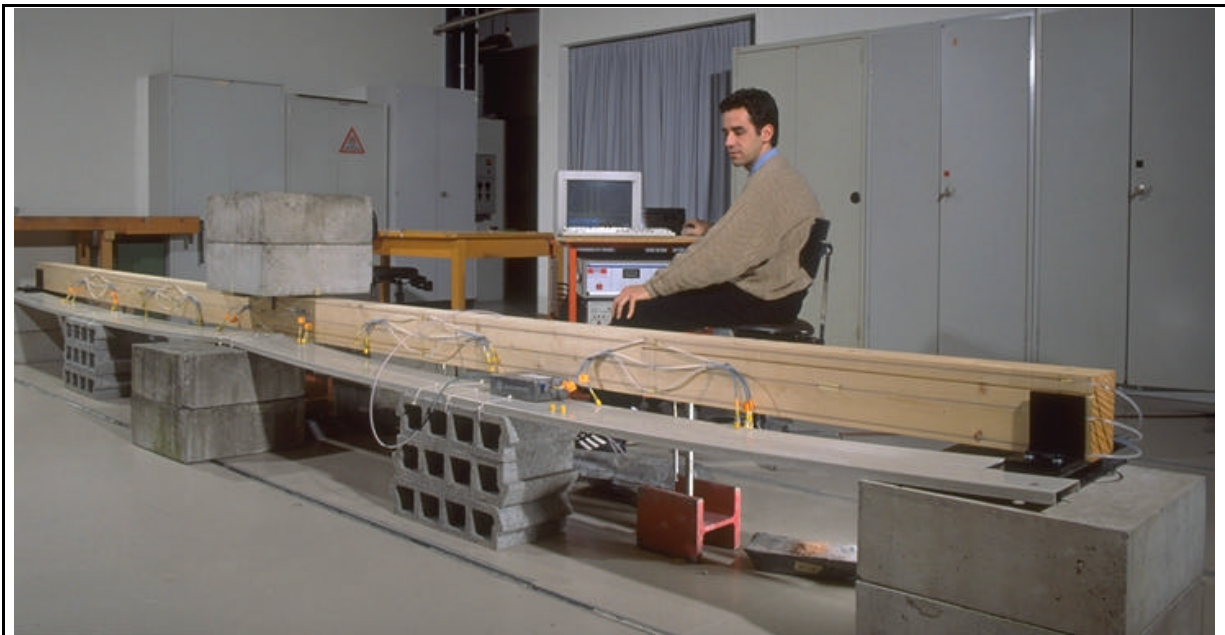
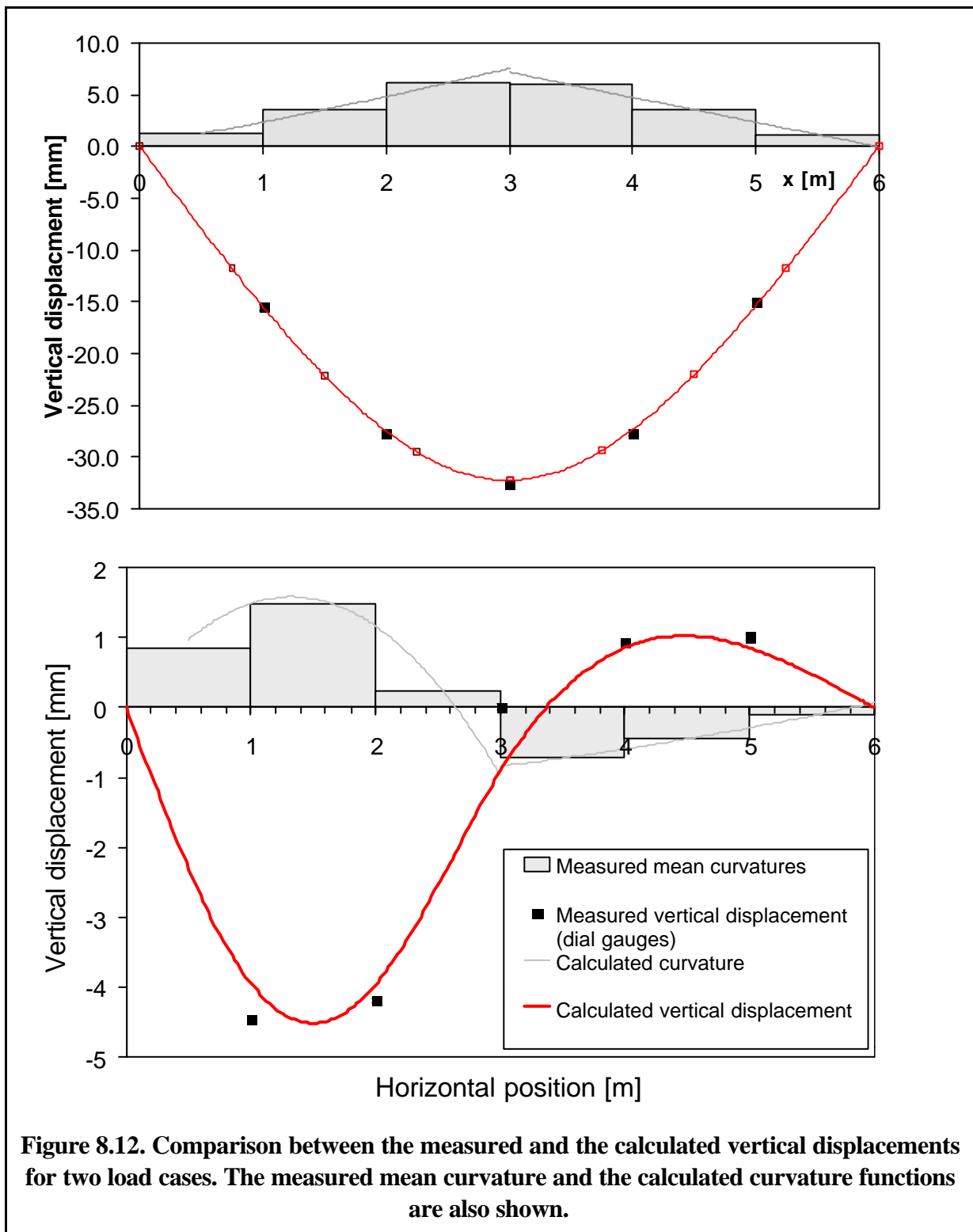


Figure 8.11. Timber beam subdivided in six measurement cells each equipped with two fiber optic sensors. One near the top of the beam and the other near the bottom .

curvatures. The curvatures were measured by installing twelve 1 m long optical fiber sensors above and below the neutral axis of the beam (see Figure 8.11). If for example the beam is loaded from the top, the fibers above the neutral axis will measure a shortening while the one below will get longer. This allows the calculation of the mean curvature of each of the six beam sections in which the beam is subdivided. By double integration of the curvature function and proper definition of the border conditions, it is possible to retrieve the vertical displacement function and compare it with the measurements of several dial gages placed under the beam. Sensors were installed on both sides of the beam. On one side classical sensors (with needle coupling and acrylate coated fibers), on the other with partial reflectors (also with needle coupling, but with polyimide coating).

- **Main results for the SOFO system:** First application of the double integration of the curvature to retrieve the vertical displacements. This algorithm is now part of the data treatment software package. First application on a structure of a partial reflector sensor chain.

- **Main results:** Different load cases were tried including concentrated and distributed loads on two and three supports. The first case shown in Figure 8.12, the beam is on two supports and the load is applied locally at the center of the beam. In this case the vertical



displacement is retrieved with high accuracy and compares well with the dial gages. The curvature is triangle shaped as expected from the theory. In the second example, the beam is on three supports and loaded uniformly on the left span, only. As expected, the curvature

of the loaded side is parabolic shaped while the one of the unloaded side is linear. The double integration gives a vertical displacement which fairly well corresponds to the real one. Note that the maximal displacement is much lower than in the first case. Furthermore, the algorithm finds the central support and even predicts a sinking at this point. This effect was later related to a local compression of the wood.

- **Bibliography:**

- "Mathematical model for the determination of the vertical displacement from internal horizontal measurements of a bridge" S. Vurpillot, D. Inaudi, A. Scano, Smart Structures and materials, San Diego February 1996, SPIE Volume 2719-05.
- "Coherence multiplexing of in-line displacement and temperature sensors", D. Inaudi, Opt. Eng., Vol. 34, No. 7, July 1995
- "In-line coherence multiplexing of displacement sensors: a fiber optic extensometer", D. Inaudi, S. Vurpillot, S. Lloret, Smart Structures and materials, San Diego February 1996, SPIE Volume 2718-28.

8.8 Vertical displacement measurements: Concrete beam

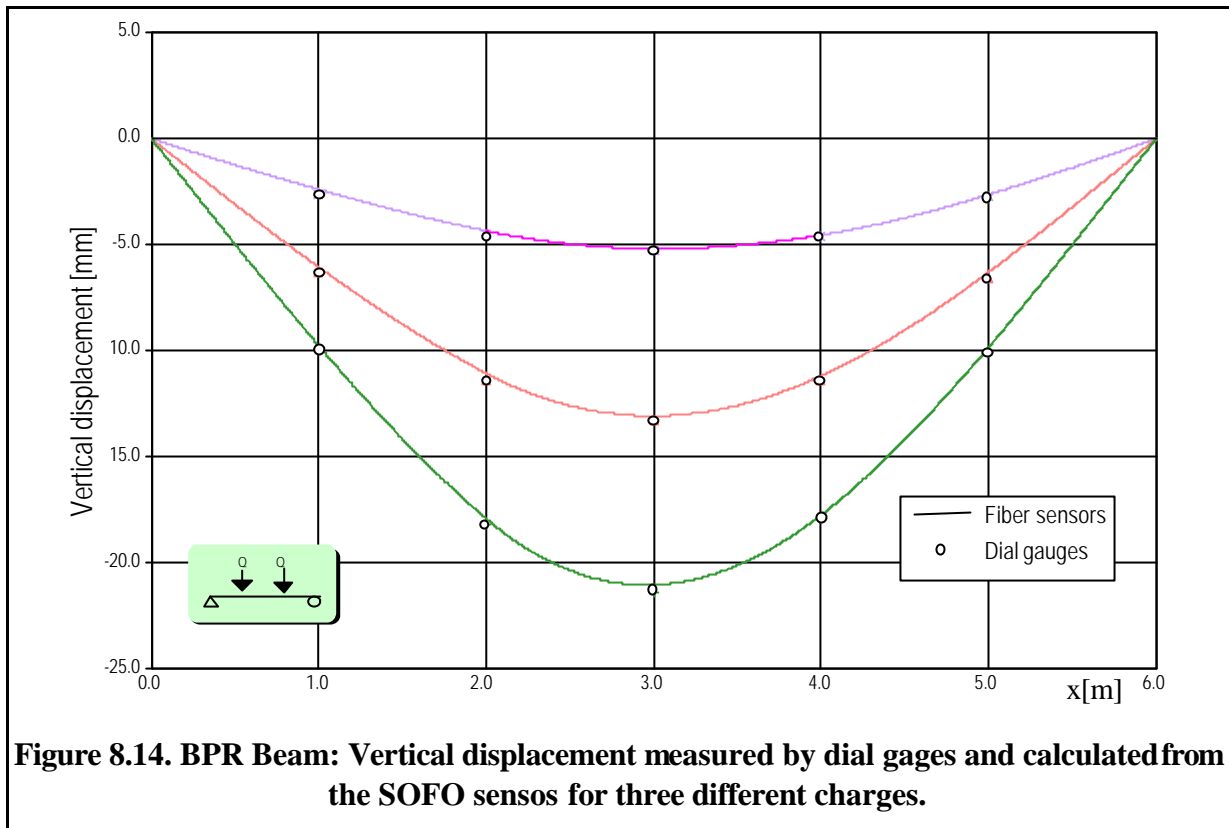
- **Date:** 1996
- **Location:** Hall IMM, Lugano
- **People involved:** Nicoletta Casanova, Samuel Vurpillot, Daniele Inaudi, Antonio Scano, Pascal Kronenberg, Claudio Rigo (IMM).
- **Sponsors:** CERS/CTI, DIAMOND, CABLOPTIC.
- **Short description of the experiment:** Measurement of the vertical displacement of a 6 m long BPR (Béton à Poudres Réactives: very high performance concrete) beam on two



Figure 8.13. BPR concrete beam subdivided in six measurement cells each equipped with two fiber optic sensors. One near the top of the beam and the other near the bottom .

supports by double integration of the mean local curvatures. The curvatures were measured by installing 18 one meter long optical fiber sensors above, on and below the neutral axis of the beam (see Figure 8.13). The measurements were performed as in the timber beam described above.

- **Main results for the SOFO system:** First “field” application of partial reflection chains.



- Main results:** The sensors were connected in chains and the whole beam could be monitored with just a few measurements. The mean curvature was analyzed in each of the six 1 m long sections by measuring the deformation near the top and near the bottom of the beam. The variations in the shape of the curvature function and in the position of the neutral axis, allowed the early detection of cracks at charge levels much lower than those producing visible cracks. By double integration of the curvature function and taking into account the boundary conditions, it was possible to retrieve the vertical displacement of the beam. Figure 8.14 shows a comparison between the displacements calculated from the SOFO data and those obtained by dial gauges placed under the beam. Excellent agreement is found even for loads far exceeding the elastic domain.

8.9 Venoge bridge

- **Date:** 1995
- **Location:** Near Lausanne on the Lausanne-Geneva Highway
- **People involved:** Samuel Vurpillot, Jean-Marc Ducret (ICOM-EPFL), Daniele Inaudi, Simone Bassi (IMM).
- **Sponsors:** Etat de Vaud, CERS/CTI, CABLOPTIC.
- **Short description of the experiment:** Measurement of the shrinkage of the concrete deck of a mixed steel-concrete highway bridge. The Venoge highway bridge near



Figure 8.15. The Venoge highway bridge near Lausanne. General view.

Lausanne (see Figure 8.15) is a four-spans bridge consisting in two parallel steel girders of $1.0 \div 1.9$ m in height and supporting a 23 cm thick concrete deck. To widen the bridge, two identical bridges were built on each side creating a third traffic lane and a new emergence lane in each direction. The Venoge bridge widening and the different phases of its construction allowed the observation of different interesting phenomena. The monitoring of the real behavior of this steel-concrete bridge under direct and indirect loads was the general aim of this experiment, which can be divided in three main objectives:

- Monitoring of the shrinkage effects, especially during the first hours after concreting. It is very interesting to control the thermal expansion phases to understand the real behavior of the steel-concrete interaction.
- Verification of the bridge behavior under static forces.
- Measurement of the bridge behavior under the traffic loads.

More than 30 fiber optic sensors (of the final junction type design), a few wire strain gauges and about 24 thermoelectric couples were installed in the deck and on the steel girders. Forty eight strain gauges were fitted on the steel girders, while four instrumented bearings were installed on the 2 extremities of the first span.

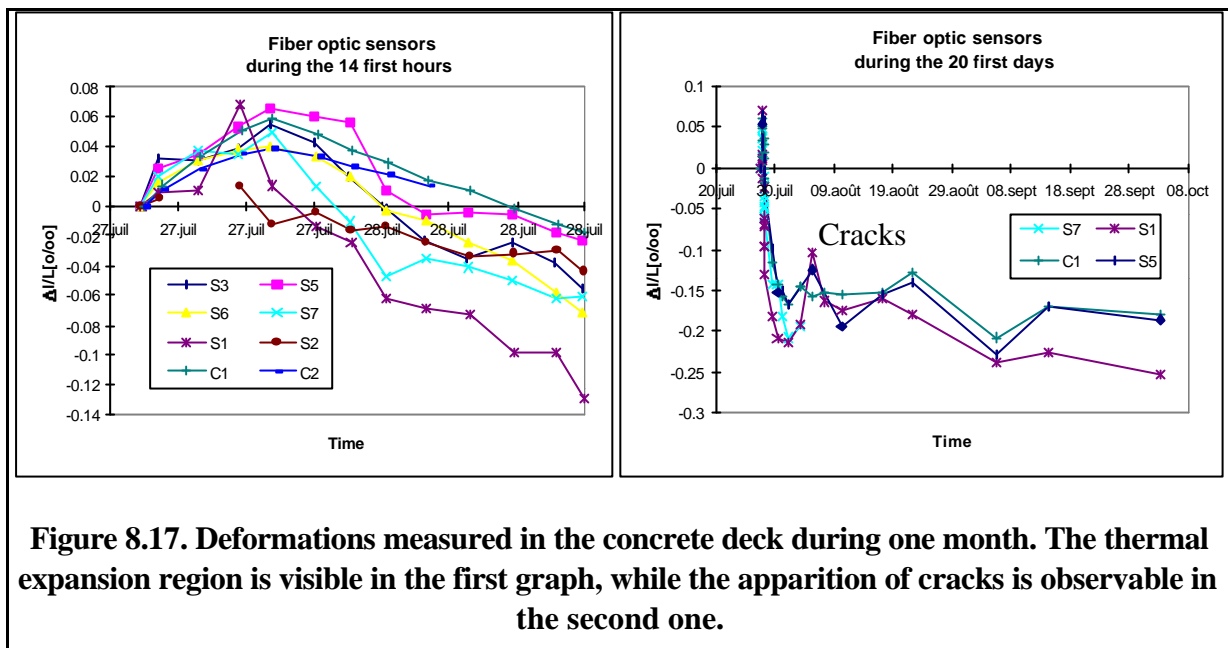
- **Main results for the SOFO system:** First application of the SOFO system in real building-site conditions. The problems of the installation rapidity, the protection of the connectors and mating adapters (see Figure 8.16) as well as the use of the SOFO reading



Figure 8.16. The Venoge highway bridge near Lausanne. Typical measurement session.

unit in adverse conditions had to be addressed. About 95% of the sensors survived installation and concrete pouring and allowed measurements to be performed for a few days or weeks. However, more than half of the sensors failed after some time. This problem was traced back to the mechanical removal of the acrylate fiber coating at the locations of the anchorage points. This operation, while having eliminated the problem of creep than was never observed in this experiment, made the fiber fragile and led to failure. After this experiment all sensors were built with polyimide coated fibers that solved both problems. For the first time, a coupler was integrated in some of the sensors. This solution proved effective and the precision of the sensors was increased by almost an order of magnitude. The SOFO reading unit performed well in the field conditions encountered on this bridge (including mud, wind, rain and snow).

- **Main results:** Thanks to the measurements obtained with the SOFO system, it was possible to observe the apparition of transversal cracks a few days after concreting. This effect was predicted by a theoretical model and is the consequence of the partially hindered



thermal shrinkage. Being the SOFO system unaffected by the temperature effects it was possible to measure the apparition of the cracks and the associated redistribution of the deformations in a quantitative way . Measurements were also performed during the charging tests where heavy trucks were placed at specific locations on the bridge and the associated deformations were observed.

- **Bibliography:**
 - "Bridge monitoring by fiber optic deformation sensors: design, emplacement and results", S. Vurpillot, D. Inaudi, J.-M. Ducret, Smart Structures and materials, San Diego February 1996, SPIE Volume 2719-16.
 - "Modeling and testing of the behavior of a composite bridge", J.-M. Ducret, J-P Lebet, Structural Assessment, The role of large and full Scale testing, City University, London, July 1-3, 1996.

8.10 Moesa bridge

- **Date:** beginning 1996
- **Location:** Near Bellinzona on the Gotthard railway line.
- **People involved:** Nicoletta Casanova, Simone Bassi (IMM), Daniele Inaudi, DIAMOND R&D team, Pascal Kronenberg.
- **Sponsors:** DIAMOND, IMM, Passera + Pedretti, Swiss Railways, CERS/CTI
- **Short description of the experiment:** Measurement of the shrinkage of the concrete deck of a mixed steel-concrete railway bridge. The Moesa railway bridge near Bellinzona



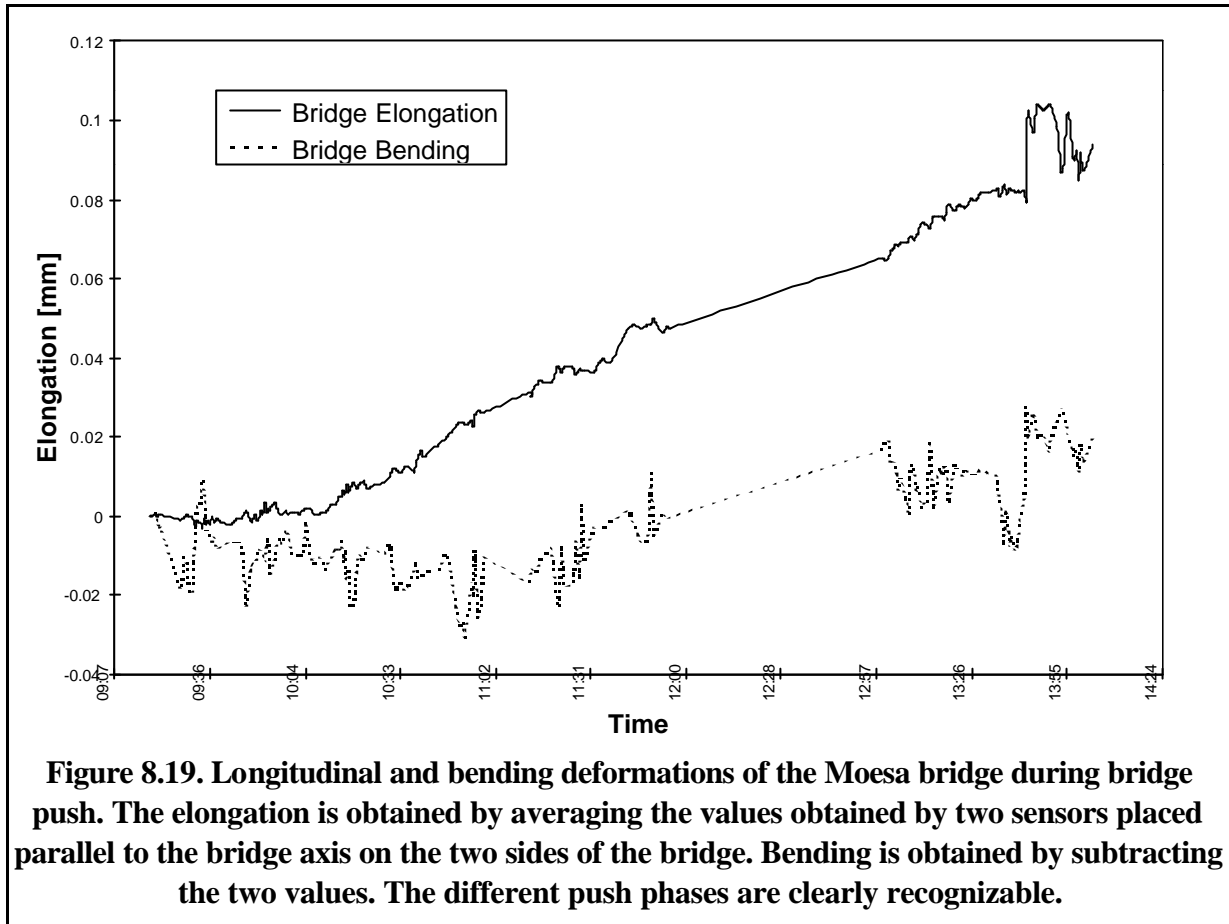
Figure 8.18. The Moesa railway bridge near Bellinzona.

(see Figure 8.18) is a three-spans bridge consisting in two parallel steel girders with their lower part supporting a 50 cm thick concrete deck. This new bridge was built parallel to the old steel bridge. After dismantling this later, the new bridge was then pushed on the old and refurbished pillars. This was the first application of the SOFO system to a railway bridge and the first field application of the DIAMOND sensor.

- **Main results for the SOFO system:** The bridge was concreted in six sections with about two weeks pace. This allowed IMAC, DIAMOND and IMM to analyze the results of each section and improve on the sensors design. A particularly fine and abrasive dust was encountered on this bridge and allowed the test of adequate connector protection. Some sensors were affected by a flaw in the fabrication procedure that resulted in a path unbalance between the sensors larger than the one measurable with the SOFO system. A few broke during installation because of excessive fiber surplus in the passive region, others were fabricated with nylon coated fibers and became more temperature than deformation sensitive. During the push phase, additional sensors were attached under the concrete slab and measured the curvature of the bridge due to uneven push. Although not a complete success from the measurement side, this experiment greatly contributed to the technology

transfer between IMAC and DIAMOND. Many improvements on the DIAMOND sensor were realized during this experiment.

- **Main results:** The sensors that were usable after installation gave nice shrinkage curves similar to those encountered at Venoge. A discontinuity due to the heating produced by the concrete setting in the successive section was also visible. During the push phase, additional



sensors were attached under the concrete slab and measured the curvature of the bridge due to uneven push (see Figure 8.19)

- **Bibliography:**
 - “Bridge Monitoring by interferometric deformation sensors”, D. Inaudi, S. Vurpillot, N. Casanova, SPIE Photonics China, Beijing, 4-7 November 1996
 - “Structural monitoring by curvature analysis using interferometric fiber optic sensors”, D. Inaudi, S. Vurpillot, N. Casanova, P. Kronenberg, submitted to “Smart Materials and Structures”.

8.11 Versoix bridge

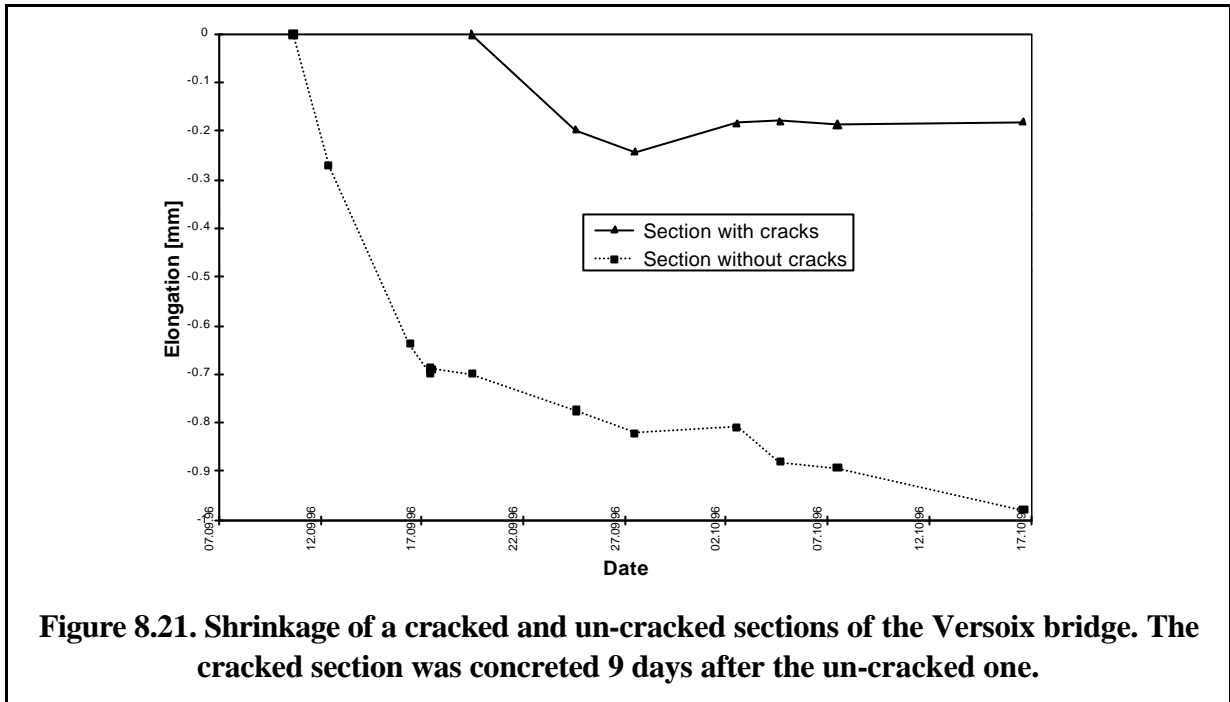
- **Date:** end 1996
- **Location:** Versoix near Geneva.
- **People involved:** Samuel Vurpillot, Pascal Kronenberg, Daniele Inaudi, Raymond Delez.
- **Sponsors:** State of Geneva, DIAMOND, Passera+Pedretti.
- **Short description of the experiment:** Curvature measurement on an enlarged and refurbished concrete highway bridge. Measurement of the interface behavior between hold



Figure 8.20. The Versoix highway bridge.

and new concrete.

- **Main results for the SOFO system:** First large-scale application of the SOFO system. More than 100 sensors are installed inside the new concrete and on the old concrete. Most sensors are of DIAMOND type, a few IMAC sensors are added for comparison purposes. All sensors are routed to a central connection box using optical cables. The installation is ready for remote and automatic monitoring with optical switches. The curvature are analyzed in the horizontal and vertical planes. At the time of writing, all sensors have been installed, only 5 of which did not survive concreting.



- Main results:** After concreting the first 6 sections it was possible to observe different shrinkage patterns characteristic of zones with or without cracks as shown in Figure 8.21. Further research is necessary to interpret these patterns in a quantitative way and characterize the cracking state.

8.12 Lully viaduct

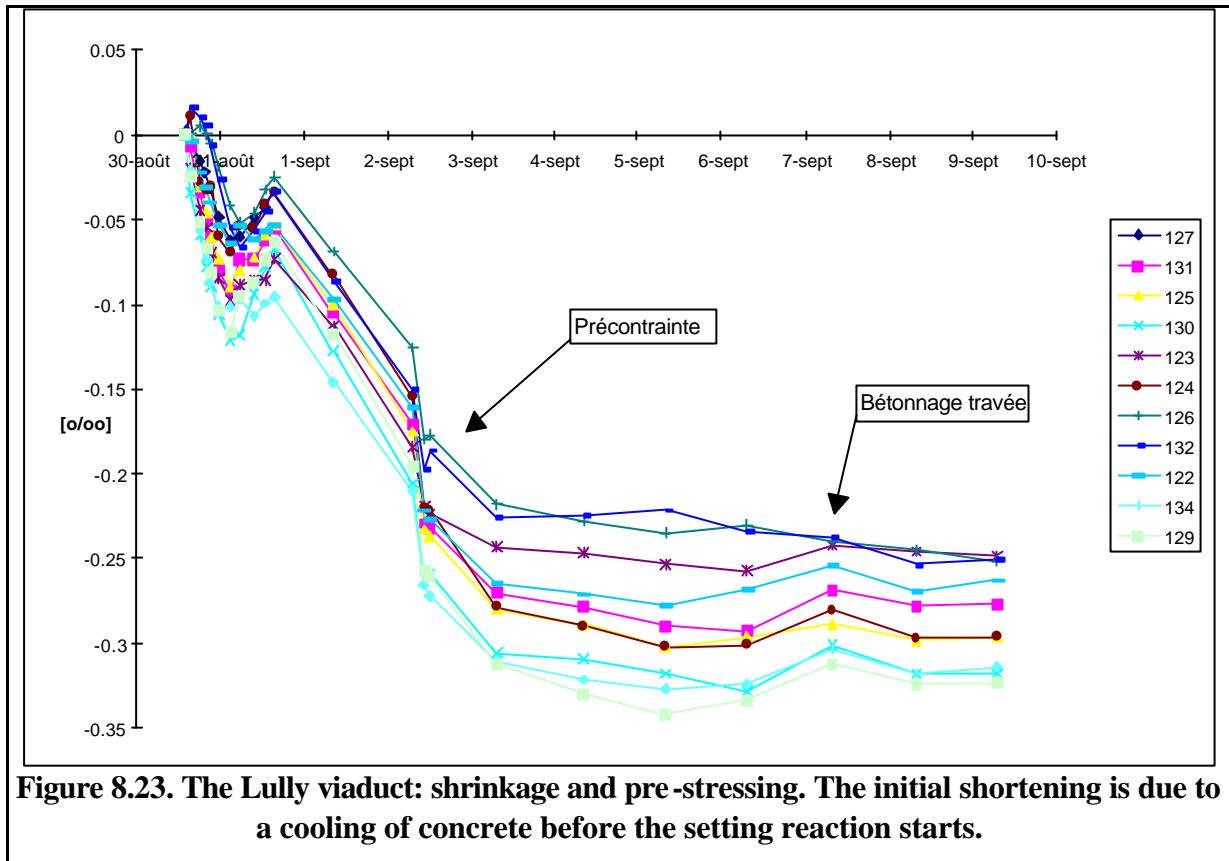
- **Date:** 1996
- **Location:** Lully, Fr.
- **People involved:** Jean-Marc Ducret, Samuel Vurpillot, Daniele Inaudi, Pascal Kronenberg.
- **Sponsors:** State of Fribourg, CERS/CTI
- **Short description of the experiment:** Measurement of the deformation of the concrete slab of a steel-concrete during concrete setting, pre-stressing and one year life.
- **Main results for the SOFO system:** First application of the DIAMOND sensors on a



Figure 8.22. The Lully viaduct

full-scale real structure.

- **Main results:** Determination of the setting properties of concrete and of the real amount of pre-stressing. Measurement of the pre-stressing transfer from the concrete slab to the metallic truss (see Figure 8.23).



8.13 Lutrive bridge

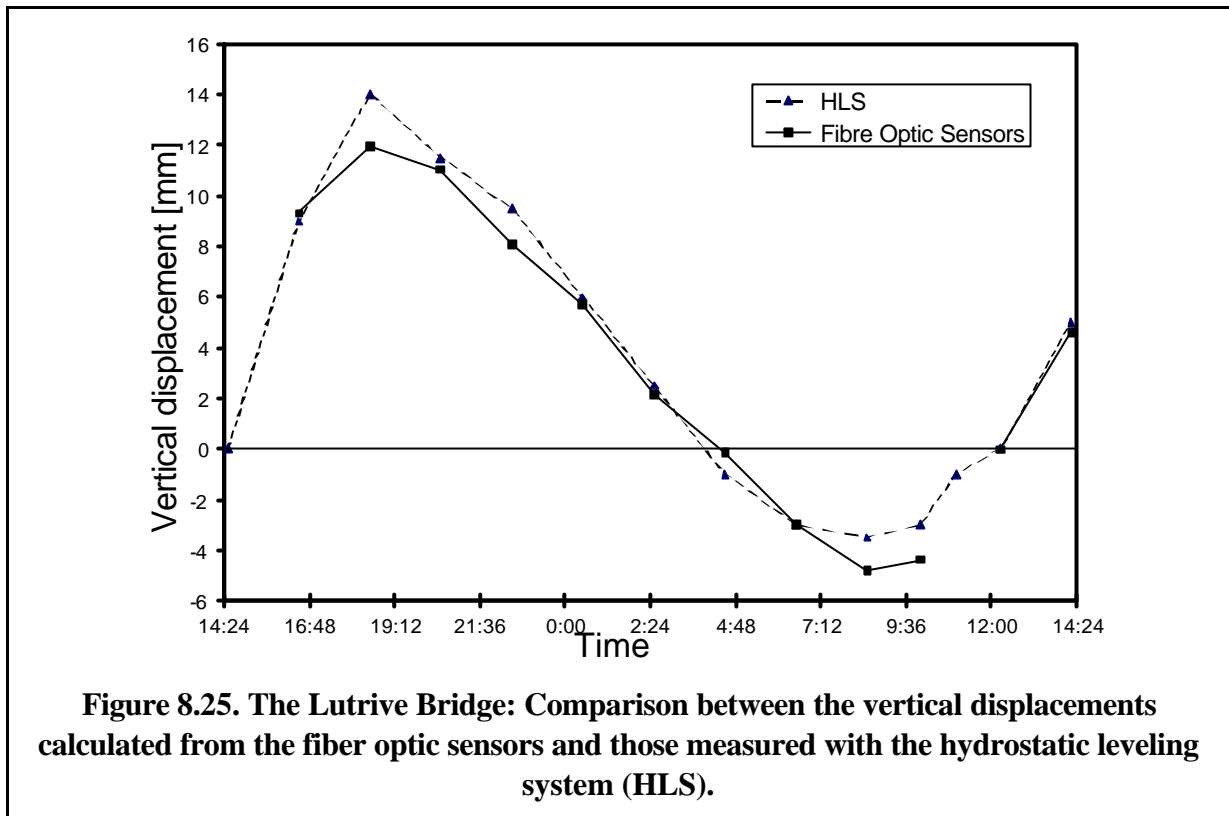
- **Date:** 1996
- **Location:** Belmont, VD
- **People involved:** Samuel Vurpillot, Gaston Krüger, David Benouaich, Denis Clément, Daniele Inaudi.
- **Short description of the experiment:** Measurement of the vertical displacement under thermal loading of an existing box girder concrete highway bridge by double integration of the curvatures. Ten meters long sensors were attached inside the box girder. Three cells



Figure 8.24. The Lutrive Bridge

with two sensors each have been installed.

- **Main results for the SOFO system:** First in-situ application of the curvature algorithm. Inclinometer measurements were used to improve the border conditions for the integration of the curvatures.



- **Main results:** Retrieval of the vertical displacement of the bridge over one day. Good agreement was found with measurements performed with water leveling systems.
- **Bibliography:**
 - “Vertical displacement of a pre-stressed concrete bridge deduced from deformation sensors and inclinometer measurements”, S. Vurpillot, G. Krüger, D. Benouaich, D. Clément, D. Inaudi, submitted to “American Concrete International”.

8.14 Emosson Dam

- **Date:** 1996
- **Location:** Emosson VS.



Figure 8.26. The Emosson dam.

- **People involved:** Daniele Inaudi, Raymond Délez, Pascal Kronenberg, Samuel Vurpillot.
- **Sponsors:** Emosson Dam (see Figure 8.26).
- **Short description of the experiment:** Replace two mechanical extensometers (rockmeter) with fiber optic sensors of the SOFO type. Monitoring of the rock deformations during one year with measurements every month. Continuous measurements during one month.

- **Main results for the SOFO system:** Design, fabrication and installation of a 30 m and a 39 m long sensors (see Figure 8.27). The sensor presents a few interesting features uncommon in the shorter sensors used for concrete embedding:



- The sensor replaces the existing rockmeter and can be installed and removed like its mechanical counterpart. Special fixation points for the top and bottom anchorage points have been designed. The sensor is pre-stressed after installation.
- The whole sensor fits inside the 15mm diameter bore-hole.
- The sensor is contained inside a PVC pipe. The reference fiber is contained inside a polyethylene pipe placed inside the PVC pipe. The measurement fiber sits in a micro-tube installed between the polyethylene and the PVC pipes.
- **Main results:** At the time of writing both sensors had been installed successfully in the dam.

8.15 Other applications

Besides the applications presented in the previous paragraphs, many other smaller experiments were conducted during this work. Here are some of the more interesting ones:

8.15.1 Rails

- **Date:** 1993
- **Location:** IMAC - EPFL.
- **People involved:** Adil Elamari, Daniele Inaudi.
- **Short description of the experiment:** Measurement of the deformation under thermal loading of a 1 m long rail sample with fibers glued directly into grooves machined in the rail.
- **Main results for the SOFO system:** This experiment allowed the measurement of the thermal expansion coefficient of steel and therefore showed that the SOFO system was insensitive to temperature variations.

8.15.2 Piles in Morges

- **Date:** 1995
- **Location:** Morges.
- **People involved:** Annette Osa-Wyser (LMS-EPFL), Xavier Rodicio (LMS-EPFL), Samuel Vurpillot, Daniele Inaudi.
- **Short description of the experiment:** Measurement of the vertical deformations in a pour-in-place concrete pile. The 15 m long sensors were based on the needle coupling design. The experiment was mainly a feasibility test and a certain number of sensors indeed survived the concrete pour.
- **Main results for the SOFO system:** This experiment proved once and for all the unsuitability of the FORMOS system for field applications. It also confronted us with the problem of installing fibers in piles. The connectors have to be accessible during all construction phases (after pile concreting, after foundation pouring and so on). Sometimes piles are even cut, the question on how to install fibers in them remains open.
- **Bibliography:**
 - "Development of interferometric fiber optic extensometers to monitor geostuctures", L. Vulliet, D. Inaudi, A. Wyser, S. Vurpillot, L. Pflug, Field Measurements in Geomechanics 4th International Symposium, Bergamo April 1995.

8.15.3 Vignes Tunnel

- **Date:** 1995
- **Location:** Tunnel des Vignes, near Fribourg.
- **People involved:** Annette Osa-Wyser (LMS-EPFL), Xavier Rodicio (LMS-EPFL), Samuel Vurpillot, Daniele Inaudi.
- **Short description of the experiment:** Measurement of the deformations in a prefab concrete vault installed in a highway tunnel. It was planned to perform convergence measurements by installing 25 cm long sensors near the inside and the outside of the vaults. The sensors used were early versions of the final junction-piece sensor and most failed for the same reason as those in the Venoge bridge. The measurement performed on the

remaining ones gave inconsistent results because of the use of uncharacterized and nylon coated (and therefore temperature and creep sensitive) patch cords.

- **Main results for the SOFO system:** This project confronted us with the problems typical of the instrumentation of a tunnel. When successive layers of waterproofing are added inside the tunnel, patch cords have to be added or displaced. The protection of the connectors and their accessibility is also a concern. This experiment, although not particularly successful will prove invaluable for further application of the SOFO system in other tunnels.

8.15.4 High temperature sensors for a nuclear power plant mock-up

- **Date:** 1995
- **Location:** IMAC - EPFL.
- **People involved:** Samuel Vurpillot, Ange Pontier (Freysinet), Daniele Inaudi.
- **Short description of the experiment:** Development of deformation sensors for installation in the 1 m thick concrete wall of a nuclear power plant mock-up to be loaded with high pressure vapor to simulate a major accident. The sensors have to perform according to the normal specifications at temperatures up to 180°C.
- **Main results for the SOFO system:** This project allowed to gain a lot of experience in the fabrication of sensors and in the properties of the different coatings and glues used to attach the fibers to the junction pieces. The final SOFO sensor and the DIAMOND industrial version, are evolution of the sensor developed for this peculiar application.
- **Main results:** The mock-up was still waiting for completion at the time of writing.

8.15.5 Fatigue tests

- **Date:** 1995-1996
- **Location:** Hall ISS, EPFL
- **People involved:** Pascal Kronenberg, Samuel Vurpillot, Max Schläfli (MSC-EPFL), Daniele Inaudi.
- **Short description of the experiment:** Measurement of the deformations in concrete slab submitted to fatigue tests. The measurement fibers were installed on the surface by gluing them on small metallic blocs adhered to concrete. In a successive experiment, DIAMOND sensors were embedded in the slab.
- **Main results for the SOFO system:** This test proved that optical fiber sensors are unaffected by fatigue. Measurements were performed after a given number of cycles. No single fiber failure or creeping problems was encountered for up to ten million cycles.
- **Main results:** Measurement of the crack-induced deformations. The measurements compared well to those performed with electrical foil strain gauges and direct measurements of crack openings with a magnifier.

8.16 Conclusions

These experiments show that the SOFO system is indeed applicable in useful experiments and real building-yard conditions. They also show how the evolution of the system as a whole (sensors, reading unit, software) followed and was driven by real needs and problems found outside the lab. The issues of sensor installation in civil structures were addressed in an original way by our multidisciplinary team including specialists from both optics and civil

engineering. These practical problems that are sometimes either underestimated or judged uninteresting have become for us a challenge and brought some of the biggest satisfactions on the local and international level.

9. Conclusions

This final section resumes the main achievements of this dissertation and presents an outlook about interesting extensions of the SOFO system as well as possible spin-offs of some of the technologies developed during this work.

9.1 Summary

The main result of this work is the design and realization of a complete deformation monitoring system based on low-coherence interferometry in optical fiber sensors and adapted to civil engineering applications. The SOFO system comprises:

- A series of sensors for direct concrete embedding and surface mounting on metallic and existing structures (see paragraph 6.6).
- A reading unit adapted to field-applications (see section 6).
- A number of multiplexing schemes allowing the measurement of multiple sensors with a single reading unit (see section 7).
- Software packages allowing the organization of the measurements in a relational database system, as well as the retrieval, visualization and analysis of all the gathered data (see paragraph 6.10).

The SOFO system has been applied successfully to the monitoring of a number of civil structures (see section 8).

9.2 Main accomplishments

The next paragraphs resume the main original contributions of this work. Being SOFO a multidisciplinary project involving many researchers from different domains, some of the achievements cited below are not the fruit of only my personal work.

9.2.1 Sensors

- **Fiber-coating-structure interaction** (see paragraph 6.6).

It was found that polyimide coatings transmit strain well and are adapted for local-coupling sensors. Nylon coated fibers are best suited for full-length distributed coupling. Acrylate coated fibers transmit strain well only at temperatures below 35°C and tensions below 0.5%, they present creeping problems for long-term applications. Two different epoxy glues were selected to cement the coated optical fibers to the anchorage pieces for low- and high-temperature applications.

- **Fiber-coating-structure temperature sensitivity** (see paragraph 4.3).

Experiments and theoretical models showed that polyimide and acrylate coatings do not alter significantly the low thermal expansion coefficient of silica fibers and are therefore well suited for reference fibers. Nylon coated reference fibers introduce an important parasitic sensitivity to temperature. Coatings do not influence the temperature properties of the measurement fibers.

- **Sensors for concrete embedding and surface mounting** (see paragraph 6.6).

A sensor for direct concrete embedding (including in mortars and grout) was designed and realized in different successive versions. The same sensor can be surface-mounted on existing structures and on materials that do not allow direct embedding (e.g. metals). In other cases the sensors can be installed into machined grooves (e.g. wood and concrete). Sensors of this type and with

lengths of up to 6 m are now produced industrially by DIAMOND SA and distributed by SMARTEC SA.

- **Long sensors** (see paragraph 8.14).
Sensors with length up to 40 m were designed and produced for anchorage monitoring and as rockmeter replacements for dam instrumentation.
- **Small sensors** (see paragraph 6.6.5).
Sensors with small diameter based on full-length distributed coupling and adapted to mortar and glue embedding were also developed and tested.
- **Chained sensors** (see paragraphs 8.7 and 8.8).
Sensor chains using air-gap connectors as partial reflector were designed and tested. The sensors are similar to those for concrete but dispose of connectors on both ends.

9.2.2 Reading unit

- **Realization of a portable reading unit for field applications** (see section 6).
A portable and battery powered reading unit was realized. This unit is adapted to building-size applications being rugged and waterproof. An industrial version is being developed by SMARTEC SA.
- **Optimization of the delay line** (see paragraph 6.7.3.1).
A mathematical model was proposed to help in the optimization of the double-pass delay line. The influence of the ferule curvature was also studied and optimized to obtain a good and relatively constant back-coupled power for all mirror positions.
- **Demodulation techniques** (see paragraph 6.9).
Different analog and digital demodulation techniques were compared. Digital demodulation on the under-sampled fringe signal was retained as the solution that offers the best compromise between noise resistance and data processing performance.

9.2.3 Measurement and analysis software

- **SOFO16 and SOFO95** (see paragraph 6.10.1.2)
These are the first software packages developed for use with the SOFO system. They allow automatic peak analysis as well as primitive project and sensor history management.
- **Definition of a database structure** (see paragraph 6.10.1.3).
A relational database structure was designed to store all the data relative to a given project into a single file. This database contains all the measurements and other related data useful for the successive analysis of the results. This database is also an important tool for the application of total quality management to projects based on the SOFO system.
- **SOFO DB** (see paragraph 6.10.1.3).
This software package implements the database structure, stores, retrieves and displays the data obtained with the SOFO reading unit. It is designed to work

with all types of SOFO sensors (including sensor chains) and reading units. It also comprises advanced scripting functions and allows the use of optical switches for unattended measurements.

9.2.4 Multiplexing

- **Analysis of possible multiplexing solutions** (see section 7).
A complete study on the possible multiplexing solutions for low-coherence sensors has been realized. Many solutions were tested experimentally and compared for their power and cost-efficiency. A few of these solutions can be considered as novel setups:
- **In-line coherence multiplexing** (see paragraph 7.4.1).
By using partial reflector pairs it is possible to multiplex many sensors in-line (i.e. in a chain). This type of multiplexing offers a very good power efficiency. Solutions for the unambiguous correlation of the interference peaks with the reflector pairs have also been proposed.
- **Phase pulses** (see paragraph 7.4.3.2).
Phase pulses can be used to identify the partial reflectors by their physical position in the sensor chain.
- **Double-pass phase modulation** (see paragraph 7.4.3.5).
This setup is an evolution of the phase pulses and allows a spatial resolution down to a few centimeters. The delicate time measurement is transformed into a much simpler amplitude measurement.
- **Hi-bi fibers** (see paragraph 7.4.2.4).
A setup using hi-birefringence fibers as reference fibers in a sensor or sensor chain has been presented. This configuration allows the identification of the different peaks by a simple measurement of the peak splitting between the two polarizations. This setup also allows the simultaneous measurement of deformations and integrated temperature.
- **Realization and characterization of partial reflectors** (see paragraph 7.6).
Different types of partial reflectors were tested including air-gap connectors, bubble reflectors and fiber Bragg gratings. Air-gap connectors offer the most flexible solution for civil engineering applications.

9.2.5 Applications

- **Deformation monitoring of concrete during setting** (see paragraphs 8.2, 8.9, 8.10, 8.11 and 8.12).
With the SOFO system it is possible to measure the concrete deformation during the setting reaction and starting right after concrete pouring. Thank to the temperature insensitivity of the setup, the heating due to the setting reaction does not influence the measurements.
- **Evaluation of interface behavior in mixed structures** (see paragraphs 8.3, 8.4, 8.5, 8.9, 8.11 and 8.12).

The SOFO system was used to study the interface behavior of mixed structures including steel-concrete, old-new concrete and timber-concrete slabs and beams. It was possible to analyze how the efforts are transmitted between the two materials and how differential shrinkage affects the properties of the structures.

- **Geometrical analysis of beams, bridges and plates** (see paragraphs 8.7, 8.8, 8.11 and 8.13).

Using deformation sensors it was possible to analyze the behavior of a structure with a purely geometrical analysis, i.e. through the measurement of the distance variations between points in the structure. It was found that curvature monitoring offers a powerful tool to analyze a structure with a reduced number of sensors.

- **Bridge monitoring** .

The SOFO system has been used to monitor the Venoge (VD, see section 8.9), Versoix (GE, see paragraph 8.11), Lully (FR, see paragraph 8.12), Lutrive (VD see paragraph 8.13) and OA402 (GE) highway bridges and viaducts, the Moesa (TI, see paragraph 8.10) railway bridge, and the Bissone (TI) road bridge.

- **Dam monitoring** (see paragraph 8.14).

The Emosson dam (VS) was instrumented with two long SOFO sensors replacing two steel rockmeters.

- **Tunnel monitoring** (see paragraph 8.15.3).

The Vignes highway tunnel (FR) and a tunnel near the Luzzzone Dam (TI) were instrumented with SOFO sensors for the monitoring of the tunnel's ovaling.

9.3 Outlook

This paragraph discusses desirable extensions of the SOFO system and possible spin-offs of the technologies developed in this project that could be applied in other domains. Some applications in structural engineering that could benefit from the SOFO system are also cited

9.3.1 Extensions of the SOFO system

- **Automatic and remote monitoring**

The automatic and remote measurement of structures is an important and relatively simple extension of the present SOFO system. A project in this direction has been launched.

- **Automatic analysis of the SOFO measurements**

Conventional and automatic measurements on a large number of sensors installed in a structure generate a huge amount of data that is impossible to analyze manually. Only automatic tools allowing the analysis of this data can extract the relevant information reliably, rapidly and cost-efficiently. The data obtained with the SOFO system should be integrated with other measurements (e.g. GPS, inclinometers, thermometers, force sensors,...) in order to obtain a

complete understanding of the structure's behavior. Samuel Vurpillot is preparing a dissertation on this interesting and important topic.

- **Measurement of temperature, pressure, humidity, pH, salt,...**

The SOFO system can be extended to measure other quantities than a displacement. We have seen that it is possible to obtain a temperature sensor, but many other quantities can be converted into a deformation and could therefore be measured by SOFO. Examples include pressures, humidity, pH, salt penetration and rust. A joint project with the University of Strathclyde aims to the development of chemical sensors for civil engineering applications based on the SOFO system and on the use of hydrogels.

- **Very long sensors**

Sensors with active lengths of 100 m and more could be interesting for the monitoring of large structures including suspension and cable stayed bridges, dams, off-shore platforms, pipelines, tunnels and power lines. The main problems to be solved include the design of a truly free reference fiber and of the sensor to structure bonding.

- **Short strain gages**

On the opposite end, sensors with only a few centimeters in length could offer an interesting alternative to resistive strain gages in applications where electromagnetic disturbances are present. To obtain a good resolution it will probably be necessary to fold the sensor to increase the measured deformation. For this application, fiber Bragg grating will probably offer a better alternative once their price gets lower.

- **Demodulation of fiber Bragg gratings**

The SOFO system can be used to demodulate multiple fiber Bragg gratings by Fourier transform spectroscopy. Preliminary tests were encouraging, but showed that the resolution of the translation stage supporting the mobile mirror should be increased in order to obtain a useful strain and temperature resolution.

9.3.2 Possible spin-offs

- **Use of SOFO sensors with other techniques: FBG, EFPI, ILFPI, Brillouin,...**

The SOFO sensors can be adapted to other fiber optic measurement techniques. Fiber Bragg Gratings (FBG), Extrinsic Fabry-Perot Interferometers (EPPI), In-Line Fabry-Perot Interferometers (ILEPI) and other 'point' sensors can be transformed into deformations sensors by installing them inside a SOFO sensor. The strained measurement fiber will turn any deformation into a variation of its tension that can be measured by the 'point' sensor. Another sensor can be manufactured on the reference fiber to compensate for parasitic temperature dependencies. Other systems measuring directly the strain state of the fiber and in particular stimulated Brillouin amplification can also be used to read multiplexed SOFO sensors. A collaboration with the Naval Research Laboratory in Washington has been established to explore on SOFO sensors containing fiber Bragg gratings and other applications of FBG to civil

engineering. Applications to civil structures of the Brillouin system developed at the Metrology laboratory (MET) at EPFL are also foreseen.

- **Dynamic measurement of SOFO sensors.**

It would be interesting if it was possible to measure SOFO sensors at much higher rates to obtain information about the dynamic properties of bridges and other structures. A large palette of methods based on coherent, low coherence and incoherent (e.g. microwave modulation) is available and should be explored. The same sensors could then be used for material testing during construction, static and dynamic testing and long term static and dynamic monitoring.

- **Extension of SOFO DB to other measurement methods**

The database structure of SOFODB can be easily extended to record measurements obtained with other measuring systems, both optical fiber-based as conventional. Integrated analysis tools would then combine the data from different types of sensors to give a complete understanding of the structure's behavior.

9.3.3 Other possible applications of the SOFO system

- **Mortars and shotcrete**

Short and small sensors can be used to characterize mortars, shotcrete and glues during setting and in the long-term. This is especially useful in the case of refurbishing, in order to guarantee a good cohesion between the added materials and the underlying ones.

- **Suspended and cable-strayed bridges**

Long sensors could be used to monitor long bridges. Dynamic measurements under traffic and wind loads would be important in this case.

- **Domes, roofs, space trusses**

Large domes and other extended roofs could benefit from the geometrical monitoring possible with the SOFO system. Highly non-linear structures like the 'tensegrity' system proposed by Passera + Pedretti Engineering for the Swiss expo2001 roofs are examples of structures that could benefit from a deformation monitoring system. It would even be possible to introduce active elements like hydraulic jacks to actively damp these structures.

- **Road pavements**

The high-temperature sensors developed for the monitoring of EDF's nuclear power plant mockup could be used to monitor road pavement deformations.

- **Off-shore structures**

Off-shore structures like drilling platforms are subject to extreme stresses and certainly require a continuous monitoring. In particular the long cables anchoring the platforms to the seabed could benefit from a fiber optic monitoring system.

- **Historical monuments and heritage structures**

Old buildings and structures with particular historical value or precarious static conditions should be monitored regularly or continuously to guarantee their security and allow early interventions to avoid irrecoverable damages.

- **Pipe-lines**

Pipeline joints should be monitored to avoid spillage and the associated ecological and economical consequences.

- **Containers**

Large containers for liquids, gases and cryogenic fluids can undergo large deformations when filled and emptied. An adequate monitoring system could monitor these deformations. Containers for nuclear wastes should be monitored.

9.4 Epilogue

I hope this work has brought a contribution towards a more generalized monitoring of civil engineering structures and a better understanding of the real structural and material behaviors. The SOFO project was (and is) not only a scientific and industrial adventure. It was for me a great experience in human interaction. Throughout the project, I had the opportunity to work with passionate peoples with whom I have shared the satisfactions and the inevitable disappointments associated with every project. I have learned that the best results are obtained by seeking the help and advice from the specialists. Everyone has however to adapt himself to the needs of the others and a common language has to be found to communicate and build a true team spirit. Through this interaction I have found out how fascinating civil engineering can be. All the buildings, bridges and tunnels that surround me are now seen under a new light (and sometimes with a little more concern!). It was also a satisfaction to transmit my passion for optics and metrology my colleagues. In our project, it is not rare to hear a civil engineer reason about “the influence of birefringence on the visibility of interference fringes” or on the definition of “coherence”, while a physicist argues about “stress diagrams” and “pH changes due to concrete degradation”. I believe that this degree of osmosis is only possible when people from different domains physically work together towards a common goal and vision. A weekly meeting will never replace the complicity that can be created by sharing the same offices and laboratories. This is probably the true essence of the IMAC spirit and Prof. Plug’s philosophy: bring together researchers from civil engineering, optics and other domains, give them freedom, support and a pleasant working environment and wait for the spark to ignite...

Lugano, May 1997

Daniele Inaudi

General Bibliography

Cited bibliography by first author name.

- Distributed and multiplexed fiber optic sensors IV, San Diego, CA, Jul. 27-28, 1994, SPIE Vol. 2294
- Distributed and multiplexed fiber optic sensors V, Munich, FRG, Jun. 22-23, 1995, SPIE Vol. 2507
- Fiber Optics Reliability: Benign and Adverse Environments IV (1990), SPIE vol. 1366
- Optical Fiber Sensor Conference Series OFS: 1 London 1983, 2 Stuttgart 1984, 3 San Diego 1985, 4 Tokyo 1986, 5 New Orleans 1988, 6 Paris 1989, 7 Sydney 1990, 8 Monterey 1991, 9 Florence 1993
- Smart Structures and Materials 1993: Smart sensing, processing, and instrumentation, Albuquerque, NM, Feb. 1-4, 1993, SPIE Vol. 1918
- Smart Structures and Materials 1994: Smart sensing, processing, and instrumentation, Orlando, FL, Feb. 14-16, 1994, SPIE Vol. 2191
- Smart Structures and Materials 1995: Smart sensing, processing, and instrumentation, San Diego, CA, Feb. 27- Mar. 1, 1995, SPIE Vol. 2444
- Tenth International Conference on Optical Fiber Sensors, Glasgow, UK, Oct. 11-13, 1994, SPIE Vol. 2360
- C. G. Askins, M. A. Putman, G. M. Williams, E. J. Friebele, "Contiguous Fiber Bragg Grating Arrays Produced On-line During Fiber Draw," Smart Structures and Materials 1994: Smart sensing, processing, and instrumentation, Orlando, FL, 1994, SPIE Vol. 2191, pp. 80-85
- M. K. Barnoski, S. M. Jensen, "A Novel Technique for Investigating Attenuation Characteristics," Applied Optics, Vol. 15, 1976, pp. 2112
- A. J. Bruinsama, B. Culshaw, Fiber Optic Sensors: Engineering and applications, The Hague, The Netherlands, Mar. 14-15, 1991, SPIE Vol. 1511
- C. D. Butter and G. B. Hocker "Fiber optics strain gage", Applied Optics, Vol. 17, No. 18, Sept. 1978
- C.-C. Chang, J. Sirkis, "Optical Fiber Sensors Embedded in Composite Panels for Impact Detection," Smart Structures and Materials 1995: Smart sensing, processing, and instrumentation, San Diego, CA, Feb. 27- Mar. 1, 1995, SPIE Vol. 2444, pp. 502-513
- S. Chen, A. J. Rogers, B. T. Mergitt "Electronically Scanned Optical-Fiber Young's White-light interferometer", Optics Letters, Vol. 16, No. 10, May 1991, pp. 761-763.
- S. Chen, B. T. Mergitt, A. J. Rogers "Novel electronic Scanner for Coherence Multiplexing in a Quasi-distributed Pressure Sensor", Electronics letters, Vol. 26, No. 17, August 1990, pp. 1367-1369
- J. Dakin, B. Culshaw, Optical fiber sensors, Norwood, MA, Artech House,

1988

- A. Dandridge, A. B. Tveten, A. D. Kersey, A. M. Yurek, "Multiplexing of Interferometric Sensors Using Phase Generated Carrier Techniques," IEEE Journal of Lightwave Technology, Vol. 5, 1987, PP. 947
- K. Danker, B. G. Rabbat, "Why America's Bridges are crumbling", Scientific American, March 1993, 66-70
- M. A. Davis, D. G. Bellemore, T. A. Berkoff, A. D. Kersey, "Design and Performance of a Fiber Bragg Grating Distributed Strain Sensor System," Smart Structures and Materials 1995: Smart Systems for Bridges, Structures, and Highways, San Diego, CA, Feb. 28 - Mar. 3, 1995, SPIE Vol. 2446, p. 227-235
- A. Elamari, D. Inaudi, J. Breguet, L. Pflug, N. Gisin, S. Vurpillot, "Low Coherence Fiber Optic Sensors for Structural Monitoring", Structural Engineering International, Volume 5, Number 1, 43-47
- D. A. Flavin, R. McBride, J. D. C. Jones, J. G. Burnett, A. H. Greenaway, "Combined Temperature and Strain Measurement with a Dispersive Optical Fiber Fourier-transform Spectrometer," Optics Letters, Vol. 19, 1994, pp. 2167-2169
- I. P. Giles, D. Uttam, B. Culshaw, D. E. N. Davies, "Coherent Optical Fiber Sensors with Modulated Laser Sources," Electronics Letters, Vol. 20, 1983, pp. 14
- N. Gisin, J.-P. Von der Weid, J.-P. Pellaux "Polarization Mode Dispersion of Short and Long Single-mode Fibers", Journal of Lightwave technology, Vol.9, No. 7, July 1991, pp. 821-827
- J. W. Goodman, "Statistical Optics", Wiley, 1985
- J. A. Green et al. "Photoinduced Fresnel reflectors for point-wise and distributed sensing applications" Smart Structures and Materials 95, S. Diego, SPIE vol. 2444, p 64
- P. de Groth, L. Deck "Three-dimensional imaging by sub-Nyquist sampling of white-light Interferograms", Optics Letters, Vol. 18, No. 17, September 1993, pp. 1462-1464.
- V. Gusmensoli, M. Martinelli, "Absolute measurements by low-coherence sources", Advances in Optical Fiber Sensors, Wuhan, China, October 1991
- V. Gusmensoli, M. Martinelli, "Non-incremental Interferometric Fiber-optic measurement method for simultaneous detection of temperature and strain," Optics Letters, Vol. 19, 1994, pp. 2164-2166
- W. R. Habel, D. Hofmann, "Strain Measurements in Reinforced Concrete Walls During the Hydration Reaction by Means of Embedded Fiber Interferometers," Second European Conference on Smart Structures and Materials, Glasgow, UK, Oct. 12-14, 1994, SPIE Vol. 2361, pp. 180-183
- W. R. Habel, M. Höpcke, F. Basedau, H. Polster, "The Influence of Concrete and Alkaline Solutions on Different Surfaces of Optical Fibers for Sensors," Second European Conference on Smart Structures and Materials, Glasgow, UK, Oct. 12-14, 1994, SPIE Vol. 2361, pp. 168-171

- E. Hecht "Optics", Addison-Wesley, 1974-1987
- G. B. Hocker "Fiber-optic sensing of pressure and temperature", Applied Optics, Vol. 18, No. 9, May 1979
- S. H. Huang, M. M. Ohn, M. LeBlanc, R. Lee, R. M. Measures, "Fiber Optic Intra-grating Distributed Strain Sensor," Distributed and Multiplexed Fiber Optic Sensors IV, San Diego, CA, Sept. 1994, SPIE Vol. 2294
- D. Inaudi "Coherence multiplexing of in-line displacement and temperature sensors", Optical Engineering, Vol. 34, Nr.7, July 1995
- D. Inaudi, A. Elamari, L. Pflug, N. Gisin, J. Breguet, S. Vurpillot, "Low-coherence deformation sensors for the monitoring of civil-engineering structures", Sensor and Actuators A, 44 (1994), 125-130.
- D. Inaudi, A. Elamari, S. Vurpillot, "Low-coherence interferometry for the monitoring of civil engineering structures", Second European Conference on Smart Structures and Materials, Glasgow October 1994, SPIE Volume 2361, 216-219.
- D. Inaudi, L. Vulliet, L. Pflug, S. Vurpillot, A. Wyser, "Low-coherence interferometry for the monitoring of underground works", 1995 North American Conference on Smart Structures and Materials, San Diego February 1995, Volume 2444, 171-178.
- D. Inaudi, S. Vurpillot, S. Lloret, "In-line coherence multiplexing of displacement sensors: a fiber optic extensometer", Smart Structures and materials, San Diego February 1996, SPIE Volume 2718-28.
- D. Inaudi, S. Vurpillot, Nicoletta Casanova, Annette Osa-Wyser, "Development and field test of deformation sensors for concrete embedding", Smart Structures and materials, San Diego February 1996, SPIE Volume 2721-16.
- A. D. Kersey, A. Dandridge, A. B. Tveten, "Dependence of visibility on input polarization in interferometric fiber-optic sensors", Optics Letters, Vol. 13, No. 4, April 1988
- A. D. Kersey, M. A. Davis, T. Tsai "fiber optic Bragg grating sensor with direct reflectometric interrogation", OFS11, Sapporo, May 1996, p. 634
- A. D. Kersey, M. J. Marrone, "Nested interferometric sensors utilizing Bragg grating reflectors", OFS11, Sapporo, May 1996, p. 618
- A. D. Kersey, T. A. Berkoff, W. W. Morey, "Multiplexed Fiber Bragg Grating Strain-sensor System with a Fiber Fabry-Perot Wavelength Filter," Optics Letters, Vol. 18, 1993, pp. 1370-1372
- A. Koch, R. Ulrich "Fiber-optic Displacement Sensor with 0.02 μm Resolution by White-light Interferometry", Sensors and Actuators A, 25-27 (1991), 201-207
- D. G. Luke, R. McBride, P. Lloyd, J. G. Burnett, A. H. Greenaway, J. D. C. Jones, "Strain and temperature measurement in composite-embedded highly-birefringent optical fiber using mean and differential group delay", OFS 11, Sapporo, may 1996, p. 200.

- A. Mabrouky, M. Gadonna and R. Le Naour, "Polarization characterization of a Mach-Zehnder interferometer", *Applied Optics*, Vol. 35, No. 19, July 1996
- I. F. Markey, "Enseignements tirés d'observations des déformations de ponts en béton et d'analyses non linéaires", Thèse EPFL n° 1194, 1993
- B. Mason, T. Valis, D. Hogg, "Commercialization of Fiber-optic Strain Gauge Systems," *Fiber optic and laser sensors X*, Boston, MA, Sept. 8-11, 1992, SPIE Vol. 1795, p. 215-222.
- R. M. Measures, et al. "Structurally Integrated Fiber Optic Damage Assessment System for Composite Materials," *Applied Optics*, Vol. 28, 1989, pp. 2626-2633
- G. Meltz, W. W. Morey, W. H. Glenn "Formation of fiber Bragg gratings in optical fibers by a transverse holographic method", *Optics letters*, 14, 1989, p. 823
- W. C. Michie, B. Culshaw, I. McKenzie, M., Konstantakis, N. B. Graham, C. Moran, F. Santos, E. Bergqvist, B. Carlstrom, "Distributed Sensor for Water and pH Measurements Using Fiber Optics and Swellable Polymeric Systems," *Optics Letters*, Vol. 20, 1995, pp. 103-105
- W. W. Morey, J. R. Dunphy, G. Meltz, "Multiplexing fiber Bragg Grating sensors", SPIE Vol. 1586, p.261
- H. Murata "Handbook of optical fibers and cables", Dekker, 1988
- M. Niklès, L. Thévenaz, P. A. Robert, "Simple Distributed Temperature Sensor Based on Brillouin Gain Spectrum Analysis," *Tenth Optical Fiber Sensors Conference*, Glasgow, UK, Oct. 11-13, 1994, SPIE Vol. 2360, pp. 138-141
- Y. N. Ning, K. T. V. Grattan, B. T. Mergitt, A. W. Palmer "Characteristics of laser diodes for interferometric use", *Applied optics*, Vol. 28, No. 17, September 1989, pp. 3657-3661.
- Y. J. Rao, Y. N. Ning, D. A. Jackson "Synthesized Source for White-light sensing system", *Optics letters*, Vol. 18, No 6, March 1993, pp. 462-464
- K. Shimitzu, T. Horiguchi, Y. Koyamada, "Measurement of Distributed Strain and Temperature in a Branched Optical Fiber Network by Use of Brillouin Optical Time-Domain Reflectometry," *Optics Letters*, Vol. 20, 1995, pp. 507-509
- J. S. Sirkis, C. T. Mathews, "Experimental Investigation of Phase-Strain-Temperature Models for Structurally Embedded Interferometric Fiber-optic Sensors," *Experimental Mechanics*, vol. 33, 1993, pp. 26-31
- J. S. Sirkis, "Unified Approach to Phase-Strain-Temperature Models for Smart Structure Interferometric Optical Fiber Sensors: Part 1, Development," *Optical Engineering*, Vol. 32, 1993, pp. 752-761
- J. S. Sirkis, "Unified Approach to Phase-Strain-Temperature Models for Smart Structure Interferometric Optical Fiber Sensors: Part 2, Applications," *Optical Engineering*, Vol. 32, 1993, pp. 762-773
- J. S. Sirkis, D. D. Brennan, M. A. Putman, T. A. Berkoff, A. D. Kersey and E. J. Friebele, "In-line fiber étalon for strain measurement", *Optics Letters*, Vol. 18,

No. 22, pp. 1973-1975, 1993

- A. S. Subdo, "An optical time domain reflectometer with low power InGaAsP diode lasers", IEEE J. of Lightwave technology, LT-1, 616-618, 1983
- L. Thévenaz, J.-P. Pellaux, N. Gisin, J.-P. Von der Weid "Birefringence Measurements in Fibers Without Polarizer", Journal of Lightwave technology, Vol.7, No. 8, August 1989, pp. 1207-1212
- E. Udd "Fiber Optic Sensors", Wiley, 1990
- E. Udd, "Three axis and temperature fiber optic grating sensor", Smart Structures and Materials 1996, San Diego, CA, Feb. 27- 29, 1996, SPIE Vol. 2718
- Udd, E., Fiber optic smart structures, Wiley, New York, 1995
- A. M. Vengsarkar, W. C. Michie, L. Jankovic, B. Culshaw, R. O. Claus, "Fiber-optic Dual-technique for Simultaneous Measurement of Strain and Temperature," Journal of Lightwave Technology, Vol. 12, 1994, pp. 170-177
- J.-P. Von der Weid, L. Thévenaz, J.-P. Pellaux, "Interferometer measurements of chromatic dispersion and polarization mode dispersion in highly birefringent singlemode fibers", Electr. Lett., vol. 23, pp. 151-152, 1987
- S. Vurpillot, D. Inaudi, P. Mivelaz, "Low-coherence interferometry for the monitoring of concrete structures", European Symposium on Optics for Environmental and Public Safety, Munich June 1995, SPIE Volume 2507, 35-44
- M. G. Xu, J.-L. Archambault, L. Reekie, J. P. Dakin, "Discrimination Between Strain and Temperature Effects Using Dual-wavelength fiber grating sensors," Electronics Letters, vol. 30, 1994, pp. 1085-1087

Curriculum Vitae

Name: Daniele Andrea INAUDI

Date and Place of Birth: 25th June 1968, Lugano Switzerland.

Nationality: Swiss

Education:

1983-1987	High school, Scientific orientation, Lugano.
1987-1992	Physics, Swiss Federal Institute of Technology, Zurich, Switzerland.
1992-1996	Ph.D. student at the Laboratory of Stress Analysis (IMAC) of the Swiss Federal Institute of Technology in Lausanne, Switzerland.

Academic and Professional Qualifications: Physics degree, Swiss Federal Institute of Technology.
SPIE Member.

Awards:

1992	ETHZ Medal for the graduation work “Design, characterization and modeling of external grating tunable diode lasers”.
------	--

Professional Activities:

1992-1996	Research engineer, IMAC-EPFL. SOFO project manager. Advisor for the following graduation works: “Applicazione dell’interferometria in bassa coerenza alla ricerca della deformata di una trave”, Antonio Scano. “Detection and ranging of reflective markers on optical fibers by low-coherence interferometry”, Sandra Lloret. "Analyse d’une poutre fléchie / Application à un barrage-voûte en exploitation", Pascal Kronenberg. Assistant for practical works on holographic interferometry and holographic optical elements for micro-technology students.
1996	Co-founder of the company SMARTEC SA in Grancia, active in the domain of optical fiber instrumentation for civil engineering monitoring.

Author's Bibliography

Books:

- "Fiber optic smart sensing" D. Inaudi in "Optical Measurement Techniques and Applications" edited by P. K. Rastogi, Artech house, 1997

Peer reviewed journals:

- "Polarization state of the emission of external grating diode lasers", D. Syvridis, D. Inaudi, G. Guekos, IEEE Journal of quantum electronics, Vol. 30, Number 4, April 1994, pp.966-974.
- "Low-coherence deformation sensors for the monitoring of civil-engineering structures", D. Inaudi, A. Elamari, L. Pflug, N. Gisin, J. Breguet, S. Vurpillot, Sensor and Actuators A, 44 (1994), 125-130.
- "Low Coherence Fiber Optic Sensors for Structural Monitoring", A. Elamari, D. Inaudi, J. Breguet, L. Pflug, N. Gisin, S. Vurpillot, Structural Engineering International, Volume 5, Number 1, 43-47.
- "Coherence multiplexing of in-line displacement and temperature sensors", D. Inaudi, Opt. Eng., Vol. 34, Nr. 7, July 1995.
- "Milestone in chaos theory: Experimental evidence of the butterfly effect", D. Inaudi, X. Colonna de Lega, A. Di Tullio, C. Forno, P. Jacquot, M. Lehmann, M. Monti, S. Vurpillot, Annals of Improbable Research, Vol. I, No. 6, November/December 1995.
- "Structural monitoring by curvature analysis using interferometric fiber optic sensors", D. Inaudi, S. Vurpillot, N. Casanova, P. Kronenberg, submitted to Smart Materials and Structures Journal.
- "Vertical displacements of a pre-stressed concrete bridge deduced from deformation sensors and inclinometer measurements", S. Vurpillot, G. Krüger, D. Benouaich, D. Clément, D. Inaudi, submitted to American Concrete International.
- "Ranging of reflective markers in optical fiber sensors by double-pass phase modulation", D. Inaudi, S. Lloret, to be published in Optical Engineering.

Invited papers:

- "Bridge Monitoring by Interferometric Deformation Sensors", D. Inaudi, S. Vurpillot, N. Casanova, Laser Optoelectronics and Microphotonics: Fiber Optics Sensors, SPIE, Beijing November 1996

Conferences:

- "Low-coherence interferometry for the monitoring of civil engineering structures", D. Inaudi, A. Elamari, S. Vurpillot, Second European Conference on Smart Structures and Materials, Glasgow October 1994, SPIE Volume 2361, 216-219.
- "Mesure des déformation de grandes ouvrages par fibres optiques en interférométrie basse cohérence", D. Inaudi, Conférence "Mesure optique des formes 3D et des grandes déformations" Tours novembre 1994.
- "Low-coherence interferometry for the monitoring of underground works", D. Inaudi, L. Vulliet, L. Pflug, S. Vurpillot, A. Wyser, 1995 North American Conference on Smart Structures and Materials, San Diego February 1995, Volume 2444, 171-178
- "Development of interferometric fiber optic extensometers to monitor geostuctures", L. Vulliet, D. Inaudi, A. Wyser, S. Vurpillot, L. Pflug, Field Measurements in Geomechanics 4th International Symposium, Bergamo April 1995.
- "Low-coherence interferometry for the monitoring of concrete structures", S. Vurpillot, D. Inaudi, P. Mivelaz, European Symposium on Optics for Environmental and Public Safety, Munich June 1995, SPIE Volume 2507, 35-44
- "SOFO: Surveillance d'ouvrages par senseurs à fibres optiques", Daniele Inaudi, S. Vurpillot, IAS: Ingénieur et Architecte Suisse, 121ème année, numéro 26, 6 décembre 1995, 522-529.
- "Mesure des déformations de grandes structures par senseurs à fibre optique", D. Inaudi, S. Vurpillot, L. Pflug, Research and development in the field of Dams, Crans-Montana, September 1995
- "Mathematical model for the determination of the vertical displacement from internal horizontal measurements of a bridge" S. Vurpillot, D. Inaudi, A. Scano, Smart Structures and materials, San Diego February 1996, SPIE Volume 2719-05.
- "Development and field test of deformation sensors for concrete embedding", D. Inaudi, S. Vurpillot, Nicoletta Casanova, Annette Osa-Wyser, Smart Structures and materials, San Diego February 1996, SPIE Volume 2721-16.
- "Bridge monitoring by fiber optic deformation sensors: design, emplacement and results", S. Vurpillot, D. Inaudi, J.-M. Ducret, Smart Structures and materials, San Diego February 1996, SPIE Volume 2719-16.
- "In-line coherence multiplexing of displacement sensors: a fiber optic extensometer", D. Inaudi, S. Vurpillot, S. Lloret, Smart Structures and materials, San Diego February 1996, SPIE Volume 2718-28.
- "Development and laboratory tests of deformation fiber optic sensors for civil engineering applications", L. Vulliet, N. Casanova, D. Inaudi, A. Osa-Wyser, S. Vurpillot, International Symposium on Lasers, Optics and Vision for Productivity in Manufacturing, Europto Series, Besançon, 10-14 June 1996.
- "Dam monitoring with fiber optic sensors", P. Kronenberg, N. Casanova, D. Inaudi, S. Vurpillot, Smart Structures and materials, San Diego February 1997

- "Bridge spatial deformation monitoring with 100 fiber optic deformation sensors", P. Kronenberg, N. Casanova, D. Inaudi, S. Vurpillot, Smart Structures and materials, San Diego February 1997
- "Railway bridge monitoring during construction and bridge sliding", P. Kronenberg, N. Casanova, D. Inaudi, S. Vurpillot, Smart Structures and materials, San Diego February 1997
- "Embedded and surface mounted sensors for civil structural monitoring", P. Kronenberg, N. Casanova, D. Inaudi, S. Vurpillot, Smart Structures and materials, San Diego February 1997

